Counteraction of APOBEC3 Proteins by Herpesvirus Ribonucleotide Reductases

A Dissertation
Presented to
The Academic Faculty of
The University of Minnesota

By

Adam Z. Cheng

In Partial Fulfillment
of the Requirements for the Degree of
Doctor of Philosophy

Advisor: Reuben S. Harris

August 2019

Counteraction of APOBEC3 Proteins by Herpesvirus Ribonucleotide Reductases

Approved by:

Dr. Peter J. Southern
Department of
Microbiology & Immunology
Committee Chair

Dr. Stephen A. Rice
Department of
Microbiology & Immunology
Committee Member

Dr. Ryan A. Langlois
Department of
Microbiology & Immunology
Committee Member

Dr. Hideki Aihara
Department of Biochemistry,
Molecular Biology, & Biophysics
External Committee Member

Dr. Reuben S. Harris
Department of Biochemistry,
Molecular Biology, & Biophysics
Advisor

Date Approved: June 24, 2019

Science is a Feeling.

Anonymous

Dedicated to my Matthew.

ACKNOWLEDGEMENTS

I would like to thank:

My thesis advisor, Dr. Reuben S. Harris, who entranced me with science and filled my days with fantastical ideas, novel experiments, and boundless wisdom.

Members of the Harris lab, who trained and laughed with me, especially Brett & Nadine, who trained me well, and Mike, who is my personal "letmegooglethatforyou".

Collaborators who shared with me many, many reagents, protocols, ideas, and data.

My thesis committee, Drs. Peter J. Southern, Stephen A. Rice, Ryan A. Langlois, and Hideki Aihara, for their time and expertise in guiding me through this journey we call PhD. In particular, Dr. Southern, who led me through medical school microbiology, preliminary exams, and my thesis with invaluable advice throughout the way.

The many people who have shaped my childhood years and sparked my love of science, especially Mr. Brad Graba & Mr. Karl Craddock.

Previous research mentors, Drs. Petra Levin & Beth Levine, who drove my excitement for research and encouraged me to continue down a path of science and medicine.

C.P., you are like a brother to me.

Skittles, you taught me to be brave.

Grace, you showed me to be compassionate.

John, you guided me to love.

My dear brother with whom I grew up and with whom I found joy in life.

My parents, who told me I could do anything.

And to Matthew.

ABSTRACT

The APOBEC3 family of DNA cytosine deaminases plays an important role in antiviral innate immunity. In this thesis, we describe the novel function of APOBEC3B as a physiologic restriction factor against herpesviruses such as Epstein-Barr virus and herpes simplex virus type 1. We additionally define the counteraction mechanism imparted by herpesviruses using the virus-encoded ribonucleotide reductase large subunit. These viral proteins directly bind A3B to inhibit enzymatic activity, relocalize it away from replicating viral DNA, and protect the virus from A3B-mediated hypermutation for preservation of the viral genome. These results have the potential to reveal new modes of antiviral therapy and have implications in the treatment of A3B-driven cancers.

TABLE OF CONTENTS

LIST OF TABLES

LIST OF FIGURES

LIST OF ACRONYMS

A	Adenosine (in the context of DNA)
APE	Apurinic endonuclease
A1	APOBEC1
A2	APOBEC2
A3	APOBEC3
A3X	APOBEC3A, APOBEC3B, etc.
A4	APOBEC4
AAV	Adeno-associated virus
AID	Activation-induced deaminase
AP-MS	Affinity purification-mass spectrometry
APOBEC	Apolipoprotein B mRNA editing enzyme, catalytic polypeptide-like
BIV	Bovine immunodeficiency virus
BKPyV	BK polyomavirus
BORF2	EBV ribonucleotide reductase large subunit
C	Cytosine (in the context of DNA)
CAEBV	Chronic active EBV infection
cDNA	Complementary DNA
co-IP	Co-immunoprecipitation
CTD	C-terminal domain
CYPA	Cyclophilin A
dsDNA	Double-stranded DNA
EBNA	EBV-encoded nuclear antigen
EBV	Epstein-Barr virus
EdU	5-Ethynyl-2'-deoxyuridine

ERV	Endogenous retrovirus
FV	Foamy virus
G	Guanine (in the context of DNA)
GC	Gastric carcinoma
GM-P	Granulocyte-macrophage progenitors
HBV	Hepatitis B virus
HCMV	Human cytomegalovirus
HIV-1	Human immunodeficiency virus type 1
HIV-2	Human immunodeficiency virus type 2
hpi	Hours post-infection
HSC	Hematopoietic stem cell
HSV-1	Herpes simplex virus type 1
HSV-2	Herpes simplex virus type 2
HTLV-1	Human T-cell lymphotropic virus type 1
HV	Herpesvirus
IM	Infectious mononucleosis
KSHV	Kaposi's sarcoma-associated herpesvirus
JCPyV	JC polyomavirus
LAT	Latency-associated transcript
LINE	Long interspersed nuclear element
LMP	Latent membrane protein
LTR	Long terminal repeat
MCMV	Murine cytomegalovirus
MCPyV	Merkel cell polyomavirus
MDM	Monocyte-derived macrophage
MVV	Maedi-visna virus

NaB	Sodium buytrate
NC	Nucleocapsid
NKTL	Natural kill and T-cell lymphoma
NPC	Nasopharyngeal carcinoma
NTD	N-terminal domain
PyV	Polyomavirus
R1	Ribonucleotide reductase large subunit
R2	Ribonucleotide reductase small subunit
RNR	Ribonucleotide reductase
RT	Reverse transcriptase
ssDNA	Single-stranded DNA
SINE	Short interspersed nuclear element
T	Thymine (in the context of DNA)
TPA	12-O-tetradecanoylphorbol-13-acetate
TK	Thymidine kinase
U	Uracil (in the context of DNA)
UDG	Uracil DNA glycosylase
UGI	Uracil glycosylase inhibitor

CHAPTER 1

Introduction and Background: APOBECs in Virus Restriction

Author: Adam Z. Cheng

1.1 Chapter Synopsis

CHAPTER one provides an introduction and background to APOBEC enzymes in virus restriction. I first provide a general overview of the APOBEC family of cytosine deaminases, their functions, and roles in antiviral innate immunity. The relationship between APOBEC3 family of enzymes and HIV-1 is then highlighted as an archetypal example of virus restriction and APOBEC counteraction. I also compare and contrast other known examples of APOBEC3 counteraction including those mediated by other retroviruses and endogenous retroelements, hepadnaviruses, and double-stranded DNA viruses. Next, I cover important aspects of herpesvirus virology with a focus on herpes simplex virus type 1, human cytomegalovirus, and Epstein-Barr virus as representative viruses from each of the α-, β-, and γ-herpesvirus subfamilies. Here, I provide in-depth background on herpesvirus replication, lytic versus latency, and pathogenesis. Lastly, I describe the functions of viral ribonucleotide reductases and how they relate to APOBEC3 counteraction.

1.2 The APOBEC Family of Cytosine Deaminases

The human APOBEC (apolipoprotein B mRNA editing enzyme, catalytic polypeptide-like) family of cytosine deaminases is composed of nine proteins with the conserved function of single-stranded (ss)DNA cytosine (C) to uracil (U) deamination [1–3] (**Figure 1.1**). The superfamily includes APOBEC1 (A1), activation-induced deaminase (AID), APOBEC2 (A2), seven APOBEC3 (A3) paralogs, and APOBEC4 (A4) [1–3]. A1 serves as the namesake of the family for which the primary function is the RNA-editing of *APOB* pre-mRNA [4]. The *APOB* transcript encodes for APOB100 (full length) and APOB48 (truncated, 48% of full length) [4]. The truncated transcript arises from A1-mediated editing of CAA to UAA, which generates an early stop codon that encodes the shorter protein variant [4]. AID shares structural homology with A1, but functions in somatic hypermutation of rearranged immunoglobulin genes in B cells, which generates antibody diversity [5–7]. It is also required for class-switch recombination by deamination of adjacent cytosines on opposite strands which leads to double-strand DNA breaks after uracil processing [8]. A2 and A4 do not yet have an attributed physiologic function and lack cytosine deaminase activity *in vitro* [9].

AID and A2 have existed since at least the evolution of bony fish [1] with likely ancestral roots in jawless fish (although APOBEC-like deaminases have existed since early metazoans) [10–12]. A4 has even more ancient ancestral roots in cnidaria-algae [12]. In vertebrates, the duplication of *AID* in an inverted direction resulted in *APOBEC1*, likely in the ancestor of placental and marsupial mammals. A more recent *AID* duplication led to the development of *APOBEC3* in placental mammals after their divergence from marsupials [1, 12]. The *A3* locus has undergone numerous

expansion and contraction events since its origin in the ancestral placental mammal [13, 14]. The resulting gene copy number ranges from one in mice and rats, two in pigs, three in cows and sheep, four in cats, six in horses, seven in humans and non-human primates, and eighteen in megabats [13, 14] (**Figure 1.2**).

The human APOBEC3 family members (APOBEC3A-D and APOBEC3F-H) are encoded in tandem on chromosome 22 [1–3]. A3-mediated inhibition or restriction of viruses has been described for a variety of viruses including human immunodeficiency virus type 1 and 2 (HIV-1/2) [15–18], human T-cell lymphotrophic virus (HTLV-1) [19], foamy viruses (FV) [20], hepatitis B virus (HBV) [21–23], endogenous retroviruses (ERV) and retroelements (*e.g.*, LINE-1 and Alu) [24, 25], human papillomavirus (HPV) [26, 27], JC & BK polyomaviruses (JCPyV, BKPyV) [28, 29], and most recently, the family of double-stranded DNA (dsDNA) herpesviruses (HV) (*e.g.*, herpes simplex virus, Epstein Barr virus, and Kaposi's sarcoma-associated herpesvirus) [30, 31]. Chapter 2 defines the mechanism of A3B counteraction by an early lytic EBV protein, BORF2, the large subunit of viral ribonucleotide reductase (RNR). Chapter 3 then describes the overall conservation between RNR large subunits and A3 family proteins.

Most studies on APOBEC3-mediated restriction to date have focused on deaminase-dependent mechanisms, but deaminase-independent mechanisms of APOBEC-mediated restriction have also been described. In general, these mechanisms are RNA-dependent and arise from steric hindrance of RNA processing, such as A3G-mediated inhibition of HIV-1 reverse transcription [32]. Deaminase-dependent mechanisms of APOBEC3-mediated virus restriction rely on the conversion of cytosines-to-uracils on ssDNA to generate mutations in the viral DNA. Specificity of ssDNA substrates is determined by flexible loops adjacent to the catalytic zinc-

coordinating pocket [33]. Loop 7 governs di- and trinucleotide preferences such that 5'-TC is the preferred context for all enzymes except A3G, which prefers 5'-CC [33–35]. Moreover, chimeric loop swaps in this region can confer the reciprocal dinucleotide specificity [36]. Loop 1 undergoes conformational changes when engaging ssDNA and differences in this loop alter overall activity of the enzyme by providing more open or closed conformations for ssDNA entry. For example, chimera studies swapping A3B loop 1 for A3A loop 1 enhances A3B activity to levels similar to wild-type A3A [37]. Thus, structural loop differences between APOBEC3 enzymes provides some specificity in ssDNA substrates as well as overall enzymatic activity. Using bioinformatic and *in vitro* analyses of human and viral genomes, we can also infer tri-nucleotide preferences for each enzymes [38], summarized in **Table 1.1**.

After cytosine deamination, downstream processing of uracils can result in numerous outcomes (**Figure 1.3**). If the uracil is not repaired, the next round of replication will cause it to template as adenine and generate C-to-T mutations [39]. For faithful repair, cellular or viral uracil DNA glycosylase (UDG) must first remove the uracil base and then apurinic endonuclease (APE) excises the abasic site, followed by repair with DNA polymerase β [40]. Alternatively, the abasic site can be replicated over without repair, which leads to C-to-N mutations [40]. Uracil lesions can also be recognized my mismatch repair machinery (MutSα/MutSβ), which recruits exonuclease I to generate a long stretch of ssDNA[40, 41]. Translesion synthesis over this by DNA polymerase η can then lead to mutations at A:T base pairs [40, 41]. Additionally, these long stretches of ssDNA can be susceptible to further A3-mediated deamination and lead to kataegis[1] [42]. Finally, double strand

[1] Here, kataegis refers to localized somatic hypermutation associated with somatic rearrangements in cancer cells first observed and coined in 2012 by Nik-Zainal S., *et al.* [42]. In Greek, kataegis means shower or thunderstorm, a reference to regions of mutational shower in the genome.

breaks can occur when multiple cytosine residues are converted to uracils on opposite strands (*e.g.*, during class-switch recombination [8]), also reviewed in [40, 41]). The overall consequence of APOBEC-mediated deamination is increased mutagenic load in the genome. In viruses, this can lead to missense mutations or early stop codons, which can be lethal to virus replication.

The targets of A3-mediated deamination are partially determined by gene expression in different cell types [43, 44]. For example, the primary site of HIV-1 replication is in $CD4^+$ T cells, which express high levels of the HIV-1 restrictive APOBECs, A3C, A3D, A3F, A3G, and A3H [44, 45]. *A3* expression in these cells is also induced by HIV-1 infection and T cell-specific mitogens such as phytohemaglutinin and interleukin 2 [44]. In contrast, *A3A* expression is primarily limited to monocytes and macrophages, which may play a role in restriction of CCR5-tropic HIV-1 or other viruses that infect these cell types (*e.g.*, Kaposi's sarcoma-associated herpesvirus, KSHV). Finally, *A3B* expression is low or undetectable in T cells, but high in B and epithelial cells [30, 44, 46]. There is also a naturally circulating 29.5 kb *A3B* deletion polymorphism that results in an *A3A/B* fusion gene that encodes a protein idential to A3A at the amino acid level [47]. This deletion polymorphism has different geographic distributions, being most common in Oceania (allele frequency of 0.93) and also higher in southeast Asia (AF=0.37), and native North and South Americans (AF=0.48) [47]. Clinically, the deletion polymorphism is not definitely associated with disease pathologies. Some studies have shown associations with increased cancer risk in certain populations [48–51] while other studies have found no correlation [52–55]. Similarly, studies looking at the impact of *A3B* deletion on risk of HIV-1, HBV, and other infections have not revealed a clear associated phenotype [56–60].

In addition to cell- and tissue-specific A3 expression patterns, access to viral DNA is partially regulated by A3 localization in different subcellular compartments. Endogenous A3A is cytoplasmic in primary $CD34^+$ monocytes and the THP-1 monocyte cell line, but overexpression of A3A in a variety of other cell types is cell wide with a predominant nuclear localization *in vitro* [61–64]. A3B localization is unique in that it is the only solely nuclear A3 and is excluded from the nucleolus [61–63, 65]. When upregulated in cancer, A3B has the capacity to mutate genomic DNA, contributing to worse prognosis and chemotherapy resistance [46, 66]. A3H is cytoplasmic and nucleolar without significant nuclear localization due to its tight binding with RNA [34, 61–63, 67]. A3C has different reported localization patterns, either whole cell or cytoplasmic, which likely depends on cell type [61–63, 68]. The other A3s (A3D, A3F, and A3G) have a strictly cytoplasmic distribution [61–63]. The combination of cell- and tissue-specific expression patterns and physiologic subcellular A3 localization is likely to dictate the restrictive capacities of each APOBEC3 enzyme against viral infections.

1.3 APOBEC Counteraction by Retroviruses

APOBEC3G[2] was the first A3 family member found to be involved in antiviral innate immunity with the capacity to inhibit the replication of HIV-1 lacking the viral accessory protein Vif [15, 16]. In the absence of HIV-1 Vif, A3G is packaged into budding virions in an HIV-infected cell through interactions with HIV-1

[2] In 2002, Sheehy A., *et al.* identified the cellular gene *CEM15* by using a cDNA subtractive analysis between two cell lines, CEM, which is not permissive to HIV-1Δ*Vif* infection and a derivative, CEM-SS, which is permissive [15]. CEM15 was observed share homology to APOBEC1 and it was speculated that RNA editing activity may be involved in HIV-1 restriction. CEM15/APOBEC3G was independently shown to be a DNA deaminase [69] and soon after, found to inhibit retrovirus infection by DNA deamination [16, 71, 72].

Table 1.1: *APOBEC3* expression patterns and trinucleotide context preference. C denotes the deaminated cytosine.

Enzyme	Physiologic Localization[α]	Expression[β]	Activity[γ]	Additional References
A3A	Cytoplasmic[1]	Monocytes, Macrophages	5'-TCW[†]	[33, 64]
A3B	Nuclear	B, Epithelial cells[2]	5'-TCW	[30, 37, 46, 65]
A3C	Whole Cell	Most cell types	5'-TCA	[45, 68, 69]
A3D	Cytoplasmic	T cells, PBMCs	5'-TCA	[]
A3F	Cytoplasmic	T cells, PBMCs	5'-TCA	[70]
A3G	Cytoplasmic	T cells, PBMCs	5'-CCC	[16, 69–72]
A3H	Cytoplasmic Nucleolar	T cells, PBMCs	5'-TCW	[34, 67]
A1	Cytoplasmic Nuclear[3]	Hepatocytes	5'-CAA[4]	[69, 73–75]
AID	Cytplasmic Nuclear[5]	B cells	5'-WRC[‡]	[73, 74, 76, 77]

[α] [61–63, 78]
[β] [43, 44, 78–81]
[γ] [33–35, 46]
[1] A3A can also be cell-wide or predominantly nuclear in overexpressed systems.
[2] A naturally occurring *A3A/B* deletion polymorphism generates functional deletion of A3B [47].
[3] A1 shuttles between nucleus for RNA editing and cytoplasm as an inactive complex with A1CF [73–75].
[4] On RNA.
[5] AID is active in the nucleus for editing of immunoglobuin locus and retained in the cytoplasm with cellular factors [73, 74, 77].
[†] W refers to either A or T nucleotides.
[‡] R refers to either A or G nucleotides.

Gag and RNA [82, 83]. Upon infection of a subsequent target cell, A3G mediates hypermutation of viral complementary DNA (cDNA) after the first round of reverse transcription [2, 84–86]. The mechanism of HIV-1 restriction by A3C, A3D, A3F, and A3H is similar with exception of different di/tri-nucleotide context preferences [45, 78, 84] (A3G prefers 5'-CC while others prefer 5'-TC, **Table 1.1**). Here, both expression and cytoplasmic localization are required for effective HIV-1 restriction. In contrast, the nuclear A3B enzyme is not restrictive against HIV-1Δ*Vif* in T cells [78,

87]. However, experiments utilizing cytoplasmic A3G/B chimeras (A3G N-terminal domain with A3B C-terminal domain) or cytoplasmic A3B point mutants (Y18S, D19Y, E22Y, E24R) led to gain-of-function restriction activity against HIV-1 in 5'-TC contexts, suggesting that localization imparts some specificity for restriction [87].

To overcome A3-mediated restriction, HIV-1 encodes the accessory protein, Vif, which interacts with cellular co-factor CBF-β and members of a cullin-RING E3 ubiquitin ligase complex (comprised of CUL5, ELOB, ELOC, and RBX2) to coordinate the ubiquitination and degradation of A3C, A3D, A3F, A3G, and A3H [81, 88, 89] (**Figure 1.4**). The interaction with CBF-β is essential for Vif-mediated degradation of A3s. This requirement was initially unexpected because CBF-β normally functions as a co-factor for the family of runt-related transcription factors (RUNX) to regulate B and T cell lineage differentiation [90]. Disruption of CBF-β-RUNX1 interactions by HIV-1 Vif leads to down-regulation of RUNX1-driven genes, which includes *APOBEC3* genes [81]. Additionally, the formation of Vif-CBF-β-E3 ligase complexes leads to degradation of A3s at the protein level [81, 88, 89]. Thus, recruitment of CBF-β by Vif gives rise to the A3 counteraction at both transcriptional and post-translational levels.

Other viruses in the *Retroviridae* also have mechanisms of APOBEC3 evasion. For example, foamy viruses (FV) from the *Spumaretrovirinae* subfamily encode a protein with no homology with lentiviral Vif called Bet, which directly antagonizes A3 activity [20, 91]. However, it utilizes a distinct mechanism for counteraction that does not rely on host E3 ubiquitin ligases for degradation. Instead, interactions between FV Bet and A3G lead to the formation of a stable Bet-A3G complex that prevents A3G from incorporating into virions [92]. The mechanism of counteraction for the other human A3s has not been well defined, but presumably functions in a similar manner.

HTLV-1 nucleocapsid (NC) also functions in A3 evasion by yet another mechanism [93]. Here, a unique 20 amino acid C-terminal extension of NC is responsible for excluding the incorporation of A3G into particles [93]. Additionally, this portion of the nucleocapsid does not affect RNA incorporation suggesting a specific function for blocking A3G binding to RNA.

Counteraction of A3 proteins is not limited to viruses that infect humans either. The mouse mamary tumor virus (MMTV) can evade restriction by both mouse and human APOBEC3 enzymes. This virus packages mouse A3 and human A3G similar to HIV-1ΔVif, but encodes a reverse transcriptase (RT) that is more processive, resulting in faster kinetics of DNA polymerization during reverse transcription [94]. This decreases the overall time in which DNA remains single-stranded. Thus, despite packaging similar amounts of A3 into viral particles, these A3 molecules cause fewer overall mutations because of insufficient time to access viral genomes before reverse transcription finishes [94].

The last example discussed here focuses on endogenous retroelements which consist of long terminal repeat (LTR) and non-LTR-based retroelements, both of which are susceptible to A3-mediated deamination during reverse transcription [24, 25, 95]. A3F and A3G have been shown to inhibit the retrotransposition of LTR-based endogenous retroviruses (ERV) such as MusD elements and also leave signatures of G-to-A (complement of C-to-T) mutations in integrated regions of the human genome [24, 96]. Non-LTR-based retroelements like long and short interspersed nuclear elements (LINE, SINE) are susceptible to deamination by all A3 enzymes [25, 97]. Because retroelements are relatively simple in structure, they do not encode any known viral antagonists against APOBEC enzymes. As such, expansion of the *A3* locus has also been associated with gradual decline of LINE-1 (L1) activity and

diseases associated with L1 transposition [95]. For example, mice possess 50-60 times the number of active L1 elements which are associated with 35-fold more L1-associated diseases than in humans [98]. These data suggest that inhibition of retroelements may be one of the primary ancestral functions of A3 enzymes [97].

1.4 APOBEC Restriction of DNA Viruses

Most APOBEC3 research to date has focused on the restriction and counteraction of HIV-1 and related retroviruses due to its initial discovery as an HIV-1 inhibitor and the clinical significance of the AIDS pandemic [15, 16, 69]. However, A3-mediated restriction is not limited to retroviruses. Hepadnaviruses such as hepatitis B virus are DNA viruses with a virus-encoded polymerase that has reverse transcriptase activity. HBV RT acts upon an obligate pre-genomic RNA intermediate to generate a partially double-stranded, relaxed closed DNA genome (rcDNA) [99]. Upon infection of a cell, the rcDNA genome is converted to a covalently closed circular DNA genome (cccDNA) where it functions as a nuclear minichromosome [100, 101]. Persistence of HBV cccDNA provides the template for new virions and is likely the reservoir for chronic HBV infection [101]. A subset of A3 proteins (A3A, A3B, A3F, A3G) has been shown to edit HBV genomes [21, 22]. Upon interferon-α stimulation, A3A and A3B are upregulated and this induction was shown to clear HBV cccDNA in primary hepatocytes [22]. The mechanism underlying HBV cccDNA clearance is currently unclear and, surprisingly, there is no known HBV counteraction factor against A3A and A3B. Recently, HBV X protein (HBx) was found to decrease levels of A3G by increasing exosome-mediated secretion of A3G (**Figure 1.4**); however, this was only demonstrated with transfected and not endogenous A3G [102]. Whether

or not a HBx represents a physiological barrier to APOBEC3-mediated restriction remains to be established.

The dsDNA papillomavirus family, which includes several oncogenic human papillomaviruses (HPV), is also susceptible to A3-mediated deamination. Interestingly, the HPV E6 and E7 oncoproteins upregulate *A3B* expression by binding to a region in the A3B promoter normally occupied by TEAD family of transcription factors [26, 103]. This upregulation leads to detectable C-to-T mutations of HPV genomes *in vitro* in keratinocytes and *in vivo* in plantar warts and precancerous cervical biopsies [27, 104]. In a similar mechanism, HPV E7 mediates A3A stabilization and upregulation leading to A3A-mediated restriction [105, 106]. It has been proposed that upregulation of A3A and A3B in the context of HPV infection provides some proviral advantage, such as increasing the chance of HPV genome integration and immune escape [107] or providing a basis for cellular mutagenesis and oncogenesis [38, 46]. Whatever the reason, *A3* upregulation is not without consequence as HPV genomes are marked with patterns of 5'-TC depletion and 5'-TT enrichment suggestive of A3A/B mutagenesis pressure over evolutionary time [108, 109].

The related family of polyomaviruses, which includes BK and JC polyomaviruses (BKPyV, JCPyV), the causative agents of BK-associated nephropathy and JC-induced progressive multifocal leukoencephalopathy [110, 111], also mediates *A3B* upregulation [29]. The polyomavirus T antigen inhibits the tumor suppressor protein RB and this action disrupts normal interactions between RB and the E2F family of transcription factors [29, 112]. This then derepresses the E2F transcription factors, which function to induce *A3B* expression [29, 112]. Clinically, this results in A3B-mediated deamination of viral genomes and studies of intra-patient BKPyV evolution

show that mutagenesis is a highly dynamic process [28]. A3B-specific mutagenesis is directly associated with polyomavirus VP1 mutations, which confers resistance to antibody-mediated neutralization as well as modify receptor glycans which could potentially alter cell tropisms [28]. This story mirrors HPV-mediated upregulation of A3A/B and suggests that mutagenesis can be harnessed for accelerated viral evolution and immune evasion.

Covered here are only a few classes of viruses; however, any virus that replicates with a DNA intermediate should theoretically be susceptible to A3-mediated restriction. The lack of detection in other viruses could be due to a number of reasons. First, successful evasion of A3 enzymes in the presence of a viral counteraction factor would clearly result in little to no A3 deamination. In this scenario, only prior knowledge of the counteraction factor and its deletion or inhibition would result in a defect in virus replication. From the known examples of APOBEC3 counteraction/evasion, there is no homology between any protein and the mechanisms of overcoming A3 enzymes all differ (HIV-1 Vif, HTLV-1 NC, FV Bet, HBV HBx, **Figure 1.4**). This increases the difficulty of homology-based structure-function predictions. We can sometimes infer A3 deamination if the counterdefense is not perfect by using bioinformatic analyses of 5'-TC depletion and 5'-TT enrichment (or 5'-CC depletion/5'-CT enrichment for A3G); however such inferences require confirmation studies *in vitro* and *in vivo*.

Second, physical separation of ssDNA from APOBEC3 enzymes could prevent access to viral DNA especially during replication. Several families of large DNA viruses like poxviruses utilize nucleocytoplasmic replication centers that reorganize microtubules and cellular structures for virus-specific mRNA expression, DNA replication, and protein synthesis [113]. For example, the prototype poxvirus,

vaccinia virus, reorganizes host rough endoplasmic reticulum (ER) to form mini-nuclei adjacent to the host nucleus for virus-specific replication [114]. It is unknown whether or not APOBEC3 enzymes have access to these replication centers, but physical exclusion would prohibit deamination of these viral genomes and early studies suggest that A3s have no impact on poxvirus replication [115]. All other human pathogenic DNA viruses (papillomavirus, polyomavirus, parvovirus, adenovirus, herpesvirus) replicate in the nucleus. Without known counteraction factors or mechanisms to evade A3 restriction, these viruses should be vulnerable to nuclear A3-mediated deamination.

The thesis work presented here aims to shed light on the mechanism of APOBEC restriction of the *Herpesviridae* family and A3 counteraction mediated by the large subunit of the virally-encoded ribonucleotide reductase.

1.5 *Herpesviridae*

Herpesviruses are large double-stranded DNA viruses with linear viral genomes ranging between 120 to 240 kilobasepairs which encode for about 140 to 250 open reading frames [116]. Structurally, herpesviruses are about 100-200 nm in size with an internal a genomic core that is enclosed by an ordered icosohedral capsid [116, 117]. Surrounding the capsid is a layer of proteinaceous tegument comprised of RNAs and viral proteins required for initial steps of genome replication after entry [116, 118, 119]. Lastly, a lipid bilayer envelope surrounds the tegument and it is interspersed with viral glycoproteins that mediate virus attachment to cell surface receptors and entry into the cell [116, 119] (**Figure 1.5**).

A defining characteristic of herpesviruses is their ability to establish latency inside host cells and reactivate to a lytic cycle to produce virions for new infections [116, 117]. Although the exact molecular mechanisms governing latency and lytic infection differ between viruses (due to differences in protein expression, transcriptional regulation, microRNAs, etc.), a few general principles remain constant [116, 117]. First, upon infection of a new cell, the viral linear dsDNA genome must enter the nucleus, circularize, and form a stable extrachromosomal episome which undergoes DNA methylation, histone modification, and chromatinization [116, 117, 120] (**Figure 1.5**). These modifications aid in disguising the viral genome as cellular DNA [121] and also help regulate viral gene expression to repress lytic genes while maintaining expression of essential latent genes [122, 123]. Replication of viral episomes requires both viral factors (*e.g.*, EBV EBNA1 for recognition of its origin of replication, *oriP*) and host DNA replication machinery (*e.g.*, origin recognition and minichromosome maintenance complexes) [116, 124]. Stable maintenance of the episome is essential for latency and requires both competent replication of the minichromosome as well as segregation into daughter cells during cell division.

After establishing latency, only a few viral proteins and RNAs are produced [116, 119, 124]. While there are no known pathological consequences of α- or β-herpesvirus latent infection, γ-herpesvirus latency is associated with a number of diseases including cancer due to viral manipulation of cellular processes [117, 125]. For example, EBV expresses seven proteins (two latent membrane proteins, LMP, and five EBV-encoded nuclear antigens, EBNA) and two classes of RNAs (EBV-encoded small RNA, EBER, and microRNAs transcribed from BART and BHRF1 genes) during latency [124]. These proteins and microRNAs have a variety of functions including regulation of viral replication, interference of cell signaling pathways, and

inhibition of apoptosis, which can result in cell immortalization and oncogenesis [126–129].

The latent phase of the virus life cycle is defined by persistence within a cell with limited or no viral activity, but retaining the ability to reactivate full gene expression and produce infectious virions [130]. Sporadically, all herpesviruses have the ability to undergo a switch in modes of replication from latency to lytic phase [116, 117, 119] (**Figure 1.6**). The molecular mechanisms that govern this switch are not well understood, but environmental triggers such as stress, immunosuppression, and UV damage are associated with increased risk of herpesvirus reactivation [116, 117, 120, 131]. In contrast to latency, the lytic phase is characterized by regulated gene expression leading to accumulation of virus-encoded proteins required for genomic DNA replication and progeny virion assembly and release. Virus replication occurs in the cell nucleus and then requires capsid assembly around the nuclear membrane, egress to the surface of the cell, and maturation for production of infectious enveloped virions [116, 119, 132, 133]. Of the approximately 40 proteins with conserved functions across human herpesviruses, nearly all of them are involved in DNA replication and nucleotide metabolism, reinforcing the importance of these proteins (*e.g.*, viral DNA polymerase, ATPase, dUTPase, UDG, and RNR large subunit) [116].

On the other hand, viral proteins involved in immune evasion often differ structurally between herpesvirus subfamilies and species, but share commonalities in function. For example, the NF-κB signalling pathway has numerous cellular effects including cytokine secretion, cell proliferation, and inhibition of apoptosis [134, 135]. Regulation of this pathway can have different effects depending on the cell type or stage in viral replication. Activation of the NF-κB pathway can be achieved by several heterologous viral proteins including HSV-1 $\gamma_1$34.5 [136], HCMV pTRS1 and IRS1

[137], EBV dUTPase (BLLF3) [138], and KSHV vGPCR [139]. A separate subset of viral proteins functions in differential modulation or inactivation of the NF-κB pathway with numerous downstream targets [116, 134].

Herpesviruses often also have multiple overlapping factors that target distinct pathways that converge on essential cellular functions. Anti-apoptotic phenotypes can be achieved through modulation of the NF-κB pathway. However, inhibition of apoptosis is also (in)directly mediated by HSV-1 ICP6 (RNR large subunit), U_S3 protein kinase, glycoproteins gD and gJ, HCMV viral mitochondrial localized inhibitor of apoptosis (vMIA) and viral inhibitor of caspase 8 activation (vICA), EBV BHRF1 and BNLF1, KSHV ORF16, ORF13, K7, and K9 [116, 140–142]. The abundance of viral proteins with convergent functions demonstrates the importance of targeting programmed cell death as a way to overcome this aspect of immunity. There are many other examples of viral immune evasion like disruption of interferon signaling and interferon responsive genes [143], overcoming the TRIM family of restriction factors [144], and circumventing adaptive immune responses [116]. As previously discussed, an important arm of the innate immune response is the APOBEC3 family of enzymes, which poses a threat to the genomic integrity of several retroviruses and dsDNA viruses. It was not previously known if and how herpesviruses evaded these proteins. The studies here focus on understanding the mechanism by which human herpesviruses overcome innate immunity mediated by human A3 enzymes.

The nine herpesviruses known to infect humans can be classified into three subfamilies: α, β, and γ-herpesvirus (**Figure 1.7**). The α-herpesviruses include herpes simplex virus type 1/2 (HSV-1/2) and varicella zoster virus (VZV), β-herpesviruses include human cytomegalovirus (HCMV), human herpesvirus 6A/B (HHV6A/B), human herpesvirus 7 (HHV7), and γ-herpesviruses include Epstein-Barr

virus (EBV) and Kaposi's sarcoma-associated herpesvirus (KSHV) [145]. Each of these human herpesviruses are associated with a wide array of clinical manifestations and diseases. Highlighted in three next subsections are HSV-1, HCMV, and EBV as representative viruses from each subfamily.

1.5.1 Herpes Simplex Virus Type 1

The prototypic α-herpesvirus is HSV-1 with the other two family members being the closely related, HSV-2, and varicella zoster virus, which causes chickenpox and shingles [116]. The worldwide seroprevalence of HSV-1 is approximately 67% with higher prevalence rates in less developed nations (*e.g.*, 87% in Africa versus 49% in the Americas) and older age (*e.g.*, 27% seroprevalence under the age of 5, 57% under the age of 10, and 66% by age of 15) [146]. Primary infection usually occurs through transfer of saliva and clinically manifests as gingivostomatitis, or oral herpes, which leads to vesicular oral lesions, sore throat, and fever [116, 147]. Transmission can also occur sexually giving rise to genital herpes, which produces a range of symptoms including genital ulcers, lymphadenopathy, and fevers [116, 147].

Because the targets of HSV-1 infection are epithelial cells and neurons, primary infection can occur nearly anywhere on the skin [116, 119, 147]. For example, herpetic whitlow, or infection of the fingers, can occur from biting one's fingers or in dental professionals who commonly come in contact with oral herpes lesions [148]. Infection of ocular epithelium can cause HSV-1 keratoconjunctivitis and is one of the leading infectious causes of blindness [149]. In immunocompromised individuals, spread of the virus can lead to esophagitis, pneumonitis, hepatitis, and encephalitis [150–153]. Neonatal HSV-1 is also frequently transmitted mother-to-child during delivery and

a small proportion occurs *in utero* (congenital HSV-1 infection), which can result in skin and eye infections, microcephaly and other CNS abnormalities, or disseminated infection [154].

Productive lytic infection of epithelial cells produces new virions for secondary infection of innervating sensory neurons. Here, the viral capsid migrates retrograde along the axon to the dorsal root ganglia where it establishes latency [116, 119, 147]. Because neurons do not divide, HSV-1 also does not replicate during latency. The HSV-1 genome is heavily silenced by nucleosomes [155] and the only region of the genome that is active encodes the latency-associated transcripts (LAT) [156]. The major LAT is approximately 2 kb in length, which can produce two proteins that partially function in reactivation into lytic cycle [157]. The less stable minor LAT pre-RNA has also been implicated in reactivation, which requires the first 1.5 kb of this transcript [158]. However, the precise mechanism or trigger for reactivation or persistence of latency is not well defined [116].

Antiviral therapy can be used for treatment or prevention of herpesvirus reactivation. Currently, there are FDA-approved antivirals including acyclovir [159] (and its produg valaciclovir [160]), penciclovir (and its prodrug, famciclovir) [161], ganciclovir [162] (and its prodrug valganciclovir [163]), cidofovir [164], and foscarnet [165]. The drugs listed here have partial inhibition of all herpesviruses due to homology in the viral thymidine kinase or DNA polymerase. The first three are first-line nucleoside analogues (*e.g.*, acyclovir is a deoxyguanosine analogue), which are selectively monophosphorylated by the viral thymidine kinase. Downstream processing results in drug triphosphates, which inhibit the viral DNA polymerase and subsequent viral DNA synthesis. Acyclovir is most active against HSV-1 and EBV while ganciclovir most active against CMV. These two drugs are both orally

bioavailable while penciclovir is used topically for treatment of HSV-1 skin lesions. Cidofovir is administered intravenously as a TK-independent nucleotide analogue that selectively inhibits the viral DNA polymerase with highest activity against CMV. Foscarnet is the only drug that is not a nucleoside or nucleotide analogue. It is administered intravenously and selectively inhibits viral DNA polymerases by preventing the cleaveage of trinucleotides. It inhibits all herpesviruses as well as HIV-1.

1.5.2 Human Cytomegalovirus

There are four human β-herpesviruses including HCMV, HHV6A, HHV6B (previously recognized as one species), and HHV7 [145]. Of these, HCMV is the best studied virus of the β-herpesviruses family and clinically important for its role in numerous diseases occurring throughout life including CMV mononucleosis and post-transplantation associated diseases [166]. Similar to HSV-1, seroprevalence of CMV increases with age (*e.g.*, in the U.S., seroprevalence is 36% under age of 12, 49% under the age of 30, and increases to 91% above the age of 80 [167]. It is also the only herpesvirus capable of routinely crossing the maternal-placental barrier and causing congenital herpesvirus infections [168]. Thus, epidemiological surveillance for CMV starts during pregnancy.

Primary infection of previously CMV-negative mothers poses the greatest risk for maternal to fetal transmission (34% risk of transmission) whereas the rate of transmission during reactivation is much lower (1.4%) [169]. *In utero* infection can result in miscarriage or a number of birth defects, most commonly neurologic malformations like periventricular calcifications [170]. CMV transmission rates are high during the early postnatal period with various transmission routes such as vaginal

secretions, blood, saliva, urine, and breast milk [171]. However, postnatal infection is often asymptomatic or with mild symptoms like fever, vomiting, and diarrhea which typically resolve without intervention. In immunocompetent hosts, primary infection after infancy is also asymptomatic, but can sometimes cause CMV mononucleosis which is associated with fever, fatigue, lymphocytosis, and lymphadenopathy [172]. In immunosuppressed patients, disseminated infection can occur and spread to most organs such as liver, gastrointestinal tract, lungs, retina, and central nervous system [147].

Unlike HSV-1, which typically only infects epithelial cells and neurons, CMV can infect a wide range of cell types including epithelial cells, fibroblasts, smooth muscle cells [173], endothelial cells [174], dendritic cells [175], and other leukocytes including neutrophils and monocytes [176, 177]. These differences in tropism are likely due to interstrain variation as clinical isolates often have mutations or deletions in a number of glycoprotein-encoding genes [178, 179]. Although CMV has a wide cell tropism, the efficiency of replication is not equal in all cell types. For example, infection of neutrophils is abortive and does not produce new virions [180], but phagocytosed viruses can still be transmitted to other cell types using cell-to-cell spread [181]. Infection of trophoblasts, which is required for maternal-to-fetal transmission, is also inefficient and produces about 3 log lower levels of virus titers than infection in fibroblasts [182]. Thus, variations in glycoprotein genes contribute to cell tropism, while differences in cellular or viral factors affect the capacity or efficiency of virus replication.

Although lytic infection occurs in a variety of cell types, it is believed that latent CMV resides in myeloid lineage cells with several studies implicating $CD14^+$ monocytes and monocyte-derived macrophages (MDM) [183, 184]. However, because

these cells are short lived, it is likely that a progenitor cell type, such as $CD34^+$ hematopoietic stem cells (HSC) or $CD33^+$ granulocyte-macrophage progenitors (GM-P), are the source of CMV latency [183–185]. Importantly, latent virus in these cell types can be reactivated to produce new virions by either allogeneic stimulation or differentiation to dendritic cells [185]. The main site of replication for CMV persistence, however, is not the same as the latent cell reservoir. Instead, endothelial cells are able to foster CMV replication with minimal cytopathic changes to the cellular structure and are routinely cultured from *ex vivo* samples [186, 187]. Together, endothelial and myeloid lineage cells contribute to CMV persistence and latency which allow for lifelong infection while lytic infection in other cell types leads to significant clinical diseases.

1.5.3 Epstein-Barr Virus

Epstein-Barr virus and Kaposi's sarcoma-associated herpesvirus belong to the γ-HV subfamily and are associated with diseases during both lytic and latent infection. EBV is extremely common and seroprevalence reaches almost 90% by the second decade of life in the United States [188]. Transmission normally occurs during early stages of life via saliva, such as sharing of food or utensils. Primary infection occurs in oral epithelial cells and then secondary infection becomes established in B cells [189]. It can also be transmitted through blood transfusions, solid organ or bone marrow transplantation, and sexual contact [190].

If primary infection occurs during childhood, it is usually asymptomatic, but if it occurs during adolescence or adulthood, primary infection can cause infectious mononucleosis (IM) [191]. The clinical syndrome of IM typically consists of fever,

malaise, pharyngitis, and cervical lymphadenopathy, but can also involved other organs leading to hepatitis, splenomegaly, rash, and nausea and vomiting [192]. These symptoms are also associated with acute lymphocytosis (>4500 cells/μL) due to the rapid expansion of EBV-specific $CD8^+$ cytotoxic T cells [193]. Natural killer (NK) cells and monocytes also contribute the control and spread of EBV infection [194]. Most symptoms and laboratory abnormalities resolve within a month, but fatigue and lymphadenopathy can persist for several months [195]. Rarely, acute complications of IM can occur which include splenic rupture, Guilllain-Barré syndrome, asplastic anemia, myo/pericarditis, and others [196].

A chronic form of IM has also been described called chronic active EBV infection (CAEBV) where EBV replication is uncontrolled owing to a lack of EBV-specific immune cells. The only effective treatment is HSC transplantation and, if left untreated, it eventually leads to progressive immunodeficiency, EBV-positive lymphoma, or multi-organ failure [197, 198]. Interestingly, there are geographic differences in CAEBV phenotypes. EBV normally infects B cells and in white or African American patients in the United States, most cases of CAEBV are associated with EBV replication in B cells and subsequent B cell depletion with hypogammaglobulinemia [199]. CAEBV is more frequent in eastern Asia (Japan, Taiwan, Korea) and in contrast to CAEBV cases in the United States, EBV predominantly infects T (60% of cases) and NK (40%) cells as opposed to B cells [200, 201]. A similar pattern of T and NK cell infection is observed in native Americans from Mexico or Central America [202]. It is unclear what underlying factors mediate these differences in EBV infection, but differences in genetic factors involved in the immune response have been proposed [198].

EBV and KSHV are also known to cause latency-associated diseases, most notably

several different cancers. For example, EBV is present in almost all cases of endemic Burkitt's lymphoma from which EBV was first isolated in 1964 [203] and is strongly influenced by malarial co-infection [204]. Outside of malarial regions, EBV is only partially associated with Burkitt's lymphoma and most AIDS-related Burkitt's lymphoma are not EBV-associated [205]. Additionally, a significant proportion of Hodgkin's lymphomas and extranodal NK- and T-cell lymphomas are EBV-associated, and these cancers have similar patterns of EBV latent gene expression suggesting similar mechanisms of EBV-driven pathogenesis [206, 207]. Other cancers are more frequently observed during immunosuppression such as post-transplant lymphoproliferative disease (PTLD) [208], AIDS-related brain lymphoma [209], and non-Hodgkin's lymphoma [210].

Epithelial cancers are also associated with EBV infection, such as gastric and nasopharyngeal carcinoma (NPC). About 10-15% of gastric carcinomas (GC) are EBV-related and because the global incidence of this cancer type is relatively high, it is one of the most common cancers associated with EBV [116]. NPC is rare globally ($\sim$1 case per 100,000). It has higher incidence rates in southeastern Asia, northern Africa, indigenous Inuits, and in particular, the Canton region of southern China, with rates approaching 25 per 100,000 [211, 212]. EBV infection is almost universally present in NPCs from these endemic regions while absent in other types of NPCs from other regions of the world [213]. While some environmental factors have been attributed to increased risk of endemic NPC (*e.g.*, N-nitrosamines in traditional Cantonese salted fish [214]), host genetic factors that contribute to increased susceptibility of EBV-related NPC may also be causally involved [215–217].

A major difference in the mechanism of oncogenesis between EBV-associated lymphomas and epithelial cancers is the influence of latent and lytic modes of

replication for these cancers, respectively [116]. Most EBV-associated lymphomas are driven by a few EBV latent proteins that alter programmed cell-death or cell survival (*e.g.*, LMP-1 mediated activation of NK-κB pathway to promote cell growth [218]). Distinct patterns of latent gene expression are correlated with these different types of lymphomas, termed Latency Programs I, IIa, IIb, and III (for detailed reviews, see [116, 124, 219, 220]). On the other hand, the induction of EBV lytic cycle and expression of lytic genes has been shown to important in the pathogenesis of epithelial cancers [221]. In particular mutations in the transcriptional co-activator of lytic cycle, BZLF1/Zta, are associated with viral reactivation and oncogenesis [221–223]. Because EBV-associated epithelial cancers are always monoclonal, these mutations often precede the onset of cancer, likely in combination with environmental and genetic factors [224, 225]. Moreover, viral DNA load prior to treatment is an important prognostic factor with higher levels corresponding to worse outcomes [226, 227].

The diversity in clinical manifestations of EBV-related diseases compared to solely lytic diseases associated with α- and β-herpesviruses is due to differential protein expression patterns during the lytic and latent replication programs [116]. Whereas α- and β-herpesviruses only have origins of replication for lytic gene expression, γ-herpesviruses utilize a unique *oriP* for latent genome replication and two lytic origins (*oriLyt*) for transcription of lytic genes [116]. Maintenance of viral episomes during EBV latency requires expression of EBNA1, which is necessary and sufficient for *oriP*-driven replication [228]. *oriLyt*-dependent lytic replication requires the transcription factor, BZLF1, binding to these origins. BZLF1 is also important for promoting the transcription of other essential replication genes including BMRF1, the DNA polymerase processivity factor [229]. In total, seven proteins (BZLF1, BMRF1,

BALF5, BBLF2, BBLF4, BSLF1, and BBLF 2/3) and *oriLyt* are required for lytic replication [116]. During lytic phase, about 70 of the 80 EBV genes are transcribed for efficient genome replication, virion production, and immune evasion [230, 231]. Of these, an immediate early gene is *BORF2*, which encodes the large subunit of the viral ribonucleotide reductase and was found to be a potent antagonist of APOBEC3B (**Chapter 2**).

1.6 Ribonucleotide Reductases

RIBONUCLEOTIDE reductases reduce the 2'-OH of ribonucleotide di- or triphosphates to deoxyribonucleotide building blocks for DNA synthesis [232–235] (**Figure 1.8**). Nearly all DNA-based forms of life encode or utilize a RNR, which can be classified into three classes I-III based on dependence on oxygen and generation of radical intermediates [234, 235]. Class III RNRs do not require oxygen and are encoded by bacteriophages, archaebacteria, and anaerobic eubacteria. They are most likely the closest to the ancestral RNR since oxygen was scarce on early Earth. Class II RNRs arose next, with no preference for oxygen, as a result of increasing oxygen-producing photosynthetic organisms. Class I RNRs, which can be subdivided into Ia and Ib, have most recent origins and are found in most eukaryotes, aerobic eubacteria, and animal viruses including herpesviruses [234, 235].

Herpesviruses encode Class Ia RNRs which consist of two homodimeric proteins (large subunit, R1/α_2, and small subunit, R2/β_2) forming a heterotetramer ($\alpha_2\beta_2$) [233–235] (**Figure 1.9**). Class Ia R2 is involved in generation of a stable tyrosyl radical using an diferric center that interacts with oxygen to produce a diferric

peroxide (Fe-O-Fe) and a stable tyrosyl radical (Y•) [236] (**Figure 1.10**). The tyrosyl radical is then transferred to a conserved cysteine in R1, forming a thiyl radical (S•). This in turn mediates the reduction of NDP substrates to dNDP in the catalytic R1 pocket using reducing equivalents provided by two additional conserved R1 tyrosine residues (for EBV BORF2, this corresponds to YY725/726) and generating a disulfide bond (Tyr-S=S-Tyr). This bond is broken by exogenous reducing agents such as thioredoxin or glutaredoxin, which recycles R1 for subsequent rounds of reduction.

Apart from ribonucleotide reduction, viral R1s have been noted to have alternative functions. HSV-1 RI, ICP6, (encoded by *UL39*) has been well characterized in having the ability to inhibit FasL-induced apoptosis and initiating necroptosis [237–239]. The related HSV-2 R1, ICP10, has similar functions [239, 240]. Both of these functions are mediated by unique N-terminal extensions that interact directly with caspase-8 to prevent its downstream signalling [237–239]. In β-herpesviruses, R2 is deleted leaving the overall RNR catalytically inactive. However, other functions have been ascribed to CMV R1. In particular, murine CMV (MCMV) R1 has been shown to have similar anti-apoptotic properties encode on its N-terminal domain [241, 242]. Interestingly, HCMV R1, UL45, only has partial ability to inhibit Fas-induced apoptosis, but has the ability to inhibit NF-κB signalling by targeting RIP1 [243, 244].

In contrast to α- and β-HVs with alternative R1 functions, there was previously no attributed alternative function to γ-HV R1 proteins, EBV BORF2 and KSHV ORF61. To our knowledge, no studies have specifically examined the function of KSHV ORF61. One prior study showed that EBV BORF2 failed to interact with caspase-8 and had no effect on apoptosis [238]. Our collaborator, Dr. Lori Frappier at the University of Toronto, was the first to show that EBV BORF2 has at least one alternative function by contributing to G_1/S phase arrest [245]. In this study, a

panel of EBV lytic proteins were transfected into Fucci cells, which are HeLa cells expressing Cdt1 with a red fluorescent marker and geminin with a green fluorescent marker [246]. During G_1, cells express Cdt1 and fluoresce red while cells in $S/G_2/M$ fluoresce green due to geminin expression. Cells that are yellow are at the interface of G_1/S transition. BORF2 expression in these Fucci cells led to a 1.8-fold increase of cells in G_1/S [245]. BORF2 overexpresion was also found to induce p53 and Ser15-phosphorylated p53 levels without any effect on downstream p21 activation [245]. It is currently unclear how EBV BORF2 induces G_1/S arrest.

These observations indicate that, like many viral proteins, herpesvirus R1 proteins are multifunctional and have alternative non-catalytic functions. For HSV-1/2 and HCMV R1, these are mediated by unique N-terminal extensions that have conserved binding domains to cellular factors involved in inhibiting apoptosis and NF-κB signalling. No such N-terminal extensions exist for EBV BORF2 or KSHV ORF61, but these R1 proteins do have unique C-terminal extensions of unknown significance.

1.7 Concluding Introductory Remarks

Following the discovery that EBV BORF2 can mediate G_1/S arrest, the Frappier lab utilized a series of immunoprecipitation-mass spectrometry experiments to identify candidate interacting proteins involved in BORF2-mediated cell cycle arrest. These studies were performed in 293T cells, which have almost undetectable levels of endogenous A3B. Despite this, BORF2-FLAG robustly and reproducibly pulled down cellular A3B as the top candidate interaction protein. This knowledge sparked a robust, ongoing collaboration with the Frappier Lab at the Unviersity of Toronoto. **Chapter 2** details the interaction, mechanism, and significance of the EBV BORF2-A3B and KSHV ORF61-A3B interactions. **Chapter 3** comprehensively analyzes the interactions between HSV-1, HCMV, EBV, and KSHV R1 proteins and all seven human A3 enzymes to show conservation of R1-A3 interactions across *Herpesviridae*. Lastly, I discuss the implications and significance of these discoveries in **Chapter 4** and how the R1-A3 axis may be harnessed for therapeutic benefit. Data from separate projects that contributed to co-author publications are included in **Appendices A**, **B**, and **C**.

1.8 Figures

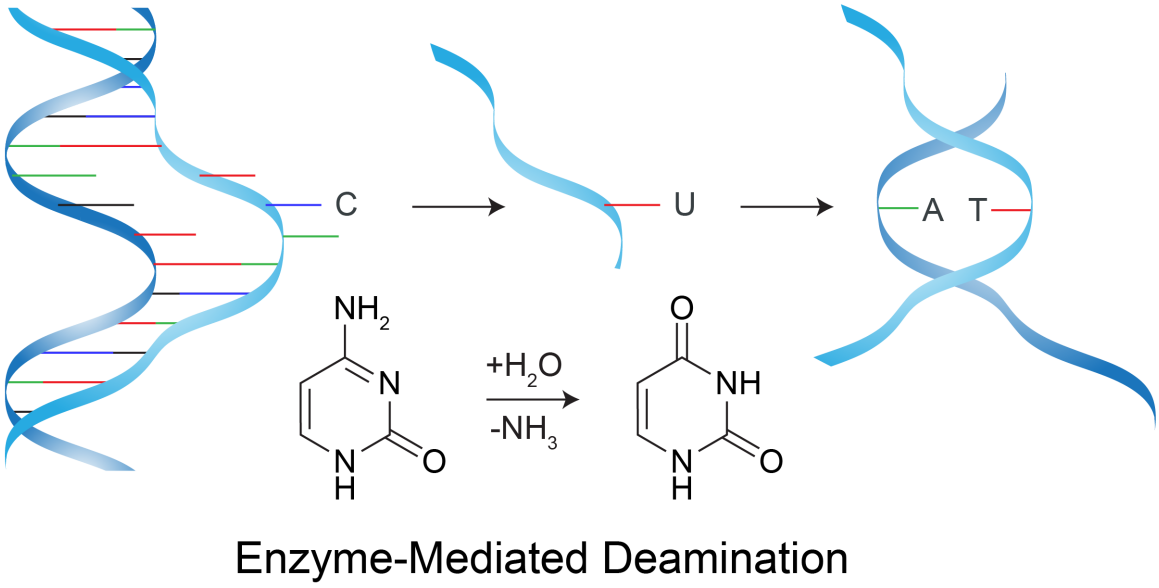

Figure 1.1: Mechanism of APOBEC-mediated deamination.
Schematic depicting an exposed cytosine base in single-stranded DNA, which can be deaminated by APOBECs. Uracil intermediates are replicated over as thymines if left unrepaired leading to overall C-to-T and G-to-A mutations.

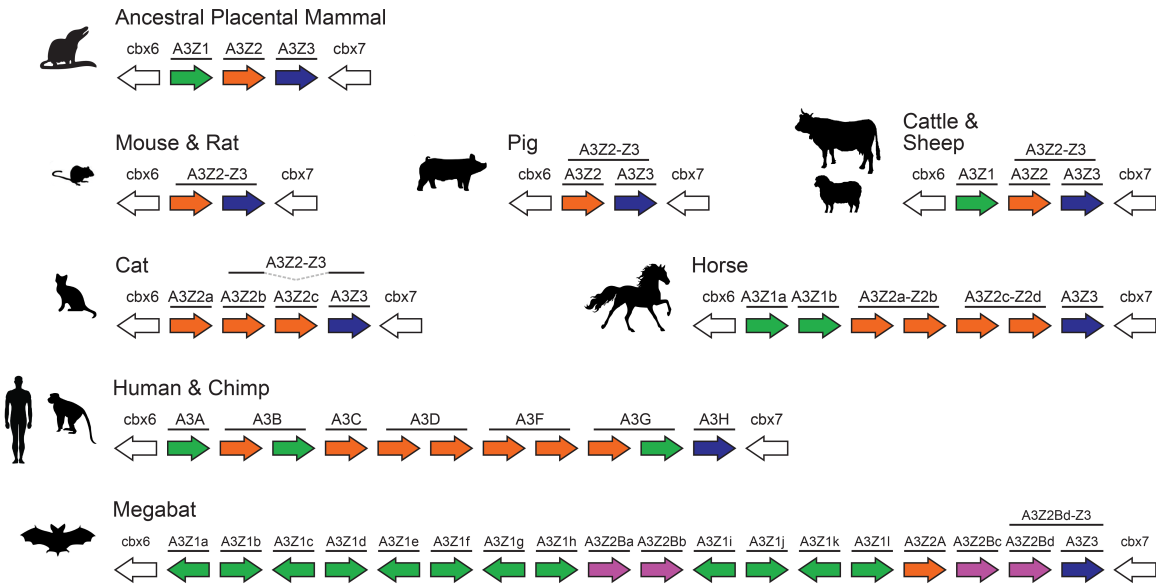

Figure 1.2: Mammalian *APOBEC3* loci.
Schematic showing *A3* loci in humans & chimps, horses, cats, cattle & sheep, pigs, and mice & rats. Green arrows depicted related *Z1* genes, orange arrows depict related *Z2* genes, and blue depicts *Z3* genes. The bat A3 repertoire is expanded to include *Z2b* genes. Names of proteins encoded by each gene are listed above the arrows. Double-domain A3s are depicted by longer lines encompassing two genes.

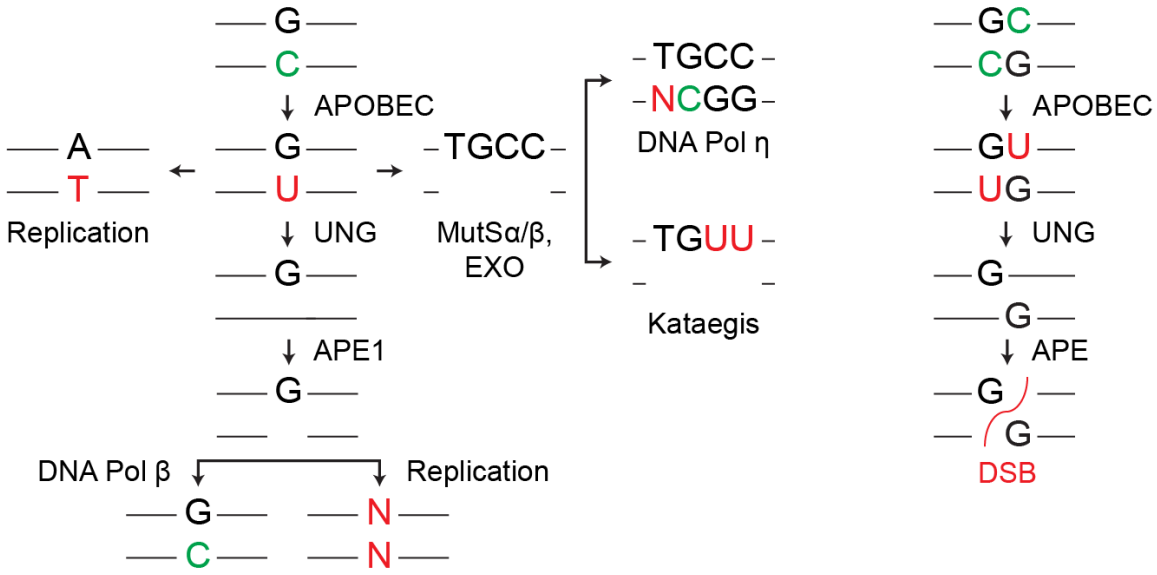

Figure 1.3: Pathways of uracil processing in mammalian cells.
Schematic based on mechanisms of somatic hypermutation and class-switch recombination showing possible outcomes of uracil lesions after APOBEC-mediated deamination [8, 39–42].
Left: uracils can be read over during replication resulting in C-to-T mutations.
Bottom Left: Uracil DNA glycosylase (UNG) can remove uracil bases resulting in an abasic site, which can further be excised by apurinic endonuclease (APE1). The resulting gap can be correctly repaired by DNA polymerase β or replicated over leading to C-to-N mutations.
Center: Uracil bases can also be recognized by mismatch repair machinery including MutSα/MutSβ and exonuclease I (EXO), leading to large stretches of single-stranded DNA. Polymerization by DNA Pol η can lead to mutations at A:T base pairs (on either strand). Exposed ssDNA is also susceptible to further APOBEC-mediated deamination resulting in kataegis.
Right: If adjacent cytosines on opposite strands are mutated to uracils, the resulting downstream processing can result in double-stranded breaks (DSB), which occurs frequently during class-switch recombination. Green letters represent initial cytosine base(s) and correctly repaired outcomes. Red letters represent bases after mutagenic outcomes.

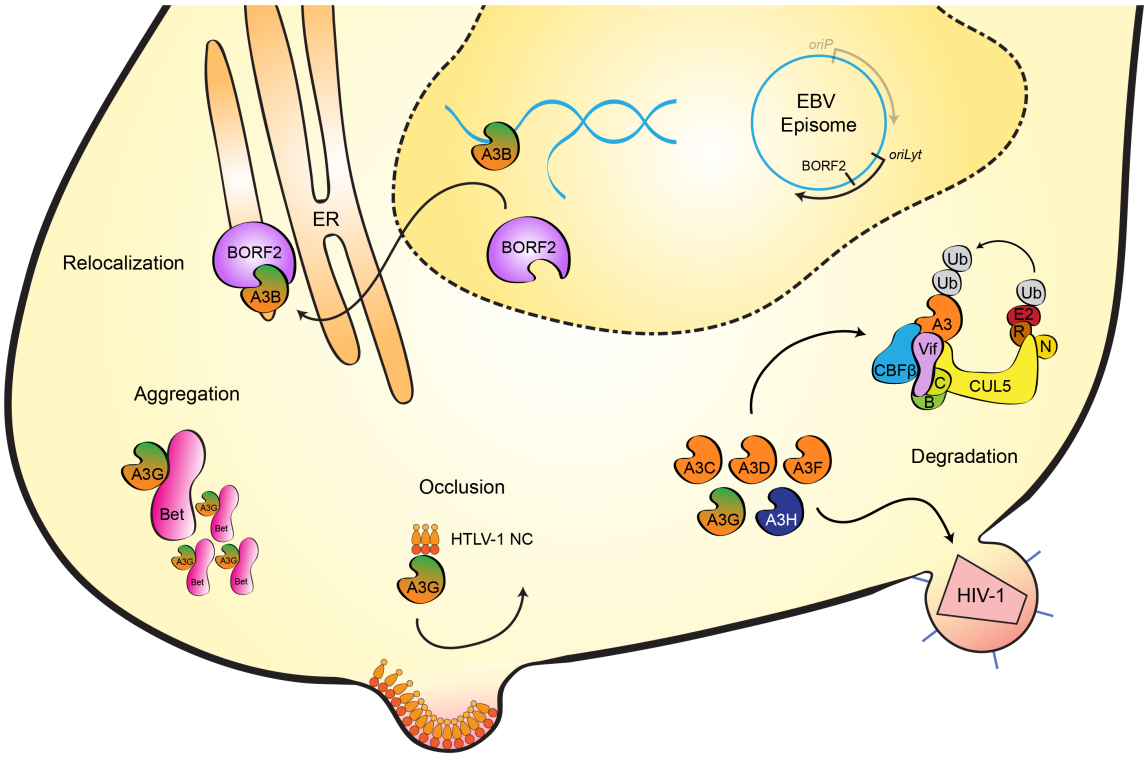

Figure 1.4: Viral counteraction of APOBEC3 enzymes.
Schematic summarizing multiple mechanisms of A3 counteraction by viruses.
Relocalization: Nuclear A3B is counteracted by EBV BORF2, the large subunit of the viral ribonucleotide reductase. BORF2 interacts with A3B directly, inhibits its enzymatic activity, and relocalizes it to cytoplasmic aggregates in the endoplasmic reticulum (ER). In the absence of a counteraction factor, A3B can deaminate EBV genomic DNA.
Aggregation: Foamy virus Bet protein can interact with cellular A3G and prevent its incorporation into budding virions. It also decreases A3G solubility and forms cytoplasmic aggregates.
Occlusion: HTLV-1 nucleocaspid (NC) can also interact with A3G to prevent packaging into HTLV-1 particles. A unique C-terminal extension is capable of inhibiting A3G without affecting RNA binding capacity.
Degradation: Five restrictive APOBEC3 enzymes (A3C, A3D, A3F, A3G, and A3H) are targeted by HIV-1 Vif for degradation by hijacking a host E3 ubiquitin ligase complex comprised of CBF-β, CUL5, ELOB (B), ELOC (C), RBX (R), NEDD8 (N), and E2 ligase which transfers ubiquitin molecules (Ub) to A3s. In the absence of Vif, these A3s can package into particles and deaminate HIV-1 genomes after the first round of reverse transcription in the target cell.

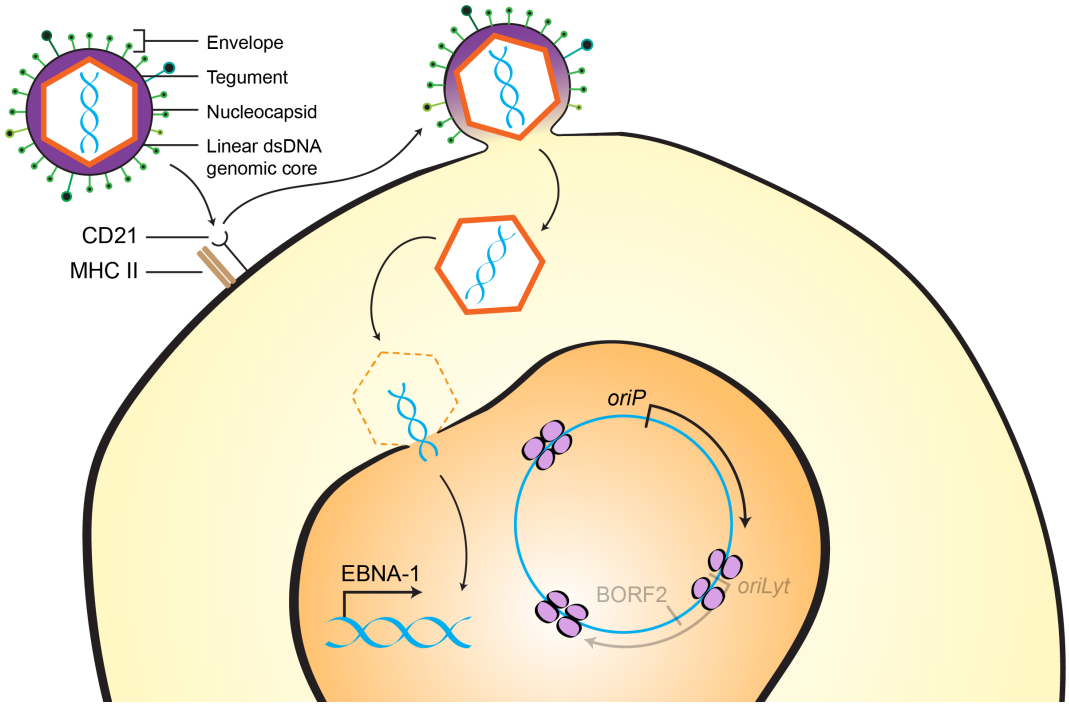

Figure 1.5: Herpesvirus structure and entry.
Schematic depicting the structure of a representative herpesvirus particle, which is composed of an inner genomic core with linear double-stranded DNA (blue). This is surrounded by an icosohedral nucleocapsid lattice (orange) followed by a proteinaceous tegument (purple). The outermost envelope layer is composed of a lipid bilayer and studded with various viral glycoproteins (green) necessary for attachment and entry of host cells. Entry occurs through interactions between viral glycoproteins and cell surface receptors such as CD21 and MHC class II using EBV as a representative virus. Fusion with the cell membrane delivers the capsid into the cell, which migrates to the nucleus. After delivery of the linear dsDNA genome to the nucleus, the viral genome circularizes and is maintained as a nuclear episome throughout latency. EBV has a unqiue latency-associated *oriP* that expresses a few proteins and RNAs during latency for maintenance.

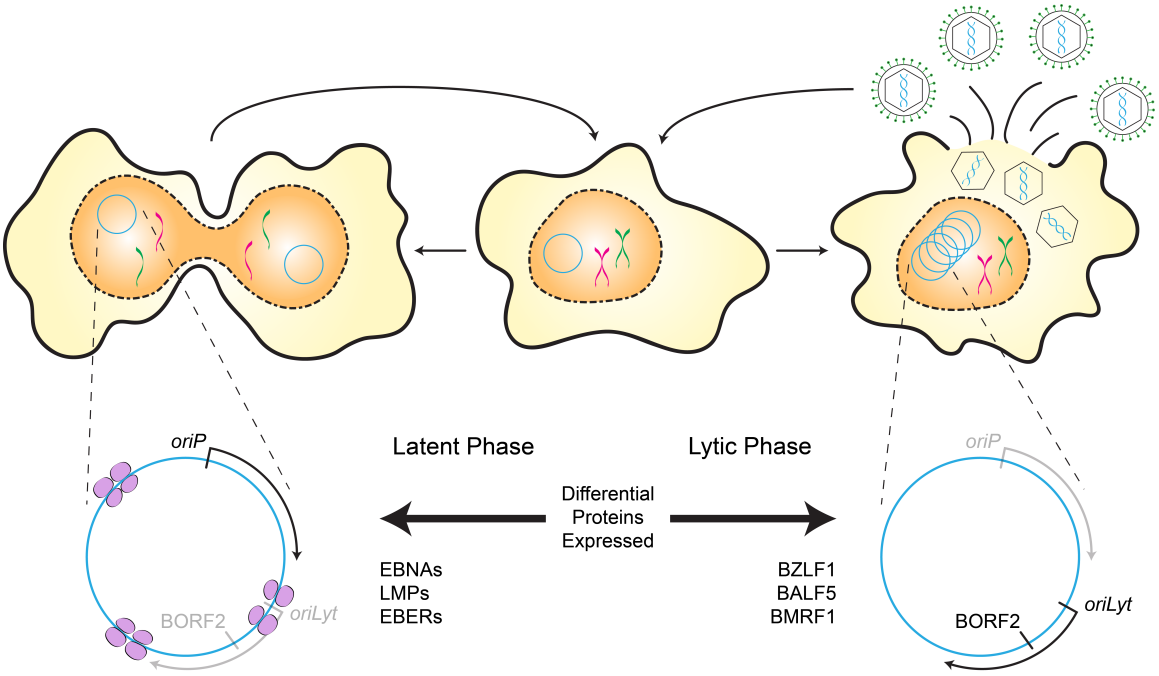

Figure 1.6: Lytic and latent EBV life cycles.
Schematic highlighting the differences between lytic (left) and latent (right) phases of EBV. Latent gene expression leads to production of a few proteins (*e.g.*, EBNAs and LMPs) and RNAs (*e.g.*, EBERs) and driven by *oriP*. Lytic gene expression can occur at one of two *oriLyt* sites (other not shown) and leads to production of about 70 viral proteins, including BORF2. Lytic phase also leads to production of new virions. Note that α- and β-herpesviruses do not have a separate latent origin of replication (*oriP*) and viral gene expression is driven only by lytic origins.

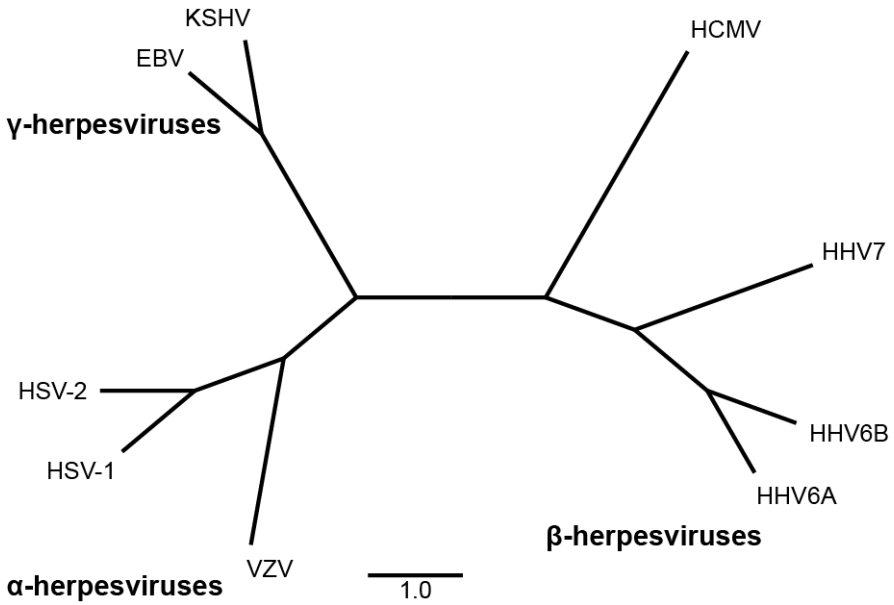

Figure 1.7: Phylogenetic tree of herpesviruses.
Phylogeny based on amino acid sequences of the RNR large subunit from respective viruses. Alignment was performed using Multiple Sequence Comparison by Log Expectation (MUSCLE) and phylogeny was generated as a neighbor-joining tree without corrections. Branches are scaled for equal lengths (scale = 1.0). Herpesvirus subfamilies are indicated in bolded text.

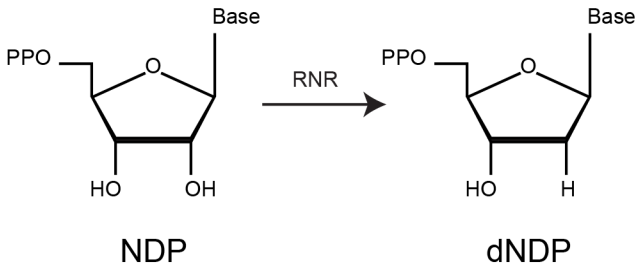

Figure 1.8: Mechanism of ribonucleotide reduction.
Schematic showing the conversion of ribonucleotide diphosphate to deoxyribonucleotide diphosphate by ribonucleotide reductases.

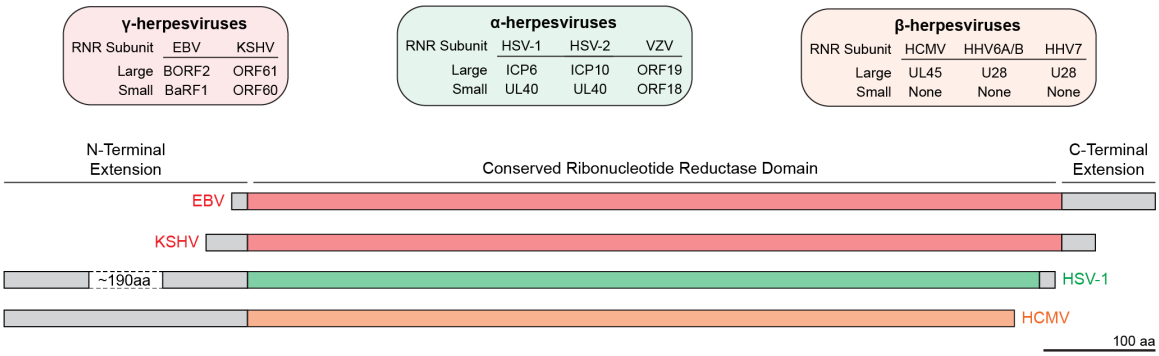

Figure 1.9: Herpesvirus ribonucleotide reductases.
Top: Protein names of herpesvirus R1 and R2 proteins, grouped by virus subfamilies. **Bottom:** Schematic of representative herpesvirus R1 proteins from α- (green), β- (orange), and γ-herpesviruses (red) (bottom). Scale bar=100 amino acids (aa).

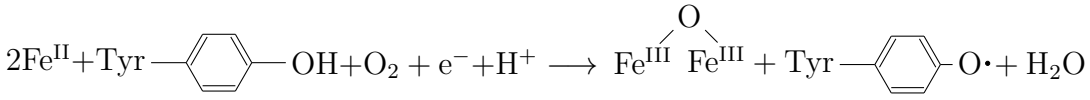

Figure 1.10: Mechanism of tyrosine reduction by R2 proteins.
Balanced chemical equation showing the generation of a stable tyrosyl radical by R2. Reduction of the R2 tyrosine is mediated by a two iron molecules reacting with oxygen, which generates an iron-oxygen complex (Fe-O-Fe), a stable tyrosyl radical, and water. The tyrosyl radical is then transferred to R1 for subsequent reduction of ribonucleotide diphosphates.

CHAPTER 2

Epstein-Barr Virus BORF2 Inhibits Cellular APOBEC3B to Preserve Viral Genome Integrity

This chapter was adapted with permission from:

*Cheng AZ, Yockteng-Melgar J, et al. Nat Microbiol. (2019). **4**(1):78-88.*

Authors: Adam Z. Cheng[1,2,3,4,9], Jaime Yockteng-Melgar[5,9], Matthew C. Jarvis[1,2,3,4], Natasha Malik-Soni[5], Ivan Borozan[6], Michael A. Carpenter[1,2,3,4,8], Jennifer L. McCann[1,2,3,4], Diako Ebrahimi[1,2,3,4], Nadine M. Shaban[1,2,3,4], Edyta Marcon[7], Jack Greenblatt[5,7], William L. Brown[1,2,3,4], Lori Frappier[5] & Reuben S. Harris[1,2,3,4,8]

Affiliations:

[1] Department of Biochemistry, Molecular Biology and Biophysics, University of Minnesota, Minneapolis, Minnesota, USA, 55455.

[2] Masonic Cancer Center, University of Minnesota, Minneapolis, Minnesota, USA, 55455.

[3] Institute for Molecular Virology, University of Minnesota, Minneapolis, Minnesota, USA, 55455.

[4] Center for Genome Engineering, University of Minnesota, Minneapolis, Minnesota, USA, 55455.

[5] Department of Molecular Genetics, University of Toronto, Toronto, Ontario, Canada, M5S 1A8.

[6] Ontario Institute for Cancer Research, MaRS Centre, South Tower, 101 College Street, Suite 800, Toronto, Ontario, Canada, M5G 0A3.

[7] Donnelly Centre, University of Toronto, Toronto, Ontario, Canada, M5S 1A8.

[8] Howard Hughes Medical Institute, University of Minnesota, Minneapolis, Minnesota, USA, 55455.

[9] These authors contributed equally to this work.

2.1 Summary

The apolipoprotein B messenger RNA editing enzyme, catalytic polypeptide-like (APOBEC) family of single-stranded DNA (ssDNA) cytosine deaminases provides innate immunity against virus and transposon replication [2, 85, 86, 247]. A well-studied mechanism is APOBEC3G restriction of human immunodeficiency virus type 1, which is counteracted by a virus-encoded degradation mechanism [2, 85, 86, 247]. Accordingly, most work has focused on retroviruses with obligate ssDNA replication intermediates and it is unclear whether large double-stranded DNA (dsDNA) viruses may be similarly susceptible to restriction. Here, we show that the large dsDNA herpesvirus Epstein-Barr virus (EBV), which is the causative agent of infectious mononucleosis and multiple cancers [248], utilizes a two-pronged approach to counteract restriction by APOBEC3B. Proteomics studies and immunoprecipitation experiments showed that the ribonucleotide reductase large subunit of EBV, BORF2 [233, 249], binds APOBEC3B. Mutagenesis mapped the interaction to the APOBEC3B catalytic domain, and biochemical studies demonstrated that BORF2 stoichiometrically inhibits APOBEC3B DNA cytosine deaminase activity. BORF2 also caused a dramatic relocalization of nuclear APOBEC3B to perinuclear bodies. On lytic reactivation, BORF2-null viruses were susceptible to APOBEC3B-mediated deamination as evidenced by lower viral titres, lower infectivity and hypermutation. The Kaposi's sarcoma-associated herpesvirus homologue, ORF61, also bound APOBEC3B and mediated relocalization. These data support a model where the genomic integrity of human γ-herpesviruses is maintained by active neutralization of the antiviral enzyme APOBEC3B.

2.2 Results

During the course of an Epstein-Barr virus (EBV) proteomics analysis, APOBEC3B (A3B) was identified as the dominant cellular protein co-purifying with FLAG-tagged ribonucleotide reductase (RNR) large subunit of EBV, BORF2, in three independent affinity purification-mass spectrometry experiments in HEK293T cells (**Figure 2.1a**), whereas no other APOBEC enzymes were recovered. A3B was identified based on the recovery of 9 unique peptides spanning 36% of this 382-amino acid protein (**Supplementary Figure S2.1a**). This result was surprising because HEK293T cells express endogenous A3B at levels that are undetectable by immunoblot and barely detectable by quantitative reverse transcription PCR (RT-qPCR) (**Figure 2.1b** and **Supplementary Figure S2.1b**). Co-immunoprecipitation experiments confirmed that BORF2-FLAG binds endogenous A3B in HEK293T cells as well as in AGS gastric adenocarcinoma cells, an established model for EBV studies (for example, see Kraus *et al.* [250], Hagemeier *et al.* [251] and Verma *et al.* [252]; **Figure 2.1b** and **Supplementary Figure S2.1c,d**). Mechanistic conservation was indicated by similarly strong interaction with the large ribonucleotide reductase subunit from Kaposi's sarcoma-associated herpesvirus (KSHV), ORF61, and undetectable interactions with homologous proteins from more distantly related herpesviruses (herpes simplex virus type 1 (HSV-1) UL39 and human cytomegalovirus (HCMV) UL45) or human ribonucleoside-diphosphate reductase large subunit (RRM1) (**Supplementary Figure S2.2a**). In addition, a BORF2 deletion analysis mapped the A3B interaction to the conserved core RNR domain, and showed that the required region is more extensive than that needed for interaction with the EBV RNR small subunit, BaRF1 (**Supplementary Figure S2.3a-d**). Furthermore, BORF2 catalytic residues were dispensable for interacting with A3B,

suggesting an RNR-independent function (**Supplementary Figure S2.3e**).

Interaction specificity was further evidenced by comparisons with related APOBEC family members, which revealed a prominent interaction with A3B-HA, barely detectable interactions with A3A-HA and A3F-HA, and undetectable interactions with A3C-HA, A3D-HA, A3G-HA, and A3H-HA (**Figure 2.1c** and **Supplementary Figure S2.4**). The interaction mapped to the A3B C-terminal domain via co-immunoprecipitation experiments using BORF2-FLAG and individually expressed hemagglutinin (HA)-tagged N- and C-terminal domains (ntd, ctd) (**Figure 2.1d**). Additional co-immunoprecipitation experiments using chimeras of A3B and A3G (A3Bntd-A3Gctd or A3Gntd-A3Bctd) confirmed the C-terminal specificity of this interaction (**Figure 2.1e**). A3Bctd and A3Gctd belong to the same deaminase subgroup [13] and the majority of amino acid differences are confined to surface-exposed regions; this enabled the construction of a series of chimeras with exchanged loop regions. The BORF2 interaction was abolished using an A3B construct with loop 7 (L7) from A3G and, conversely, it was enabled using an A3G construct with L7 from A3B (**Figure 2.1f**). These data indicated that BORF2 interacts preferentially with A3Bctd and specifically with a region involving L7 residues.

Recent structural studies have shown that A3Bctd L7 is essential for binding to 5'-TC containing ssDNA substrates [33]. The specificity of the BORF2 interaction with the L7 region of A3B suggested that BORF2 may function by directly inhibiting ssDNA deaminase activity. To test this mechanism, recombinant BORF2 and A3Bctd were purified from *E. coli* and used in a series of *in vitro* ssDNA deaminase assays (**Figure 2.2a** and **Supplementary Figure S2.5**). The related enzyme, A3H, which also prefers 5'-TC ssDNA substrates [253] and does not interact with BORF2

(see earlier), was purified and tested in parallel as a negative control. A clear dose-dependent inhibition of A3Bctd catalytic activity, approaching near complete inhibition at equimolar concentrations, was observed in multiple independent BORF2 titration experiments ($P=2.7*10^{-5}$, one-tailed one sample t-test; **Figure 2.2b,c**). In comparison, BORF2 had no significant effect on A3H enzymatic activity even at eightfold molar excess concentrations (P=0.1575, one-tailed one sample t-test). These results demonstrated that an alternative function of BORF2 is specific inhibition of A3B catalytic activity and that other viral (for example, BaRF1) or cellular factors are not required for this activity.

The archetypal mechanism for virus-mediated neutralization of APOBEC3 enzymes is target engagement followed by polyubiquitination and proteasomal degradation [2, 85, 86, 247]. In contrast, BORF2 expression stabilizes steady-state levels of cellular A3B, suggesting a degradation-independent mechanism (**Figure 2.3a**). In support, proteasome inhibition by MG132 had little effect on cellular A3B levels with or without BORF2 (**Supplementary Figure S2.6**). To gain further insights into this unique mechanism and to assess the interaction of these proteins in the context of EBV lytic replication, immunofluorescence microscopy was used to examine the subcellular localization of endogenous A3B and BORF2 produced after reactivation of AGS cells latently infected with EBV (AGS-EBV) [254, 255]. A3B was predominantly pan-nuclear in latent AGS-EBV cells before reactivation (**Figure 2.3b**, upper panel), consistent with prior reports for A3B localization in a variety of non-infected cell types (for example, see Bogerd *et al.* [63] and Burns *et al.* [46]). After reactivation to the lytic cycle, nuclear and perinuclear bodies containing both A3B and BORF2 accumulated rapidly and, as the lytic phase progressed, additional cytoplasmic bodies containing BORF2 and A3B increased in

abundance (**Figure 2.3b**, bottom panels, and **Figure 2.3c**). Additional imaging studies with markers for cytoplasmic organelles indicated that the BORF2/A3B bodies accumulated within the endoplasmic reticulum (**Figure 2.3d**). In particular, three-dimensional reconstructions of image z-stacks showed that these aggregates are surrounded on all sides by the integral endoplasmic reticulum component binding immunoglobulin protein (BiP)/GRP-78 (**Supplementary Section 2.7 1**) [30]). A similar result was obtained in reactivated AGS-EBV cells using a second endoplasmic reticulum marker, translocon-associated protein subunit (TRAP; **Supplementary Section 2.7 2** [30]). BORF2 alone also caused A3B relocalization in other cell types, including U2OS, HeLa, HEK293T, and AGS cells (**Figure 2.3d,e**, **Supplementary Figure S2.7** and **Supplementary Section 2.7 3** and **4** [30]). In addition, relocalization of endogenous A3B and colocalization with BORF2 was observed in M81 EBV-transformed B cells that spontaneously enter the lytic cycle [256] (**Figure 2.3f** and **Supplementary Figure S2.7g,h**). Importantly, ORF61 of KSHV also sequestered A3B in perinuclear and cytoplasmic bodies, further indicating mechanistic conservation (**Supplementary Figure S2.2b,c**).

To directly test whether A3B relocalization is dependent on BORF2, CRISPR-Cas9 was used to disrupt the *BORF2* gene in AGS-EBV cells and in AGS cells containing GFP-tagged viral genomes (AGS-EBV(Bx1g) [255, 257]; **Supplementary Figure S2.8a**). Despite numerous EBV genome copies in these cells, a near complete ablation of BORF2 expression was achieved as evidenced by immunoblotting and by sequencing the DNA region targeted by Cas9-gRNA complexes (**Supplementary Figure S2.8b,c**). BORF2 knockout viruses were then reactivated to the lytic cycle, and cells containing lytic replicating EBV were identified by staining for the EBV DNA polymerase processivity factor BMRF1 and for new viral DNA synthesis

by 5-ethynyl-2'-deoxyuridine (EdU) incorporation. In these cells, perinuclear and cytoplasmic A3B bodies were not observed, indicating that A3B relocalization from the nucleus is completely dependent on BORF2 (**Figure 2.3g**). In addition, a proportion of A3B colocalized with BMRF1 and EdU indicating that A3B associates with viral DNA replication intermediates in the absence of BORF2.

Our findings that BORF2 directly inhibits and relocalizes A3B away from viral replication centres strongly suggested that this DNA cytosine deaminase could be a threat to EBV genomic integrity. Based on the hallmark DNA deamination activity of A3B, we hypothesized that viral ssDNA replication intermediates would become susceptible to A3B-catalysed DNA cytosine deamination in the absence of BORF2. To test this possibility, we analysed viral genomic DNA C/G-to-T/A hypermutation by sequencing individual differential DNA denaturation (3D)-PCR products representing multiple regions of the viral genome. 3D-PCR estimates the lowest denaturation temperature required for amplification of any DNA substrate; thereby, it enables recovery of C/G-to-T/A hypermutated sequences by virtue of preferential amplification at lower than wild-type (WT) DNA denaturation temperatures [258, 259] (**Figure 2.4a**). Indeed, in a series of pilot experiments, a segment of the *BRRF2* gene was amplified at lower denaturation temperatures from reactivated AGS-EBV cells containing BORF2-null EBV genomes compared to cells containing WT EBV genomes (**Supplementary Figure S2.9a**). Low temperature amplicons were not recovered from latently infected cell pools (before reactivation). Cloning and sequencing of individual PCR products revealed the highest level of mutation in amplicons from lytic, replication-induced, BORF2-null conditions (**Supplementary Figure S2.9b**).

We next generated a clonal system to extend these studies. Virus-containing

supernatants from pooled AGS-EBV(Bx1g) cells with BORF2-null EBV were harvested and used to infect new parental AGS cells. A clonal AGS cell line with a single isogenic BORF2-null EBV was generated (AGS-EBV(Bx1g)ΔBORF2). These cells were first stably complemented with control or BORF2-FLAG-expressing lentivirus. Second, they were transduced with short hairpin RNA (shRNA) to knockdown endogenous A3B or with a non-targeting control (**Figure 2.4b**). Third, a control vector or uracil glycosylase inhibitor (UGI) was added by transduction of cells from each condition to inhibit the repair of A3B-mediated uracil lesions and potentially exacerbate the effects of A3B-mediated viral hypermutation. UGI uses a structurally conserved mechanism to inhibit uracil DNA glycosylases (UDGs) across kingdoms, including bacterial, human, and EBV enzymes [260, 261] (**Supplementary Figure S2.10**). Cells from each of these 8 conditions were cultured to maintain EBV latency (uninduced) or treated with 12-O-tetradecanoylphorbol-13-acetate (TPA) and sodium butyrate for 48 h to reactivate EBV lytic replication (induced); then, DNA was collected and mutations were analysed by sequencing individual 3D-PCR products.

Under normal cell culture conditions that maintain EBV latency, low temperature BRRF2 amplicons were rarely observed for any of the eight conditions (**Figure 2.4c**). Similarly, BORF2-complemented cells, regardless of cell culture treatments or other genetic manipulations, did not yield lower-temperature BRRF2 PCR amplicons. In contrast, after induction of EBV lytic replication, lower-temperature PCR amplicons could be generated from AGS-EBV(Bx1g)ΔBORF2 cells expressing endogenous levels of A3B, and this phenotype was exacerbated by UGI treatment. The accumulation of lower-temperature amplicons was completely dependent on A3B activity since no lower-temperature BRRF2 amplicons were recovered from A3B knockdown cells

that were otherwise treated identically. Similar results were obtained by 3D-PCR analysis of a region of Epstein-Barr virus nuclear antigen 2 (EBNA2; **Supplementary Figure S2.9c**).

A sequence analysis of individual 3D-PCR products confirmed these results, showing extensive mutagenesis of BRRF2 sequences from AGS-EBV(Bx1g)ΔBORF2 cells expressing endogenous A3B, both with and without UGI treatment (**Figure 2.4d** and **Supplementary Figure S2.11a** and **Figure S2.12**). Interestingly, diverse mutational events were observed, including strong enrichments for C/G-to-T/A mutations and deletions. A high deletion frequency was unexpected and, based on precedents with activation-induced deaminase (AID) in antibody diversification [7, 262], was probably due to processing of A3B-induced lesions by cellular DNA damage response mechanisms. This is supported by a trend towards more deletions without UGI, since uracil excision can readily lead to single-stranded nicks and broken DNA. However, A3B-attributable hypermutation was not observed in Sanger sequences of >20 high-temperature BRRF2 amplicons from BORF-null conditions (**Supplementary Figure S2.11b**), but enrichments for mutations in A3B-preferred 5'-TCA/T motifs [46] were apparent by deep-sequencing high-temperature amplicons representing four different viral genomic DNA regions (**Figure 2.4e**). Therefore, we inferred that the hypermutation frequency is relatively low for a given region of EBV. This may be explained by low reactivation rates and by a viral DNA replication mechanism that may only periodically expose ssDNA to deamination by A3B.

The potential for this viral DNA hypermutation mechanism to exert a multiplicative effect is supported by BORF2-null viruses showing 60-70% lower titres and, even on titre normalization, a further 50-60% less infectivity after one round of

lytic replication in AGS-EBV(Bx1g) cells (**Figure 2.4f,g**). Specific knockdown of endogenous A3B resulted in a near-full restoration of viral infectivity (**Figure 2.4h**). A dependence on A3B is further evidenced by Akata cells, which we found are homozygous for a 29.5 kb deletion spanning the entire *A3B* gene [47], producing BORF2-null and WT viruses with similar titres and infectivity (**Supplementary Figure S2.13**). Combined, these hypermutation and infectivity results indicated that BORF2 is dispensable during EBV latency, but required to protect viral DNA from A3B mutagenesis during conditions of induced lytic replication.

2.3 Discussion

The A3B neutralization mechanism described here for γ-herpesvirus proteins, EBV BORF2, and KSHV ORF61, is fundamentally different from the A3 degradation mechanism used by lentiviral Vif proteins [2, 85, 86, 247]. In addition to the stark differences of direct inhibition and relocalization versus proteasomal degradation, the replication cycles of EBV and KSHV may be fundamentally less tolerant of APOBEC mutagenesis. This inference is supported by bioinformatics analyses of all sequenced EBV isolates indicating that BORF2 is under negative selection and that the domain of BORF2 that binds A3B contains few non-synonymous mutations (**Supplementary Figure S2.14a-c**). APOBEC-hypermutated sequences are also absent from databases. (Only one prior publication detected hypermutation in EBV by 3D-PCR and implicated a different APOBEC family member [263].) Nevertheless, A3B-preferred 5'-TCA deamination substrate motifs are depleted from EBV genomes and, correspondingly, 5'-TTA product motifs are enriched, consistent with periodic A3B-catalysed mutation events (despite

BORF2) and long-term evolutionary pressure (**Supplementary Figure S2.14e**).

In comparison to EBV, KSHV, and related large DNA viruses with low mutation rates [264], retroviruses have much higher mutation rates and frequent scars from APOBEC mutagenesis [265, 266] (for example, ∼10% of patient samples contain human immunodeficiency virus type 1 (HIV-) sequences with APOBEC signature hypermutations). This mechanistic difference may be due, at least partly, to γ-herpesviruses using a coordinated leading/lagging strand replication mechanism to copy viral dsDNA, whereas HIV-uses reverse transcription to copy genomic RNA into an obligate single-stranded complementary DNA (cDNA) intermediate before conversion into dsDNA for integration into the host genome. Therefore, EBV and KSHV may have fewer exposed ssDNA replication intermediates during the lytic phase that can be attacked by A3B. Thus, although the frequency of BORF2-null EBV hypermutation is lower than that documented for Vif-null HIV-, the overall effect has the potential to be similarly catastrophic because even localized hypermutation could inactivate an essential viral gene or trigger degradation of the full episome. Furthermore, cumulative viral DNA deamination over the lifespan of an infected cell is likely to lead to depletion and potentially even clearance of viral episomes. Disrupting the BORF2/A3B and ORF61/A3B interactions *in vivo* may have merit for compromising the genetic integrity of EBV and KSHV, thereby limiting lytic infection that induces infectious mononucleosis and contributes to EBV- and KSHV-driven tumours.

2.4 Materials and Methods

DNA constructs for expression in human cell lines

The full set of pcDNA3.1(+) human APOBEC-HA expression constructs has been described [78] (A3A (GenBank accession number: NM_145699); A3B (NM_004900); A3C (NM_014508); A3D (NM_152426); A3F (NM_145298); A3G (NM021822); A3H (haplotype II; FJ376615)). A3Bntd1-190, A3Bctd191-382, A3Bntd-A3Gctd, and A3Gntd-A3Bctd constructs were cloned by overlap extension PCR as described [267]. The HIV-IIIB Vif-Myc construct was also described previously [268]. A3B and A3G L7 swaps were generated by overlap extension PCR on A3B-HA and A3G-HA constructs with primers introducing mutations in L7 to generate the reciprocal amino acid sequence (A3B GL7YDPLYK(132-137)DQGRCQ and A3G BL7DQGRCQ(132-137)YDPLYK). The primers used for A3B GL7 were RSH5336 5'-TAC GAC CCC CTA TAT AAG GAG GGG CTG CGC ACC CT-3' and RSH5337 5'-CTT ATA TAG GGG GTC GTA ATC ATA GAT GCG GGC-3'; the primers used for A3G BL7 were RSH5338 5'-GAT CAA GGA AGA TGT CAG GAG GCG CTG CAA ATG C-3' and RSH5339 5'-CTG ACA TCT TCC TTG ATC ATC ATA GAT GCG GGC-3'. A3B with a C-terminal 2xStrep-tag (WSHPQFEK) was subcloned using high-fidelity PCR from pcDNA3.1(+)-A3B-3xHA using primers 5'-NNA AGC TTA TGA ATC CAC AGA TCA GA-3' and 5'-NNG CGG CCG CCC GTT TCC CTG ATT CTG GA-3'. PCR products were digested with *Hind*III-HF (New England Biolabs) and *Not*I-HF (New England Biolabs) and ligated into pcDNA4/TO (Thermo Fisher Scientific) with a C-terminal 2xStrep-tag. Tetracycline-inducible A3B with a C-terminal mCherry tag was cloned using high-fidelity PCR of previously described A3B-mCherry [61] using primers RSH7018 5'-NNN NNA AGC TTA CCA CCA TGA ATC CA-3' and RSH7016 5'-AGA GTC GCG GCC GCT TAC TTG TAC

A-3'. PCR products were digested with *Hind*III-HF and *Not*I-HF and ligated into similarly digested pcDNA5/TO (Thermo Fisher Scientific). The A3B-enhanced green fluorescent protein (eGFP) construct has been described34. The pLKO construct expressing an A3B-specific shRNA has been described and validated [46, 66, 269, 270]; the construct used here has a blasticidin resistance gene in place of the puromycin resistance gene. The pLKO construct expressing a non-targeting shRNA control [271] (5'-CCT AAG GTT AAG TCG CCC TCG-3') was a gift from Keith Mostov (Addgene plasmid).

BORF2 (GenBank accession number: V01555.2) with a C-terminal 3xFLAG-tag (DYKDDDDK) was subcloned using high-fidelity PCR from the previously described PMZS3F-BORF2 [272] using primers RSH12971 5'-NNN NGA TAT CGC CGA CAC CAT GGC AAC GAC C-3' and RSH12848 5'-NNN NGC GGC CGC CCT TGG CAA GAT TCA CAG GC-3'. PCR products were digested with *Eco*RV-HF (New England Biolabs) and *Not*I-HF and ligated into pcDNA4 (Thermo Fisher Scientific) with a C-terminal 3xFLAG [88]. BORF2 with a C-terminal eGFP tag was generated using high-fidelity PCR of pcDNA4-BORF2-3xFLAG using primers RSH13422 5'-NNN NAT GCA TCA TGG CAA CGA CCA GTC ATG TC-3' and RSH13424 5'-NNN NAC GCG TCC TTG GCA AGA TTC ACA GGC TCG-3'. PCR products were digested with *Nsi*I-HF (New England Biolabs) and *Mlu*I-HF (New England Biolabs) and cloned into the previously described pQCXIP (Clontech) with a C-terminal eGFP tag [273]. BORF2 with a C-terminal 3xFLAG-tag was cloned into a murine leukaemia virus (MLV)-based pQCXIP lentivirus vector (Clontech) for complementation experiments by PCR of pcDNA4-BORF2-3xFLAG using primers RSH13422 5'-NNN NAT GCA TCA TGG CAA CGA CCA GTC ATG TC-3' and RSH13423 5'-NNN NTT AAT TAA TTA AAC GGG CCC CTT GTC GTC-3'.

The PCR product was digested into *Nsi*I-HF and *Pac*I (New England Biolabs) and ligated into pQCXIP digested with *Sbf*I-HF (New England Biolabs) and *Pac*I. BORF2 truncation mutants were generated by subcloning portions of pcDNA4-BORF2-3xFLAG using high-fidelity PCR, digesting the PCR products with *Eco*RV-HF and *Not*I-HF, and ligating into pcDNA4-3xFLAG as described earlier. The PCR primers are as follows: N-terminal BORF2 25-826 mutant (RSH14011 5'-NNN NGA TAT CGC CAC CAT GTC AGA CCC CGA GGC TGA TGT C-3' and RSH12848); BORF2 50-826 (RSH14012 5'-NNN NGA TAT CGC CAC CAT GGC CGA ATA TCT GGA GGT CTT C-3' and RSH12848); C-terminal BORF2 1-739 mutant (RSH12971 and RSH13396 5'-NNN NGC GGC CGC TCC ATC ACC CCC AGA TCG GCG GC-3'); and BORF2 1-687 (RSH12971 and RSH13612 5'-NNN NGC GGC CGC ACA AAG GGG GCC CTG TCC C-3'). BORF2 catalytic mutants were generated in pcDNA4-BORF2-3xFLAG by site-directed mutagenesis using PfuUltra II Fusion HS DNA polymerase (Agilent) with the following primers for YY725/6AA (RSH13776 5'-GGC CTG AAG ACT ATC ATG GCG CTT TGT CGC ATT GAG AAG GC-3' and RSH13777 5'-GCC TTC TCA ATG CGA CAA AGC GCC ATG ATA GTC TTC AGG CC-3') and YY725/6FF (RSH13774 5'-GGC CTG AAG ACT ATC ATG TTC TTT TGT CGC ATT GAG AAG GC-3' and RSH13775 5'-GCC TTC TCA ATG CGA CAA AAG AAC ATG ATA GTC TTC AGG CC-3').

BaRF1 (GenBank accession number V01555.2) with C-terminal 3xHA-tag (YPYDVPDYA) was cloned using high-fidelity PCR from a gBlock purchased from Integrated DNA Technologies using primers RSH13621 5'-NNN NGA ATT CGC CGC CAC CAT GTC CAA GTT G-3' and RSH13622 5'-NNN NCT CGA GAA GGT CAT CTA CCA CCA GCA T-3'. The PCR products were digested with *Eco*RI-HF (New England Biolabs) and *Xho*I (New England Biolabs) and cloned into pcDNA3.1(+)

(Thermo Fisher Scientific) with a C-terminal 3xHA-tag.

The original pLentiCRISPR [274] vector, which was a gift from Feng Zhang (Addgene plasmid), was modified to improve gRNA expression and introduce a *loxP* site into the viral 3'-long terminal repeat (pLentiCRISPR-*loxP*; Carpenter *et al.*, manuscript in preparation). A guide RNA (gRNA) targeting BORF2 was designed using crispr.mit.edu with a protospacer adjacent motif site of AGG at +119 and predicted cut site at +122 on the antisense strand (relative to the BORF2 start codon). gRNA primers (RSH13690 5'-CAC CGG TGT AAC TGA CTC GGC CTT A-3' and RSH13691 5'-GAA CTA AGG CCG AGT CAG TTA CAC C-3') were annealed, cut with *Bsm*BI, and ligated into similarly digested pLentiCRISPR-*loxP*.

UGI (GenBank accession number: J04434.1) was amplified with high-fidelity polymerase from pcDNA3.1(+)-UGI [39] using primers RSH7505 5'-NNN NCT CGA GAC CAT GAC AAA TTT ATC TGA CAT CAT TG-3' and RSH7506 5-NNN ACG CGT TTA TAA CAT TTT AAT TTT ATT TTC TCC-3', digested with *Xho*I and *Mlu*I-HF, and ligated into similarly digested pLenti4/TO (Thermo Fisher Scientific). EBV UDG (BKRF3) (GenBank accession number: MG021307.1) was amplified with a high-fidelity polymerase from AGS-EBV(Bx1g) genomic DNA using primers RSH15814 5'-GAA GCT TGG TAC CAT GGC ATC GCG GG-3' and RSH15815 5'-TCT AGA CTC GAG CTA CAG CCT CCA ATC-3', followed by restriction digest with *Kpn*I-HF (New England Biolabs) and *Xho*I, and ligation into similarly digested pcDNA3.1/V5 [275]. A gRNA targeting human UDG (UNG2) was designed using crispr.mit.edu with a protospacer adjacent motif site of TGG at +274 and predicted cut site at +271 on the sense strand (relative to the UNG2 start codon). gRNA primers (RSH11189 5'-CAC CGC GCG GCC CGC AAC GTG CCC G-3' and RSH11190 5'-GAA CCG GGC ACG TTG CGG GCC GCG C-3') were annealed, cut

with *Bsm*BI, and ligated to similarly digested pLentiCRISPR-*loxP*.

All RNR large subunit homologues were cloned into the previously described pCMV-3F plasmid[276]. Human RRM1 (GenBank accession number: BC006498) was amplified using high-fidelity PCR from a plasmid provided by the SPARC BioCentre using primers 5'-GTA CGA GCT CGC CAC CAT GCA TGT GAT CAA GCG AGA TGG-3' and 5'-GAC TTC TAG AGG ATC CAC ACA TCA GAC ATT CAT C-3', digested with *Sac*I (New England Biolabs) and *Xba*I (New England Biolabs), and ligated into similarly digested pCMV-3F. KSHV ORF61 [277] (GenBank accession number: U75698.1) was kindly provided by Britt Glausinger (University of California, San Francisco), amplified using 5'-GTA CAG ATC TGC CAC CAT GTC TGT CCG GAC ATT TTG-3' and 5'-GAC TTC TAG ACT GAC AGA CCA GGC ACT CG-3', digested with *Bgl*II and *Xba*I (New England Biolabs), and ligated into similarly digested pCMV-3F. Herpes simplex virus type 1 UL39 (GenBank accession number JN555585.1) was amplified from a library described previously [272] using primers 5'-GAC TGA ATT CGC CAC CAT GGC CAG CCG CCC AGC-3' and 5'-GCA TTC TAG ACA GCG CGC AGC TCA TGC-3', digested with *Eco*RI (New England Biolabs) and *Xba*I, and ligated into similarly digested pCMV-3F. HCMV UL45 (GenBank accession number: FJ527563.1) was amplified from a library described previously [272] using primers 5'-GTA CAG ATC TGC CAC CAT GAA TCC GGC TGA CGC GGA-3' and 5'-GAC TTC TAG AAG AGG CAC AGT ACT TAT ATA CTC-3', digested with *Bgl*II and *Xba*I, and ligated into similarly cut pCMV-3F. All new plasmid constructions were confirmed by restriction fragment analysis and DNA sequencing.

Human cell culture

Unless indicated, cell lines were derived from established laboratory collections.

All cell cultures were supplemented with 10% heat-inactivated Gibco foetal bovine serum (FBS; Thermo Fisher Scientific), 1x penicillin-streptomycin (Thermo Fisher Scientific), and periodically tested for Mycoplasma (MycoAlert PLUS Mycoplasma Detection Kit; Lonza). HEK293T cells were cultured in high glucose HyClone DMEM (Thermo Fisher Scientific), U2OS cells in HyClone McCoy's 5A media (Thermo Fisher Scientific), HeLa, AGS (gastric adenocarcinoma), AGS-EBV, and Ramos (EBV-negative Burkitt's lymphoma) cells were cultured in Roswell Park Memorial Institute (RPMI) 1640 media (Corning). The Akata B cell line (EBV-positive Burkitt's lymphoma) used in the current study was a gift from Kristin Hogquist and Samantha Dunmire (University of Minnesota). The Akata EBV strain was engineered previously to express neomycin resistance [278] and GFP19. The neomycin-resistant Akata EBV strain was introduced previously into AGS cells to yield the AGS-EBV; the neomycin-resistant, GFP-expressing virus was used to derive the AGS-EBV(Bx1g) line used in the current study14,15,19. Akata EBV-containing cell cultures were additionally supplemented with 0.4 mg ml^{-1} G418 (geneticin). B cells transformed with the M81 EBV strain18 were a gift from Henri-Jacques Delecluse (German Cancer Research Centre (DKFZ)) and were cultured in RPMI. This EBV strain spontaneously reactivates to the EBV lytic cycle without external treatment. Cells transduced with shCtrl or shA3B lentivirus were selected with 5 μg ml^{-1} blasticidin S (Gold Biotechnology). Cells transduced with pLentiCRISPR targeting BORF2 or pQCXIP-BORF2 complementation lentiviruses were selected with 1 μg ml^{-1} puromycin. Cells transduced with pLenti/TR to express tetracycline repressor (TR) were selected with 5 μg ml^{-1} blasticidin S.

Affinity purification and mass spectrometry

Five 10 cm dishes of HEK293T cells were transfected with 6 μg of PMZS3F-BORF2

[272] using PolyJet at a 1:2 ratio; 48 h after transfection cells were collected and pooled. Cells were washed twice in PBS followed by lysis (50 mM Tris pH 7.9, 420 mM NaCl, 10% glycerol, 0.1% NP-40, protease inhibitors (P8340; Sigma-Aldrich), 1 mM NaF). Lysates were subjected to three cycles of freeze-thaw followed by sonication. Benzonase (25 U ml^{-1}; Sigma-Aldrich) was added to the lysate and incubated on ice for 30 min. Lysates were then cleared by centrifugation (15,000 r.p.m.) in a table top microcentrifuge for 30 min. Cleared lysate was then added to 50 μl of anti-FLAG M2 resin (Sigma-Aldrich) followed by end-over-end rotation for 3 h at 4 °C. Following immunoprecipitation, the anti-FLAG resin was washed twice in lysis buffer, followed by three additional washes in lower-salt, detergent-free wash buffer (10 mM Tris pH 7.9, 150 mM NaCl, 10% glycerol). Protein was eluted from the resin with three washes of 0.5 M ammonium hydroxide (15 min each at 25 °C with rotation). Samples were lyophilized in a SpeedVac (Savant DNA120; Thermo Fisher Scientific) and washed with 400 μl HPLC-grade water (Gibco). Samples were lyophilized once more to remove traces of ammonium hydroxide, and then subjected to trichloroacetic acid precipitation, tryptic digestion, and tandem mass spectrometry (MS/MS) as described [279]. RAW files were submitted for database searching using X! TANDEM (v2007.07.01.3) and Trans-Proteomic Pipeline (version 4.3) under standard workflow and a modified UniProt/Swiss-Prot protein database FASTA file. The modification consisted of adding BSA (Swiss-Prot accession number P02769). Search parameters were set to allow for two missed cleavage sites, variable modification by methionine oxidation, and one fixed modification by cysteine carbamidomethylation. A 10 ppm filter was used for peptide identification. The search results were uploaded to ProHits [280] and compared using at least 99% Trans-Proteomic Pipeline probability.

RNA isolation, cDNA synthesis and RT-qPCR

RNA isolation, cDNA synthesis, and qPCR primers were described previously [44]. In brief, RNA was collected from $2*10^6$ cells using the High Pure RNA Isolation Kit (Roche Molecular Systems); cDNA libraries were generated with reverse transcriptase (Roche Molecular Systems); and qPCR was performed on a LightCycler 480 instrument (Roche Molecular Systems). The housekeeping gene *TBP* was used for normalization.

Co-immunoprecipitation experiments and immunoblots

Semi-confluent HEK293T cells were grown in 6-well plates and transfected with plasmids and 0.6 μl TransIT-LT1 (Mirus) per 100 ng DNA in 100 μl serum-free Opti-MEM reduced serum medium (Thermo Fisher Scientific). In most experiments, 100 ng DNA was used for each unique plasmid transfection (for example, **Figure 2.1b,c-f**, **Supplementary Figure S2.3**, and **Figure S2.4**). For the A3 panel and RNR homologue co-immunoprecipitation experiments (**Figure 2.4c** and **Supplementary Figure S2.2a**), a titration series was performed to achieve roughly equivalent protein expression by immunoblot. Growth medium was removed after 48 h and whole cells were collected in 1 ml PBS-EDTA by pipetting. Cells were spun down, PBS-EDTA was removed, and cells were resuspended in 300 μl of ice-cold lysis buffer (150 mM NaCl, 50 mM Tris-HCl, 0.5% Tergitol, and Roche cOmplete EDTA-free protease inhibitor cocktail tablet (Sigma-Aldrich), pH 7.4). Cells were vortexed vigorously and left on ice for 30 min, then sonicated for 5 s in an ice water bath; 30 μl of whole cell lysate was aliquoted for immunoblot. Lysed cells were spun down at 13,000 r.p.m. for 15 min to pellet debris and supernatant was added to the clean tube with 25 μl resuspended anti-FLAG M2 Magnetic Beads (Sigma-Aldrich) for overnight incubation at 4 °C with gentle rotation. Beads were then washed three times in 700 μl of ice-cold lysis buffer. Bound protein was eluted in 30 μl of

elution buffer (0.15 mg ml^{-1} FLAG peptide (Sigma-Aldrich) in 150 mM NaCl, 50 mM Tris-HCl, 0.05% Tergitol, pH 7.4). Proteins were analysed by immunoblot; the antibodies used included mouse monoclonal anti-FLAG 1:5,000 (Sigma-Aldrich), mouse monoclonal anti-BORF2 1:1,000 (Santa Cruz Biotechnology), mouse anti-BZLF1 1:3,000 (Santa Cruz Biotechnology), mouse monoclonal anti--tubulin 1:10,000 (Sigma-Aldrich), mouse anti-β-actin 1:10,000 (Santa Cruz Biotechnology), rabbit monoclonal anti-HA-tag 1:3,000 (Cell Signalling), rabbit polyclonal anti-Strep-tag II 1:5000 (Abcam), and rabbit anti-A3B 1:1,000 (5210-87-1336).

Protein purification from *E. coli* and DNA deaminase activity assays

pE-6xHis-SUMO-A3Bctd187-378-DM (L230K/F308K) [37] and pE-6xHis-SUMO A3H Hap II 1-183 [34] have been reported previously for *E. coli* expression and protein purification. Codon-optimized BORF2 was synthesized by Bio Basic, digested with *Bsm*BI (New England Biolabs), and ligated into pE-6xHis-SUMO (LifeSensors) for *E. coli* expression and protein purification. CaCl2-competent BL21(DE3) *E. coli* were transformed, grown overnight on lysogeny broth-kanamycin plates, and single-cell colonies were inoculated in 1 L 2x YT media with 50 μg ml $^{-1}$ kanamycin and grown at 37 °C until ∼A600 nm=0.8. Cells were then induced with 0.5 mM isopropyl-β-D-thiogalactoside and grown at 16 °C overnight for protein expression. Cells were centrifuged and resuspended in 30 ml of ice-cold lysis buffer (300 mM NaCl, 50 mM Tris-HCl, 20 mM imidazole, 200 μg ml^{-1} RNase A, 100 μg ml $^{-1}$ lysozyme, cOmplete EDTA-free protease inhibitor, pH 7.4). Cells were incubated on ice for 30 min, then lysed by pulse sonication twice for 2 min in an ice water bath (Branson Sonifer). Lysed cells were spun down at 13,000gfor 30 min to remove debris. The supernatant was added to 2 ml of Ni-NTA agarose beads (QIAGEN) and incubated at 4 °C for 30 min with gentle rocking. Beads were then washed twice with 10 ml of wash buffer

(300 mM NaCl, 50 mM Tris-HCl, 40 mM imidazole, pH 7.4). Bound protein was eluted twice with 500 μl of elution buffer (300 mM NaCl and 250 mM imidazole).

Recombinant purified proteins were mixed with 2x reducing sample buffer (100 mM Trish-HCl pH 6.8, 20% glycerol, 4% SDS, 5% β-mercaptoethanol, 0.05% bromophenol blue), run on 4-20% SDS-polyacrylamide gel electrophoresis (PAGE) gels, stained with Coomassie Brilliant Blue stain (40% methanol, 10% acetic acid, 0.1% Coomassie R-250), then quantified by densitometric analyses on ImageJ (https://imagej-nih-gov.ezp1.lib.umn.edu/ij/) using BSA as a standard. A3 proteins were titrated to achieve equivalent enzymatic cleavage of a fluorescent oligo substrate (RSH5194 5'-ATT ATT ATT ATT CAA ATG GAT TTA TTT ATT TAT TTA TTT ATT T-fluorescein-3') by mixing together 1 μl recombinant A3, 1 μl 10.7 μM oligo, 0.5 μl 1 mg ml^{-1} RNase, 0.025 μl UDG (New England Biolabs), and 7.47 μl modified 2-hydroxyethyl disulfide (HED) buffer (20 mM HEPES, 50 mM NaCl, 0.1 mM EDTA, 0.1 mg ml^{-1} BSA, pH 7.4) and incubating at 37 °C for 30 min; 1 μl of 1.1 M NaOH (100 mM final) was then added and heated to 98 °C for 5 min to cleave the DNA at abasic sites. The reaction was then mixed with 11 μl 2x formamide buffer (80% formamide, 1x Tris/borate/EDTA (TBE), bromophenol blue, and xylene cyanol) and run on a 15% TBE-urea PAGE gel. Separated DNA fragments were visualized on a Typhoon FLA 7000 scanner on fluorescence mode (GE Healthcare). A3 deaminase activity was quantified by densitometric analyses on ImageJ by dividing product band intensity by the sum of product and substrate band intensities. Approximately equivalent deaminase activity was achieved at 350 nM A3Bctd and 80 nM A3H. Recombinant proteins were then diluted to specified concentrations in HED buffer; 5 μl of recombinant BORF2 was equilibrated with 2 μl of A3 proteins for 15 min and added to 3 μl of an oligo master mix containing 1 μl of 10.7 μM fluorescent oligo, 0.5

μl 1 mg ml^{-1} RNase, 0.025 μl UDG (New England Biolabs), and 1.475 μl HED buffer for a total reaction volume of 10 μl, which was incubated at 37 °C for 30 min. The deaminase activity assay then proceeded as stated earlier.

Normalized percentage A3 deaminase activity was calculated for n=3 independent biological replicates by defining 100% deaminase activity as the no BORF2 condition for both A3Bctd and A3H. Normalized percentage activities were averaged and standard deviations were calculated. Assuming normal data distributions, one-tailed one sample t-tests were performed at each concentration of BORF2 to determine if mean A3Bctd or A3H deaminase activity differed from the null hypothesis μ=1 (100% activity) with the alternative hypothesis μ<1, d.f.=2. P values for A3Bctd are as follows for the following concentrations of BORF2: P=0.0237 at 43.75 nM; P=0.00206 at 87.5 nM; P=9.56*10^{-5}at 175 nM; P=2.51*10^{-6} at 350 nM; P=2.685*10^{-5} at 700 nM). P values for A3H are P=0.970 at 43.75 nM; P=0.816 at 87.5 nM; P=0.424 at 175 nM; P=0.440 at 350 nM; P=0.1575 at 700nM.

MG132 experiments

Semi-confluent HEK293T cells were transfected with 100 ng of each indicated plasmid and 1.8 μl TransIT-LT1 transfection reagent in 100 μl serum-free Opti-MEM in 6 wells. After 42 h post-transfection, media was removed and replaced with fresh media containing 10 μM MG132 (Sigma-Aldrich) or dimethylsulfoxide control. Cells were collected after 4 h of MG132 treatment, washed twice with PBS, and analysed by immunoblot. Antibodies used included rabbit polyclonal anti-c-Myc 1:3,000 (Sigma-Aldrich), rabbit anti-HA, mouse anti-FLAG 1:5,000, and mouse anti-tubulin 1:10,000.

Immunofluorescence microscopy

For immunofluorescence imaging of endogenous proteins, AGS-EBV or BORF2-null

AGS-EBV cells were grown on acid-washed and poly(lysine)-treated 22x22x1.5 mm3 coverslips (Fisherbrand, Thermo Fisher Scientific) until they reached 80% confluency. Cells were either left untreated (latent infection samples) or treated with 20 ng ml $^{-1}$ TPA and 3 mM sodium butyrate (NaB) for 8, 16, or 24 h to reactivate the virus into the lytic cycle. Coverslips were then washed with PBS, fixed in 4% methanol-free formaldehyde (Thermo Scientific Scientific) for 15 min, and rinsed three times for 5 min in PBS with gentle rocking. Cells were permeabilized with 0.2% Triton X-100 in PBS for 10 min, washed three times for 5 min in PBS, then blocked overnight in 5% BSA. Cells were incubated with rabbit anti-A3B 1:1,000 (5210-87-13)[270] and mouse anti-BORF2 1:400 (Santa Cruz Biotechnology) in AGS-EBV cells, or mouse monoclonal anti-BMRF1 1:400 (Merck Millipore) in BORF2-null AGS-EBV cells to indicate reactivated cells for 48 h in a humid chamber at 4 °C. Coverslips were washed three times with PBS, followed by incubation with secondary antibodies, goat anti-rabbit polyclonal Alexa Fluor 488 1:1,000 (Thermo Fisher Scientific) or donkey anti-mouse polyclonal Alexa Fluor 647 1:1,000 (Thermo Fisher Scientific) in 5% BSA for 1 h. After washing in PBS, coverslips were mounted onto slides using ProLong Gold antifade mountant (Thermo Fisher Scientific) containing 4',6-diamidino-2-phenylindole. Images were captured using the 40x oil objective on a Leica inverted fluorescence microscope and analysed with the Leica Application Suite X (version 3.3.0) software. For each TPA/NaB-treated sample, 50 reactivated cells were analysed for colocalization of BORF2 and A3B. For latent AGS-EBV cells and reactivated cells containing the BORF2 knockout virus, the overall localization of A3B was scored for 50 cells. For immunofluorescence of M81 cells, approximately $5*10^6$ cells were collected during log-phase growth. The immunofluorescence protocol then proceeded as stated earlier except for permeabilization in 0.5% instead of 0.2% Triton X-100 and primary antibody incubation for 24 h in constant rotation at 4 °C.

For EdU staining of AGS-EBV, cells were grown on coverslips until they reached 80% confluency. Cells were then treated with 10 μM EdU (Thermo Fisher Scientific) for 1 h before collection and fixed in 4% formaldehyde followed by washing in PBS, permeabilization in 0.5% Triton X-100, and blocking in 5% BSA for 1 h. Staining of EdU was done according to the manufacturer's protocol. Cells were incubated with rabbit anti-A3B 1:1,000 (5210-87-13)[270] and mouse monoclonal anti-BMRF1 (Merck Millipore) 1:1,000 antibody for 48 h in a humid chamber. The immunofluorescence protocol then proceeded as stated earlier. For immunofluorescence imaging of transfected cells, HEK293T, HeLa, or AGS cells were plated on coverslips and, after 24 h, transfected with 200 ng pcDNA4-BORF2-3xFLAG, 200 ng pcDNA5/TO-A3B-eGFP, or both. After 48 h, cells were collected, fixed in 4% formaldehyde, and permeabilized in 0.2% Triton X-100 as stated earlier. Cells were then incubated in blocking buffer (0.0028 M KH2PO4, 0.0072 M K2HPO4, 5% Gibco goat serum (Thermo Fisher Scientific), 5% glycerol, 1% cold water fish gelatin (Sigma-Aldrich), 0.04% sodium azide, pH 7.2) for 1 h. Cells were then incubated in blocking buffer with primary mouse anti-FLAG 1:1,000 antibody for 2 h to detect BORF2-FLAG. Cells were washed three times for 5 min with PBS then incubated in secondary antibodies diluted in blocking buffer for 1 h at room temperature with goat anti-mouse Alexa Fluor 594 1:1,000 antibody in the dark. Cells were then counterstained with 1 μg ml^{-1} Hoechst 33342 for 10 min, rinsed twice for 5 min in PBS, and once in sterile water. Coverslips were mounted on pre-cleaned slides (Gold Seal Rite-On; Thermo Fisher Scientific) using one drop (10-15 μl) of mounting medium (dissolve 1 g n-propyl gallate (Sigma-Aldrich) in 30 ml glycerol overnight, add 0.35 ml 0.1 M KH2PO4, then pH to 8-8.5 with K2HPO4, quantum satis to 50 ml with water). Slides were imaged on a Nikon Inverted Ti-E Deconvolution Microscope and analysed with NIS Elements (Nikon).

For the KSHV ORF61 experiments, HEK293T and AGS cells were transfected with 500 ng pcDNA5/TO-A3B-eGFP, 500 ng pCMV3F-ORF61, or both. After 48 h, cells were collected, fixed in 3.7% formaldehyde, and permeabilized in 0.2% Triton X-100 as stated earlier. Cells were then blocked in 5% BSA and incubated for 1 h. Cells were then incubated with mouse anti-FLAG 1:1,000 antibody for 2 h; then, the immunofluorescence protocol proceeded as stated earlier. Cell images were taken with a Leica inverted fluorescence microscope and analysed with the Leica Application Suite X software.

For the live cell imaging experiments, HEK293T cells were transfected with pLenti6/TR (Thermo Fisher Scientific), gag/pol polyprotein, and vesicular stomatitis virus G (VSV-G) protein to produce lentivirus- expressing TR. Other HEK293T cells were transfected with MLV-based pQCXIP-BORF2-eGFP, MLV gag/pol polyprotein, and VSV-G to produce lentiviral expression for BORF2-eGFP transduction. U2OS cells were first transduced with pLenti6/TR; after 48 h, the virus was washed off and cells were selected with 5 μg ml^{-1} blasticidin S for 2 weeks. Limiting dilution was used to generate single-cell clones and screened for TR expression and gene repression. U2OS-TR cells were then transfected with pcDNA5/TO-A3B-mCherry and put under 200 μg ml^{-1} hygromycin selection. After 2 weeks, the limiting dilution was used to generate a second generation of single-cell clones and screened. U2OS-TR-A3B-mCherry cells were plated on coverslips in 6-well plates for live cell imaging. A3B-mCherry expression was induced after 24 h with 10 ng ml^{-1} doxycycline, and then transduced with pQCXIP-BORF2-eGFP lentivirus 24 h after induction. One hour after transduction, cells were imaged on a Nikon BioStation IM machine every 15 min for 48 h. Images were analysed and stitched into a movie using NIS Elements. In the reciprocal experiment, U2OS-TR-A3B-mCherry cells were plated

and transduced with pQCXIP BORF2-eGFP; after 24 h, they were induced with 10 ng ml^{-1} doxycycline. Image acquisition began 1 h after A3B-mCherry induction as previously stated.

For immunofluorescence imaging of BiP, U2OS-TR-A3B-mCherry cells were plated on coverslips and induced with 10 ng ml^{-1} doxycycline for A3B-mCherry expression and transduced with pQCXIP-BORF2-eGFP lentivirus. After 48 h, cells were fixed and blocked as stated earlier and stained with rabbit polyclonal anti-GRP-78 BiP 1:1,000 antibody (Abcam) overnight to detect the endoplasmic reticulum. Cells were washed three times for 5 min each with PBS then incubated in goat anti-rabbit Alexa Fluor 647 1:1,000 diluted in blocking buffer for 1 h at room temperature in the dark. The immunofluorescence protocol then proceeded as stated earlier for the transfected proteins. Slides were imaged on a Nikon Inverted Ti-E Deconvolution Microscope and analysed with NIS Elements, including deconvolution of images. For 3D reconstruction of the endoplasmic reticulum experiments, z-stacks were captured every 0.6 μm throughout the entire cell depth. Deconvolution was performed for each z-stack; then, a movie of the 3D reconstruction was generated using NIS Elements (**Supplementary Section 2.7 1** [30]). For endoplasmic reticulum colocalization with TRAP, reactivated AGS-EBV cells were stained with primary mouse anti-BORF2 1:400 antibody, rabbit anti-TRAP 1:1,000 antibody, or both for 1 h (gift from Alexander Palazzo [281]); then, the immunofluorescence protocol proceeded as stated earlier. z-stacks were captured every 0.3 μm throughout the entire cell depth and stitched together into a z-series movie (**Supplementary Section 2.7 2** [30]).

Generation of BORF2-null EBV with CRISPR-Cas9

gRNAs targeting BORF2 were generated using the CRISPR Design Tool (http://crispr.mit.edu.ezp1.lib.umn.edu/). Oligonucleotides were purchased from

Integrated DNA Technologies and cloned into a pLentiCRISPR-*loxP* vector (see DNA constructs section). HEK293T cells were transfected with pLentiCRISPR, gag/pol polyprotein, and VSV-G. The supernatant containing the knockout lentivirus was collected after 48 h and used to transduce AGS-EBV, AGS-EBV(Bx1g), or Akata B cells. After 48 h, lentivirus was washed off and cells were subjected to antibiotic selection with media supplemented with 1 μg ml^{-1} puromycin for 4 weeks. Pooled cells were screened for successful BORF2 knockout from EBV genomes by immunoblot with mouse anti-BORF2 1:1,000 antibody. Sanger sequencing was completed on viral genomic DNA collected from BORF2-null AGS-EBV(Bx1g) cells (**Supplementary Figure S2.4**). To generate a clonal AGS cell line with isogenic BORF2-null EBV(Bx1g), described in this article as AGS-EBV(Bx1g)ΔBORF2, pooled cells were supplemented with exogenous deoxy-nucleoside monophosphates (dAMP/dCMP/dGMP/dTMP, each 400 μM) for 72 h and then induced with 3 mM sodium butyrate and 20 ng ml^{-1} TPA to produce EBV particles. After 48 h, the virus-containing supernatant was collected, filtered, and ultra-centrifuged at 22,000 r.p.m. for 2 h to obtain the concentrated cell-free, BORF2-null EBV stock. This virus stock was used to infect non-EBV-infected AGS cells at various empirically determined dilutions. Virus was washed off after 48 h and AGS cells were subjected to antibiotic supplementation with 0.4 mg ml^{-1} G418 for 2 weeks to select for successful EBV infection. These EBV-infected AGS cells were split into 96-well plates to obtain single-cell colonies by limiting dilution. Colonies were then screened for BORF2-null virus infection by immunoblot. Knockout clones were screened for successful isogenic EBV infection using Sanger sequencing (n>10 sequences per clone). The isogenic AGS-EBV(Bx1g)ΔBORF2 clone used in the current study has a 1,426 bp deletion spanning nucleotides +88 to +1,514 relative to the start codon.

Complementation, shRNA knockdown, and UGI experiments

HEK293T cells were transfected with MLV-based pQCXIP-BORF2-FLAG or empty pQCXIP vector, MLV gag/pol polyprotein, and VSV-G to produce complementation lentivirus. Other HEK293T cells were transfected with pLKO constructs expressing A3B-targeting shRNA or control non-targeting shRNA, gag/pol polyprotein, and VSV-G to produce knockdown lentivirus. Other HEK293T cells were transfected with pLenti4-UGI or empty pLenti4 vector, gag/pol polyprotein, and VSV-G to produce UGI lentivirus. The AGS-EBV(Bx1g)ΔBORF2 clone was first transduced with BORF2 or control complementation lentivirus. After 48 h, virus was washed off and cells were selected with 1 μg ml^{-1} puromycin for 2 weeks. These cells were then transduced with either A3B or control knockdown lentivirus. After 48 h, virus was washed off and cells were selected with 5 μg ml^{-1} blasticidin S for 2 weeks. These cells were then transduced with either UGI or control treatment lentivirus; 48 h after transduction, virus was washed off and split into two arms for either virus induction with TPA/NaB or mock induction. After 48 h of lytic reactivation, DNA and protein were collected and analysed by 3D-PCR or immunoblot, respectively.

Generation of AGSΔUNG2 cell line with CRISPR-Cas9

gRNAs targeting human UNG2 were generated using the CRISPR Design Tool. Oligonucleotides were purchased from Integrated DNA Technologies and cloned into a pLentiCRISPR-*loxP* vector. HEK293T cells were transfected with pLentiCRISPR-*loxP*, gag/pol polyprotein, and VSV-G. The supernatant containing the knockout lentivirus was collected after 48 h and used to transduce AGS cells. After 48 h, lentivirus was washed off and cells were subjected to antibiotic selection with media supplemented with 1 μg ml^{-1} puromycin for 2 weeks. Limiting dilution was then used to generate single-cell clones, which were screened for successful UNG2 knockout by

immunoblot and UDG (BKRF3) activity. Antibodies used included rabbit anti-UNG2 1:1,000 (gift from Sal J. Caradonna, Rowan University) and anti-tubulin 1:10,000.

UDG activity assays

AGS or AGSΔUNG cells were transfected with 1 μg BKRF3 or vector control using 3 μl TransIT-LT1 in serum-free RPMI. Cells were collected after 30 h and lysed in 300 μl modified HED buffer (20 mM HEPES, 15 mM EDTA, cOmplete EDTA-free protease inhibitor cocktail tablet, pH 7.4) per 106 cells. Activity assays were carried out as described12 using a 10 min incubation with a dU-containing oligonucleotide (RSH12955 5'-AAA AAA AAA UCG GGA AAA AAA-fluorescein-3'); 2 μl of UGI (4 units; New England Biolabs) were used to inhibit UDG. Products were separated by a 20% TBE-Urea PAGE. Separated DNA fragments were visualized on a Typhoon FLA 7000 scanner on fluorescence mode.

3D-PCR and sequencing

Total genomic DNA was collected from cells using the Gentra Puregene Cell Kit (QIAGEN). Genomic DNA was used as a template for first-round PCR with ChoiceTaq DNA polymerase (Denville) using the manufacturer's protocol with primers for BRRF2 (5'-GTA GCA TCT CTG TCT GGT GAC CTT GAA-3' and 5'-TTT TGG GGT CTC CGG ACA CCA TCT CTA-3') and EBNA2 (5'-TAA CGT GCA AGA CGC TAA ACT TAA CCA A-3' and 5'-AGC CTC GGT TGT GAC AGA GGT GAC AA-3'). First-round PCR products were run on a 3% agarose gel by gel electrophoresis, normalized by densitometry, and then used for second-round PCR. Second-round PCR used Phusion High-Fidelity DNA Polymerase (New England Biolabs) using primers for BRRF2 (5'-AGG CCT GGC TTG AGG CTC AGG ACG CAA-3' and 5'-GAC ATG ATT CAC ACT AAA AGA GAT CAA-3') and EBNA2 (5'-ACA ATC TTT GTT GGG GAA AAC ACG GGG G-3' and 5'-

CGT CAT ATC CTA GCG GAT CCC TAT CAA-3'). The following PCR conditions were used for BRRF2 (87-91 °C melting, 60 °C annealing, 72 °C extension) and EBNA2 (84-88 °C melting, 60 °C annealing, 72 °C extension). Second-round PCR products were run on a 3% agarose gel and the lowest-temperature PCR amplicons were gel-extracted with the GeneJET Gel Extraction Kit (Thermo Fisher Scientific), blunt-end cloned with the CloneJET PCR Cloning Kit (Thermo Fisher Scientific), and transformed into CaCl2-competent DH10B *E. coli*. Single-cell colonies were picked for colony PCR using Phusion High-Fidelity DNA polymerase with the primers provided by the manufacturer (5'-CGA CTC ACT ATA GGG AGA GCG GC-3' and 5'-AAG AAC ATC GAT TTT CCA TGG CAG-3'). PCR products were enzymatically purified using Exonuclease I (*E. coli*; New England Biolabs) and shrimp alkaline phosphatase (New England Biolabs) treatment. Sanger sequencing of purified PCR products used the 5'-AAG AAC ATC GAT TTT CCA TGG CAG-3' primer, sequenced by GENEWIZ (https://www.genewiz.com/), and results were analysed with the SnapGene software (http://www.snapgene.com/).

A3B genotyping

The PCR breakpoint assay to identify WT versus the 29.5 kb A3B deletion genotype was previously described26. Briefly, PCR primers within the *A3B* gene (blue arrows in **Supplementary Figure S2.13b**) generate a 490 bp PCR product while the primers flanking the A3A/B fusion (red arrows in **Supplementary Figure S2.13b**) generate a 700 bp PCR product.

Deep-sequencing analysis

The AGS-EBVΔBORF2 clone was complemented with a mock vector or BORF2-FLAG, and transduced with shCtrl or shA3B lentivirus. Genomic DNA was collected from cells 3 days after induction with TPA/NaB and portions of the EBV genome

were PCR-amplified using PfuTurbo Hotstart DNA Polymerase (Agilent). The PCR products correspond to regions near the genes *BRRF2* (95085-95584), *LMP1* (167979-168514), *BHRF1* (42090-42595), and *BcLF1* (124082-124598). Base numbers correspond to the Akata reference genome (GenBank accession number: KC207813), which was also used for both the assembly and variant calling described later. Primers were designed with Nextera-compatible adapter sequences: forward 5'-TCG TCG GCA GCG TCA GAT GTG TAT AAG AGA CAG-[locus-specific]-3' and reverse 5'-GTC TCG TGG GCT CGG AGA TGT GTA TAA GAG ACA G-[locus-specific]-3'. Locus-specific primers were designed as follows: BRRF2 (RSH15191 5'-ACC GTC CAG CAA AAA GGG-3' and RSH15192 5'-CCC CTT TGC AGC CAA TGC-3'); LMP1 (RSH15195 5'-CTG CCA CAC TAC CCT GAC-3' and RSH15196 5'-AGC CGC CAG AGA ATC TCC-3'); BHRF1 (RSH15205 5'-GTG TTG GAG CTA GCA GCA AGA G-3' and RSH15206 5'-CCG CAG GCC CAA TGA CCC-3'); and BcLF1 (RSH15207 5'-CCT GCT GGT GGG CAA GGA-3' and RSH15208 5'-AGA TGC CTC TTG AAC ATG GC-3'). The PCR products were enzymatically purified using Exonuclease I and shrimp alkaline phosphatase treatment. Illumina amplicon sequencing was performed at the University of Minnesota Genomics Center as a $\geq$16 million read, 2x 300 bp paired-end MiSeq v3 run. Sequences were aligned and assembled with the Burrows-Wheeler Aligner [282], GATK toolkit [283], Picard Tools (http://broadinstitute.github.io/picard/), and SAMtools [284, 285]. VarScan2 [286] was used to call variation compared to the Akata reference genome. SAMtools and R (http://www.R-project.org) were used for subsequent read and sequence filtering, processing, and visualization.

Viral infectivity assays

AGS-EBV(Bx1g) or BORF2-null cells were plated on ten 15 cm plates, each at equal

density, and grown until 70-80% confluency. Medium was then replaced with fresh RPMI containing 10% FBS, 1x penicillin-streptomycin, 20 ng ml^{-1} TPA, and 3 mM sodium butyrate to induce lytic reactivation (without G418). Cells were grown for 4 days and media was collected and centrifuged briefly to pellet cells; the resulting supernatant was passed through a 0.45 μm filter (VWR). Filtered supernatant was centrifuged at 25,000 r.p.m. for 2.5 h using a Beckman Coulter JLA-16.250 rotor at 4 °C in a floor model centrifuge. The supernatant was then removed and the bottle walls were washed extensively with PBS to remove residual TPA/NaB, taking care not to disturb the visible viral pellet. The virus pellet was then resuspended in 1 ml RPMI with 10% FBS and 1x penicillin-streptomycin; 19 μl concentrated virus was then mixed with 1 μl DNase (QIAGEN) and incubated at 37 °C for 10 min followed by 10 min of heat inactivation at 98 °C. A quantity of 1 μl DNase-treated virus was used to quantify viral titres in quadruplicate by RT-qPCR using a SsoFast EvaGreen Supermix (Bio-Rad) and the primer set for EBV gp350 (5'-GTC AGT ACA CCA TCC AGA GCC-3' and 5'-TTG GTA GAC AGC CTT CGT ATG-3'). Known quantities of EBV B98.5 bacterial artificial chromosome DNA were used as a standard curve (gift from Ya-Fang Chiu, Chang Gung University). Equal titres of viral DNA were then used to infect 50,000 Ramos cells in 200 μl in a 96-well plate. Fresh RPMI was used as mock infection. After 22 h, Ramos cells were collected, washed twice with PBS, resuspended in 200 μl PBS-EDTA, and analysed by flow cytometry.

Akata or Akata BORF2-null cells were grown in 400 ml media until a confluency of $\sim$1-2*10^6 cells ml^{-1}. Cells were pelleted and resuspended at a density of 4*10^6 cells ml^{-1} in 100 ml of RPMI with 10% FBS, 1x penicillin-streptomycin, and 6 μg ml^{-1} goat anti-human serum immunoglobulin G fraction (MP Biomedicals) to induce

lytic reactivation (without G418). After 2 days, the media volume was doubled with RPMI supplemented with 10% FBS and 1x penicillin-streptomycin. After 4 days post-induction, cells were briefly centrifuged to pellet cells; the resulting supernatant was passed through a 0.42 μm filter. Filtered supernatant was treated in a similar fashion to the one already described for the virus produced from the AGS-EBV cells. All infectivity studies were performed with at least two independent biological replicates for virus production, each quantified by n=3-4 independent reporter cell infections.

Flow cytometry

Analysis was done on a BD FACSCanto II system immediately after cell collection and completed within 1 h. Acquisition occurred for 75 s or until 10,000 cells were collected. Cells were gated on live cells using side scatter-area versus forward scatter-area; then, mock-infected cells were gated on GFP versus forward scatter-area to determine the threshold for the GFP-negative gates.

Bioinformatics analysis

EBV whole-genome sequences previously isolated from patient gastric adenocarcinoma and normal samples were analysed for evidence of APOBEC-related mutation [287]. Phylogenetic analyses were used to determine novel mutations that only occur once on an EBV sequence compared to all other whole-genome sequences in the data set (n=142). This phylogeny was constructed from an alignment to a consensus sequence using the MAFFT (v7) software (https://mafft.cbrc.jp/alignment/software/) and classified into a neighbour-joining tree using an Hasegawa-Kishino-Yano model [288]. All single base substitutions compared to an ancestral EBV sequence (GenBank accession number: NC_007605.1) were used to calculate the dN/dS ratios. Whole genomes for the Akata EBV strain (GenBank accession number: KC207813), rhesus lymphocryptovirus (GenBank

accession number: NC_006146.1), and murine herpesvirus 68 strain WUMS (GenBank accession NC_001826.2) were used for trinucleotide motif enrichment analyses (substrate 5'-TCA and product 5'-TTA) based on Markov modelling [29, 289]. Sliding window analyses across herpesvirus genomes were calculated using 15 kb windows and an overlapping interval rate of 1 kb. Smoothed fitted lines and 95% confidence intervals of these densities were calculated and plotted using the ggplot2 package in the R statistical environment (https://cran.r-project.org/web/packages/ggplot2/index.html).

Acknowledgements

We thank B. Anderson for technical advice and RT-qPCR data, Y.F. Chiu for sharing BAC EBV B95.8, H.-J. Delecluse for M81 transformed B cells, K. Hogquist and S. Dunmire for providing Akata cells, T. Ikeda and C. Richards for cell culture assistance, M. Sanders and staff at the University of Minnesota Imaging Center for assistance with fluorescence microscopy and live cell imaging, A. Serebrenik for the gRNA construct targeting UNG2, G. Starrett for technical programming advice, and R. Khanna, S. Rice, S. Simon, and P. Southern for thoughtful comments. This work was supported by NCI R21-CA206309 (RSH), the University of Minnesota (College of Biological Sciences, Academic Health Center, and Masonic Cancer Center to RSH), and Canadian Institutes for Health Research grant 153014 (to LF). NIH training grants provided salary support for AZC (F30 CA200432 and T32 GM008244) and MCJ (T32 CA009138). Salary support for JLM was provided by a National Science Foundation Graduate Research Fellowship. JY-M was funded by Secretaría Nacional de Educación Superior, Ciencia, Tecnología e Innovación (SENESCYT). LF is a tier 1 Canada Research Chair in Molecular Virology. RSH is the Margaret Harvey Schering Land Grant Chair for Cancer Research, a Distinguished University

McKnight Professor, and an Investigator of the Howard Hughes Medical Institute.

Author Contributions

AZC, JY-M, LF, and RSH conceived and designed the studies. AZC and JY-M performed the bulk of experimental work. NM-So, EM, and JG did AP-MS analyses. MCJ, MAC, JLM, NMSh, and WLB provided technical training and advice. JLM helped validate the BORF2-A3B interaction and MAC performed UDG experiments. AZC, IB, MCJ, and DE conducted bioinformatics analyses. AZC, JY-M, LF, and RSH drafted the manuscript, and all authors contributed to revisions.

Competing Interests

RSH is a co-founder, shareholder, and consultant of ApoGen Biotechnologies Inc. The other authors declare no competing interests.

Correspondence and requests for materials should be addressed to LF (lori.frappier@utoronto.ca) or RSH (rsh@umn.edu).

2.5 Figures

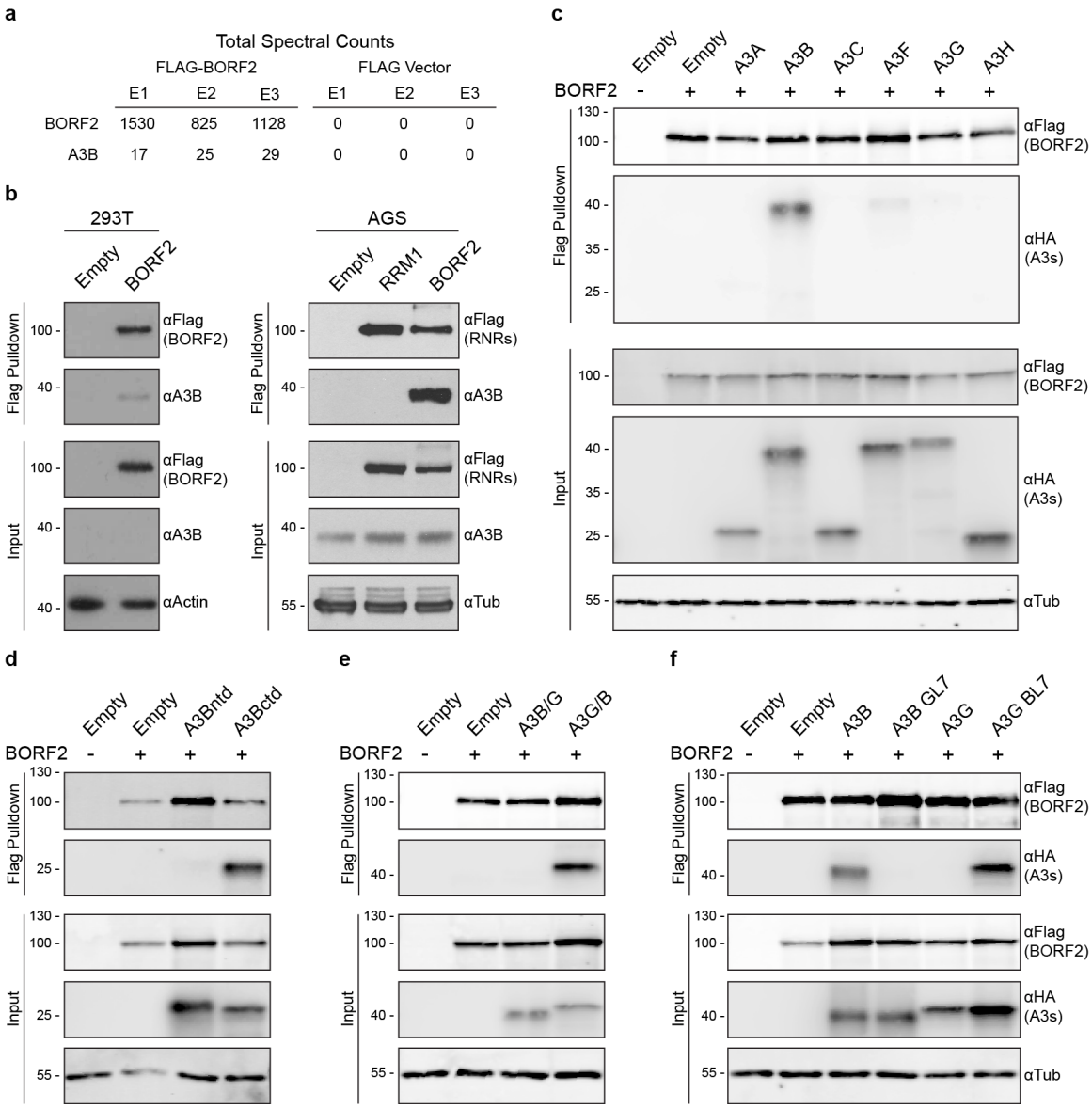

Figure 2.1: EBV BORF2 interacts with cellular A3B.
a, Total spectral counts from three independent affinity purification-mass spectrometry experiments using transfected BORF2-FLAG as bait and empty FLAG vector as negative control in HEK293T cells.
b, Co-immunoprecipitation of endogenous A3B in HEK293T and AGS cells with BORF2-FLAG, RRM1-FLAG, or an empty vector control.

Figure 2.1 (Continued):
c-f, Co-immunoprecipitation of indicated HA-tagged A3 constructs in HEK293T cells with BORF2-FLAG. Immunoblot labels (**b-f**) are provided in kDa. These data (**a-f**) are each representative of at least n=3 biologically independent experiments.

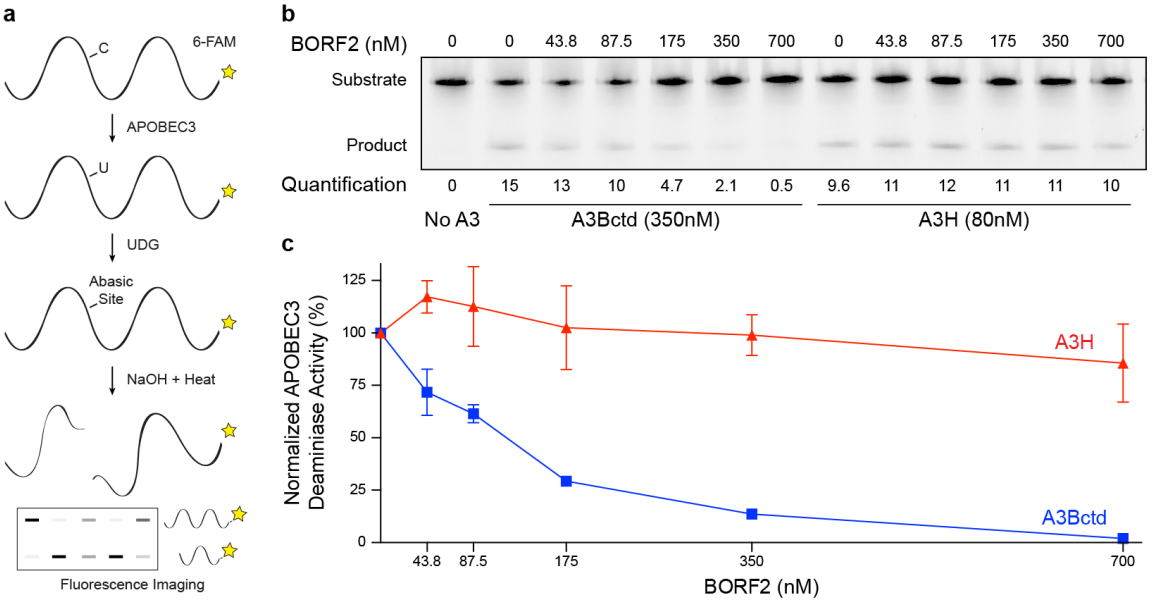

Figure 2.2: EBV BORF2 inhibits A3B catalytic activity specifically.
a, Schematic of deaminase activity assay in which A3-mediated deamination of cytidine-to-uridine in ssDNA substrate, uracil excision by UDG, and abasic site cleavage by sodium hydroxide (NaOH) treatment yields a shorter product (6-fluorescein amidite (6-FAM)-labelled for quantification by fluorescence scanning).
b, Representative TBE-urea PAGE analysis of A3Bctd and A3H deaminase activity in the presence of increasing concentrations of EBV BORF2 (product percentage indicated below each lane).
c, Quantification of the DNA deaminase activity data in panel b and two additional biologically independent experiments (normalized mean±s.d. with some error bars smaller than the symbols). These data (**b,c**) are representative of n=3 biologically independent experiments.

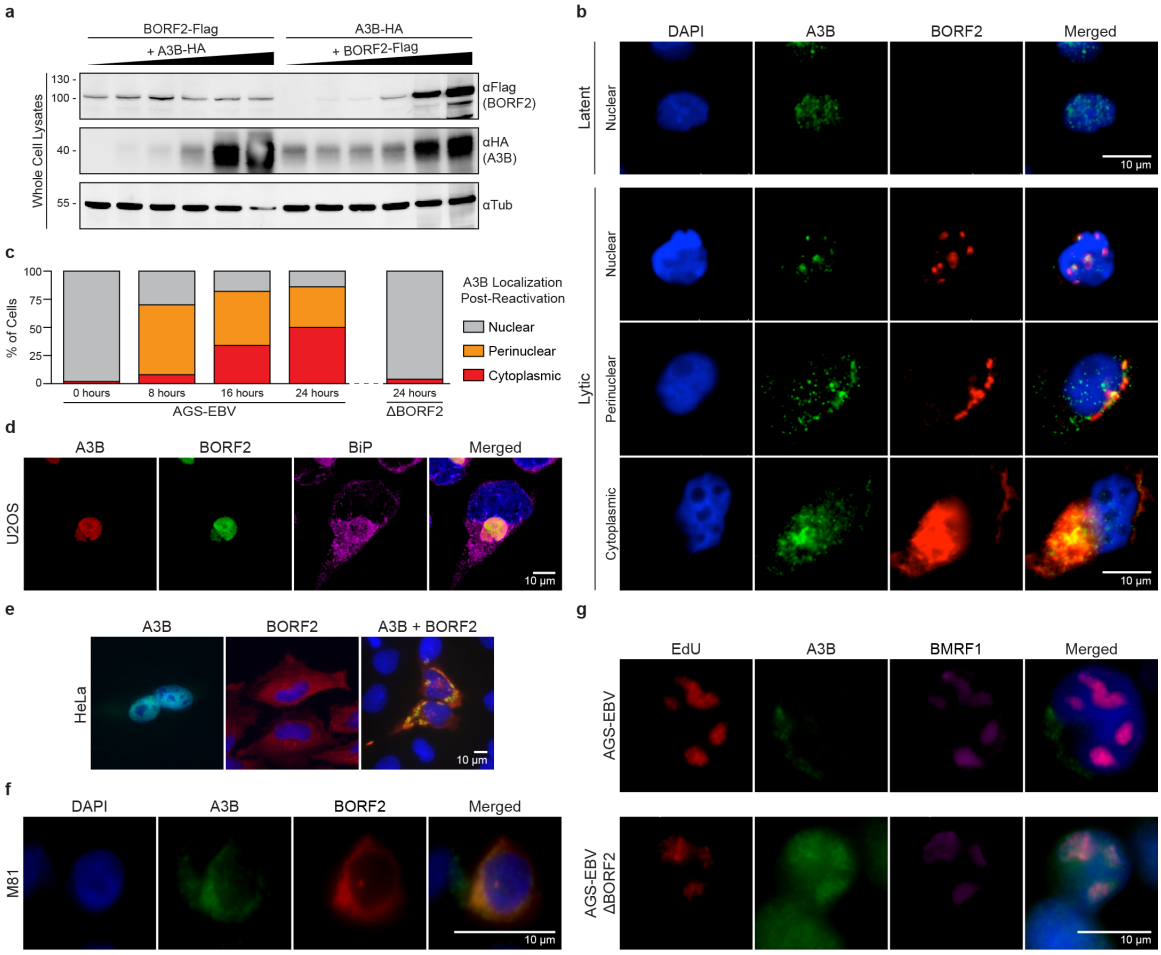

Figure 2.3: BORF2 relocalizes A3B from the nuclear compartment to the endoplasmic reticulum.

a, Immunoblots of lysates from HEK293T cells transfected with equal amounts of BORF2-FLAG and increasing amounts of A3B-HA (left) or the reciprocal set-up (right).

b, Representative immunofluorescence microscopy images of latent (top panel) or lytic (bottom three panels) AGS-EBV stained with 4,6-diamidino-2-phenylindole (DAPI, blue) and antibodies against endogenous A3B (green) or BORF2 (red).

c, Quantification of A3B localization in AGS-EBV cells grown under latent (0 h) or lytic (8, 16, 24 h) conditions (n=50 cells per condition). Parallel quantification of A3B localization in lytic BORF2-null AGS-EBV cells (24 h; n=50 cells).

Figure 2.3 (Continued):
d, Representative immunofluorescence microscopy images of U2OS expressing A3B-mCherry and BORF2-eGFP, and stained with an antibody against the endoplasmic reticulum protein, BiP/GRP-78 (purple; also see **Supplementary Section 2.7 1** [30]).
e, Representative immunofluorescence microscopy images of HeLa cells transiently expressing A3B-eGFP alone, BORF2-FLAG alone, or both proteins together.
f, Representative immunofluorescence microscopy images of endogenous A3B (green) and BORF2 (red) in a M81-transformed B cell that has spontaneously entered the lytic cycle.
g, Representative immunofluorescence microscopy images of endogenous A3B (green) in AGS-EBV and ΔBORF2 derivative pools 24 h after lytic reactivation. Anti-DNA polymerase processivity factor BMRF1 (purple) marks sites of viral DNA replication in lytic cells and EdU (red) shows newly synthesized DNA. These data are representative of n=2 (**a,d,f,g**) or n=3 (**b,c,e,f**) biologically independent experiments. Scale bars (**b,d-g**), 10 μm.

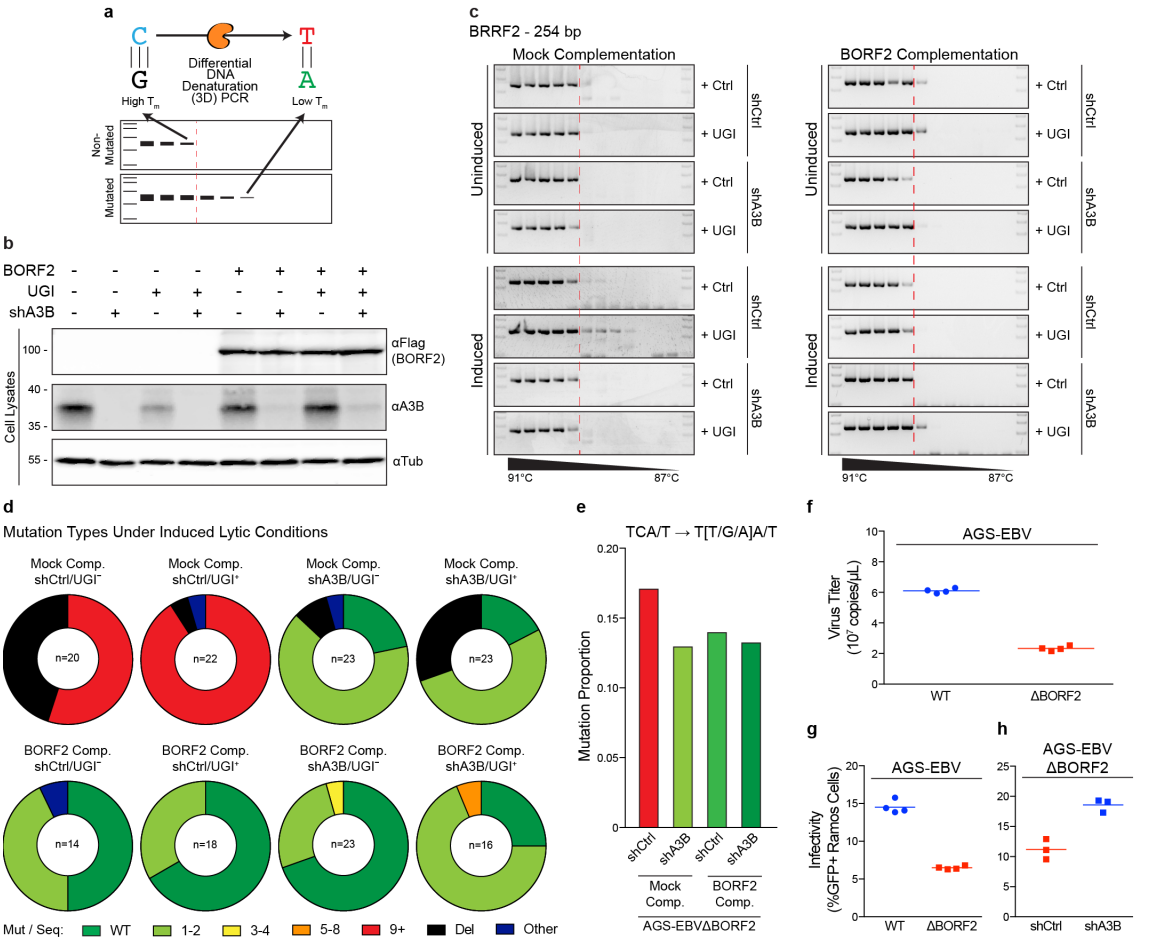

Figure 2.4: BORF2 functions to preserve EBV genome integrity from A3B.
a, 3D-PCR differentiates between non-mutated and mutated DNA substrates by virtue of product accumulation at higher versus lower denaturation temperature (T_m) thresholds (for example, A3B (orange enzyme) causes C/G-to-T/A mutations through uracil intermediates).
b, Immunoblots of an AGS-EBV(Bx1g)ΔBORF2 clone engineered to express BORF2-FLAG or vector control, shA3B or shCtrl, and UGI or vector control (see text for details).
c, Representative agarose gel images showing the results of 3D-PCR experiments involving a 254 base pair (bp) *BRRF2* gene segment of AGS-EBV(Bx1g)ΔBORF2. The dashed red line shows the point at which non-mutated BRRF2 DNA fails to amplify under high-denaturation conditions; visible PCR products below this T_m threshold represent lower-temperature amplicons (that is, mutated sequences). The right panels show the effect of complementing each condition with BORF2 expression.

Figure 2.4 (Continued):
d, Pie charts showing the types of mutational events observed in Sanger sequences of cloned lower T_m amplicons from the eight induced conditions shown in the bottom half of panel **c**. WT non-mutated sequences are depicted in green; base substitutions with the number of mutations per sequence are depicted in light green, yellow, orange, and red; deletions are depicted in black; other types of mutations (for example, combination of base substitution and deletion) are depicted in navy.
e, A summary of cytosine mutations detected in multiple EBV DNA regions under the indicated conditions following recovery by high-fidelity PCR (high T_m) and deep sequencing.
f, Titres of WT and ΔBORF2 viruses after lytic induction of AGS-EBV(Bx1g). Each symbol represents data from an independent culture (n=4); the horizontal line shows the mean.
g, Infectivity of WT and ΔBORF2 viruses produced by lytic replication in AGS-EBV(Bx1g). Each symbol represents the percentage of GFP-positive Ramos reporter cells from an independent infection (n=4); the horizontal line shows the mean.
h, Infectivity of ΔBORF2 EBV produced by lytic replication in AGS-EBV(Bx1g) with endogenous A3B intact (shCtrl) or depleted (shA3B). Each symbol represents the percentage of GFP-positive Ramos reporter cells from an independent infection (n=3); the horizontal line shows the mean. These data are representative of n=2 (**f,g**) or n=3 (**b,c,h**) biologically independent experiments.

2.6 Supplementary Figures

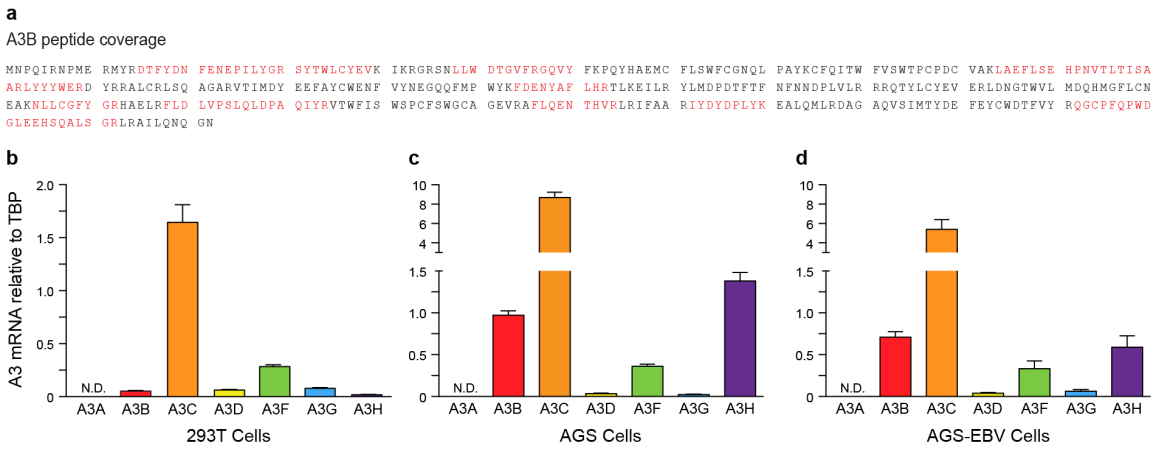

Supplementary Figure S2.1: AP-MS coverage and A3B expression in human cell lines used in these studies.

a, Amino acid sequence of A3B with residues highlighted in red de*Not*Ing total peptide coverage from **Figure 2.1a**.

b-d, mRNA expression levels of indicated A3 family members measured by RT-qPCR of (**b**) 293T, (**c**) AGS, or (**d**) AGS-EBV cells, normalized to housekeeping gene *TBP* (mean +/- SD of technical triplicate reactions, N.D., not detectable). These data are representative of n=2 (**c,d**) or n=3 (**a,b**) biologically independent experiments. RT-qPCR was performed in technical triplicates.

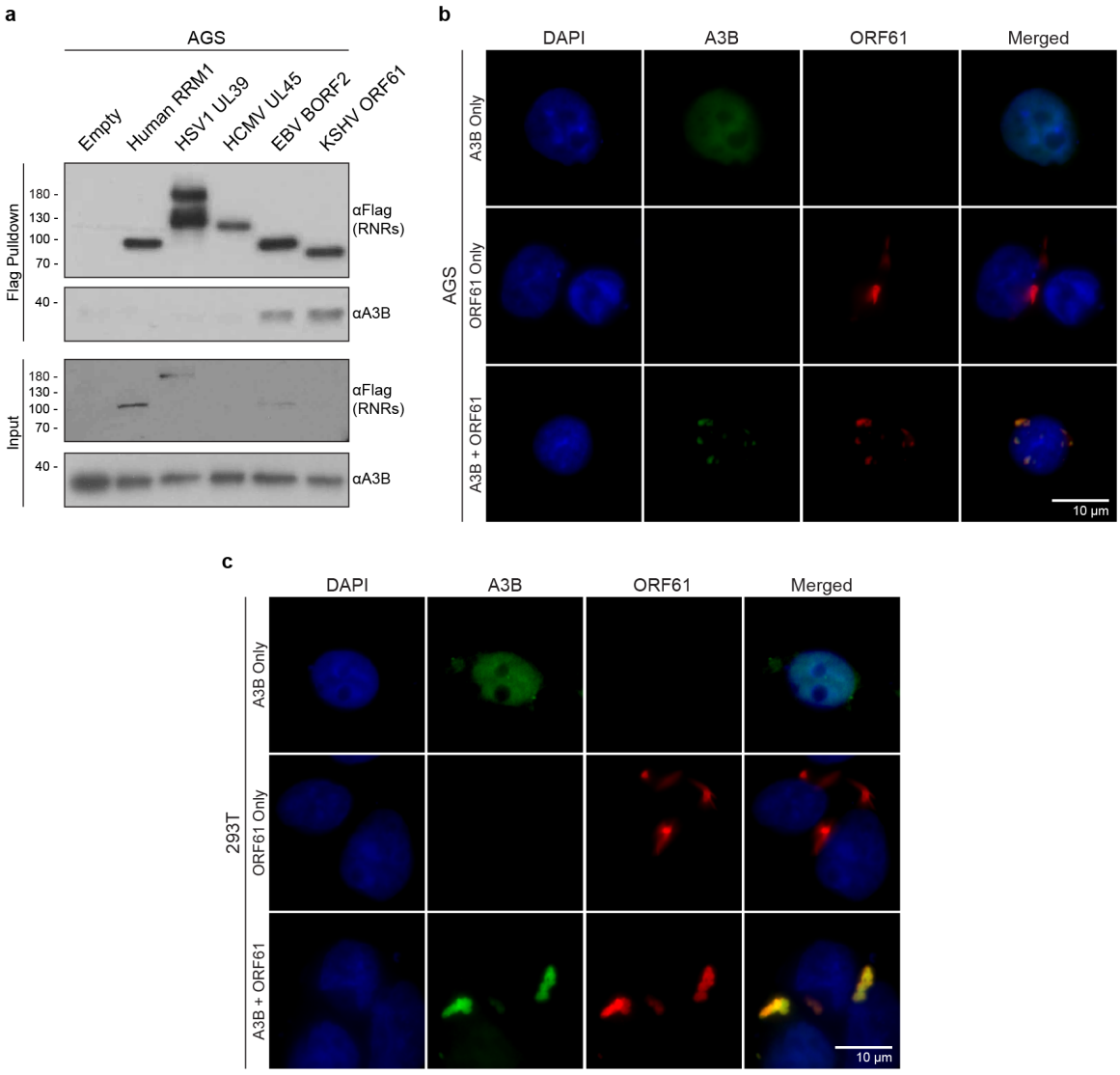

Supplementary Figure S2.2: KSHV ORF61 also binds A3B and relocalizes it to perinuclear regions.

a, Co-IP of endogenous A3B in AGS cells with indicated Flag-tagged RNRs. Several RNRs were expressed below detectable levels in whole cell extracts (despite clear detection after IP). Near-equivalent loading of each reaction was indicated by similar levels of endogenous A3B in the whole cell extract input immunoblot.

b-c, Representative fluorescent microscopy images of A3B-eGFP, ORF61-Flag, and the two proteins together in AGS and 293T cells, respectively. A 10 μm scale is shown in the merged panel images. These data are representative of n=2 (**b**), n=3 (**c**), or n=4 (**a**) biologically independent experiments.

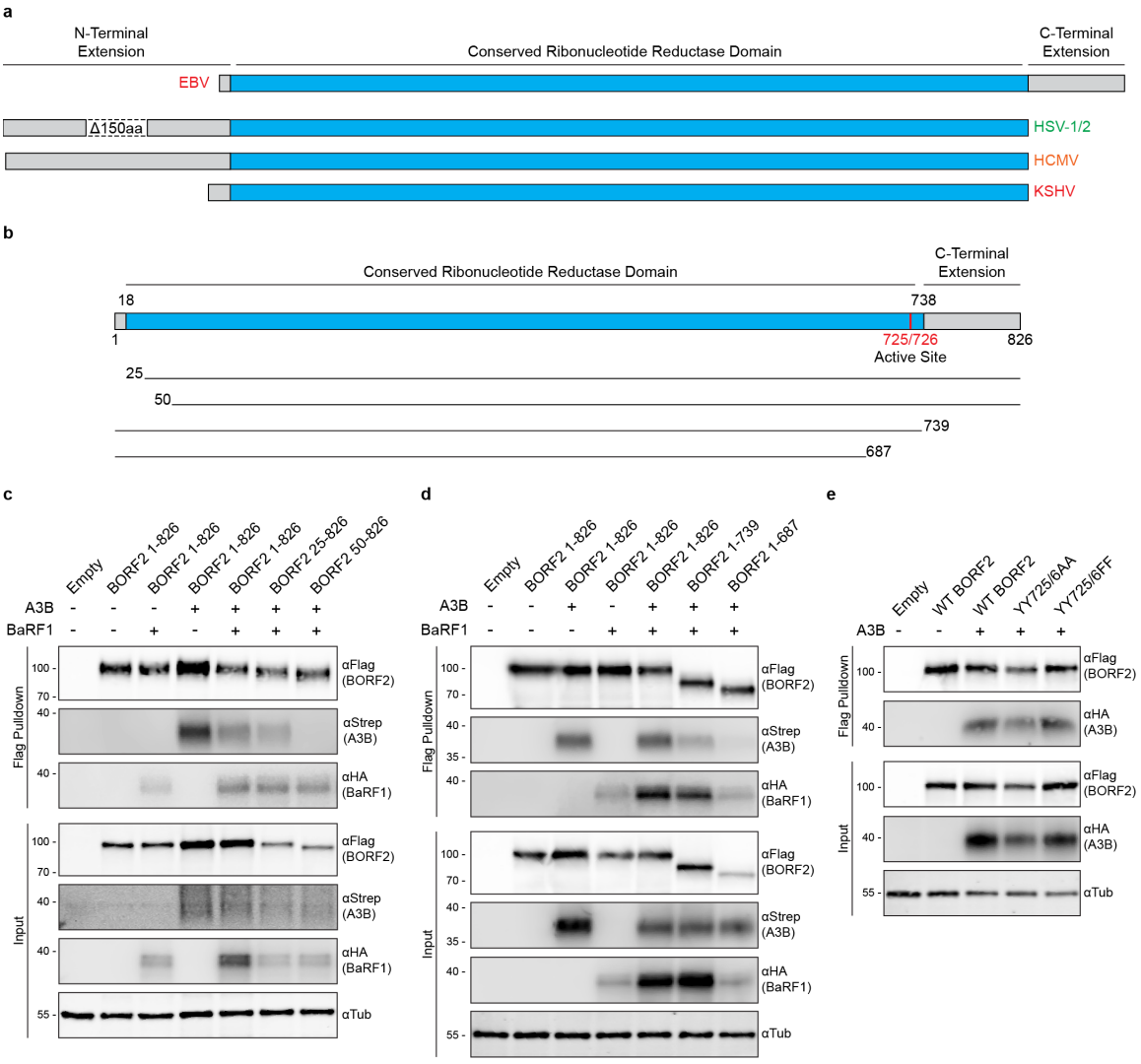

Supplementary Figure S2.3: The conserved RNR domain of EBV BORF2 is required for interaction with A3B.

a, Schematics of BORF2 and related RNRs from the indicated herpesviruses.

b, Schematics of BORF2 N- and C-terminal deletion mutants with residue positions indicated.

c, Co-IP results in which the indicated BORF2-Flag N-terminal deletion constructs were pulled-down from 293T cells co-expressing A3B-Strep and/or EBV BaRF1-HA. The BORF2 interaction with A3B requires BORF2 residues 26-50, whereas the interaction with BaRF1 does not.

d, Co-IP results in which the indicated BORF2-Flag C-terminal deletion constructs were pulled-down from 293T cells co-expressing A3B-Strep and/or EBV BaRF1-HA. The BORF2 interaction with A3B requires BORF2 residues 688-739, whereas the interaction with BaRF1 is less dependent on these residues.

Supplementary Figure S2.3 (Continued):
e, Co-IP results in which BORF2-Flag and the indicated catalytic mutant derivatives were pulled-down from 293T cells co-expressing human A3B-HA. These data indicated that the catalytic residues of BORF2 are dispensable for interacting with A3B. These data (**b-e**) are representative of n=3 biologically independent experiments.

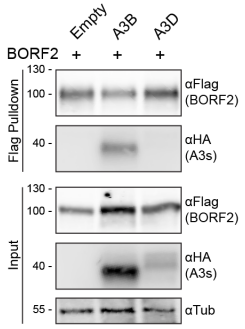

Supplementary Figure S2.4: BORF2 does not interact with A3D.
A co-IP experiment using BORF2-Flag to attempt to pull-down A3D-HA from 293T cell lysates. A reconstruction of the experiment in **Figure 2.1c** was necessary for A3D because it is expressed poorly relative to related A3 family members and required higher amounts of transfected DNA to achieve similar expression levels. These data are representative of n=3 biologically independent experiments.

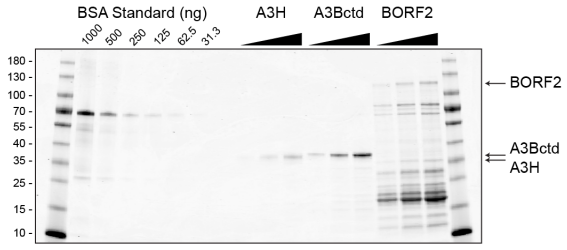

Supplementary Figure S2.5: *In vitro* purification of A3H, A3Bctd, and BORF2.

Coomassie stain of SDS-PAGE gel loaded with a BSA standard and aliquots of purified His-SUMO-A3H, His-SUMO-A3Bctd, and His-SUMO-BORF2 from *E. coli*. These proteins were used for deaminase activity assays in **Figure 2.2**. Arrows point to the intact epitope-tagged proteins. As for many EBV proteins, BORF2 was difficult to purify from *E. coli*, but these contaminants do not compromise the conclusions in **Figure 2.2** where even this relatively crude BORF2 preparation was able to specifically inhibit the activity of A3Bctd but not that of A3H. These data are representative of n=3 biologically independent experiments

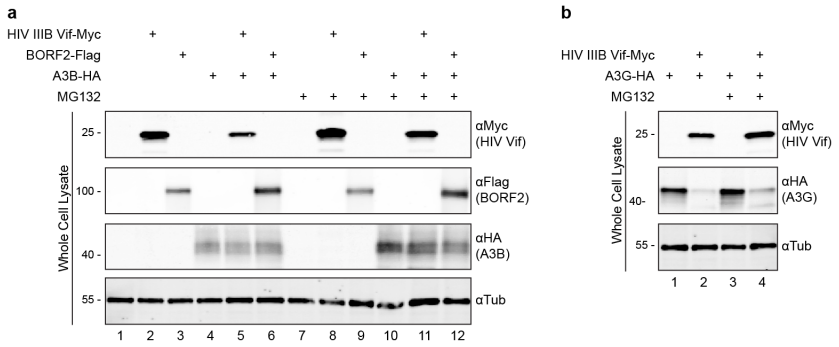

Supplementary Figure S2.6: A3B and BORF2 levels are unaffected by MG132 treatment.

a, Immunoblots of whole cell extracts from 293T cells co-transfected with constructs expressing A3B-HA, BORF2-Flag, and/or HIV-IIIB Vif-Myc. Cells were transfected and, after 42 hrs, treated for 4 hrs with 10 μM MG132 or vehicle control (DMSO), and harvested for immunoblotting. Neither HIV-Vif nor BORF2 caused a significant change in A3B protein levels.

b, Parallel immunoblot control experiment as in panel (a) except using A3G-HA (instead of A3B-HA). Expression of BORF2-Flag caused a proteasome-independent drop in cellular A3G levels (perhaps due to competition for ribosomes), whereas HIV-Vif caused the degradation of A3G through an established proteasome-dependent mechanism (compare band intensities in lanes 2 and 5). These data (**a,b**) are representative of n=3 biologically independent experiments.

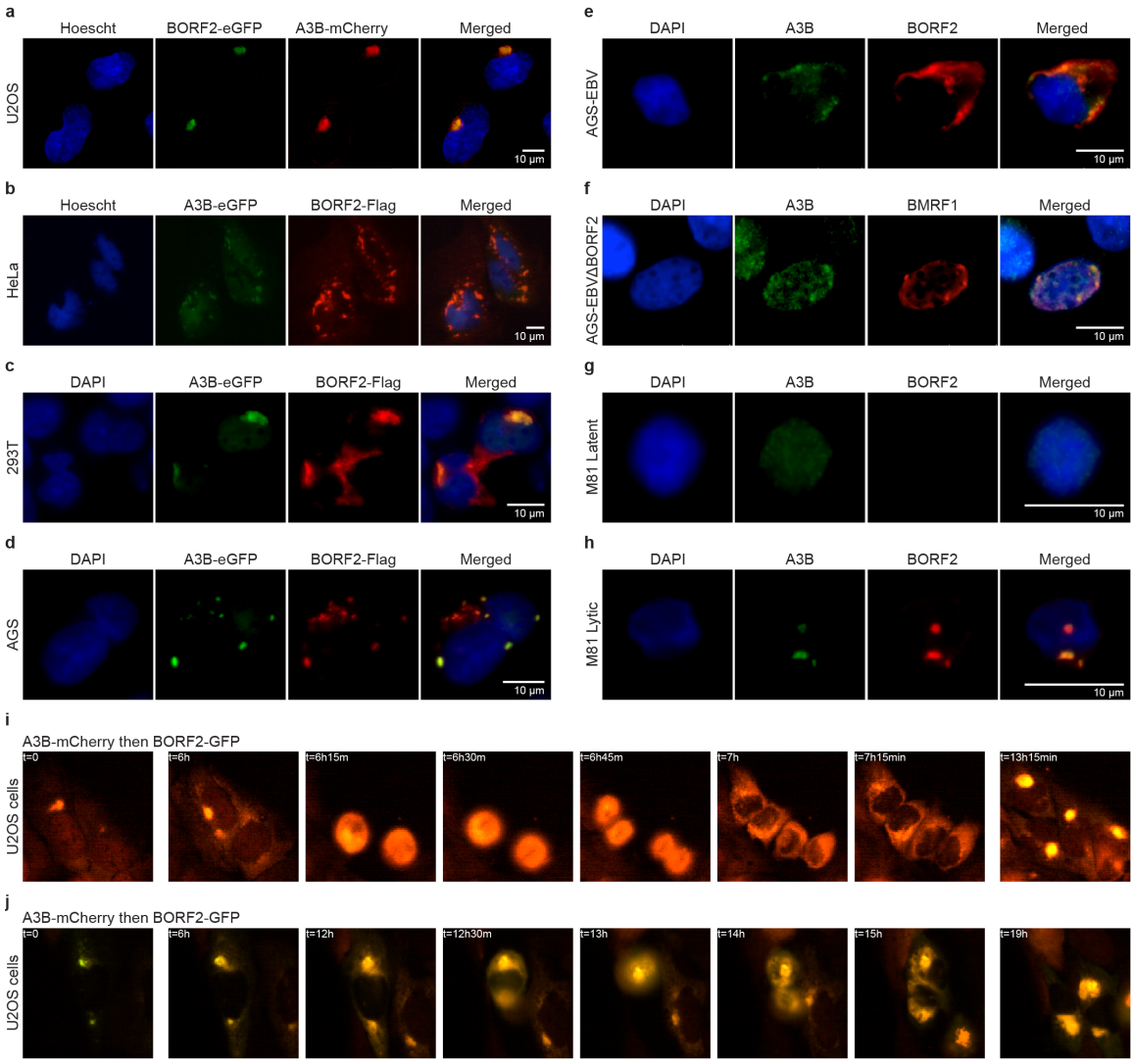

Supplementary Figure S2.7: Examples of BORF2 relocalization of A3B in multiple cell types.

a-h, Representative immunofluorescence microscopy images with the indicated proteins and cell lines. Panels (**a-d**) show transfected proteins with the indicated C-terminal tags. Panels (**e-h**) show endogenous proteins stained with antibodies.

i-j, Representative still images from live cell imaging experiments (**Supplementary Section 2.7 3** & **4**, respectively [30]). These data are representative of n=2 (**f-j**), n=3 (**a,b,d**), or n≥4 (**c,e**) biologically independent experiments.

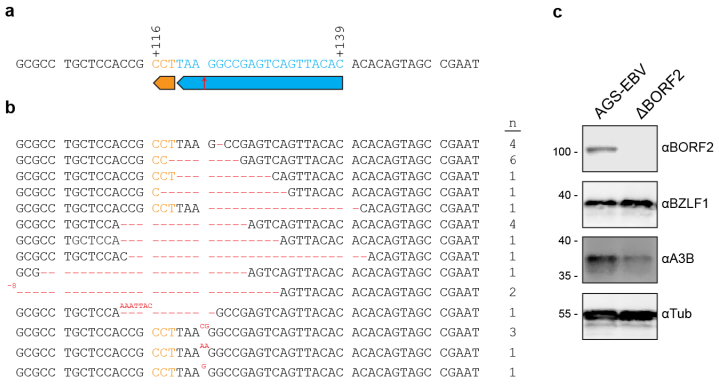

Supplementary Figure S2.8: Deletion of BORF2 in EBV episomes in AGS-EBV(Bx1g) and Akata.

a, Schematic of a portion of the *BORF2* gene targeted by Cas9 with gRNA complementarity shown in blue, PAM site shown in orange, and predicted endonuclease cut site shown by the red arrow (nucleotide numbers +116 and +139 are relative to BORF2 ATG codon).

b, Sanger sequences of the Cas9/gRNA targeted region of BORF2 PCR cloned from DNA purified from a pool of engineered AGS-EBV(Bx1g) cells. Only mutant sequences were recovered (some multiple times indicated by n), suggesting near complete knockout of BORF2 in the engineered pool.

c, Immunoblots of extracts from parental AGS-EBV(Bx1g) cells and the Cas9/gRNA engineered BORF2-null pool after lytic reactivation. BORF2 protein is undetectable in the engineered pool consistent with the sequencing data in (**b**). These data (**c**) are representative of n=3 biologically independent experiments.

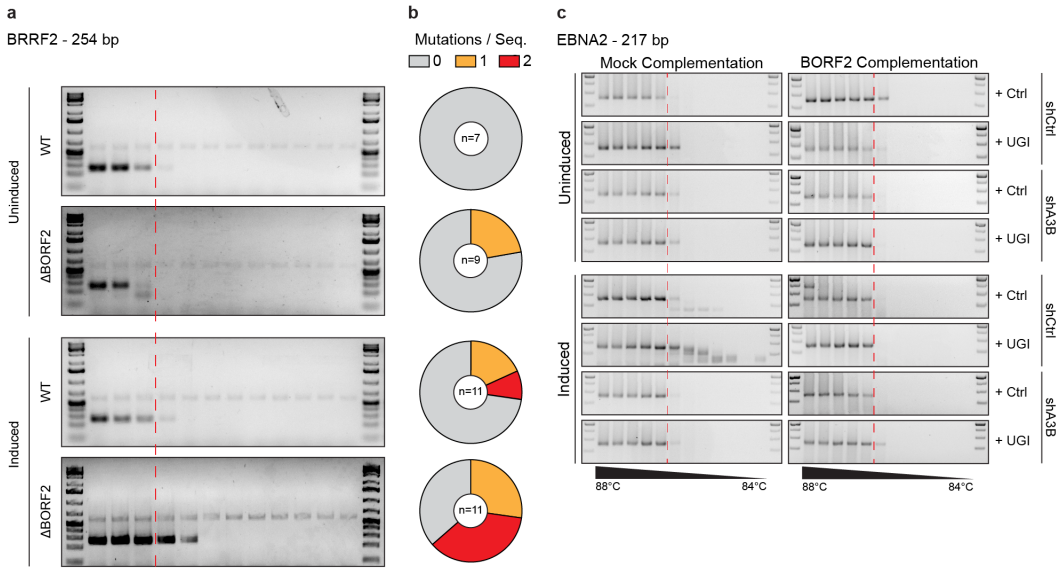

Supplementary Figure S2.9: BORF2 functions to preserve EBV genome integrity from A3B.

a, Representative images of agarose gels showing 3D-PCR results of the 254 bp *BRRF2* gene segment from pooled BORF2-null AGS-EBV(Bx1g) cells (**Supplementary Figure S2.7**).

b, Pie charts showing number of mutations observed in Sanger sequences of cloned lower temperature amplicons from (**a**). Wild-type non-mutated sequences depicted in gray and base substitutions shown in orange and red.

c, Agarose gel images of 3D-PCR results using the 217 bp *EBNA2* gene segment of derivatives of the AGS-EBV(Bx1g)ΔBORF2 clone. The 16 different conditions labeled below are described in the main text. The faster mobility, low-temperature products from conditions of induced cells, ΔBORF2, shControl, and UGI represent an accumulation of deletion mutations. These data (**a,c**) are representative of n=3 biologically independent experiments.

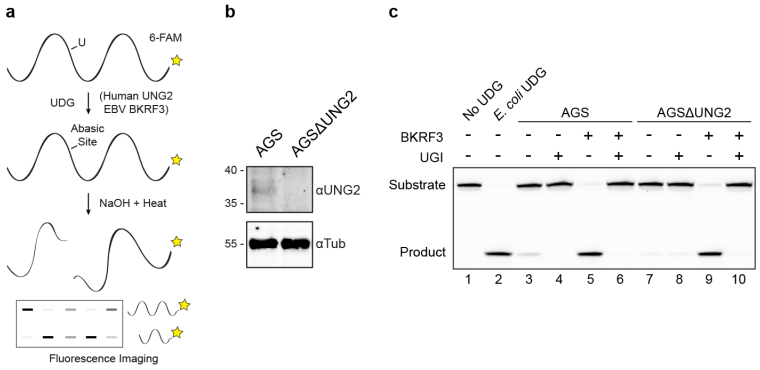

Supplementary Figure S2.10: UGI inhibits both cellular UNG2 and EBV uracil DNA glycosylase BKRF3.

a, Schematic of the uracil excision assay.

b, Immunoblot of whole cell lysates from AGS or AGSΔUNG2 cells.

c, Uracil excision experiment in which AGS or AGSΔUNG2 cells were transfected with a construct expressing viral uracil DNA glycosylase (BKRF3) and whole cell lysates were harvested after 30 hrs to test for uracil excision activity in the absence or presence of UGI (see **Section 2.4** for additional information). The uracil excision activity in AGS cells is mostly from cellular UNG2 and inhibited by UGI (compare product bands in lanes 3 vs 7 and 3 vs 4, respectively). BKRF3 expression causes a large increase in uracil excision activity that is almost completely inhibited by UGI (compare lanes 5 vs 6, and lanes 9 vs 10). Negative and positive controls are no UDG and exogenous E. coli UDG, respectively. These data are representative of n=2 (**b**) or n=3 (**c**) biologically independent experiments.

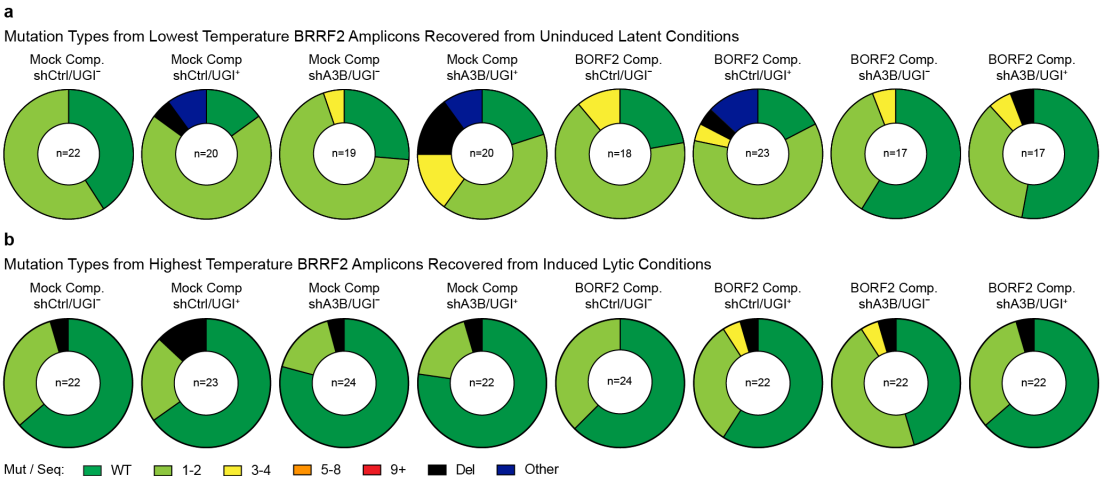

Supplementary Figure S2.11: Additional mutation data.
a, Pie charts showing mutational events observed in Sanger sequences of cloned lower temperature 3D-PCR *BRRF2* amplicons from the 8 uninduced conditions shown in **Figure 2.4c** (top half). Wild-type non-mutated sequences are depicted in green; base substitutions with numbers of mutations per sequence depicted in light green, yellow, orange, and red; deletions are depicted in black; other types of mutations (*e.g.*, combination of base substitution and deletion) are depicted in navy.
b, Pie charts showing mutational events observed in Sanger sequences of cloned highest temperature *BRRF2* amplicons from the 8 induced conditions shown in **Figure 2.4c** (bottom half). Color scheme as in panel (**a**). A low frequency of hypermutation is expected because lytic reactivation is inefficient (minority of cells in each culture), and EBV lytic replication occurs by coordinated leading- and lagging-strand DNA replication, which is not likely to leave single-stranded DNA exposed for long durations.

Supplementary Figure S2.12: Sanger sequences show massive A3B-dependent hypermutation of EBV lacking BORF2.
Sanger sequences of cloned lower temperature *BRRF2* 3D-PCR amplicons from the 16 different experimental conditions shown in **Figure 2.4c**. The parental wild-type (WT) *BRRF2* sequence is shown in blue (spanning nucleotides +1423 to +1629 relative to the *BRRF2* start codon). The pink highlighting shows base substitution mutations and deletion mutations (dashes) within the consensus region. The number of times each sequence was recovered is shown to the right.

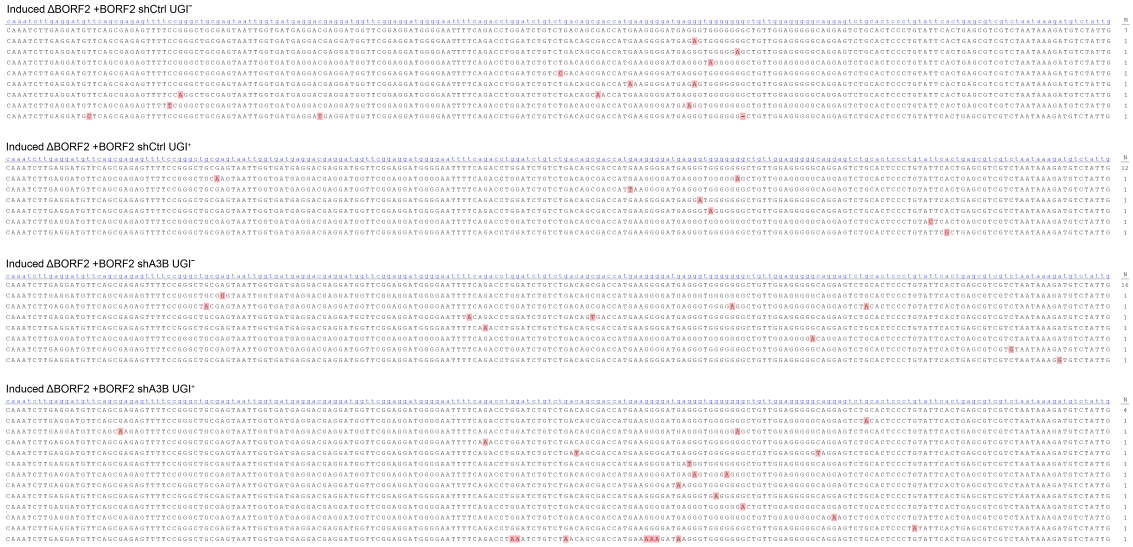

Supplementary Figure S2.12 (Continued):

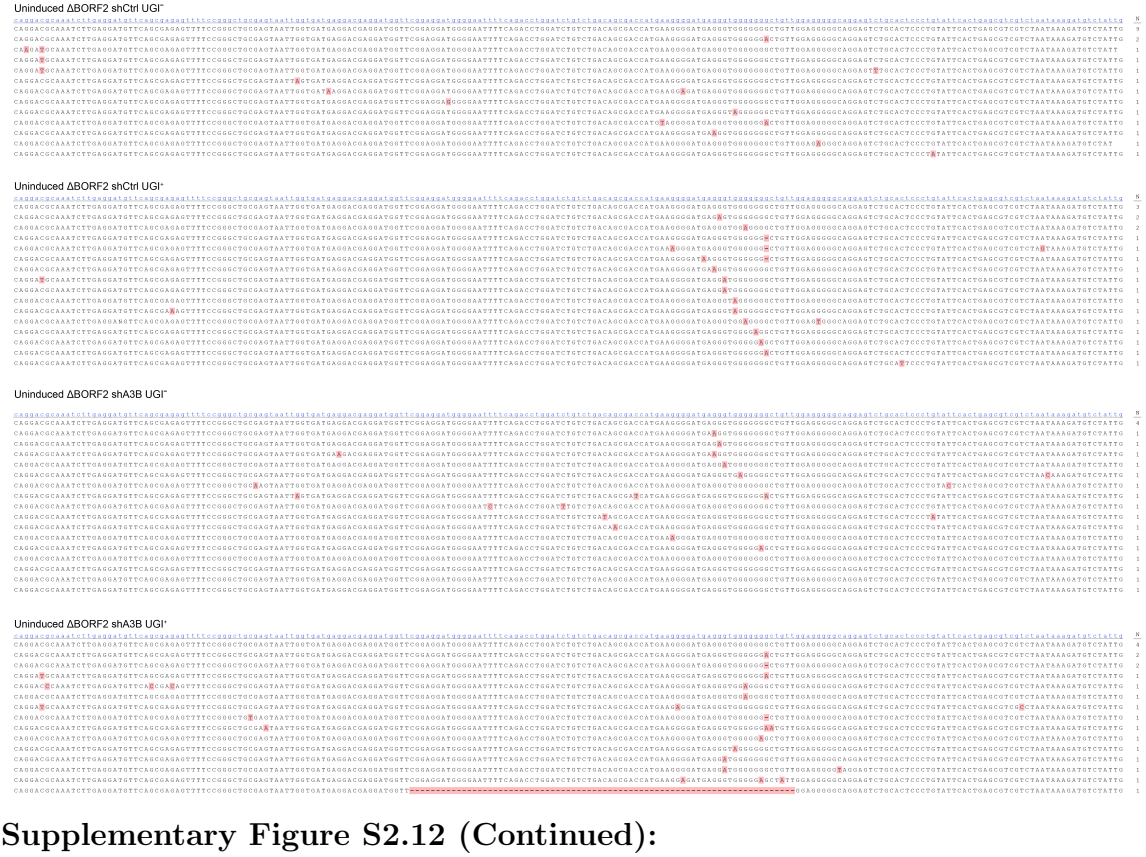

Supplementary Figure S2.12 (Continued):

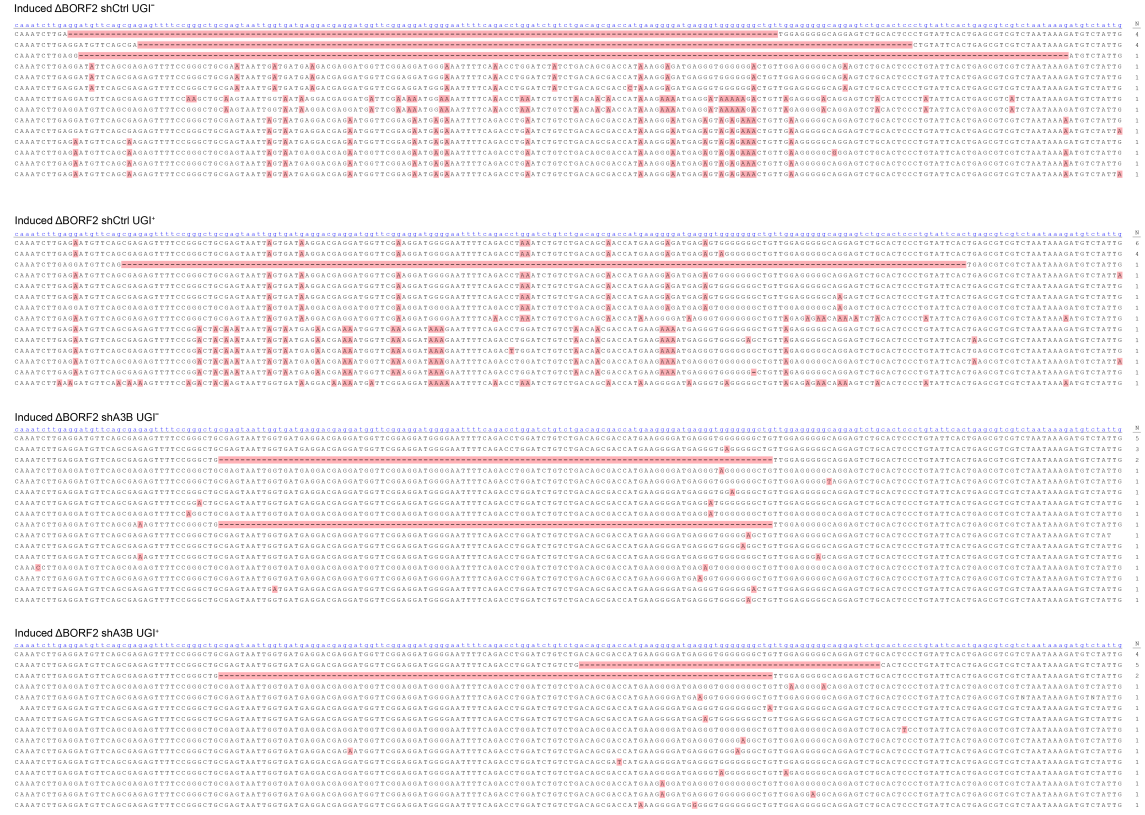

Supplementary Figure S2.12 (Continued):

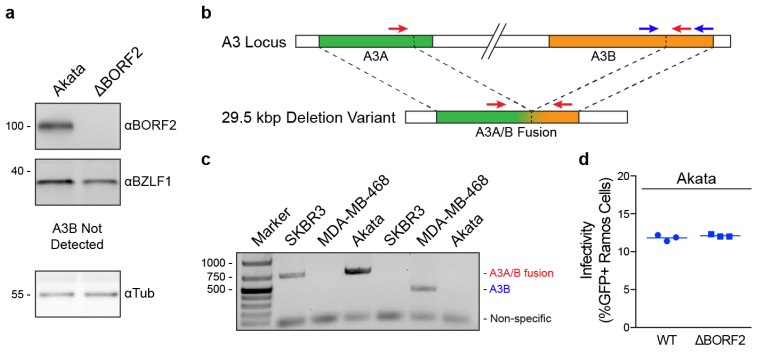

Supplementary Figure S2.13: BORF2 is dispensable for Akata EBV infectivity.

a, Immunoblots of extracts from parental Akata cells and the Cas9/gRNA engineered BORF2-null pools after lytic reactivation. Endogenous A3B is undetectable in Akata cells (blank immunoblot not shown).

b, Schematic of the *A3A* and *A3B* genes (top) and a naturally occurring 29.5 kbp deletion leading an *A3A/B* fusion gene (bottom, not to scale). Arrows correspond to primer sets used to genotype cells (blue represents the intact locus; red represents the deletion variant).

c, Agarose gel of A3A/B- and A3B-specific PCR products from SKBR3 (A3B-null), MDA-MB-468 (A3B intact), and Akata cells (A3B-null). **d**, Infectivity of wild-type and ΔBORF2 viruses produced by lytic replication in Akata cells. Each symbol represents the percent of GFP-positive Ramos reporter cells from an independent infection (n=3), and the horizontal line shows the mean. These data (**a,c,d**) are representative of n=3 biologically independent experiments.

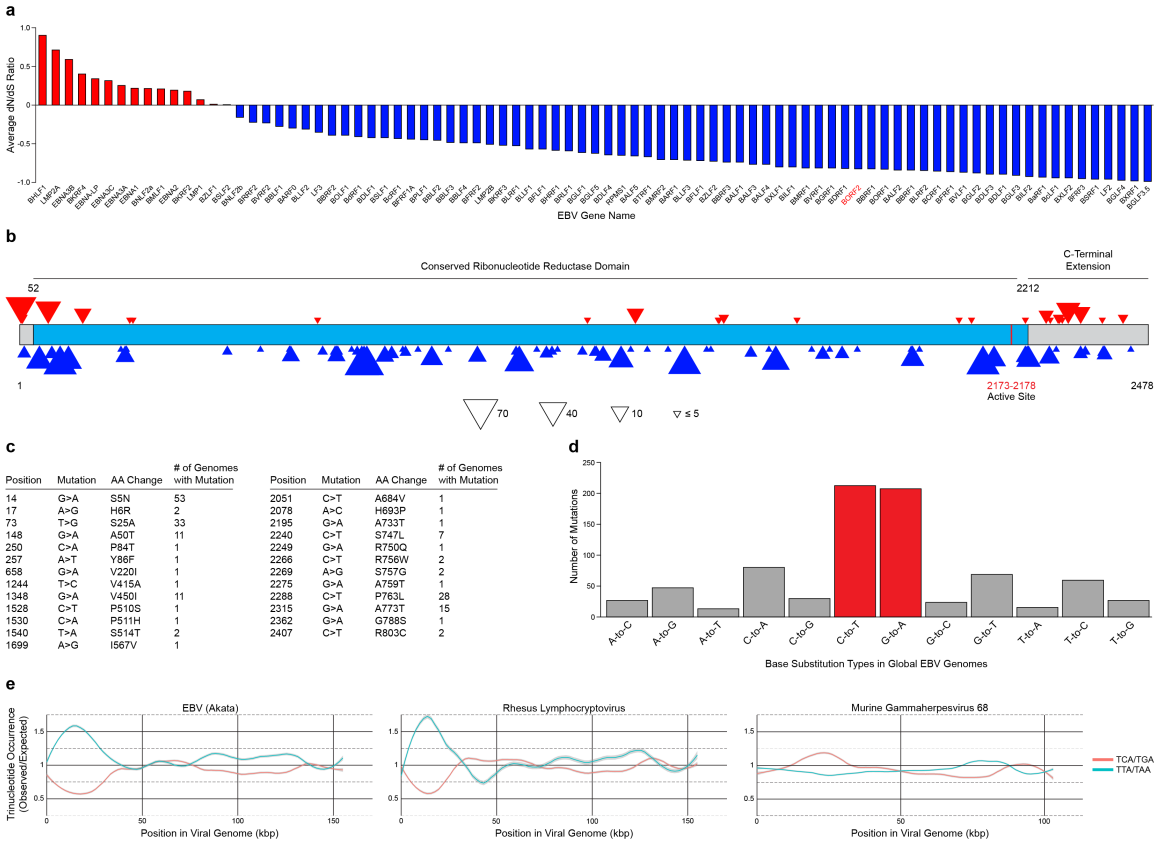

Position	Mutation	AA Change	# of Genomes with Mutation
14	G>A	S5N	53
17	A>G	H6R	2
73	T>G	S25A	33
148	G>A	A50T	11
250	C>A	P84T	1
257	A>T	Y86F	1
658	G>A	V220I	1
1244	T>C	V415A	1
1348	G>A	V450I	11
1528	C>T	P510S	1
1530	C>A	P511H	1
1540	T>A	S514T	2
1699	A>G	I567V	1

Position	Mutation	AA Change	# of Genomes with Mutation
2051	C>T	A684V	1
2078	A>C	H693P	1
2195	G>A	A733T	1
2240	C>T	S747L	7
2249	G>A	R750Q	1
2266	C>T	R756W	2
2269	A>G	S757G	2
2275	G>A	A759T	1
2288	C>T	P763L	28
2315	G>A	A773T	15
2362	G>A	G788S	1
2407	C>T	R803C	2

Supplementary Figure S2.14: EBV genomic variation in clinical isolates.
a, Bar plot of average ratios of non-synonymous (dN) to synonymous (dS) mutations in every EBV gene centered around 1 (dN=dS) using sequencing data from 142 publically available EBV genomes. Red bars show genes under positive selection while blue bars show genes under negative selection. BORF2 is under strong negative selection consistent with at least one essential function.
b, Schematic of *BORF2* gene highlighted with non-synonymous (red triangles) and synonymous (blue triangles) mutations using data from (**a**). The clustering of amino acid altering base substitutions to the N- and C-terminal ends of BORF2 indicates these regions are dispensable, whereas the majority of the central conserved RNR domain predominantly harbors silent mutations [consistent with result in panel (**a**) and deletion analysis in **Supplementary Figure S2.3**].
c, Tabulated positions, mutations, and frequencies of every non-synonymous mutation in *BORF2*.
d, Global distribution of EBV base substitution from 142 clinical EBV isolates showing preferential accumulation of C/G-to-T/A mutations.

Supplementary Figure S2.14 (Continued):
e, 1 kbp sliding window analyses in 15 kbp bins of the observed/expected distributions of A3B-preferred 5'-TCA substrates (5'-TGA on complementary strand) and of the most likely transition mutation products 5'-TTA (5'-TAA) within the indicated viral genomes. A3B-preferred deamination substrates are depleted and products are enriched in human EBV and rhesus LCV, but not in murine MHV68 (*i.e.*, A3B, if present, impacts viral trinucleotide distributions). Non-preferred motifs such as 5'-ACA (5'-TGT) are neither depleted nor enriched (data not shown).

2.7 Supplementary Videos

Supplementary Videos can be found online at:

Nature Microbiology: https://www.nature.com/articles/s41564-018-0284-6

or

PubMed Central: https://www.ncbi.nlm.nih.gov/pubmed/30420783

CHAPTER 3

A Conserved Mechanism of APOBEC Counteraction by Herpesviruses Ribonucleotide Reductase Large Subunits

This chapter was adapted with permission from:

Cheng AZ, et al. J Virol., in review.

Authors: Adam Z. Cheng[1,2,3,4], Sofia Nóbrega de Moraes[1,2,3,4], Claire Attarian[1,2,3,4], Jaime Yockteng Melgar[5], Matthew C. Jarvis[1,2,3,4], Matteo Biolatti[6], Ganna Galitska[6], Valentina Dell'Oste[6], Lori Frappier[5], Craig J. Bierle[3,7], Stephen A. Rice[3,8] & Reuben S. Harris[1,2,3,4,9]

Affiliations:

[1] Department of Biochemistry, Molecular Biology and Biophysics, University of Minnesota, Minneapolis, Minnesota, USA, 55455.

[2] Masonic Cancer Center, University of Minnesota, Minneapolis, Minnesota, USA, 55455.

[3] Institute for Molecular Virology, University of Minnesota, Minneapolis, Minnesota, USA, 55455.

[4] Center for Genome Engineering, University of Minnesota, Minneapolis, Minnesota, USA, 55455.

[5] Department of Molecular Genetics, University of Toronto, Toronto, Ontario, Canada, M5S 1A8.

[6] Laboratory of Pathogenesis of Viral Infections, Department of Public Health and Pediatric Sciences, University of Turin, 10126, Turin, Italy.

[7] Department of Pediatrics, Division of Pediatric Infectious Diseases and Immunology, University of Minnesota, Minneapolis, Minnesota, USA 55455.

[8] Department of Microbiology and Immunology, University of Minnesota, Minneapolis, Minnesota, USA, 55455.

[9] Howard Hughes Medical Institute, University of Minnesota, Minneapolis, Minnesota, USA, 55455.

3.1 Summary

An integral part of the antiviral innate immune response is the APOBEC3 family of single stranded DNA cytosine deaminases, which inhibits virus replication through deamination dependent and independent activities. Viruses have evolved mechanisms to counteract these enzymes such as HIV-1 Vif mediated formation of a ubiquitin ligase to degrade virus restrictive APOBEC3 enzymes. A new example is Epstein Barr virus (EBV) ribonucleotide reductase (RNR) mediated inhibition of cellular APOBEC3B (A3B). The large subunit of the viral RNR, BORF2, causes A3B relocalization from the nucleus to cytoplasmic bodies and thereby protects viral DNA during lytic replication. Here, we use co-immunoprecipitation and immunofluorescent microscopy approaches to ask whether this APOBEC neutralization mechanism is shared with the closely related γ-herpesvirus Kaposis sarcoma-associated herpesvirus (KSHV) and the more distantly related α-herpesvirus, herpes simplex virus type 1 (HSV-1). The large RNR subunit of KSHV, ORF61, co-precipitated multiple APOBEC3s including A3B and APOBEC3A (A3A). KSHV ORF61 also caused relocalization of these two enzymes to perinuclear bodies (A3B) and to oblong cytoplasmic structures (A3A). The large RNR subunit of HSV-1, ICP6, also co-precipitated A3B and A3A and was sufficient to promote the relocalization of these enzymes from nuclear to cytoplasmic compartments. HSV-1 infection caused similar relocalization phenotypes, and this was fully dependent on the viral RNR protein ICP6. These relocalization phenotypes could be exacerbated by infection with viruses that overexpress ICP6 due to an *ICP4* deletion. These results combine to indicate that both γ-and α-herpesviruses counteract the antiviral activities of cellular APOBEC3 enzymes through a conserved RNR-dependent mechanism.

Importance

The APOBEC3 family of DNA cytosine deaminases constitutes a vital innate immune defense against a range of different viruses. A novel counter restriction mechanism has recently been uncovered for the γ-herpesvirus EBV, in which a subunit of the viral protein known to produce DNA building blocks (ribonucleotide reductase) causes A3B to relocalize from the nucleus to the cytosol. Here, we extend these observations to a closely related γ-herpesvirus, KSHV, and to a more distantly related α-herpesvirus, HSV-1. Relocalization was also evident for these ribonucleotide reductases and A3A, which is 92% identical to A3B. These studies are important because they demonstrate a conserved mechanism of APOBEC3 evasion by large double-stranded DNA herpesviruses. Strategies to block this host-pathogen interaction may be effective for treating infections caused by these herpesviruses.

3.2 Introduction

An important arm of the innate immune response lies in the APOBEC family of single stranded DNA cytosine deaminases [2, 85, 86]. Each of the seven human APOBEC3 (A3) enzymes, A3A-D and A3F-H, have been implicated in the restriction and mutation of a variety of different human viruses including retroviruses (HIV-1, HIV-2, HTLV-1) [15–19], endogenous retroviruses (HERV) [24, 290], hepadnaviruses (HBV) [21, 23], small DNA tumor viruses (HPV, JC/BK-PyV) [26–29, 291], and most recently, the γ-herpesvirus Epstein-Barr Virus (EBV) [30, 31]. It is difficult, if not impossible, to predict *a priori* which subset of APOBEC3 enzymes has the potential to engage a given virus and, furthermore, how that virus might counteract potentially restrictive A3 enzymes. For instance, the lentiviruses HIV-1 and HIV-2 encode

an accessory protein called Vif that heterodimerizes with the cellular transcription co-factor CBF-β and recruits a cellular ubiquitin ligase complex to trigger the degradation of restrictive A3 enzymes [88, 292].

Human herpesviruses can be grouped into three distinct subfamilies (α, β, and γ; phylogeny **Figure 3.1A**). Pathogenic α- and β-herpesviruses include herpes simplex virus type 1 (HSV-1) and cytomegalovirus (CMV), respectively, and the γ-herpesvirus subfamily includes EBV and Kaposis sarcoma-associated herpesvirus (KSHV). We recently identified the APOBEC counteraction mechanism for EBV [30]. We demonstrated that the large subunit of the viral ribonucleotide reductase (RNR), BORF2, inhibits APOBEC3B (A3B) by directly binding and relocalizing it from the nucleus to the cytoplasmic compartment. This counteraction mechanism prevents the normally nuclear-localized A3B enzyme from deaminating viral genomic DNA cytosines to uracils during lytic replication. In the absence of BORF2, A3B inflicted C/G-to-T/A mutations in EBV genomes and reduced viral titers and infectivity. We also showed that the homologous protein from KSHV, ORF61, is similarly capable of binding and relocalizing A3B [30].

Here, we ask whether the viral RNR-mediated APOBEC counteraction mechanism is specific to γ-herpesviruses or more general-acting by assessing interactions between γ-herpesvirus BORF2/ORF61 and other human A3 enzymes and by determining whether the more distantly related α-herpesvirus HSV-1 has a similar A3 neutralization mechanism (RNR nomenclature in **Figure 3.1A** and protein domains depicted in **Figure 3.1B**). We found that, in addition to binding and relocalizing A3B, both BORF2 and ORF61 were also capable of co-immunoprecipitation and relocalization of A3A. Additionally, we found that the HSV-1 RNR large subunit ICP6 similarly binds and relocalizes both A3B and A3A. Overexpression studies showed

that ICP6 alone is sufficient for A3B and A3A relocalization. Infection studies with wild-type and mutant viruses demonstrated that ICP6 mediates this relocalization activity in the context of infected cells and that no other viral protein is capable of this function. These data combine to indicate that pathogenic γ- and α-herpesviruses have evolved an effective A3 counteraction mechanism, which is governed by the viral RNR large subunit.

3.3 Results

EBV BORF2 and KSHV ORF61 bind and relocalize both A3B and A3A

Our prior co-immunoprecipitation (co-IP) experiments indicated that EBV BORF2 interacts strongly with A3B and weakly with A3A and A3F (see **Figure 2.1c** in **Chapter 2** [30]). EBV BORF2 was both necessary and sufficient to relocalize A3B in a variety of different cell types including endogenous A3B in the AGS gastric carcinoma cell line and the M81 B cell line [30]. However, our original studies did not address whether EBV BORF2 could functionally interact with and relocalize any of these related human A3 enzymes. We therefore performed immunofluorescent (IF) microscopy studies of U2OS cells overexpressing A3-mCherry constructs with either empty vector or BORF2-FLAG. As reported, A3B is nuclear, A3A has a cell-wide localization, A3H is cytoplasmic and nucleolar, and the other A3s are cytoplasmic [61, 62, 65, 67, 293]. Also as expected, BORF2 caused a robust and complete relocalization of nuclear A3B to perinuclear aggregates (**Figure 3.2**). Interestingly, BORF2 co-expression with A3A led to the presence of novel linear elongated structures concomitant with normal A3A localization. The localization

patterns of the other five A3s were unchanged by BORF2 co-expression. Small BORF2 punctate structures were also noted in all conditions including the mCherry control, which is likely due to transfected BORF2 interacting with endogenous A3B (previously shown to be elevated in U2OS [28]). Similar A3B and A3A relocalization patterns were evident in Vero cells except that A3A relocalization became whole-cell without elongated structures (**Supplementary Figure S3.1**).

Like EBV BORF2, KSHV ORF61 was also shown to co-IP and relocalize A3B [30]. However, our original studies did not examine the specificity of this interaction by comparing with related human A3 enzymes. We therefore used co-IP experiments to evaluate KSHV ORF61 interactions with a full panel of human A3 enzymes. ORF61-FLAG was co-expressed with A3-HA family members in 293T cells, subjected to anti-FLAG affinity purification, and analyzed by immunoblotting (**Figure 3.3A**). The ORF61-FLAG pulldown resulted in A3B recovery as described [30]. In addition, the ORF61-FLAG IP also yielded a robust interaction with A3A and weaker interactions with A3D and A3F.

These KSHV ORF61-A3 interactions were then evaluated by IF microscopy experiments to look for changes in A3 localization in U2OS and Vero cells (**Figure 3.3B**). As expected [30], KSHV ORF61 caused A3B to relocalize to perinuclear bodies. Moreover, as above for BORF2 and A3A, ORF61 co-expression caused a portion of the cellular A3A to localize to intense elongated linear structures in the cytosolic compartment (**Figure 3.3B**). No other A3 proteins showed altered subcellular localization in these experiments. These new results with EBV BORF2 and KSHV ORF61 combined to indicate that both A3B and A3A may be cellular targets of viral RNR-mediated neutralization. The potential relevance of these interactions to the pathology of these viruses will be considered in **Section 3.4**

Discussion.

HSV-1 ICP6 binds and relocalizes A3B and A3A

To test whether RNR-mediated APOBEC antagonism is a more broadly conserved mechanism, a series of co-IP experiments was done with the large RNR subunit of HSV-1, ICP6. FLAG-ICP6 was co-expressed with each of the seven different HA-tagged human A3s in 293T cells and subjected to anti-FLAG IP as above. The EBV BORF2-A3B interaction was used as a positive control and BORF2-A3G as a negative control to be able to compare the relative strengths of pulldowns between RNRs and A3s. HSV-1 ICP6 showed a strong interaction with A3A and weaker, but detectable, interactions with A3B, A3C, and A3D (**Figure 3.4A**).

Next, IF microscopy was used to assess functional interactions between HSV-1 ICP6 and each of the human A3 enzymes. Human U2OS osteosarcoma cells were co-transfected with mCherry-tagged A3s and either empty vector or FLAG-tagged HSV-1 ICP6 and analyzed by IF after 48 hours (**Figure 3.4B**). On its own EBV BORF2 shows a cytoplasmic distribution and, as shown above and previously [30], it was able to completely relocalize A3B from the nucleus to cytoplasm. In comparison, HSV-1 FLAG-ICP6 showed a broadly cytoplasmic localization that did not change significantly with co-expression of any A3. However, co-expression of FLAG-ICP6 and A3B-mCherry or A3A-mCherry led to a near complete relocalization of these DNA deaminases from the nucleus to the cytoplasm. HSV-1 ICP6 co-expression with the other A3s did not lead to any remarkable change in localization. These results suggested that, although HSV-1 ICP6 interacted by co-IP with several A3s to varying degrees, functionally relevant interactions may only be occurring with A3B and A3A.

HSV-1 infection relocalizes A3B and A3A

To address whether HSV-1 infection similarly promotes relocalization of A3B and A3A, U2OS cells were transfected with A3-mCherry constructs 48 hours prior to either mock or HSV-1 infection. We used K26GFP, a HSV-1 strain that has a GFP moiety fused to capsid protein VP26 to allow for identification of infected cells [294]. Cells were analyzed by IF 8 hours post-infection (hpi) (**Figure 3.5A**). Similar to the ICP6 overexpression experiments described above, HSV-1 infection caused A3A to relocalize to the cytoplasmic compartment and A3B to change from a predominantly nuclear localization to a more cell-wide distribution. A3C also changed from a predominantly cytoplasmic localization to a more diffuse whole cell distribution, whereas A3D, A3F, A3G, and A3H were unchanged by HSV-1 infection. Relocalization was quantified for A3A-mCherry, A3B-mCherry, and A3G-mCherry as a representative non-altered control (**Figure 3.5B**). Similar relocalization patterns were found in HeLa cells following HSV-1 K26GFP infection (**Supplementary Figure S3.2**). Moreover, time-course experiments showed that relocalization of A3A was detectable as early as 3 hpi, whereas A3B and A3C relocalization became apparent by 6 or 9 hpi (**Supplementary Figure S3.3**). These kinetic differences may reflect a differential affinity of the viral protein(s) to bind to these cellular A3 enzymes and/or different competitions with cellular interactors.

HSV-1 mediated relocalization of A3B and A3A requires ICP6

To investigate whether the HSV-1 large RNR subunit is required for A3A/B relocalization, we next examined A3 localization in cells following infection with an HSV-1 KOS1.1 strain lacking ICP6 due to a deletion of the *UL39* gene (*UL39* encodes ICP6) [295]. Vero cells were transfected with A3-mCherry constructs 48 hours prior to mock infection or infection with KOS1.1 or KOS1.1ΔICP6. After 8 hours, cells were fixed, permeabilized, and subjected to IF analysis by staining for the HSV-1

immediate early protein ICP27 to mark infected cells, and monitoring A3 localization through mCherry fluorescence. As above, HSV-1 infection caused the relocalization of A3A, A3B, and A3C (**Figure 3.6A**). However, only the relocalization A3A and A3B was ICP6-dependent, whereas A3C redistributed regardless of the presence of ICP6. These results provide strong support for mechanistic conservation of the RNR large subunit-A3 interaction (A3A and A3B) and also indicated that A3C relocalization by HSV-1 is mechanistically distinct.

To further investigate the role of ICP6 in mediating A3A and A3B relocalization, U2OS cells were infected with an HSV-1 KOS mutant with a deletion in the *ICP4* gene [296]. ICP4, an immediate early protein, is the major transcriptional activator protein of HSV-1 [296]. *ICP4*-null mutants exhibit a strict block to expression of nearly all viral delayed-early and late genes, but are competent to express the viral immediate-early genes (*ICP0*, *ICP22*, *UL54*, and *US12*) as well the *UL39* gene, a delayed-early gene that is uniquely transactivated by ICP0 [297]. In fact, at intermediate and late times post-infection, *ICP4*-null mutants express abnormally high levels of both the immediate early proteins and ICP6 [296]. Similar to what was seen for wild-type HSV-1 infection, infection with the HSV-1 KOSΔICP4 mutant also led to A3A and A3B relocalization, but with noticeably more pronounced phenotypes (**Figure 3.6B**). For instance, this mutant virus caused A3B-mCherry to form perinuclear aggregates reminiscent of previously observed BORF2-A3B bodies [30] (**Figure 3.6B**). Interestingly, A3C localization remained predominantly nuclear upon HSV-1 KOSΔICP4 infection, suggesting that one of the other four immediate early proteins besides ICP4 induces its relocalization. Taken together, these data show that HSV-1 ICP6 is both necessary and sufficient for the relocalization of A3A and A3B, and that at least one other viral factor is responsible for A3C relocalization.

3.4 Discussion

We previously described a novel mechanism for A3B counteraction by the γ-herpesvirus RNR large subunits, EBV BORF2 and KSHV ORF61 [30]. These viral proteins interact directly with A3B, relocalize it from the nuclear to the cytoplasmic compartment, and protect lytically replicating viral genomes from A3B-mediated deamination and hypermutation. Here, we investigated the question of specificity by comparing interactions with the full repertoire of seven different human A3 enzymes, and we also addressed the potential for broader conservation by asking whether the α-herpesvirus HSV-1 has a similar APOBEC3 counterdefense mechanism. Although EBV BORF2 and KSHV ORF61 were able to interact with several different A3 proteins in co-IP experiments, these viral RNR large subunits only promoted the relocalization of A3B and A3A. HSV-1 ICP6 showed a similarly broad range of co-IP interactions but also only promoted the relocalization of A3B and A3A. Wild-type but not ICP6 deletion mutant HSV-1 infections yielded similar A3B and A3A relocalization phenotypes. These studies combine to indicate that human γ- and α-herpesviruses possess a conserved A3B/A counterdefense mediated by the viral RNR large subunits.

The γ- and α-herpesvirus subfamilies encode both large and small RNR subunits (**Figure 3.1A**). These RNRs have the canonical function of synthesizing deoxyribonucleotides by reducing the 2-hydroxyl from ribonucleotide substrates [232]. While RNRs are essential for all cellular life, the requirement for endogenous viral RNRs differs tremendously across viral families. For example, most small dsDNA viruses and single-stranded DNA viruses do not encode RNRs and instead rely on host-encoded RNRs for deoxyribonucleotide production [298, 299]. On

the other hand, RNRs are almost ubiquitous among large double-stranded DNA (dsDNA) viruses, such as herpesviruses and poxviruses, presumably due to high dNTP requirements during DNA replication [300–302]. β-herpesviruses such as CMV are an exception, however, because they lack a small subunit and the large subunit has mutations in the catalytic residues [233]. In addition to ribonucleotide reductase activity, some viral RNRs have been shown to engage in non-catalytic activities that result in proviral phenotypes. For instance, the HSV-1 and HSV-2 large ribonucleotide reductase subunits, ICP6 and ICP10, respectively, have unique N-terminal extensions that block caspase-8 activity to inhibit apoptosis and bind RIP3 to promote necroptosis [237–239, 303] (**Figure 3.1B**). CMV UL45 also has anti-apoptotic and pro-necroptotic functions suggesting this could be its predominant function [241, 243, 303].

The question of whether A3B, A3A, or both enzymes is most relevant to γ- and α-herpesvirus pathogenesis is likely to depend, at least in part, on the complex interplay between viral tropism(s) and alternating modes of latent versus lytic replication. For EBV, epithelial cells serve as the source of primary infection which are mandatory for establishing lytic replication cycles for person-to-person spread and enabling secondary infection of B lymphocytes for establishment of long-term latency [304]. B cells also support lytic reactivation for reinfection and maintenance of EBV in the blood [305]. Here, A3B may be more important than A3A simply because its expression is well-documented in these cell types [43, 46]. Likewise, KSHV infects epithelial and B cells, but also engages in infection of clinically relevant endothelial cells which can lead to Kaposis sarcoma [306]. Additionally, because monocytes are likely to be a secondary reservoir for KSHV infection [307–309], it is plausible that this virus requires the capacity to relocalize both A3B and A3A

(A3B neutralization for replication in B cells and A3A neutralization for replication in monocytes/macrophages, where A3A is interferon-inducible and capable of being expressed at extremely high levels) [43, 259, 310]. For HSV-1, although neither A3B nor A3A expression has been reported in neural/CNS cells, lytic replication in epithelial cells may require functional neutralization of A3B and/or A3A [120, 311]. Dedicated functional studies in the most disease relevant *in vivo* systems will be required to fully address the question of whether A3B, A3A, or both enzymes are most relevant to the pathogenesis of these herpesviruses.

3.5 Materials and Methods

Generation of herpesvirus phylogenetic tree

Amino acid sequences for herpesvirus ribonucleotide reductase large subunits were obtained from NCBI Protein RefSeq with the following GenBank accession numbers: HSV-1 ICP6 YP_009137114.1, HSV-2 ICP10 YP_009137191.1, VZV ORF19 NP_040142.1, EBV BORF2 YP_401655.1, HCMV UL45 YP_081503.1, HHV6A U28 NP_042921.1, HHV6B U28 NP_050209.1, HHV7 U28 YP_073768.1, KSHV ORF61 YP_001129418.1. Alignment was generated using MUSCLE: multiple sequence alignment with high accuracy and high throughput [312] and phylogenetic tree was made using a neighbor-joining tree without distance corrections. Output was made using FigTree using scaled branches [313].

DNA constructs for expression in human cell lines

The full set of pcDNA3.1(+) human APOBEC-HA expression constructs has been described [268] [A3A (GenBank accession NM_145699), A3B (NM_004900), A3C (NM_014508), A3D (NM_152426), A3F (NM_145298), A3G (NM021822), A3H

(haplotype II; FJ376615)]. The full set of APOBEC-mCherry expression constructs was PCR amplified with Phusion High Fidelity DNA Polymerase (NEB M0530) from previously described A3-mCherry constructs [61] and subcloned into pcDNA5/TO (Invitrogen V103320). The forward PCR primers are as follows: A3A (5'-NNN NAA GCT TAC CAC CAT GGA AGC C-3'), A3B and A3C (5'-NNN NNA AGC TTA CCA CCA TGA ATC CA-3'), A3D (5'-NNN NNA AGC TTA CCA CCA TGA ATC CA-3'), A3F (5'-NNN NNA AGC TTA CCA CCA TGA AGC CT-3'), A3G (5'-NNN NAA GCT TAC CAC CAT GAA GCC T-3'), and A3H (5'-NNN NAA GCT TAC CAC CAT GGC TCT G-3'). The reverse PCR primer used was 5'-AGA GTC GCG GCC GCT TAC TTG TAC A-3'. PCR fragments were digested with *Hind*III-HF (NEB R3104) and *Not*I-HF (NEB R3189) and ligated into pcDNA5/TO. The full set of pLenti-iA3i-HA constructs were previously described except the puromycin resistance gene was replaced with a hygromycin resistance gene [66]. Briefly, this is a lentiviral construct with an intron spanning the A3 gene with a C-terminal 3x-HA tag, arranged in the antisense direction, which is expressed after reverse transcription and integration. This construct bypasses limitation of self-restriction by A3-mediated deamination of its own plasmid. EBV BORF2 (GenBank accession V01555.2) with a C-terminal 3x-FLAG (DYKDDDDK) tag and EBV BaRF1 (Genbank accession V01555.2) with a C-terminal 3x-HA (YPYDVPDYA) tag was previously described [30]. Other viral RNRs were subcloned with Phusion High Fidelity DNA Polymerase from previously described pCMV-3F vectors [30].

HSV-1 UL39 (GenBank accession JN555585.1) was PCR amplified using primers 5'-NNN NGA TAT CCG CCA CCA TGG CCA GCC GCC CAG CC-3' and 5'-NNN NGC GGC CGC CCC AGC GCG CAG CT-3', digested with *Eco*RV-HF (NEB R1395) and *Not*I-HF, and ligated into pcDNA4 (Invitrogen V102020) with

a C-terminal 3x-FLAG [88]. The same construct was PCR amplified using primers 5'-NNN NGC GGC CGC GGC CAG CCG CCC AGC CGC A-3' and 5'-NNN NTC TAG ATT ACA GCG CGC AGC TCG TGC A-3', digested with *Not*I-HF and *Xba*I (NEB R0145S), and ligated into a similar pcDNA4 vector with N-terminal 3x-FLAG.

KSHV ORF61 (GenBank accession U75698.1) was PCR amplified using primers 5'-NNN NGA ATT CGC CAC CAT GTC TGT CCG GAC ATT TTG T-3' and 5'-NNN NGA ATT CGC CAC CAT GTC TGT CCG GAC ATT TTG T-3', digested with *Eco*RI-HF (NEB R3101S) and *Not*I-HF, and ligated into pcDNA4 with a C-terminal 3x- FLAG. The same construct was PCR amplified using primers 5'-NNN NGC GGC CGC GTC TGT CCG GAC ATT TTG T-3' and 5'-NNN NTC TAG ATT ACT GAC AGA CCA GGC ACT C-3', digested with *Not*I-HF and *Xba*I, and ligated into a similar pcDNA4 vector with N-terminal 3x- FLAG.

Human cell culture

Unless indicated, cell lines were derived from established lab collections. All cell cultures were supplemented with 10% heat-inactivated fetal bovine serum (Gibco 16140-063), 1x Pen-Strep (Thermo Fisher 15140122), and periodically tested for mycoplasma (Lonza MycoAlert PLUS LT07-710). No cell lines have ever been mycoplasma positive or previously treated. 293T and Vero cells were cultured in high glucose DMEM (Hyclone), U2OS cells were cultured in McCoy's 5A media (Hyclone), and HeLa cells were cultured in RPMI 1640 (Corning).

Co-immunoprecipitation experiments and immunoblots

Semi-confluent 293T cells were grown in 6-well plates and transfected with plasmids and 0.6 μL TransIT-LT1 (Mirus 2304) per 100 ng DNA in 100 μL serum-free Opti-MEM (Thermo Fisher 31985062). A titration series was performed to achieve roughly

equivalent protein expression by immunoblot for the A3 panel and RNR homologue co-IP experiments. Growth medium was removed after 48 hrs and whole cells were harvested in 1 mL PBS-EDTA by pipetting. Cells were spun down, PBS-EDTA was removed, and cells were resuspended in 300 μL of ice-cold lysis buffer [150 mM NaCl, 50mM Tris-HCl, 10% glycerol, 1% IGEPAL (Sigma I8896), Roche cOmplete EDTA-free protease inhibitor cocktail tablet (Roche 5056489001), pH 7.4]. Cells were vortexed vigorously and left on ice for 30 minutes, then sonicated for 5 seconds in an ice water bath. 30 μL of whole cell lysate was aliquoted for immunoblot. Lysed cells were spun down at 13,000 rpm for 15 minutes to pellet debris and supernatant was added to clean tube with 25 μL resuspended anti-FLAG M2 Magnetic Beads (Sigma M8823) for overnight incubation at 4°C with gentle rotation. Beads were then washed three times in 700 μL of ice-cold lysis buffer. Bound protein was eluted in 30 μL of elution butter [0.15 mg/mL 3xFLAG peptide (Sigma F4799) in 150 mM NaCl, 50 mM Tris-HCl, 10% glycerol, 0.05% Tergitol, pH 7.4]. Proteins were analyzed by immunoblot and antibodies used include mouse anti-FLAG 1:5000 (Sigma F1804), mouse anti-tubulin 1:10,000 (Sigma T5168), and rabbit anti-HA 1:3000 (Cell Signaling C29F4).

Generation and titration of HSV-1 viruses

The HSV-1 strains used were wild-type strain KOS1.1 [314], K26GFP [294], ICP6 deletion mutant ICP6Δ, and the ICP4 deletion mutant d120 [296]. HSV-1 infections were done at a multiplicity of infection of 5 PFU per cell, as previously described [315]. Titers of viral stocks were determined by plaque assay on either Vero cells (KOS1.1, K26GFP, and ICP6Δ) or ICP4-complementing E5-Vero cells [316].

Immunofluorescence microscopy

For immunofluorescence imaging of transfected cells, approximately $5*10^4$ Vero,

HeLa, or U2OS cells were plated on coverslips and after 24 hrs, transfected with 200 ng pcDNA4-RNR-3xFLAG, 200 ng pcDNA5/TO-A3-mCherry, or both. After 48 hrs, cells were fixed in 4% formaldehyde, permeabilized in 0.2% Triton X-100 in PBS for 10 minutes, washed three times for 5 minutes in PBS, and incubated in blocking buffer (0.0028 M KH2PO4, 0.0072 M K2HPO4, 5% goat serum (Gibco), 5% glycerol, 1% cold water fish gelatin (Sigma), 0.04% sodium azide, pH 7.2) for 1 hr. Cells were then incubated in blocking buffer with primary mouse anti-Flag 1:1000 overnight at 4 C to detect FLAG-tagged RNRs. Cells were washed 3 times for 5 minutes with PBS, then incubated in secondary antibody goat anti-mouse AlexaFluor 488 1:1000 (Invitrogen A11001) diluted in blocking buffer for 2 hrs at room temperature in the dark. Cells were then counterstained with 1 μg/mL Hoechst 33342 for 10 minutes, rinsed twice for 5 minutes in PBS, and once in sterile water. Coverslips were mounted on pre-cleaned slides (Gold Seal Rite-On) using 20-30 μL of mounting media (dissolve 1g n-propyl gallate (Sigma) in 40 mL glycerol overnight, add 0.35 mL 0.1M KH2PO4, then pH to 8-8.5 with K2HPO4, Q.S. to 50mL with water). Slides were imaged on a Nikon Inverted Ti-E Deconvolution Microscope instrument and analyzed using NiS Elements.

For immunofluorescence imaging of HSV-1-infected cells, approximately $5*10^4$ Vero, HeLa, or U2OS cells were plated on coverslips and after 24 hrs, transfected with 200 ng pcDNA5/TO-A3-mCherry. After 48 hours, cells were infected with HSV-1 K26GFP, HSV-1 KOS1.1, HSV-1 KOS1.1ΔICP6, or HSV-1 KOS1.1ΔICP4 at MOI 5. Cells were fixed in 4% formaldehyde 8 hours post-infection and then IF studies proceeded as above. Time course experiments were fixed at either 3, 6, 9, or 12 hours post-infection. HSV-1 K26GFP experiments did not require primary or secondary antibody staining steps. Cells infected with HSV-1 KOS1.1 and

mutants were incubated in primary antibody mouse anti-HSV-1 ICP27 H1113 (Santa Cruz sc69807) 1:1000 overnight at 4 C to detected HSV-1-infected cells. Secondary antibody staining, counterstaining with Hoechst, mounting, and imaging proceeded as above.

IF microscopy quantification

For quantification of A3 nuclear to cytoplasmic ratio, IF images were analysed using Fiji software to obtain mean fluorescence intensities (MFI) of nuclear compartments determined by Hoechst stain outline and cytoplasmic compartments determined by cell outline. MFI values for each compartment were divided and plotted using Prism. Statistical analyses were performed using an unpaired Students t-test.

Acknowledgements

We thank Sandy Weller, Neal Deluca, and Prashant Desai for HSV-1 strains, M. Sanders and staff at the University of Minnesota Imaging Center for assistance with fluorescence microscopy, J. Becker for assistance with confocal microscopy, D. Ebrahimi for bioinformatics analyses of *A3* expression in different cell types, and P. Southern for thoughtful comments. NIH training grants provided salary support for AZC (F30 CA200432 and T32 GM008244) and MCJ (T32 CA009138). JY-M was supported by Secretaría Nacional de Educación Superior, Ciencia, Tecnología e Innovación (SENESCYT). GG is a scholar under the Horizon2020 program (H2020 MSCA-ITN-2015). V.D.O. is supported by Research Grants from the University of Turin (RILO18) and from the Italian Ministry of Education, University and Research – MIUR (PRIN 2015, 2015RMNSTA). LF is a tier 1 Canada Research Chair in Molecular Virology. RSH is the Margaret Harvey Schering Land Grant Chair for Cancer Research, a Distinguished McKnight University Professor, and an Investigator of the Howard Hughes Medical Institute. The funders had no role in study design,

data collection and analysis, decision to publish, or preparation of the manuscript.

Correspondence and requests for materials should be addressed to RSH (rsh@umn.edu).

3.6 Figures

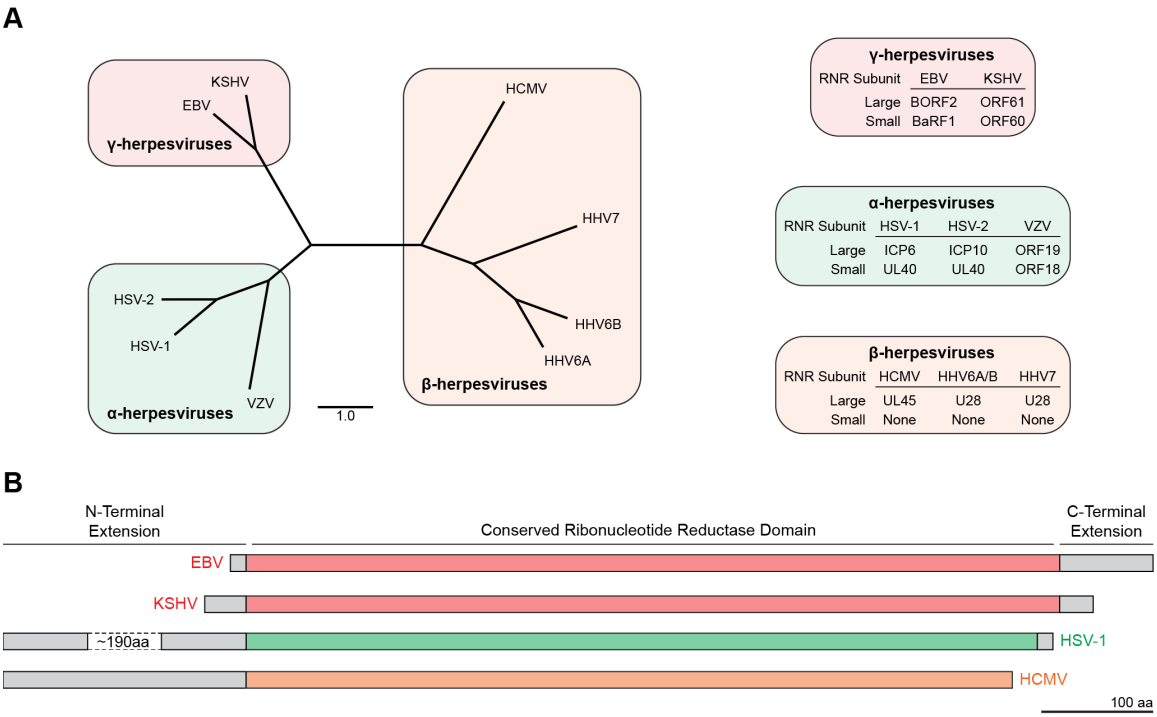

Figure 3.1: Herpesvirus ribonucleotide reductases conservation.
A) Amino acid sequences from ribonucleotide reductase large subunits were aligned using Multiple Sequence Comparison by Log-Expectation (MUSCLE) and phylogeny was constructed using neighbor-joining tree without distance corrections and scaled for equal branch lengths (scale bar = 1). Shaded boxes indicate herpesvirus subfamilies, which group closely to established phylogenetic trees. Protein names for human herpesvirus ribonucleotide reductase large and small subunits shown on the right.
(**B**) Schematic of representative RNR large subunit polypeptides from α-, β-, and γ-herpesviruses with conserved core sequences (colored) and unique N- and C-terminal extensions (gray). Diagram is approximately to scale with a $\sim$190 amino acid portion of HSV-1 ICP6 omitted to fit the figure. Scale bar is 100 amino acids.

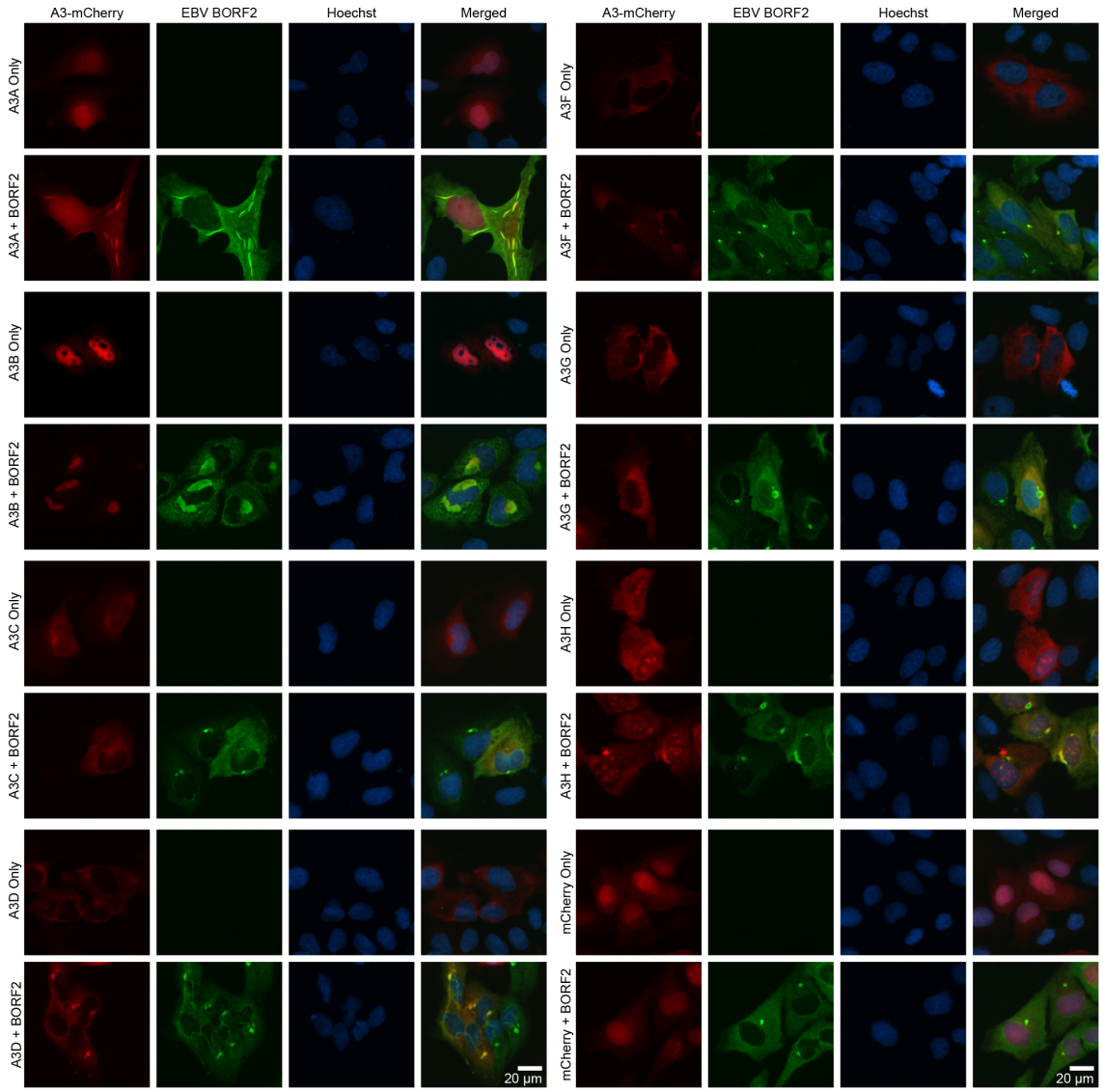

Figure 3.2: EBV BORF2 relocalizes A3B and A3A.
Representative images of U2OS cells transfected with either A3-mCherry or BORF2-FLAG constructs. Cells were fixed 48 hours post-transfection, permeabilized, and stained with anti-FLAG antibody and Hoechst. A3 localization was compared in the presence and absence of EBV BORF2-FLAG co-transfection.

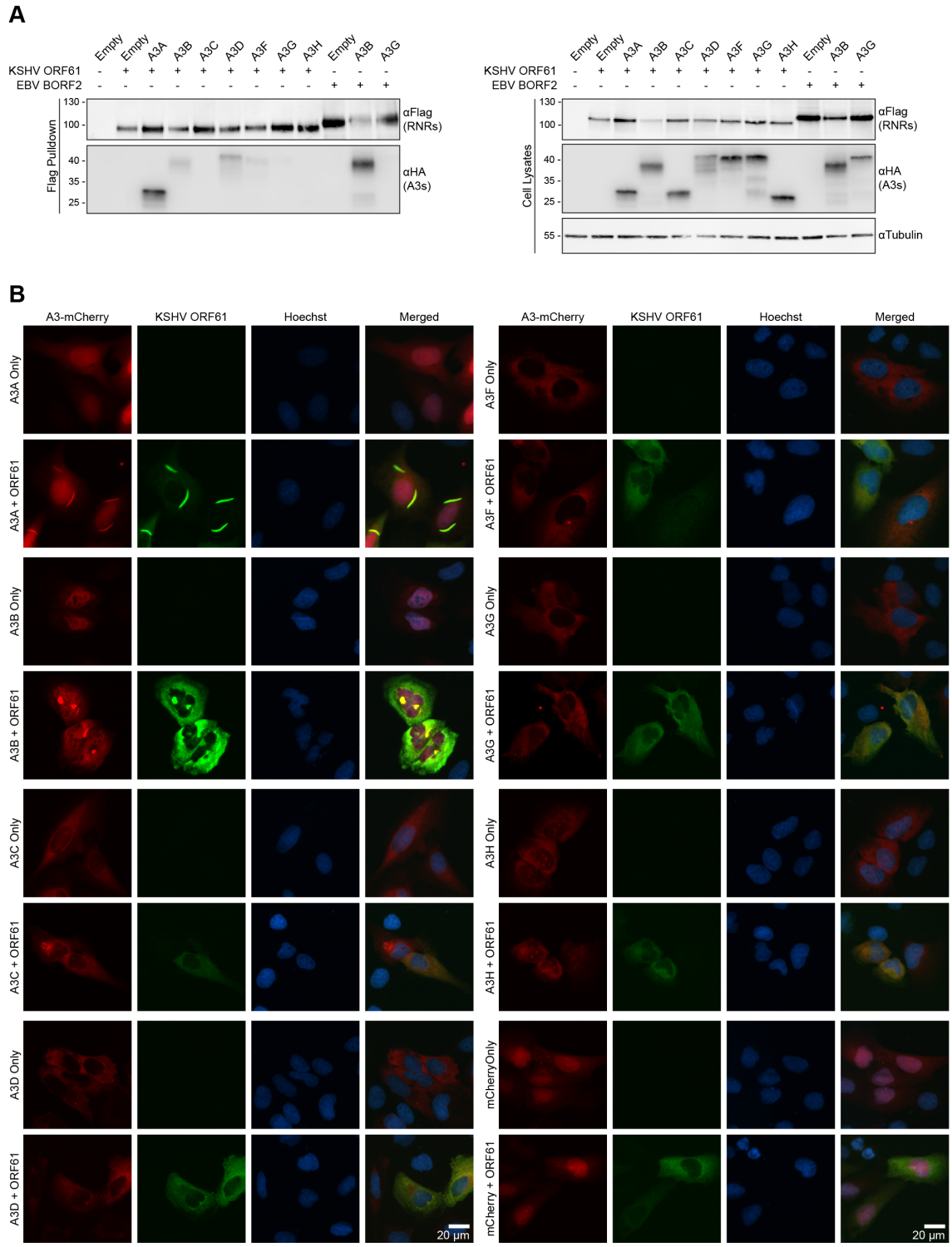

Figure 3.3: KSHV ORF61 relocalizes A3B and A3A.

Figure 3.3 (Continued):
(**A**) Co-immunoprecipitation of transfected KSHV ORF61-FLAG with the indicated A3-HA constructs in 293T cells. Cells were lysed 48 hours post-transfection for anti-FLAG pulldown and resulting proteins were analyzed by immunoblot. EBV FLAG-BORF2 transfected with A3B and A3G were used as positive and negative co-IP controls, respectively.
(**B**)Representative images of U2OS cells transfected with either A3-mCherry or FLAG-RNR constructs. Cells were fixed 48 hours post-transfection, permeabilized, and stained with anti-FLAG antibody and Hoechst. Co-transfection with A3B-mCherry and EBV BORF2-FLAG was used as positive controls for relocalization from nuclear to cytoplasmic aggregates. A3 localization was compared in the presence and absence of KSHV ORF61-FLAG co-transfection.

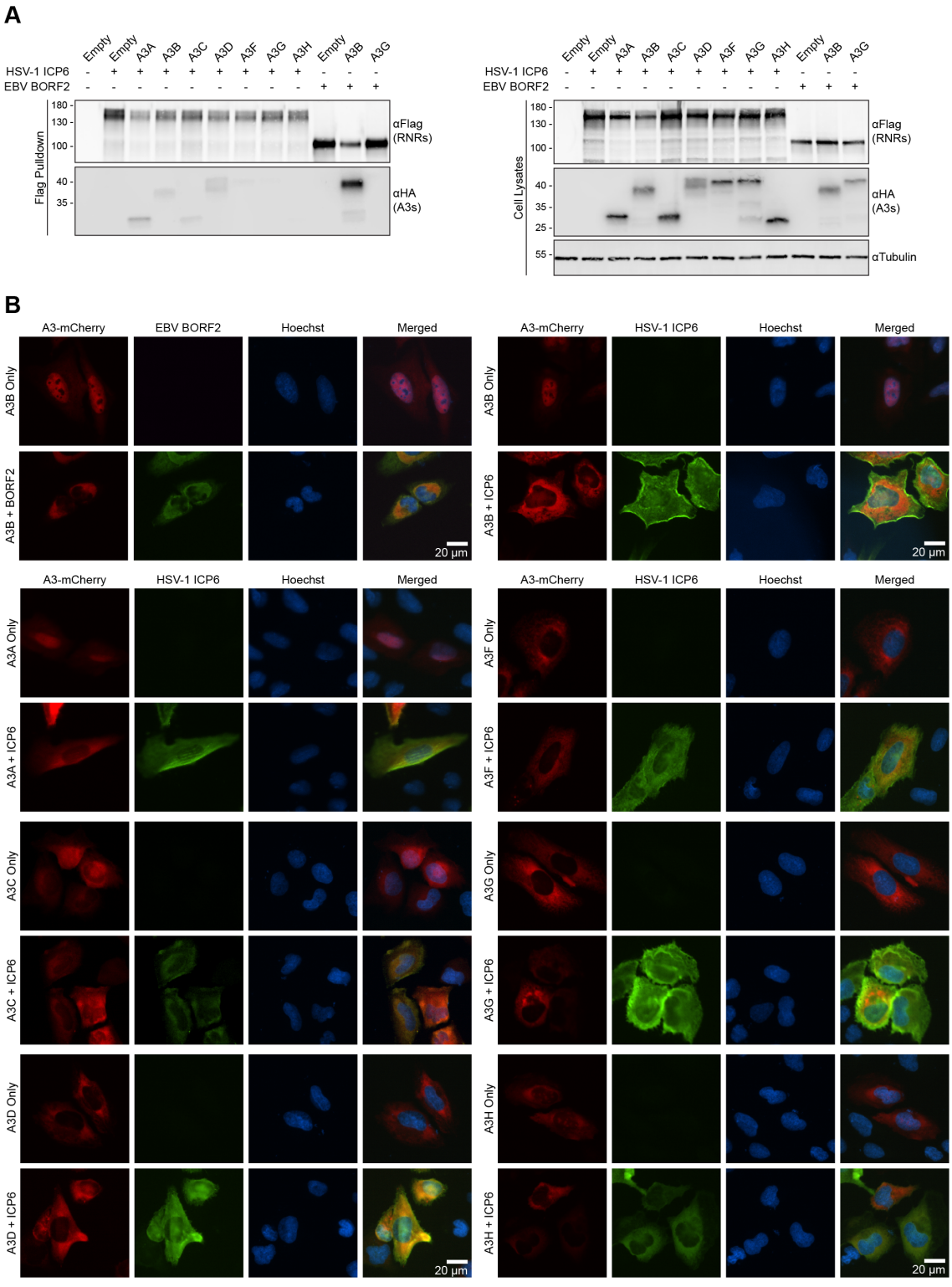

Figure 3.4: HSV-1 ICP6 binds and relocalizes A3B and A3A.

Figure 3.4 (Continued):
(**A**) Co-immunoprecipitation of transfected HSV-1 FLAG-ICP6 with the indicated A3-HA constructs in 293T cells. Cells were lysed 48 hours post-transfection for anti-FLAG pulldown and resulting proteins were analyzed by immunoblot. EBV FLAG-BORF2 transfected with A3B and A3G were used as positive and negative co-IP controls, respectively.
(**B**) Representative images of U2OS cells transfected with either A3-mCherry or FLAG-RNR constructs. Cells were fixed 48 hours post-transfection, permeabilized, and stained with anti-FLAG antibody and Hoechst. Co-transfection with A3B-mCherry and EBV FLAG-BORF2 was used as positive controls for relocalization from nuclear to cytoplasmic aggregates. A3 localization was compared in the presence and absence of HSV-1 FLAG-ICP6 co-transfection.

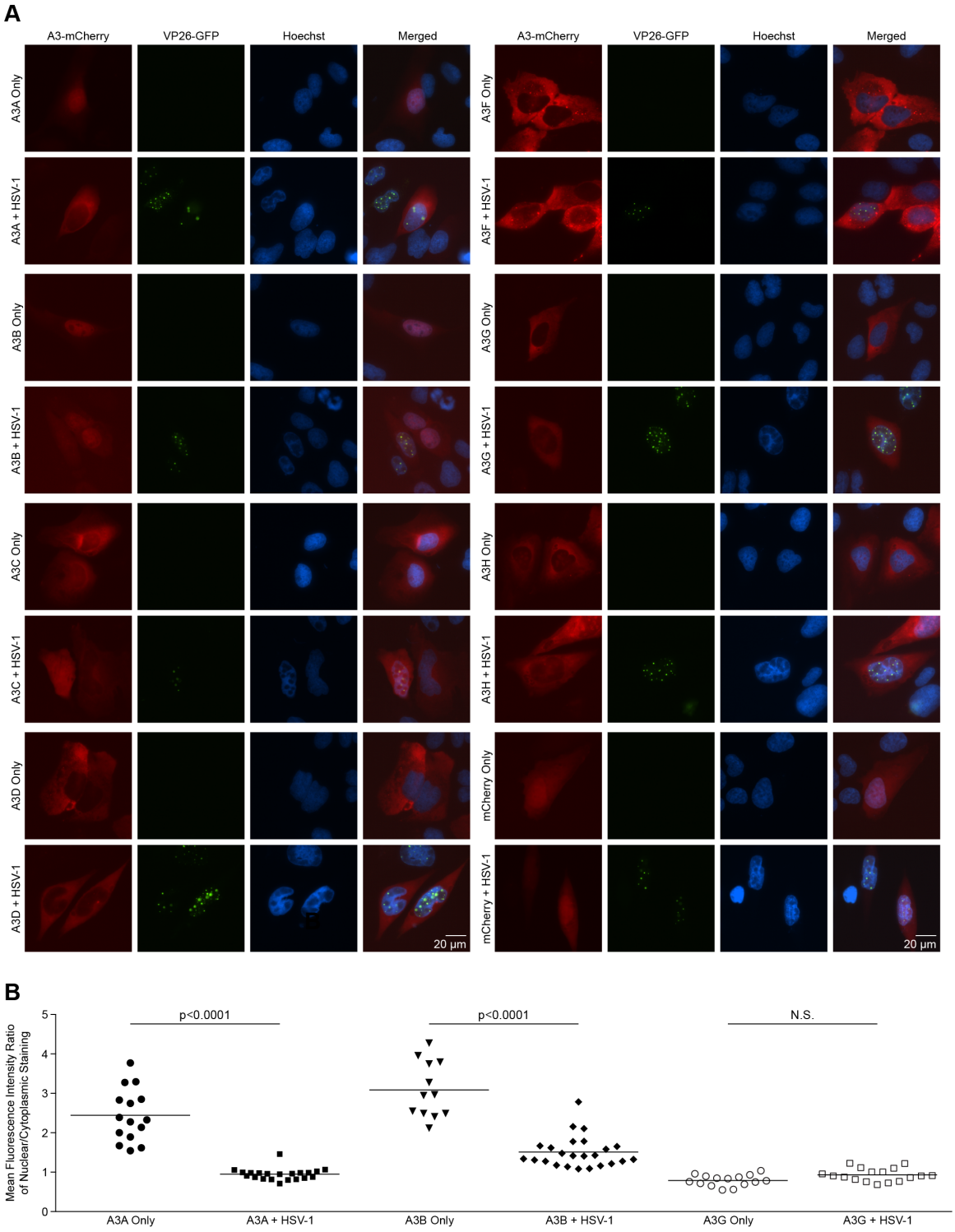

Figure 3.5: HSV-1 infection relocalizes A3B and A3A.

Figure 3.5 (Continued):
(**A**) Representative images of U2OS cells transfected with A3-mCherry constructs, followed by mock or HSV-1 K26GFP infection 48 hours post-transfection. Cells were fixed 8 hpi and stained with Hoechst, then imaged directly. The viral capsid protein VP26 is tagged with GFP which marks infected cells.
(**B**) Quantification of key IF microscopy data for HSV-1 infection. Statistical analysis was performed using an unpair Students t-test between indicated groups, NS = not significant).

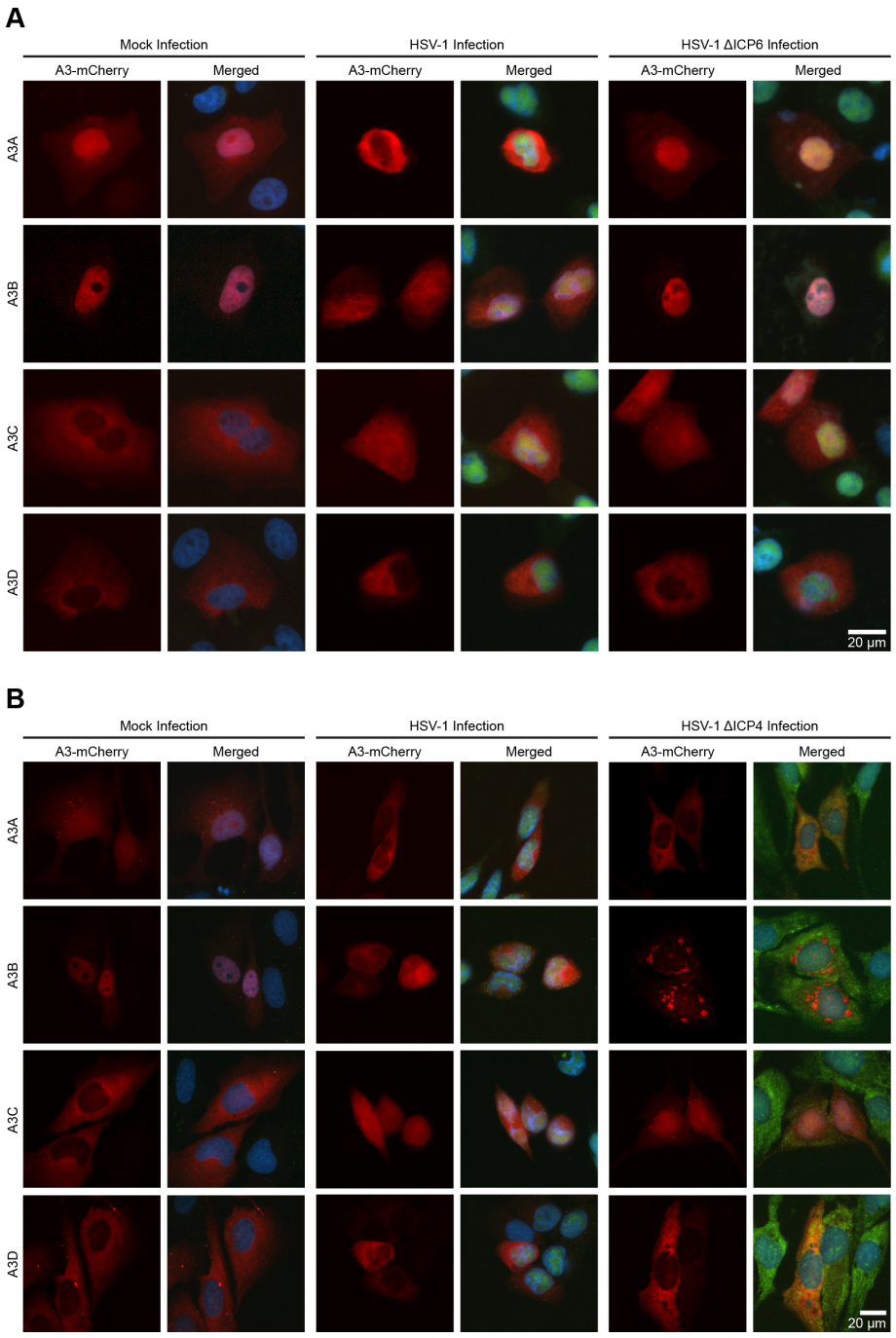

Figure 3.6: A3B and A3A relocalization is dependent on HSV-1 ICP6. (**A**) Representative images of Vero cells transfected with A3-mCherry constructs, followed by mock, wild-type HSV-1 KOS1.1, or HSV-1 KOS1.1ΔICP6 infection 48 hours post-transfection. Cells were fixed 8 hours after HSV-1 infection, permeabilized, and stained with anti-ICP27 antibody to mark infected cells and Hoechst.
(**B**) Representative images from an experiment similar to that described in panel A, except using U2OS cells and the mutant virus HSV-1 KOS1.1ΔICP4.

3.7 Supplementary Figures

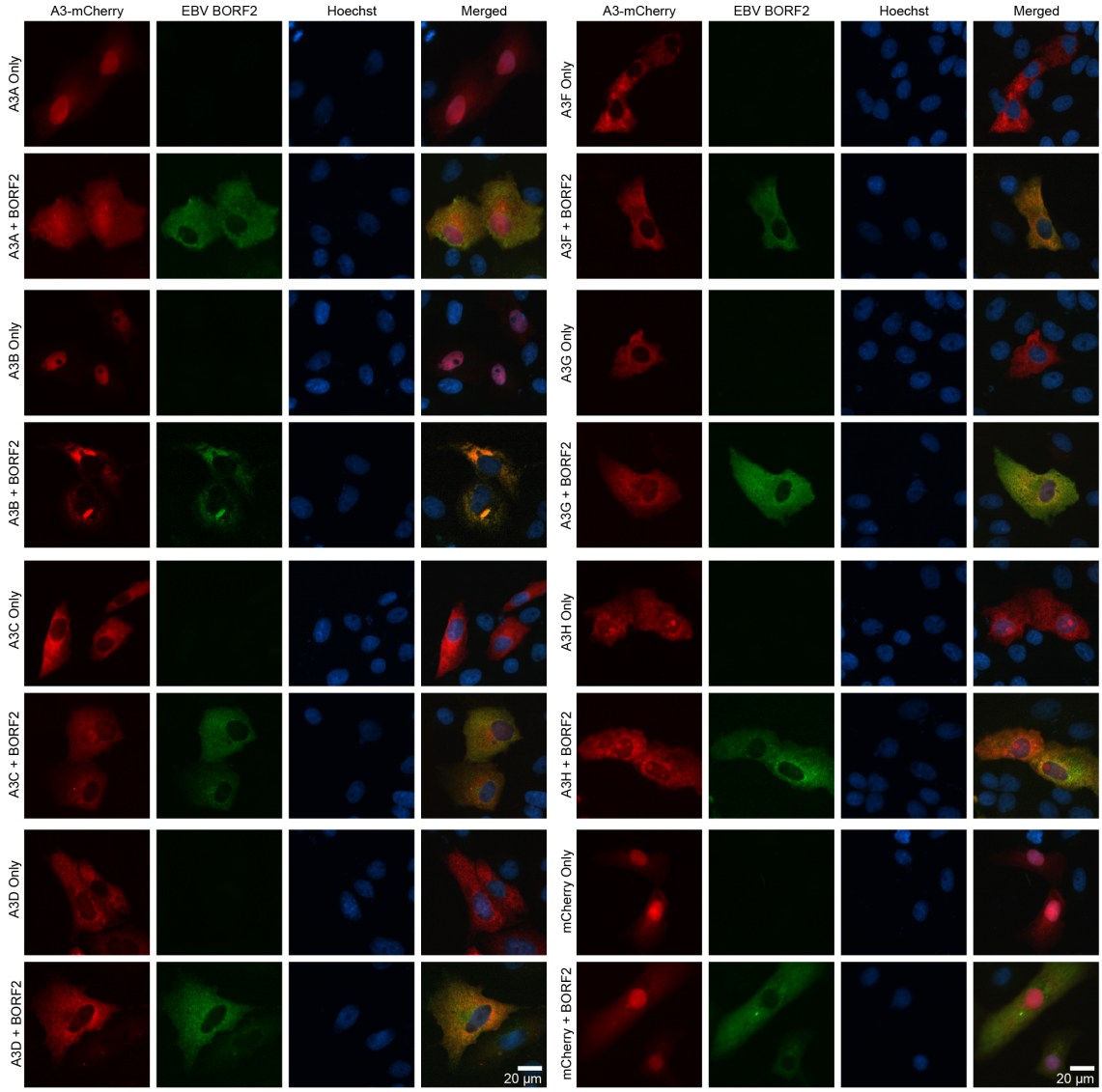

Supplementary Figure S3.1: EBV BORF2 relocalizes A3B and A3A. Representative immunofluorescence microscopy images of Vero cells transfected with either A3-mCherry or EBV BORF2-FLAG constructs. Cells were fixed 48 hours post-transfection, permeabilized, and stained with anti-FLAG antibody and Hoechst to stain the nuclear compartment.

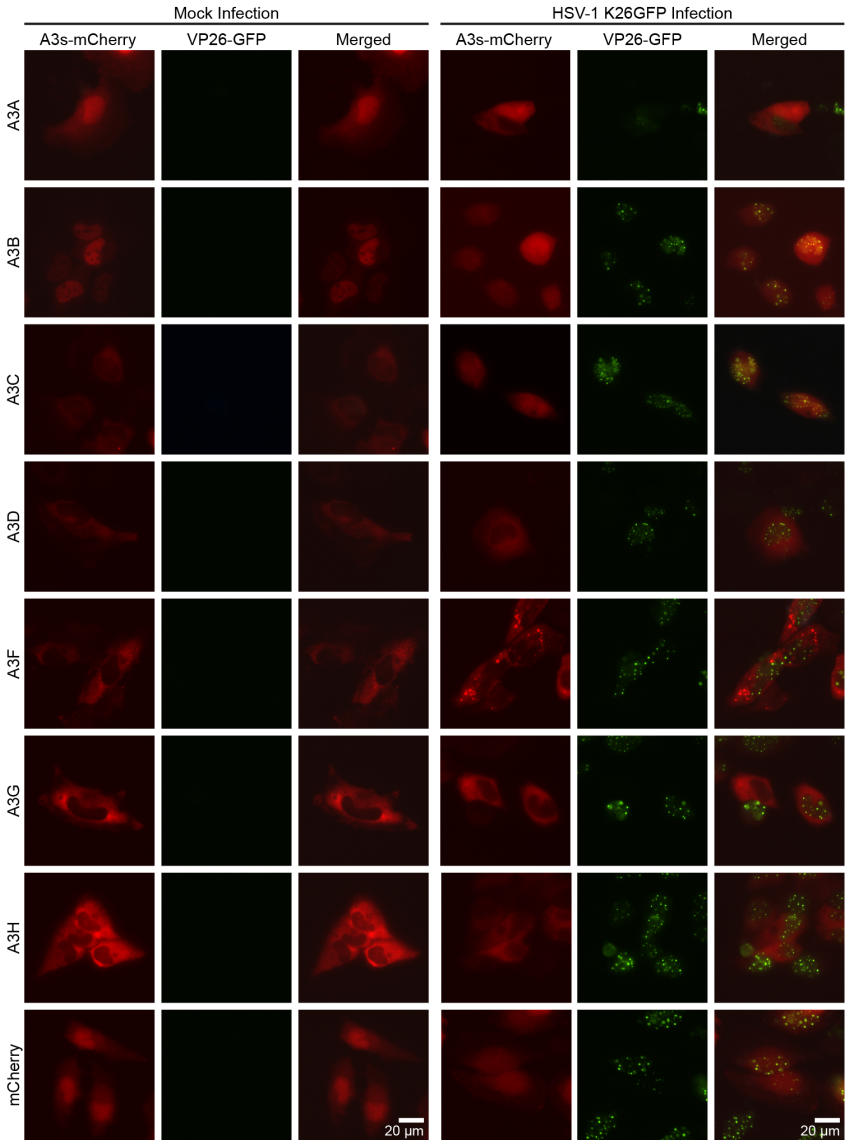

Supplementary Figure S3.2: HSV-1 infection relocalizes A3B and A3A. Representative images of HeLa cells transfected with A3-mCherry constructs, followed by mock or HSV-1 K26GFP infection 48 hours post-transfection. Cells were fixed 8 hpi and then imaged directly. The viral capsid protein VP26 is tagged with GFP to mark infected cells.

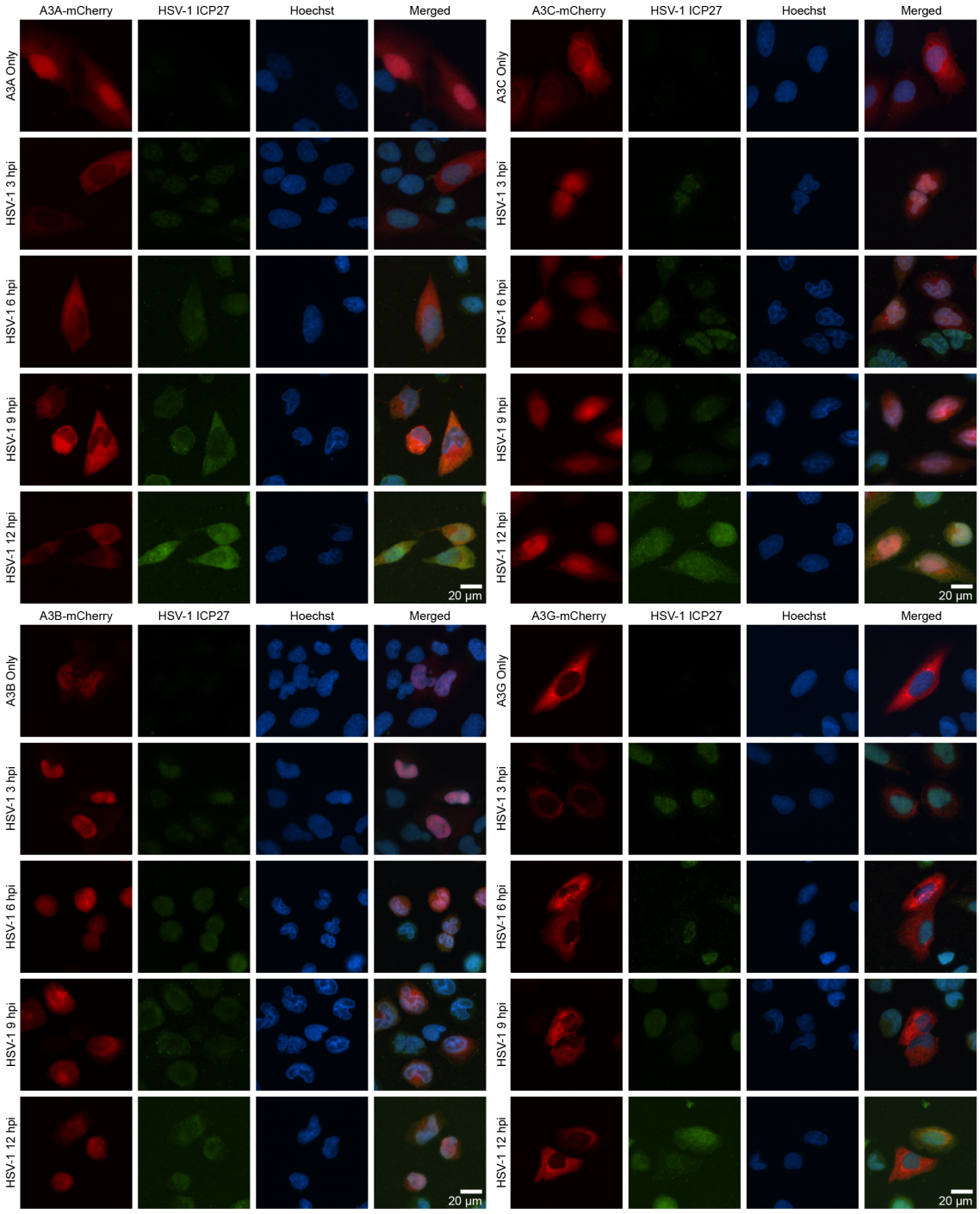

Supplementary Figure S3.3: Time course of HSV-1-mediated relocalization of A3B and A3A.

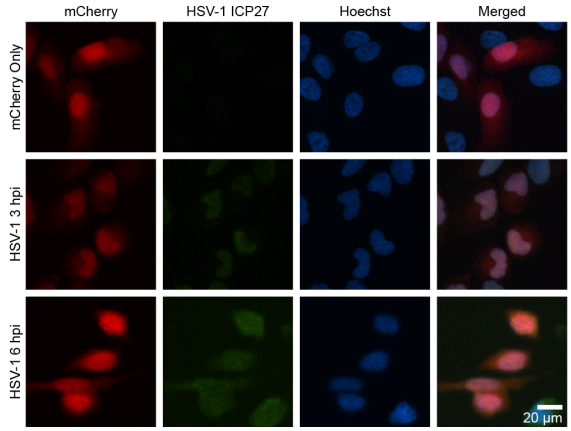

Supplementary Figure S3.3 (Continued):
Representative images of U2OS cells transfected with A3-mCherry constructs, followed by mock or HSV-1 KOS1.1 infection 48 hours post-transfection. Cells were fixed at either 3, 6, 9, or 12 hpi and stained with anti-ICP27 antibody to mark infected cells and Hoechst to stain the nuclear compartment.

CHAPTER 4

Discussion and Conclusions

Author: Adam Z. Cheng

4.1 Discussion

4.1.1 Summary

The expansion of *A3* genes since the ancestral placental mammal suggests a strong evolutionary advantage to preserve and expand upon *A3* gene function. Indeed, phylogenetic and bioinformatic analyses support the finding that these genes are under strong positive diversifying selection [317–319]. Highlighted in **Chapter 1** were some examples of convergent evolution in which viral factors antagonize human A3 proteins (*e.g.,* HIV-1 Vif, FV Bet, HTLV-1 NC, HBV HBx). Competition between virus and host survival is sometimes likened to an ongoing arms race in which both parties must continuously expand upon their armory of weapons in order to withstand and oppose the other party's assault. This analogy was formalized by Van Valen in 1973 as the "Red Queen's Hypothesis"[1] in which he proposes:

> We can think of the Red Queen's Hypothesis in terms of an unorthodox game theory. To a good approximation, each species is part of a zero-sum game against other species. Which adversary is most important for a species may vary from time to time, and for some or even most species no one adversary may ever be paramount. Furthermore, no species can ever win, and new adversaries grinningly replace the losers. [320]

In other words, viruses or other pathogens are always at constant odds against the host and, in order for the host to persist, it must be constantly "running," for failure to do so could result in extinction. Inability to adapt by the virus is similarly lethal (*e.g.,*

[1] In describing his new hypothesis on a law of evolutionary extinction, Van Valen referenced the following excerpt from Lewis Caroll's *Through the Looking Glass* (1871): "Now here, you see, it takes all the running you can do, to keep in the same place." In the following sentence of the Queen's dialogue with Alice, she states, "If you want to get somewhere else, you must run at least twice as fast as that!" Unfortunately, it seems that the rate of evolution can not yet be controlled, perhaps to the dismay of Van Valen.

extinct retroelements like LINE-1 and Alu [321, 322], endogenized bornaviruses [323] and hepadnaviruses [324]). The sub-discipline of paleovirology attempts to study these extinct viruses in order to understand when and why certain viral lineages disappeared. Were there novel host factors that arose? How did modern day viruses evolve to persist while those of the ancient past faded away?

The evolution of lentiviruses along with their hosts is a prime example of ongoing adaptation and counter-adaptation between viral Vif proteins and cellular APOBEC enzymes [325]. Based on parsimony, the ancestral lentivirus Vif most likely resembled bovine immunodeficiency virus (BIV) Vif, which degrades the simpler two APOBEC3 protein repertoire of the host [89]. This process still requires use of the host E3 ubiquitin ligase, but without CBF-β as a co-factor. During the divergence of sheep and goats from the placental ancestor, lentiviruses infecting these animals (sheep: Maedi-visna virus, MVV; goat: caprine arthritis encephalitis virus, CAEV) acquired a conserved requirement for the co-factor, cyophilin A (CypA) [89, 326]. Cats diverged independently in parallel with an expansion of the *APOBEC3* locus resulting in four genes; however, a feline immunodeficiency virus Vif co-factor has yet to be identified [13, 89]. Most recently, humans and non-human primates possess a seven member APOBEC3 family and with counteraction of at least five of them (A3C, A3D, A3F, A3G, A3H) by primate lentiviral Vif. Not only does this Vif degrade cellular A3 enzymes, it also recruits CBF-β as a co-factor, which results in downregulation at the transcriptional level [81]. Thus, as a species' innate immune repertoire becomes more advanced, so too does viral adaptation.

If A3C, A3D, A3F, A3G, and A3H are present day mediators of HIV-1 restriction and targets of Vif counter-restriction, what then is the physiological function of the other two A3 enzymes? Given that APOBEC3 enzymes are DNA cytosine

deaminases, there is a surprising paucity of examples showing A3-mediated restriction of DNA viruses. Instead, there is a trend towards deamination of single-stranded DNA intermediates after reverse transcription of retroviruses. Potentially, this is because these substrates are highly accessible compared to double-stranded DNA, which would become single-stranded only transiently during transcription or replication. To this point, the restriction of hepadnaviruses occurs during an RNA-to-DNA intermediate mediated by reverse transcriptase. Nevertheless, even dsDNA viruses must have intermittently exposed ssDNA during replication or transcription. Recent experiments in HPV and polyomaviruses suggest that these small dsDNA viruses may upregulate A3B for proviral, promutagenic activities [26, 29, 112]. However, the prior absence of a counteraction or evasion mechanism against APOBEC3 enzymes in large dsDNA viruses like herpesviruses posed a significant barrier to our understanding of antiviral innate immunity.

Prior studies by Dr. Natasha Soni-Malik (past graduate student in Frappier Lab) identified an interaction between EBV BORF2 and A3B using affinity purification-mass spectrometry (AP-MS) [327]. Subsequently, a dedicated and comprehensive investigation of the BORF2-A3B interaction has revealed novel insights on APOBEC and herpesvirus biology. ***The studies described in this doctoral thesis define a novel conserved mechanism by which herpesviruses utilize the large subunit of the virus-encoded ribonucleotide reductase to counteract APOBEC3-mediated restriction for productive lytic infection and propagation*** (**Figure 4.1**).

Using a series of biochemical, cellular, and bioinformatic approaches, we showed that EBV BORF2 specifically interacts with APOBEC3B using the surface-exposed loop 7 [30], but not loops 1 or 3 (data not shown). Because loop 7 mediates -1

nucleotide preference (*i.e.*, 5'-TC), it was suspected that binding of a large viral protein near the catalytic site of A3B would impede deaminase activity. Subsequent purification of BORF2 and A3 enzymes *in vitro* showed that BORF2 inhibited A3B, but not A3H enzymatic activity in a dose-dependent manner. At equimolar concentrations, BORF2-mediated inhibition was almost complete suggesting a stoichiometric interaction. These *in vitro* assays and tandem co-IP experiments (data not shown) indicated the BORF2-A3B interaction is direct. Immunofluorescence microscopy and live cell imaging revealed an additional layer of counteraction by BORF2-mediated relocalization of A3B from the nucleus to perinuclear ER-associated aggregates. Deletion of BORF2 using a CRISRP/Cas9-based approach led to A3B co-localization with sites of ongoing replication as marked by the thymidine analog, EdU, and EBV BMRF1, the viral processivity factor. These data suggested the possibility A3B-mediated deamination of replicating viral genomes in the absence of BORF2. Indeed, Sanger sequencing of PCR fragments and Illumina MiSeq of EBVΔBORF2 showed that regions of EBV were susceptible to hypermutation at A3B-specific 5'-TCA trinucleotide contexts. Accordingly, EBVΔBORF2 suffered in both virus production and virus infectivity, while the same EBVΔBORF2 strain produced from A3B-null Akata cells replicated as well as wild-type virus.

Bioinformatic studies indicated that BORF2 has been under strong positive selection likely to preserve this function of A3B counteraction. Moreover, analysis of all publicly available sequences of BORF2 showed no nonsynonymous mutations in the A3B-interacting region of BORF2. The EBV viral genome has also suffered A3B target site (5'-T$\underline{\text{C}}$A) depletion and product (5'-T$\underline{\text{T}}$A) enrichment that reinforces the notion that A3B has applied selective pressures on the genome over evolutionary time. Finally, the general mechanism of R1-mediated A3 counteraction by interaction

and relocalization is conserved among the α-HV homologue, HSV-1 ICP6, and γ-HV homologue, KSHV ORF61. Altogether, these data indicate that an essential noncatalytic function of herpesvirus R1 proteins is to inhibit the restrictive capacities of APOBEC3 enzymes.

4.1.2 The Physiologic Herpesvirus Restriction Factor

The role for A3B as a *physiologic* restriction factor of EBV is clear for several reasons. First, endogenous A3B is expressed in EBV-tropic cell types such as B and epithelial cells. Second, A3B is the solely nuclear A3 enzyme and endogenous A3B was able to co-localize with replicating viral DNA in the absence of BORF2 (**Chapter 2**). Third, both A3B and BORF2 are under positive selection, suggestive of host/pathogen co-evolution. Fourth, both *in vitro* and ongoing *in vivo* studies demonstrate the necessity of the viral counteraction factor for proficient virus replication. Fifth, conservation of R1-A3 interactions indicates an evolutionary advantage to preserve these functions across herpesvirus subfamilies.

A3A is less likely to be a physiologic restriction factor for EBV, but may be important in restricting other viruses. Namely, the gene expression profile of *A3A* is limited to mostly monocytes and macrophages and not expressed in B, T, NK, or epithelial cells. As such, EBV replication most likely occurs in the absence of A3A. Another possibility is that either *A3A* or *A3B* is induced after viral infection. For example, HPV E6 and BK/JC PyV T antigen can induce *A3B* expression [26, 29, 103, 112]. *A3A* expression is also interferon-inducible and likely elevated during inflammatory processes like viral infection [43, 44, 80]. In Akata (B cell) and AGS (gastric carcinoma) cell lines, we saw no changes in *A3* gene expression during latent

or lytic EBV replication for either wild-type EBV or EBVΔBORF2 (data not shown). However, we cannot rule out that infection and reactivation *in vivo* could generate chemokines that stimulate *A3* induction for downstream functions in virus restriction.

The question of whether A3A, A3B, or both enzymes serve as restriction factors for HSV-1 is more contentious. In overexpression experiments, both enzymes can be targeted by the virus for relocalization. However, this may be due to molecular mimicry since A3A is 92% similar to A3B-ctd with identical loop 7 sequences. Moreover, A3A is not expressed in epithelial cells or neurons, meaning that HSV-1 would never encounter A3A *in vivo*. On the other hand, A3B is expressed in epithelial cells making this family member more physiologically relevant. It would also imply that there are no A3 enzymes capable of targeting HSV-1 during latency in neurons due to the lack of viral replication in neurons and almost no transcription of the genome.

The targeting of a specific pathway by multiple proteins with overlapping functions is not uncommon in the field of virology (*e.g.*, NF-κB pathway and anti-apoptosis examples described in **Chapter 1**). Studies performed in **Chapter 2** indicate that viral UDG partially repairs A3B-mediated deamination in the absence of BORF2 and that UDG inhibition by exogenous UGI increases A3B mutagenesis. Potentially, there may be other viral proteins involved in uracil processing and repair that add an additional layer of protection against cytosine deamination and uracil misincorporation. For example, deletion of both viral UDG and dUTPase in murine gammaherpesvirus 68 was shown to have a synergistic effect to inhibit virus replication and increase genomic instability [328]. Would inhibition of viral R1, UDG, and dUTPase make the virus wholly susceptible to APOBEC restriction? Are there other sources of functional redudundancy in APOBEC counteraction? Further experiments

will be required to address these questions.

4.1.3 A Multitude of Herpesvirus R1 Functions

The canonical function of R1 proteins is ribonucleotide reduction in complex with its small subunit partner [233–235]. A second function of herpesvirus R1 was discovered in mouse MCMV M45 and later extended to HSV-1/2 homologues to inhibit apoptosis and promote necroptosis using conserved N-terminal extensions [237–239, 242]. The HCMV homologue, UL45, showed only a partial phenotype on this front, but was noted to also interact with RIP1 to inhibit NF-κB signalling [243, 244]. In a colorimetric cell cycle screen, EBV BORF2 was identified as a viral factor capable of inducing G_1/S arrest [245]. Studies detailed here revealed yet another function of herpesvirus R1 proteins in the counteraction of A3B [30].

How can we begin to tease apart the multitude of herpesvirus R1 functions? The significance of RNR activity can be tested by generating point mutants at catalytic sites on either R1 or R2. Because the reduction of ribonucleotides requires a stepwise transfer of a radical on tyrosine or cysteine residues, disruption of any one of these should be sufficient to abolish activity [233–236]. Anti-apoptotic functions for α- and β-herpesviruses have more or less been mapped out to the N-terminal domain [237–239, 242]. For HSV-1 ICP6, a single point mutant R950H was shown to have a significant effect on pathogenicity *in vivo* due to an impaired ability to inhibit apoptosis [329].

Separation of A3 counteraction function has been more challenging than anticipated. Initial truncation experiments narrowed the BORF2-A3B interaction to a conserved RNR core domain retaining amino acids 25-739 (out of 826), but

further truncations resulted in loss of interaction [30]. A predicted structure of BORF2 was then generated based on existing crystal structures to identify potential surface-exposed residues. Through an extensive series of site-directed mutagenesis experiments, several regions in the conserved RNR domain were found to completely abolish A3B binding as well as localization (data not shown). These mutants retained BaRF1 interactions by co-IP and expressed at levels similar to wild-type suggesting that proper protein folding remained intact. Studies to graft these mutations into EBV genomes for *in vitro* and *in vivo* infectivity studies are in progress.

The most important question to be addressed is which function is most important for herpesvirus replication. Prior studies in EBV suggest that RNR activity is not at all required for replication because BORF2-null EBV produced from Akata cells replicated similar to wild-type EBV due to the lack of endogenous A3B [30]. However, more detailed engineering of point mutants that separate function will be needed to test this completely as well as further verification in primary cells. Similar mutation analyses of HSV-1 ICP6 will also be insightful. HSV-1 ICP6 already has been shown to have important functions as an inhibitor of apoptosis [237–239, 242]. Counteraction of A3 enzymes is likely also a crucial function, but may share redundancy with another viral enzyme, such that loss of ICP6 may not have immediately revealing replication defects. These separation of function mutants can be generated by using existing bacterial artificial chromosomes methods or by applying newer CRISPR-based approaches such as base-editing or homologous recombination.

Lastly, a puzzling void in the BORF2-A3B story still remains: How does BORF2 induce G_1/S arrest? Are other cellular factors involved in the BORF2-A3B complex? *In vitro* activity and interaction studies in a heterologous *E. coli* system would argue against this possibility, but does not rule out separate A3B-independent complexes.

A G_1/S arrest phenotype would certainly be beneficial to the virus and allow more time for dNTP synthesis. Further collaborative work with the Frappier lab will be essential for elucidating this mystery.

The different R1 functions underscore the compactness of viral genomes and efficiency for encoding multiple tasks into one protein. It also reminds us of the Red Queen and her run with Alice: As A3 proteins diversified from a common ancestral AID-like protein, co-evolving pathogens also developed novel ways to persist in the face of these innate immune pressures. When and how did herpesvirus R1 proteins evolve these A3 counteraction functions? In the history of herpesvirus evolution, what are the origins of other R1 functions? Did these functional domains arise from viruses adapting to early mammals or from viruses infecting more ancient ancestors like bony fish or algae?[2] Although the evolutionary origins of these protein domains are unclear, they are almost certain to have provided an extremely beneficial advantage over earlier ancestors to combat the ongoing expansion and divergence of APOBEC enzymes. Perhaps the multifunctional R1 proteins are even more versatile than just RNR catalysis, apoptosis inhibition, and A3 counteraction.

4.1.4 Clinical Applications and Questions

The results presented in this thesis yield at least two clear potential avenues for clinical development. The first lies in disrupting the R1-A3 interaction as a novel approach for antiviral intervention. The second leverages the inhibitory effects of R1 molecules as a framework for developing drugs that specifically target A3B in cancer.

[2] The 331 kbp Paramecium bursaria Chlorella virus 1 from the large dsDNA *Phycodnaviridae* family infects eukaryotic algae [330, 331] and also encodes an R1 protein, A629R. A precursory alignment with EBV BORF2 shows 43% similarity at the protein level including regions of high conservation around the putative A3B-binding domain in BORF2.

Both routes will likely require years of further work in improving our understanding of basic biology, developing/screening drug candidates, applying animal models, and testing in clinical trials. A brief overview of potential challenges and benefits is described here.

Ribonucleotide reductases are conserved across almost all forms of DNA-based life. Numerous FDA-approved RNR inhibitors exist for anti-cancer chemotherapy including hydroxyurea, gemcitabine, gallium nitrate, and others [332–334]. The mechanisms for these drugs are based on either direct enzymatic inhibition (*e.g.*, hydroxyurea scavenges the free tyrosyl radical generated by R2 [335] and gallium nitrate substitutes for Fe^{III} in the catalytic pocket [336]) or nucleoside analogues (*e.g.*, gemcitabine is a pro-drug that is phosphorylated to a deoxycytidine analogue that inhibits the RNR [337]). However, these drugs lack specificity in terms of cellular uptake and function in chemotherapy by the principle of increased turnover and metabolism in cancer cells. Hence, these drugs often have a number of associated cytotoxic side effects such as pancytopenia, hepatitis, nephrotoxicity, paresthesia, and others [332–334].

We propose that enzymatic inhibition is likely insufficient to produce a specific therapeutic antiviral intervention due to similarities in R1 and R2 across Class Ia RNRs (*i.e.*, both humans and herpesviruses). Instead, targeting and inhibiting the R1-A3 interface has the potential to generate a more specific drug candidate. This is because human R1 does not interact with human A3s [30] and also because the R1-A3 interface is independent of the R1-R2 interaction surface (data not shown). Disruption of the R1-A3 axis is anticipated to allow A3-mediated deamination and hypermutation of viral genomes, which we previously showed *in vitro* to cause a 50-70% reduction in virus infectivity after one round of replication. Over the course

of several viral life cycles within a host, one would predict compounding effects A3-mediated hypermutation, leading to eventual extinction of the virus. Additional *in vivo* experiments will be required to demonstrate this hypothesis.

Whether or not blocking just the A3-binding domain would be sufficient for virus inhibition remains to be addressed, but epidemiological data suggest that A3B plays an important role in limiting the pathogenesis of EBV even in the presence of BORF2. As covered in **Chapter 1**, a naturally circulating *A3B* deletion polymorphism is common in Southeast Asia, Oceania, and in native North and South Americans [47]. Perhaps not coincidentally, several lytic-associated EBV diseases are much more prevalent in these same identical regions including chronic active EBV, nasopharyngeal carcinoma, and gastric carcinoma. Even some latency-associated extranodal NK and T-cell lymphomas (NKTL) show geographic differences in incidence, mechanisms of pathogenesis, and disease severity [116, 338–340].

In particular, the EBV-associated nasal subtype of NKTL is approximately 10-fold higher in Southeast Asia and South America than Europe or North America (without consideration for native American subgroups) [338, 341–343] in spite of identical EBV subtypes found in cancers from all regions [344]. This implicates the presence of an underlying environmental or genetic factor influencing the progression of disease. A few gene mutations in TP53, JAK/STAT3 signaling, and FAS receptor have been implicated with increased risk of NKTL, but these studies only showed associations and lacked experimental validation [338]. More work on this front is required to tease out the various factors involved in disease progression. It is additionally enticing to surmise a potential link between EBV disease incidence and pathogenesis with the naturally circulating *A3B* deletion polymorphism.[3]

[3] Accordingly, I would wager a bottle of good Scotch whisky that such a correlation exists and that deletion of *A3B* partially contributes to increased risk for lytic-associated herpesvirus diseases.

If endogenous A3B does indeed play a role in protection from these EBV-associated diseases, it would be logical to assume that A3B would have an even greater effect in innate immunity in the absence of the counteraction factor. If this could be achieved through chemical means, such as an orally-bioavailable once-a-daily pill, it has the potential to change the medical landscape of herpesvirus management. Presumably, such a pill could be used for treatment of lytic replication ranging from relatively benign cold sores to life-threatening diseases like EBV-associated carcinomas and lymphomas. It could also be used for prevention in patients with recurrent cases of lytic diseases or prior to transplant to mitigate the risks of post-transplant lymphoproliferative disorder.

On the flip side, misregulation of *A3B* expression has been shown to cause genomic hypermutation and instability [38, 46, 269, 345, 346]. Although it is probably not an initiating factor in oncogenesis, elevated levels of *A3B* contribute to ongoing tumor evolution, worsening prognosis, drug resistance, and metastasis in the setting of existing cancer [66, 347–349]. The current working model suggests that an unknown tumor initiating event increases *A3B* expression, which in turn generates increased levels of genomic C-to-T mutations. Finding a way to block this process would slow down both cancer evolution and immune escape, which could aid as an adjuvant in chemotherapy regimens.

This goal could be achieved by designing a BORF2-like compound to bind and relocalize A3B in cancer cells. A significant discovery of the BORF2-A3B interaction was that it did not rely on other cellular factors for enzymatic inhibition unlike other examples of A3B counteraction (*e.g.*, Vif requires a functional ubiquitin ligase [350]). Moreover, the region of interaction mapped to a few amino acids on loop 7 but not loops 1 and 3, suggesting that the interaction surface may be discrete or well defined.

It is also near the catalytic pocket making it tractable for designing small molecules to fit adjacent grooves. However, the lack of atomic-level structural data is a currently a major hurdle in our understanding of the R1-A3 interaction. Solving the crystal structure would allow for rational drug design in synthesizing peptides that mimic the interaction surface.

Apart from direct enzymatic inhibition, another route for developing anti-A3B therapies could focus on physically removing A3B from replicating genomic DNA. This function is a conserved feature of HSV-1 ICP6, EBV BORF2, and KSHV ORF61. Several A3B residues have been implicated to be essential for nuclear localization [65, 87], but the mechanism by which it trafficks to the nucleus is not yet known. It has been suggested that A3B import requires other cellular factors [65]. If this is the case, R1-mediated binding to A3B could block the interaction with its import factor such that it retains cytoplasmic localization. Identification of these factors could reveal new targets for A3B retention. In the end, drugs that target either enzymatic function or inhibit physiological nuclear import would both have the same result by preventing A3B-mediated deamination of genomic DNA and aid in the treatment of A3B-expressing cancers.

4.2 Conclusions

HE Red Queen Hypothesis states that viruses and hosts are constantly co-evolving to stay in place. Every advancement in host innate immunity is met by similar counteraction by viral factors. This doctoral thesis advances the current understanding of basic virology and antiviral innate immunity. We define a novel

and conserved mechanism of APOBEC-mediated restriction and counteraction by herpesvirus ribonucleotide reductases. The R1-A3 axis highlights the role of A3B as a physiological restriction factor for EBV, KSHV, and HSV-1. Future *in vivo*, structural, proteomic, and biochemical studies will be needed to further illuminate the importance of the R1-A3 interaction and aid in the development of new antiviral and anti-cancer drugs.

4.3 Figures

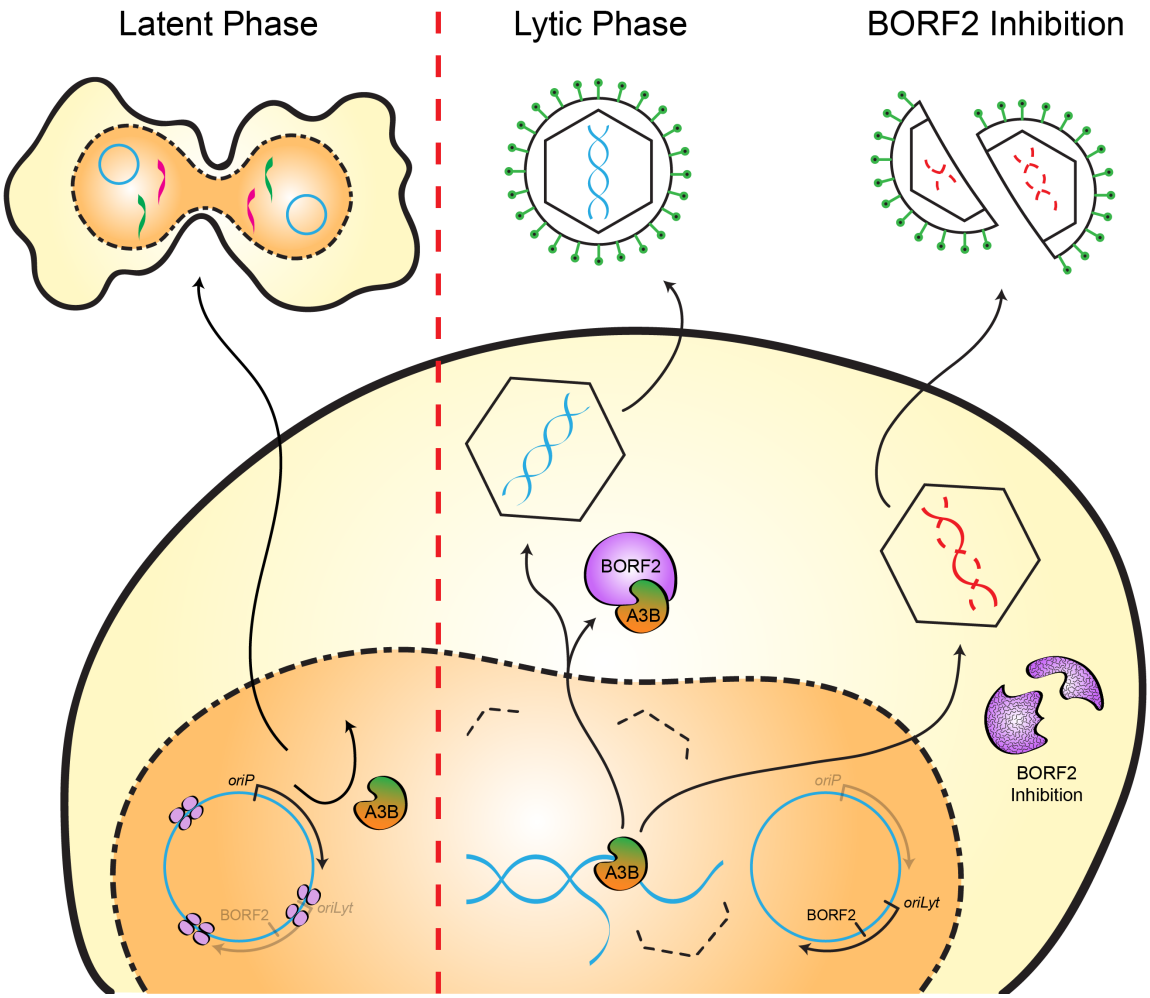

Figure 4.1: Working model of R1-mediated A3 counteraction.
Latency Phase: A3B is likely unable to access herpesvirus episomal DNA due to histone modifications and chromatinization. There is also low levels of transcriptional activity and therefore less exposed ssDNA.
Lytic Phase: The early lytic protein, BORF2, is expressed in early lytic phase. BORF2 directly interacts with A3B to inhibit enzymatic activity and relocalizes A3B to perinuclear ER-associated aggregates. This prevents A3B-mediated deamination and allows for faithful replication of the viral genome.
BORF2 Inhibition: In the absence of the viral counteraction factor, such as with CRISPR-mediated deletion or small molecule inhibition, nuclear A3B is now able to access replicating viral DNA. This leads to C-to-T mutations resulting in viral hypermutation, defects in virus production, and loss of infectivity.

References

1. Conticello, S. G. The AID/APOBEC family of nucleic acid mutators. *Genome Biol* **9,** 229 (2008).

2. Harris, R. S. & Dudley, J. P. APOBECs and virus restriction. *Virology* **479-480,** 131–45 (2015).

3. Salter, J. D., Bennett, R. P. & Smith, H. C. The APOBEC Protein Family: United by Structure, Divergent in Function. *Trends Biochem Sci* **41,** 578–594 (2016).

4. Whitfield, A. J., Barrett, P. H., van Bockxmeer, F. M. & Burnett, J. R. Lipid disorders and mutations in the APOB gene. *Clin Chem* **50,** 1725–32 (2004).

5. Conticello, S. G., Langlois, M. A., Yang, Z. & Neuberger, M. S. DNA deamination in immunity: AID in the context of its APOBEC relatives. *Adv Immunol* **94,** 37–73 (2007).

6. Muramatsu, M., Sankaranand, V. S., Anant, S., Sugai, M., Kinoshita, K., Davidson, N. O. & Honjo, T. Specific expression of activation-induced cytidine deaminase (AID), a novel member of the RNA-editing deaminase family in germinal center B cells. *J Biol Chem* **274,** 18470–6 (1999).

7. Di Noia, J. M. & Neuberger, M. S. Molecular mechanisms of antibody somatic hypermutation. *Annu Rev Biochem* **76,** 1–22 (2007).

8. Stavnezer, J., Guikema, J. E. & Schrader, C. E. Mechanism and regulation of class switch recombination. *Annu Rev Immunol* **26,** 261–92 (2008).

9. Lada, A. G., Krick, C. F., Kozmin, S. G., Mayorov, V. I., Karpova, T. S., Rogozin, I. B. & Pavlov, Y. I. Mutator effects and mutation signatures of editing deaminases produced in bacteria and yeast. *Biochemistry (Mosc)* **76,** 131–46 (2011).

10. Rogozin, I. B., Iyer, L. M., Liang, L., Glazko, G. V., Liston, V. G., Pavlov, Y. I., Aravind, L. & Pancer, Z. Evolution and diversification of lamprey antigen receptors: evidence for involvement of an AID-APOBEC family cytosine deaminase. *Nat Immunol* **8,** 647–56 (2007).

11. Holland, S. J., Berghuis, L. M., King, J. J., Iyer, L. M., Sikora, K., Fifield, H., Peter, S., Quinlan, E. M., Sugahara, F., Shingate, P., Trancoso, I., Iwanami, N., Temereva, E., Strohmeier, C., Kuratani, S., Venkatesh, B., Evanno, G., Aravind, L., Schorpp, M., Larijani, M. & Boehm, T. Expansions, diversification, and interindividual copy number variations of AID/APOBEC family cytidine deaminase genes in lampreys. *Proc Natl Acad Sci U S A* **115,** E3211–E3220 (2018).

12. Krishnan, A., Iyer, L. M., Holland, S. J., Boehm, T. & Aravind, L. Diversification of AID/APOBEC-like deaminases in metazoa: multiplicity of clades and widespread roles in immunity. *Proc Natl Acad Sci U S A* **115,** E3201–E3210 (2018).

13. LaRue, R. S., Andrsdttir, V., Blanchard, Y., Conticello, S. G., Derse, D., Emerman, M., Greene, W. C., Jonsson, S. R., Landau, N. R., Lochelt, M., Malik, H. S., Malim, M. H., Munk, C., O'Brien, S. J., Pathak, V. K., Strebel, K., Wain-Hobson, S., Yu, X. F., Yuhki, N. & Harris, R. S. Guidelines for naming nonprimate APOBEC3 genes and proteins. *J Virol* **83,** 494–7 (2009).

14. Hayward, J. A., Tachedjian, M., Cui, J., Cheng, A. Z., Johnson, A., Baker, M. L., Harris, R. S., Wang, L. F. & Tachedjian, G. Differential Evolution of Antiretroviral Restriction Factors in Pteropid Bats as Revealed by APOBEC3 Gene Complexity. *Mol Biol Evol* **35,** 1626–1637 (2018).

15. Sheehy, A. M., Gaddis, N. C., Choi, J. D. & Malim, M. H. Isolation of a human gene that inhibits HIV-1 infection and is suppressed by the viral Vif protein. *Nature* **418,** 646–50 (2002).

16. Harris, R. S., Bishop, K. N., Sheehy, A. M., Craig, H. M., Petersen-Mahrt, S. K., Watt, I. N., Neuberger, M. S. & Malim, M. H. DNA deamination mediates innate immunity to retroviral infection. *Cell* **113,** 803–9 (2003).

17. Wiegand, H. L., Doehle, B. P., Bogerd, H. P. & Cullen, B. R. A second human antiretroviral factor, APOBEC3F, is suppressed by the HIV-1 and HIV-2 Vif proteins. *EMBO J* **23,** 2451–8 (2004).

18. Dang, Y., Wang, X., Esselman, W. J. & Zheng, Y. H. Identification of APOBEC-3DE as another antiretroviral factor from the human APOBEC family. *J Virol* **80,** 10522–33 (2006).

19. Sasada, A., Takaori-Kondo, A., Shirakawa, K., Kobayashi, M., Abudu, A., Hishizawa, M., Imada, K., Tanaka, Y. & Uchiyama, T. APOBEC3G targets human T-cell leukemia virus type 1. *Retrovirology* **2,** 32 (2005).

20. Russell, R. A., Wiegand, H. L., Moore, M. D., Schafer, A., McClure, M. O. & Cullen, B. R. Foamy virus Bet proteins function as novel inhibitors of the APOBEC3 family of innate antiretroviral defense factors. *J Virol* **79,** 8724–31 (2005).

21. Turelli, P., Mangeat, B., Jost, S., Vianin, S. & Trono, D. Inhibition of hepatitis B virus replication by APOBEC3G. *Science* **303,** 1829 (2004).

22. Lucifora, J., Xia, Y., Reisinger, F., Zhang, K., Stadler, D., Cheng, X., Sprinzl, M. F., Koppensteiner, H., Makowska, Z., Volz, T., Remouchamps, C., Chou, W. M., Thasler, W. E., Huser, N., Durantel, D., Liang, T. J., Munk, C., Heim, M. H., Browning, J. L., Dejardin, E., Dandri, M., Schindler, M., Heikenwalder, M. & Protzer, U. Specific and nonhepatotoxic degradation of nuclear hepatitis B virus cccDNA. *Science* **343,** 1221–8 (2014).

23. Suspene, R., Guetard, D., Henry, M., Sommer, P., Wain-Hobson, S. & Vartanian, J. P. Extensive editing of both hepatitis B virus DNA strands by APOBEC3 cytidine deaminases in vitro and in vivo. *Proc Natl Acad Sci U S A* **102,** 8321–6 (2005).

24. Esnault, C., Heidmann, O., Delebecque, F., Dewannieux, M., Ribet, D., Hance, A. J., Heidmann, T. & Schwartz, O. APOBEC3G cytidine deaminase inhibits retrotransposition of endogenous retroviruses. *Nature* **433,** 430–3 (2005).

25. Chiu, Y. L., Witkowska, H. E., Hall, S. C., Santiago, M., Soros, V. B., Esnault, C., Heidmann, T. & Greene, W. C. High-molecular-mass APOBEC3G complexes restrict Alu retrotransposition. *Proc Natl Acad Sci U S A* **103,** 15588–93 (2006).

26. Vieira, V. C., Leonard, B., White, E. A., Starrett, G. J., Temiz, N. A., Lorenz, L. D., Lee, D., Soares, M. A., Lambert, P. F., Howley, P. M. & Harris, R. S. Human papillomavirus E6 triggers upregulation of the antiviral and cancer genomic DNA deaminase APOBEC3B. *MBio* **5** (2014).

27. Vartanian, J. P., Guetard, D., Henry, M. & Wain-Hobson, S. Evidence for editing of human papillomavirus DNA by APOBEC3 in benign and precancerous lesions. *Science* **320,** 230–3 (2008).

28. Peretti, A., Geoghegan, E. M., Pastrana, D. V., Smola, S., Feld, P., Sauter, M., Lohse, S., Ramesh, M., Lim, E. S., Wang, D., Borgogna, C., FitzGerald, P. C., Bliskovsky, V., Starrett, G. J., Law, E. K., Harris, R. S., Killian, J. K., Zhu, J., Pineda, M., Meltzer, P. S., Boldorini, R., Gariglio, M. & Buck, C. B. Characterization of BK Polyomaviruses from Kidney Transplant Recipients Suggests a Role for APOBEC3 in Driving In-Host Virus Evolution. *Cell Host Microbe* **23,** 628–635 e7 (2018).

29. Verhalen, B., Starrett, G. J., Harris, R. S. & Jiang, M. Functional Upregulation of the DNA Cytosine Deaminase APOBEC3B by Polyomaviruses. *J Virol* **90,** 6379–6386 (2016).

30. Cheng, A. Z., Yockteng-Melgar, J., Jarvis, M. C., Malik-Soni, N., Borozan, I., Carpenter, M. A., McCann, J. L., Ebrahimi, D., Shaban, N. M., Marcon, E., Greenblatt, J., Brown, W. L., Frappier, L. & Harris, R. S. Epstein-Barr virus BORF2 inhibits cellular APOBEC3B to preserve viral genome integrity. *Nat Microbiol* **4,** 78–88 (2019).

31. Martinez, T., Shapiro, M., Bhaduri-McIntosh, S. & MacCarthy, T. Evolutionary effects of the AID/APOBEC family of mutagenic enzymes on human gamma-herpesviruses. *Virus Evol* **5,** vey040 (2019).

32. Iwatani, Y., Chan, D. S., Wang, F., Maynard, K. S., Sugiura, W., Gronenborn, A. M., Rouzina, I., Williams, M. C., Musier-Forsyth, K. & Levin, J. G. Deaminase-independent inhibition of HIV-1 reverse transcription by APOBEC3G. *Nucleic Acids Res* **35,** 7096–108 (2007).

33. Shi, K., Carpenter, M. A., Banerjee, S., Shaban, N. M., Kurahashi, K., Salamango, D. J., McCann, J. L., Starrett, G. J., Duffy, J. V., Demir, O., Amaro, R. E., Harki, D. A., Harris, R. S. & Aihara, H. Structural basis for targeted DNA cytosine deamination and mutagenesis by APOBEC3A and APOBEC3B. *Nat Struct Mol Biol* **24,** 131–139 (2017).

34. Shaban, N. M., Shi, K., Lauer, K. V., Carpenter, M. A., Richards, C. M., Salamango, D., Wang, J., Lopresti, M. W., Banerjee, S., Levin-Klein, R., Brown, W. L., Aihara, H. & Harris, R. S. The antiviral and cancer genomic DNA deaminase APOBEC3H is regulated by an RNA-mediated dimerization mechanism. *Mol Cell* **69,** 75–86 e9 (2018).

35. Helleday, T., Eshtad, S. & Nik-Zainal, S. Mechanisms underlying mutational signatures in human cancers. *Nat Rev Genet* **15,** 585–98 (2014).

36. Rathore, A., Carpenter, M. A., Demir, O., Ikeda, T., Li, M., Shaban, N. M., Law, E. K., Anokhin, D., Brown, W. L., Amaro, R. E. & Harris, R. S. The local dinucleotide preference of APOBEC3G can be altered from 5'-CC to 5'-TC by a single amino acid substitution. *J Mol Biol* **425,** 4442–54 (2013).

37. Shi, K., Carpenter, M. A., Kurahashi, K., Harris, R. S. & Aihara, H. Crystal structure of the DNA deaminase APOBEC3B catalytic domain. *J Biol Chem* **290,** 28120–30 (2015).

38. Alexandrov, L. B., Nik-Zainal, S., Wedge, D. C., Aparicio, S. A., Behjati, S., Biankin, A. V., Bignell, G. R., Bolli, N., Borg, A., Borresen-Dale, A. L., Boyault, S., Burkhardt, B., Butler, A. P., Caldas, C., Davies, H. R., Desmedt, C., Eils, R., Eyfjord, J. E., Foekens, J. A., Greaves, M., Hosoda, F., Hutter, B., Ilicic, T., Imbeaud, S., Imielinski, M., Jager, N., Jones, D. T., Jones, D., Knappskog, S., Kool, M., Lakhani, S. R., Lopez-Otin, C., Martin, S., Munshi, N. C., Nakamura, H., Northcott, P. A., Pajic, M., Papaemmanuil, E., Paradiso, A., Pearson, J. V., Puente, X. S., Raine, K., Ramakrishna, M., Richardson, A. L., Richter, J., Rosenstiel, P., Schlesner, M., Schumacher, T. N., Span, P. N., Teague, J. W., Totoki, Y., Tutt, A. N., Valdes-Mas, R., van Buuren, M. M., van 't Veer, L., Vincent-Salomon, A., Waddell, N., Yates, L. R., Australian Pancreatic Cancer Genome, I., Consortium, I. B. C., Consortium, I. M.-S., PedBrain, I., Zucman-Rossi, J., Futreal, P. A., McDermott, U., Lichter, P., Meyerson, M., Grimmond, S. M., Siebert, R., Campo, E., Shibata, T., Pfister, S. M., Campbell, P. J. & Stratton, M. R. Signatures of mutational processes in human cancer. *Nature* **500,** 415–21 (2013).

39. Di Noia, J. & Neuberger, M. S. Altering the pathway of immunoglobulin hypermutation by inhibiting uracil-DNA glycosylase. *Nature* **419,** 43–8 (2002).

40. Tubbs, A. & Nussenzweig, A. Endogenous DNA Damage as a Source of Genomic Instability in Cancer. *Cell* **168,** 644–656 (2017).

41. Krokan, H. E. & Bjoras, M. Base excision repair. *Cold Spring Harb Perspect Biol* **5,** a012583 (2013).

42. Nik-Zainal, S., Alexandrov, L. B., Wedge, D. C., Van Loo, P., Greenman, C. D., Raine, K., Jones, D., Hinton, J., Marshall, J., Stebbings, L. A., Menzies, A., Martin, S., Leung, K., Chen, L., Leroy, C., Ramakrishna, M., Rance, R., Lau, K. W., Mudie, L. J., Varela, I., McBride, D. J., Bignell, G. R., Cooke, S. L., Shlien, A., Gamble, J., Whitmore, I., Maddison, M., Tarpey, P. S., Davies, H. R., Papaemmanuil, E., Stephens, P. J., McLaren, S., Butler, A. P., Teague, J. W., Jonsson, G., Garber, J. E., Silver, D., Miron, P., Fatima, A., Boyault,

S., Langerod, A., Tutt, A., Martens, J. W., Aparicio, S. A., Borg, A., Salomon, A. V., Thomas, G., Borresen-Dale, A. L., Richardson, A. L., Neuberger, M. S., Futreal, P. A., Campbell, P. J., Stratton, M. R. & Breast Cancer Working Group of the International Cancer Genome, C. Mutational processes molding the genomes of 21 breast cancers. *Cell* **149,** 979–93 (2012).

43. Koning, F. A., Newman, E. N., Kim, E. Y., Kunstman, K. J., Wolinsky, S. M. & Malim, M. H. Defining APOBEC3 expression patterns in human tissues and hematopoietic cell subsets. *J Virol* **83,** 9474–85 (2009).

44. Refsland, E. W., Stenglein, M. D., Shindo, K., Albin, J. S., Brown, W. L. & Harris, R. S. Quantitative profiling of the full APOBEC3 mRNA repertoire in lymphocytes and tissues: implications for HIV-1 restriction. *Nucleic Acids Res* **38,** 4274–4284 (2010).

45. Anderson, B. D., Ikeda, T., Moghadasi, S. A., Martin, A. S., Brown, W. L. & Harris, R. S. Natural APOBEC3C variants can elicit differential HIV-1 restriction activity. *Retrovirology* **15,** 78 (2018).

46. Burns, M. B., Lackey, L., Carpenter, M. A., Rathore, A., Land, A. M., Leonard, B., Refsland, E. W., Kotandeniya, D., Tretyakova, N., Nikas, J. B., Yee, D., Temiz, N. A., Donohue, D. E., McDougle, R. M., Brown, W. L., Law, E. K. & Harris, R. S. APOBEC3B is an enzymatic source of mutation in breast cancer. *Nature* **494,** 366–70 (2013).

47. Kidd, J. M., Newman, T. L., Tuzun, E., Kaul, R. & Eichler, E. E. Population stratification of a common APOBEC gene deletion polymorphism. *PLoS Genet* **3,** e63 (2007).

48. Nik-Zainal, S., Wedge, D. C., Alexandrov, L. B., Petljak, M., Butler, A. P., Bolli, N., Davies, H. R., Knappskog, S., Martin, S., Papaemmanuil, E., Ramakrishna, M., Shlien, A., Simonic, I., Xue, Y., Tyler-Smith, C., Campbell, P. J. & Stratton, M. R. Association of a germline copy number polymorphism of APOBEC3A and APOBEC3B with burden of putative APOBEC-dependent mutations in breast cancer. *Nat Genet* **46,** 487–91 (2014).

49. Wen, W. X., Soo, J. S., Kwan, P. Y., Hong, E., Khang, T. F., Mariapun, S., Lee, C. S., Hasan, S. N., Rajadurai, P., Yip, C. H., Mohd Taib, N. A. & Teo, S. H. Germline APOBEC3B deletion is associated with breast cancer risk in an Asian multi-ethnic cohort and with immune cell presentation. *Breast Cancer Res* **18,** 56 (2016).

50. Middlebrooks, C. D., Banday, A. R., Matsuda, K., Udquim, K. I., Onabajo, O. O., Paquin, A., Figueroa, J. D., Zhu, B., Koutros, S., Kubo, M., Shuin, T., Freedman, N. D., Kogevinas, M., Malats, N., Chanock, S. J., Garcia-Closas, M., Silverman, D. T., Rothman, N. & Prokunina-Olsson, L. Association of germline variants in the APOBEC3 region with cancer risk and enrichment with APOBEC-signature mutations in tumors. *Nat Genet* **48,** 1330–1338 (2016).

51. Chen, T. W., Lee, C. C., Liu, H., Wu, C. S., Pickering, C. R., Huang, P. J., Wang, J., Chang, I. Y., Yeh, Y. M., Chen, C. D., Li, H. P., Luo, J. D., Tan, B. C., Chan, T. E. H., Hsueh, C., Chu, L. J., Chen, Y. T., Zhang, B., Yang, C. Y., Wu, C. C., Hsu, C. W., See, L. C., Tang, P., Yu, J. S., Liao, W. C., Chiang, W. F., Rodriguez, H., Myers, J. N., Chang, K. P. & Chang, Y. S. APOBEC3A is an oral cancer prognostic biomarker in Taiwanese carriers of an APOBEC deletion polymorphism. *Nat Commun* **8,** 465 (2017).

52. Gohler, S., Da Silva Filho, M. I., Johansson, R., Enquist-Olsson, K., Henriksson, R., Hemminki, K., Lenner, P. & Forsti, A. Impact of functional germline variants and a deletion polymorphism in APOBEC3A and APOBEC3B on breast cancer risk and survival in a Swedish study population. *J Cancer Res Clin Oncol* **142,** 273–6 (2016).

53. Marouf, C., Gohler, S., Filho, M. I., Hajji, O., Hemminki, K., Nadifi, S. & Forsti, A. Analysis of functional germline variants in APOBEC3 and driver genes on breast cancer risk in Moroccan study population. *BMC Cancer* **16,** 165 (2016).

54. Revathidevi, S., Manikandan, M., Rao, A. K., Vinothkumar, V., Arunkumar, G., Rajkumar, K. S., Ramani, R., Rajaraman, R., Ajay, C. & Munirajan, A. K. Analysis of APOBEC3A/3B germline deletion polymorphism in breast, cervical and oral cancers from South India and its impact on miRNA regulation. *Tumour Biol* **37,** 11983–11990 (2016).

55. Klonowska, K., Kluzniak, W., Rusak, B., Jakubowska, A., Ratajska, M., Krawczynska, N., Vasilevska, D., Czubak, K., Wojciechowska, M., Cybulski, C., Lubinski, J. & Kozlowski, P. The 30 kb deletion in the APOBEC3 cluster decreases APOBEC3A and APOBEC3B expression and creates a transcriptionally active hybrid gene but does not associate with breast cancer in the European population. *Oncotarget* **8,** 76357–76374 (2017).

56. Zhang, T., Cai, J., Chang, J., Yu, D., Wu, C., Yan, T., Zhai, K., Bi, X., Zhao, H., Xu, J., Tan, W., Qu, C. & Lin, D. Evidence of associations of APOBEC3B

gene deletion with susceptibility to persistent HBV infection and hepatocellular carcinoma. *Hum Mol Genet* **22,** 1262–9 (2013).

57. Prasetyo, A. A., Sariyatun, R., Reviono, Sari, Y., Hudiyono, Haryati, S., Adnan, Z. A., Hartono & Kageyama, S. The APOBEC3B deletion polymorphism is associated with prevalence of hepatitis B virus, hepatitis C virus, Torque Teno virus, and Toxoplasma gondii co-infection among HIV-infected individuals. *J Clin Virol* **70,** 67–71 (2015).

58. Ezzikouri, S., Kitab, B., Rebbani, K., Marchio, A., Wain-Hobson, S., Dejean, A., Vartanian, J. P., Pineau, P. & Benjelloun, S. Polymorphic APOBEC3 modulates chronic hepatitis B in Moroccan population. *J Viral Hepat* **20,** 678–86 (2013).

59. Imahashi, M., Izumi, T., Watanabe, D., Imamura, J., Matsuoka, K., Ode, H., Masaoka, T., Sato, K., Kaneko, N., Ichikawa, S., Koyanagi, Y., Takaori-Kondo, A., Utsumi, M., Yokomaku, Y., Shirasaka, T., Sugiura, W., Iwatani, Y. & Naoe, T. Lack of association between intact/deletion polymorphisms of the APOBEC3B gene and HIV-1 risk. *PLoS One* **9,** e92861 (2014).

60. Singh, H., Marathe, S. D., Nain, S., Nema, V., Ghate, M. V. & Gangakhedkar, R. R. APOBEC3B deletion impacts on susceptibility to acquire HIV-1 and its advancement among individuals in western India. *APMIS* **124,** 881–7 (2016).

61. Lackey, L., Law, E. K., Brown, W. L. & Harris, R. S. Subcellular localization of the APOBEC3 proteins during mitosis and implications for genomic DNA deamination. *Cell Cycle* **12,** 762–72 (2013).

62. Muckenfuss, H., Hamdorf, M., Held, U., Perkovic, M., Lower, J., Cichutek, K., Flory, E., Schumann, G. G. & Munk, C. APOBEC3 proteins inhibit human LINE-1 retrotransposition. *J Biol Chem* **281,** 22161–72 (2006).

63. Bogerd, H. P., Wiegand, H. L., Hulme, A. E., Garcia-Perez, J. L., O'Shea, K. S., Moran, J. V. & Cullen, B. R. Cellular inhibitors of long interspersed element 1 and Alu retrotransposition. *Proc Natl Acad Sci U S A* **103,** 8780–5 (2006).

64. Land, A. M., Law, E. K., Carpenter, M. A., Lackey, L., Brown, W. L. & Harris, R. S. Endogenous APOBEC3A DNA cytosine deaminase is cytoplasmic and nongenotoxic. *J Biol Chem* **288,** 17253–60 (2013).

65. Salamango, D. J., McCann, J. L., Demir, O., Brown, W. L., Amaro, R. E. & Harris, R. S. APOBEC3B Nuclear Localization Requires Two Distinct N-Terminal Domain Surfaces. *J Mol Biol* **430,** 2695–2708 (2018).

66. Law, E. K., Sieuwerts, A. M., LaPara, K., Leonard, B., Starrett, G. J., Molan, A. M., Temiz, N. A., Vogel, R. I., Meijer-van Gelder, M. E., Sweep, F. C., Span, P. N., Foekens, J. A., Martens, J. W., Yee, D. & Harris, R. S. The DNA cytosine deaminase APOBEC3B promotes tamoxifen resistance in ER-positive breast cancer. *Sci Adv* **2,** e1601737 (2016).

67. Salamango, D. J., Becker, J. T., McCann, J. L., Cheng, A. Z., Demir, O., Amaro, R. E., Brown, W. L., Shaban, N. M. & Harris, R. S. APOBEC3H Subcellular Localization Determinants Define Zipcode for Targeting HIV-1 for Restriction. *Mol Cell Biol* **38** (2018).

68. Horn, A. V., Klawitter, S., Held, U., Berger, A., Vasudevan, A. A., Bock, A., Hofmann, H., Hanschmann, K. M., Trosemeier, J. H., Flory, E., Jabulowsky, R. A., Han, J. S., Lower, J., Lower, R., Munk, C. & Schumann, G. G. Human LINE-1 restriction by APOBEC3C is deaminase independent and mediated by an ORF1p interaction that affects LINE reverse transcriptase activity. *Nucleic Acids Res* **42,** 396–416 (2014).

69. Harris, R. S., Petersen-Mahrt, S. K. & Neuberger, M. S. RNA editing enzyme APOBEC1 and some of its homologs can act as DNA mutators. *Mol Cell* **10,** 1247–53 (2002).

70. Wichroski, M. J., Robb, G. B. & Rana, T. M. Human retroviral host restriction factors APOBEC3G and APOBEC3F localize to mRNA processing bodies. *PLoS Pathog* **2,** e41 (2006).

71. Mangeat, B., Turelli, P., Caron, G., Friedli, M., Perrin, L. & Trono, D. Broad antiretroviral defence by human APOBEC3G through lethal editing of nascent reverse transcripts. *Nature* **424,** 99–103 (2003).

72. Zhang, H., Yang, B., Pomerantz, R. J., Zhang, C., Arunachalam, S. C. & Gao, L. The cytidine deaminase CEM15 induces hypermutation in newly synthesized HIV-1 DNA. *Nature* **424,** 94–8 (2003).

73. Yang, Y., Yang, Y. & Smith, H. C. Multiple protein domains determine the cell type-specific nuclear distribution of the catalytic subunit required for apolipoprotein B mRNA editing. *Proc Natl Acad Sci U S A* **94,** 13075–80 (1997).

74. Ito, S., Nagaoka, H., Shinkura, R., Begum, N., Muramatsu, M., Nakata, M. & Honjo, T. Activation-induced cytidine deaminase shuttles between nucleus and cytoplasm like apolipoprotein B mRNA editing catalytic polypeptide 1. *Proc Natl Acad Sci U S A* **101,** 1975–80 (2004).

75. Sowden, M. P., Ballatori, N., Jensen, K. L., Reed, L. H. & Smith, H. C. The editosome for cytidine to uridine mRNA editing has a native complexity of 27S: identification of intracellular domains containing active and inactive editing factors. *J Cell Sci* **115,** 1027–39 (2002).

76. Pham, P., Bransteitter, R., Petruska, J. & Goodman, M. F. Processive AID-catalysed cytosine deamination on single-stranded DNA simulates somatic hypermutation. *Nature* **424,** 103–7 (2003).

77. Methot, S. P., Litzler, L. C., Trajtenberg, F., Zahn, A., Robert, F., Pelletier, J., Buschiazzo, A., Magor, B. G. & Di Noia, J. M. Consecutive interactions with HSP90 and eEF1A underlie a functional maturation and storage pathway of AID in the cytoplasm. *J Exp Med* **212,** 581–96 (2015).

78. Hultquist, J. F., Lengyel, J. A., Refsland, E. W., LaRue, R. S., Lackey, L., Brown, W. L. & Harris, R. S. Human and rhesus APOBEC3D, APOBEC3F, APOBEC3G, and APOBEC3H demonstrate a conserved capacity to restrict Vif-deficient HIV-1. *J Virol* **85,** 11220–34 (2011).

79. Chen, J. & MacCarthy, T. The preferred nucleotide contexts of the AID/APOBEC cytidine deaminases have differential effects when mutating retrotransposon and virus sequences compared to host genes. *PLoS Comput Biol* **13,** e1005471 (2017).

80. Refsland, E. W., Hultquist, J. F. & Harris, R. S. Endogenous origins of HIV-1 G-to-A hypermutation and restriction in the nonpermissive T cell line CEM2n. *PLoS Pathog* **8,** e1002800 (2012).

81. Anderson, B. D. & Harris, R. S. Transcriptional regulation of APOBEC3 antiviral immunity through the CBF-beta/RUNX axis. *Sci Adv* **1,** e1500296 (2015).

82. Wang, T., Tian, C., Zhang, W., Luo, K., Sarkis, P. T., Yu, L., Liu, B., Yu, Y. & Yu, X. F. 7SL RNA mediates virion packaging of the antiviral cytidine deaminase APOBEC3G. *J Virol* **81,** 13112–24 (2007).

83. Apolonia, L., Schulz, R., Curk, T., Rocha, P., Swanson, C. M., Schaller, T., Ule, J. & Malim, M. H. Promiscuous RNA binding ensures effective encapsidation of APOBEC3 proteins by HIV-1. *PLoS Pathog* **11,** e1004609 (2015).

84. Harris, R. S., Hultquist, J. F. & Evans, D. T. The restriction factors of human immunodeficiency virus. *J Biol Chem* **287,** 40875–83 (2012).

85. Simon, V., Bloch, N. & Landau, N. R. Intrinsic host restrictions to HIV-1 and mechanisms of viral escape. *Nat Immunol* **16,** 546–53 (2015).

86. Malim, M. H. & Emerman, M. HIV-1 accessory proteins–ensuring viral survival in a hostile environment. *Cell Host Microbe* **3,** 388–98 (2008).

87. Pak, V., Heidecker, G., Pathak, V. K. & Derse, D. The role of amino-terminal sequences in cellular localization and antiviral activity of APOBEC3B. *J Virol* **85,** 8538–47 (2011).

88. Jager, S., Kim, D. Y., Hultquist, J. F., Shindo, K., LaRue, R. S., Kwon, E., Li, M., Anderson, B. D., Yen, L., Stanley, D., Mahon, C., Kane, J., Franks-Skiba, K., Cimermancic, P., Burlingame, A., Sali, A., Craik, C. S., Harris, R. S., Gross, J. D. & Krogan, N. J. Vif hijacks CBF-beta to degrade APOBEC3G and promote HIV-1 infection. *Nature* **481,** 371–5 (2011).

89. Kane, J. R., Stanley, D. J., Hultquist, J. F., Johnson, J. R., Mietrach, N., Binning, J. M., Jonsson, S. R., Barelier, S., Newton, B. W., Johnson, T. L., Franks-Skiba, K. E., Li, M., Brown, W. L., Gunnarsson, H. I., Adalbjornsdottir, A., Fraser, J. S., Harris, R. S., Andresdottir, V., Gross, J. D. & Krogan, N. J. Lineage-Specific Viral Hijacking of Non-canonical E3 Ubiquitin Ligase Cofactors in the Evolution of Vif Anti-APOBEC3 Activity. *Cell Rep* **11,** 1236–50 (2015).

90. Collins, A., Littman, D. R. & Taniuchi, I. RUNX proteins in transcription factor networks that regulate T-cell lineage choice. *Nat Rev Immunol* **9,** 106–15 (2009).

91. Lochelt, M., Romen, F., Bastone, P., Muckenfuss, H., Kirchner, N., Kim, Y. B., Truyen, U., Rosler, U., Battenberg, M., Saib, A., Flory, E., Cichutek, K. & Munk, C. The antiretroviral activity of APOBEC3 is inhibited by the foamy virus accessory Bet protein. *Proc Natl Acad Sci U S A* **102,** 7982–7 (2005).

92. Jaguva Vasudevan, A. A., Perkovic, M., Bulliard, Y., Cichutek, K., Trono, D., Haussinger, D. & Munk, C. Prototype foamy virus Bet impairs the dimerization and cytosolic solubility of human APOBEC3G. *J Virol* **87,** 9030–40 (2013).

93. Derse, D., Hill, S. A., Princler, G., Lloyd, P. & Heidecker, G. Resistance of human T cell leukemia virus type 1 to APOBEC3G restriction is mediated by elements in nucleocapsid. *Proc Natl Acad Sci U S A* **104,** 2915–20 (2007).

94. Hagen, B., Kraase, M., Indikova, I. & Indik, S. A high rate of polymerization during synthesis of mouse mammary tumor virus DNA alleviates hypermutation by APOBEC3 proteins. *PLoS Pathog* **15,** e1007533 (2019).

95. Refsland, E. W. & Harris, R. S. The APOBEC3 family of retroelement restriction factors. *Curr Top Microbiol Immunol* **371,** 1–27 (2013).

96. Anwar, F., Davenport, M. P. & Ebrahimi, D. Footprint of APOBEC3 on the genome of human retroelements. *J Virol* **87,** 8195–204 (2013).

97. Kinomoto, M., Kanno, T., Shimura, M., Ishizaka, Y., Kojima, A., Kurata, T., Sata, T. & Tokunaga, K. All APOBEC3 family proteins differentially inhibit LINE-1 retrotransposition. *Nucleic Acids Res* **35,** 2955–64 (2007).

98. Ostertag, E. M. & Kazazian H. H., J. Biology of mammalian L1 retrotransposons. *Annu Rev Genet* **35,** 501–38 (2001).

99. Wang, G. H. & Seeger, C. The reverse transcriptase of hepatitis B virus acts as a protein primer for viral DNA synthesis. *Cell* **71,** 663–70 (1992).

100. Bock, C. T., Schwinn, S., Locarnini, S., Fyfe, J., Manns, M. P., Trautwein, C. & Zentgraf, H. Structural organization of the hepatitis B virus minichromosome. *J Mol Biol* **307,** 183–96 (2001).

101. Nassal, M. HBV cccDNA: viral persistence reservoir and key obstacle for a cure of chronic hepatitis B. *Gut* **64,** 1972–84 (2015).

102. Chen, R., Zhao, X., Wang, Y., Xie, Y. & Liu, J. Hepatitis B virus X protein is capable of down-regulating protein level of host antiviral protein APOBEC3G. *Sci Rep* **7,** 40783 (2017).

103. Mori, S., Takeuchi, T., Ishii, Y., Yugawa, T., Kiyono, T., Nishina, H. & Kukimoto, I. Human Papillomavirus 16 E6 Upregulates APOBEC3B via the TEAD Transcription Factor. *J Virol* **91** (2017).

104. Wang, Z., Wakae, K., Kitamura, K., Aoyama, S., Liu, G., Koura, M., Monjurul, A. M., Kukimoto, I. & Muramatsu, M. APOBEC3 deaminases induce hypermutation in human papillomavirus 16 DNA upon beta interferon stimulation. *J Virol* **88,** 1308–17 (2014).

105. Warren, C. J., Xu, T., Guo, K., Griffin, L. M., Westrich, J. A., Lee, D., Lambert, P. F., Santiago, M. L. & Pyeon, D. APOBEC3A functions as a restriction factor of human papillomavirus. *J Virol* **89,** 688–702 (2015).

106. Westrich, J. A., Warren, C. J., Klausner, M. J., Guo, K., Liu, C. W., Santiago, M. L. & Pyeon, D. Human Papillomavirus 16 E7 Stabilizes APOBEC3A Protein by Inhibiting Cullin 2-Dependent Protein Degradation. *J Virol* **92** (2018).

107. Kondo, S., Wakae, K., Wakisaka, N., Nakanishi, Y., Ishikawa, K., Komori, T., Moriyama-Kita, M., Endo, K., Murono, S., Wang, Z., Kitamura, K., Nishiyama, T., Yamaguchi, K., Shigenobu, S., Muramatsu, M. & Yoshizaki, T. APOBEC3A associates with human papillomavirus genome integration in oropharyngeal cancers. *Oncogene* **36,** 1687–1697 (2017).

108. Warren, C. J., Van Doorslaer, K., Pandey, A., Espinosa, J. M. & Pyeon, D. Role of the host restriction factor APOBEC3 on papillomavirus evolution. *Virus Evol* **1** (2015).

109. Hirose, Y., Onuki, M., Tenjimbayashi, Y., Mori, S., Ishii, Y., Takeuchi, T., Tasaka, N., Satoh, T., Morisada, T., Iwata, T., Miyamoto, S., Matsumoto, K., Sekizawa, A. & Kukimoto, I. Within-Host Variations of Human Papillomavirus Reveal APOBEC Signature Mutagenesis in the Viral Genome. *J Virol* **92** (2018).

110. Moens, U. Human Polyomaviruses and Papillomaviruses. *Int J Mol Sci* **19** (2018).

111. DeCaprio, J. A. & Garcea, R. L. A cornucopia of human polyomaviruses. *Nat Rev Microbiol* **11,** 264–76 (2013).

112. Starrett, G. J., Serebrenik, A. A., Roelofs, P. A., McCann, J. L., Verhalen, B., Jarvis, M. C., Stewart, T. A., Law, E. K., Krupp, A., Jiang, M., Martens, J. W. M., Cahir-McFarland, E., Span, P. N. & Harris, R. S. Polyomavirus

T Antigen Induces APOBEC3B Expression Using an LXCXE-Dependent and TP53-Independent Mechanism. *MBio* **10** (2019).

113. Schmid, M., Speiseder, T., Dobner, T. & Gonzalez, R. A. DNA virus replication compartments. *J Virol* **88,** 1404–20 (2014).

114. Schramm, B. & Locker, J. K. Cytoplasmic organization of POXvirus DNA replication. *Traffic* **6,** 839–46 (2005).

115. Kremer, M., Suezer, Y., Martinez-Fernandez, Y., Munk, C., Sutter, G. & Schnierle, B. S. Vaccinia virus replication is not affected by APOBEC3 family members. *Virol J* **3,** 86 (2006).

116. in. *Human Herpesviruses: Biology, Therapy, and Immunoprophylaxis* (eds Arvin, A., Campadelli-Fiume, G., Mocarski, E., Moore, P. S., Roizman, B., Whitley, R. & Yamanishi, K.) (Cambridge, 2007). ISBN: 9780521827140.

117. Grinde, B. Herpesviruses: latency and reactivation - viral strategies and host response. *J Oral Microbiol* **5** (2013).

118. Sciortino, M. T., Suzuki, M., Taddeo, B. & Roizman, B. RNAs extracted from herpes simplex virus 1 virions: apparent selectivity of viral but not cellular RNAs packaged in virions. *J Virol* **75,** 8105–16 (2001).

119. Fields, B. N., Knipe, D. M. & Howley, P. M. *Fields virology* 3rd. ISBN: 0781702534 (set alk. paper) (Lippincott-Raven Publishers, Philadelphia, 1996).

120. Nicoll, M. P., Proenca, J. T. & Efstathiou, S. The molecular basis of herpes simplex virus latency. **36,** 684–705 (2012).

121. Dyson, P. J. & Farrell, P. J. Chromatin structure of Epstein-Barr virus. *J Gen Virol* **66 (Pt 9),** 1931–40 (1985).

122. Jenkins, P. J., Binne, U. K. & Farrell, P. J. Histone acetylation and reactivation of Epstein-Barr virus from latency. *J Virol* **74,** 710–20 (2000).

123. Speck, S. H., Chatila, T. & Flemington, E. Reactivation of Epstein-Barr virus: regulation and function of the BZLF1 gene. *Trends Microbiol* **5,** 399–405 (1997).

124. Kang, M. S. & Kieff, E. Epstein-Barr virus latent genes. *Exp Mol Med* **47,** e131 (2015).

125. Thompson, M. P. & Kurzrock, R. Epstein-Barr virus and cancer. *Clin Cancer Res* **10,** 803–21 (2004).

126. Niedobitek, G., Agathanggelou, A., Herbst, H., Whitehead, L., Wright, D. H. & Young, L. S. Epstein-Barr virus (EBV) infection in infectious mononucleosis: virus latency, replication and phenotype of EBV-infected cells. *J Pathol* **182,** 151–9 (1997).

127. Alfieri, C., Birkenbach, M. & Kieff, E. Early events in Epstein-Barr virus infection of human B lymphocytes. *Virology* **181,** 595–608 (1991).

128. Maruo, S., Nanbo, A. & Takada, K. Replacement of the Epstein-Barr virus plasmid with the EBER plasmid in Burkitt's lymphoma cells. *J Virol* **75,** 9977–82 (2001).

129. Cai, X., Schafer, A., Lu, S., Bilello, J. P., Desrosiers, R. C., Edwards, R., Raab-Traub, N. & Cullen, B. R. Epstein-Barr virus microRNAs are evolutionarily conserved and differentially expressed. *PLoS Pathog* **2,** e23 (2006).

130. Speck, S. H. & Ganem, D. Viral latency and its regulation: lessons from the gamma-herpesviruses. *Cell Host Microbe* **8,** 100–15 (2010).

131. Stoeger, T. & Adler, H. "Novel" Triggers of Herpesvirus Reactivation and Their Potential Health Relevance. *Front Microbiol* **9,** 3207 (2018).

132. Weller, S. K. & Coen, D. M. Herpes simplex viruses: mechanisms of DNA replication. *Cold Spring Harb Perspect Biol* **4,** a013011 (2012).

133. Mettenleiter, T. C. Herpesvirus assembly and egress. *J Virol* **76,** 1537–47 (2002).

134. De Oliveira, D. E., Ballon, G. & Cesarman, E. NF-kappaB signaling modulation by EBV and KSHV. *Trends Microbiol* **18,** 248–57 (2010).

135. Santoro, M. G., Rossi, A. & Amici, C. NF-kappaB and virus infection: who controls whom. *EMBO J* **22,** 2552–60 (2003).

136. He, B., Gross, M. & Roizman, B. The gamma(1)34.5 protein of herpes simplex virus 1 complexes with protein phosphatase 1alpha to dephosphorylate the alpha subunit of the eukaryotic translation initiation factor 2 and preclude the shutoff of protein synthesis by double-stranded RNA-activated protein kinase. *Proc Natl Acad Sci U S A* **94,** 843–8 (1997).

137. Child, S. J., Hakki, M., De Niro, K. L. & Geballe, A. P. Evasion of cellular antiviral responses by human cytomegalovirus TRS1 and IRS1. *J Virol* **78,** 197–205 (2004).

138. Ariza, M. E., Glaser, R., Kaumaya, P. T., Jones, C. & Williams, M. V. The EBV-encoded dUTPase activates NF-kappa B through the TLR2 and MyD88-dependent signaling pathway. *J Immunol* **182,** 851–9 (2009).

139. Konrad, A., Wies, E., Thurau, M., Marquardt, G., Naschberger, E., Hentschel, S., Jochmann, R., Schulz, T. F., Erfle, H., Brors, B., Lausen, B., Neipel, F. & Sturzl, M. A systems biology approach to identify the combination effects of human herpesvirus 8 genes on NF-kappaB activation. *J Virol* **83,** 2563–74 (2009).

140. Guo, H., Kaiser, W. J. & Mocarski, E. S. Manipulation of apoptosis and necroptosis signaling by herpesviruses. *Med Microbiol Immunol* **204,** 439–48 (2015).

141. You, Y., Cheng, A. C., Wang, M. S., Jia, R. Y., Sun, K. F., Yang, Q., Wu, Y., Zhu, D., Chen, S., Liu, M. F., Zhao, X. X. & Chen, X. Y. The suppression of apoptosis by alpha-herpesvirus. *Cell Death Dis* **8,** e2749 (2017).

142. Lagunoff, M. & Carroll, P. A. Inhibition of apoptosis by the gamma-herpesviruses. *Int Rev Immunol* **22,** 373–99 (2003).

143. Hoffmann, H. H., Schneider, W. M. & Rice, C. M. Interferons and viruses: an evolutionary arms race of molecular interactions. *Trends Immunol* **36,** 124–38 (2015).

144. Full, F., van Gent, M., Sparrer, K. M. J., Chiang, C., Zurenski, M. A., Scherer, M., Brockmeyer, N. H., Heinzerling, L., Sturzl, M., Korn, K., Stamminger, T., Ensser, A. & Gack, M. U. Centrosomal protein TRIM43 restricts herpesvirus infection by regulating nuclear lamina integrity. *Nat Microbiol* **4,** 164–176 (2019).

145. Adams, M. J. & Carstens, E. B. Ratification vote on taxonomic proposals to the International Committee on Taxonomy of Viruses (2012). *Arch Virol* **157,** 1411–22 (2012).

146. Looker, K. J., Magaret, A. S., May, M. T., Turner, K. M., Vickerman, P., Gottlieb, S. L. & Newman, L. M. Global and Regional Estimates of Prevalent

and Incident Herpes Simplex Virus Type 1 Infections in 2012. *PLoS One* **10,** e0140765 (2015).

147. Whitley, R. J. in *Medical Microbiology* (eds th & Baron, S.) (Galveston (TX), 1996). ISBN: 0963117211.

148. Betz, D. & Fane, K. in *StatPearls* (Treasure Island (FL), 2019).

149. Whitley, R. J., Kimberlin, D. W. & Roizman, B. Herpes simplex viruses. *Clin Infect Dis* **26,** 541–53; quiz 554–5 (1998).

150. Canalejo Castrillero, E., Garcia Duran, F., Cabello, N. & Garcia Martinez, J. Herpes esophagitis in healthy adults and adolescents: report of 3 cases and review of the literature. *Medicine (Baltimore)* **89,** 204–10 (2010).

151. Taplitz, R. A. & Jordan, M. C. Pneumonia caused by herpesviruses in recipients of hematopoietic cell transplants. *Semin Respir Infect* **17,** 121–9 (2002).

152. Kaufman, B., Gandhi, S. A., Louie, E., Rizzi, R. & Illei, P. Herpes simplex virus hepatitis: case report and review. *Clin Infect Dis* **24,** 334–8 (1997).

153. Herget, G. W., Riede, U. N., Schmitt-Graff, A., Lubbert, M., Neumann-Haefelin, D. & Kohler, G. Generalized herpes simplex virus infection in an immunocompromised patient–report of a case and review of the literature. *Pathol Res Pract* **201,** 123–9 (2005).

154. Hutto, C., Arvin, A., Jacobs, R., Steele, R., Stagno, S., Lyrene, R., Willett, L., Powell, D., Andersen, R., Werthammer, J. & et al. Intrauterine herpes simplex virus infections. *J Pediatr* **110,** 97–101 (1987).

155. Deshmane, S. L. & Fraser, N. W. During latency, herpes simplex virus type 1 DNA is associated with nucleosomes in a chromatin structure. *J Virol* **63,** 943–7 (1989).

156. Stevens, J. G., Wagner, E. K., Devi-Rao, G. B., Cook, M. L. & Feldman, L. T. RNA complementary to a herpesvirus alpha gene mRNA is prominent in latently infected neurons. *Science* **235,** 1056–9 (1987).

157. Thomas, S. K., Lilley, C. E., Latchman, D. S. & Coffin, R. S. A protein encoded by the herpes simplex virus (HSV) type 1 2-kilobase latency-associated transcript is phosphorylated, localized to the nucleus, and overcomes the

repression of expression from exogenous promoters when inserted into the quiescent HSV genome. *J Virol* **76,** 4056–67 (2002).

158. Perng, G. C., Ghiasi, H., Slanina, S. M., Nesburn, A. B. & Wechsler, S. L. The spontaneous reactivation function of the herpes simplex virus type 1 LAT gene resides completely within the first 1.5 kilobases of the 8.3-kilobase primary transcript. *J Virol* **70,** 976–84 (1996).

159. Wagstaff, A. J., Faulds, D. & Goa, K. L. Aciclovir. A reappraisal of its antiviral activity, pharmacokinetic properties and therapeutic efficacy. *Drugs* **47,** 153–205 (1994).

160. Jacobson, M. A. Valaciclovir (BW256U87): the L-valyl ester of acyclovir. *J Med Virol* **Suppl 1,** 150–3 (1993).

161. Boike, S. C., Pue, M. A., Freed, M. I., Audet, P. R., Fairless, A., Ilson, B. E., Zariffa, N. & Jorkasky, D. K. Pharmacokinetics of famciclovir in subjects with varying degrees of renal impairment. *Clin Pharmacol Ther* **55,** 418–26 (1994).

162. Markham, A. & Faulds, D. Ganciclovir. An update of its therapeutic use in cytomegalovirus infection. *Drugs* **48,** 455–84 (1994).

163. Cocohoba, J. M. & McNicholl, I. R. Valganciclovir: an advance in cytomegalovirus therapeutics. *Ann Pharmacother* **36,** 1075–9 (2002).

164. Ho, H. T., Woods, K. L., Bronson, J. J., De Boeck, H., Martin, J. C. & Hitchcock, M. J. Intracellular metabolism of the antiherpes agent (S)-1-[3-hydroxy-2-(phosphonylmethoxy)propyl]cytosine. *Mol Pharmacol* **41,** 197–202 (1992).

165. Wagstaff, A. J. & Bryson, H. M. Foscarnet. A reappraisal of its antiviral activity, pharmacokinetic properties and therapeutic use in immunocompromised patients with viral infections. *Drugs* **48,** 199–226 (1994).

166. Cherry, J. D., Harrison, G. J., Kaplan, S. L., Hotez, P. J. & Steinbach, W. J. *Feigin and Cherry's textbook of pediatric infectious diseases* Seventh edition., 2 volumes. ISBN: 9781455711772 (two-volume set) (Elsevier/Saunders, Philadelphia, PA, 2014).

167. Staras, S. A., Dollard, S. C., Radford, K. W., Flanders, W. D., Pass, R. F. & Cannon, M. J. Seroprevalence of cytomegalovirus infection in the United States, 1988-1994. *Clin Infect Dis* **43,** 1143–51 (2006).

168. Manicklal, S., Emery, V. C., Lazzarotto, T., Boppana, S. B. & Gupta, R. K. The "silent" global burden of congenital cytomegalovirus. *Clin Microbiol Rev* **26,** 86–102 (2013).

169. Kenneson, A. & Cannon, M. J. Review and meta-analysis of the epidemiology of congenital cytomegalovirus (CMV) infection. *Rev Med Virol* **17,** 253–76 (2007).

170. Graham, D., Guidi, S. M. & Sanders, R. C. Sonographic features of in utero periventricular calcification due to cytomegalovirus infection. *J Ultrasound Med* **1,** 171–2 (1982).

171. Hamprecht, K., Maschmann, J., Vochem, M., Dietz, K., Speer, C. P. & Jahn, G. Epidemiology of transmission of cytomegalovirus from mother to preterm infant by breastfeeding. *Lancet* **357,** 513–8 (2001).

172. Evans, A. S. Infectious mononucleosis and related syndromes. *Am J Med Sci* **276,** 325–39 (1978).

173. Sinzger, C., Grefte, A., Plachter, B., Gouw, A. S., The, T. H. & Jahn, G. Fibroblasts, epithelial cells, endothelial cells and smooth muscle cells are major targets of human cytomegalovirus infection in lung and gastrointestinal tissues. *J Gen Virol* **76 (Pt 4),** 741–50 (1995).

174. Kahl, M., Siegel-Axel, D., Stenglein, S., Jahn, G. & Sinzger, C. Efficient lytic infection of human arterial endothelial cells by human cytomegalovirus strains. *J Virol* **74,** 7628–35 (2000).

175. Riegler, S., Hebart, H., Einsele, H., Brossart, P., Jahn, G. & Sinzger, C. Monocyte-derived dendritic cells are permissive to the complete replicative cycle of human cytomegalovirus. *J Gen Virol* **81,** 393–9 (2000).

176. Sinzger, C., Digel, M. & Jahn, G. Cytomegalovirus cell tropism. *Curr Top Microbiol Immunol* **325,** 63–83 (2008).

177. Schafer, P., Tenschert, W., Cremaschi, L., Schroter, M., Gutensohn, K. & Laufs, R. Cytomegalovirus cultured from different major leukocyte subpopulations: association with clinical features in CMV immunoglobulin G-positive renal allograft recipients. *J Med Virol* **61,** 488–96 (2000).

178. Sinzger, C., Schmidt, K., Knapp, J., Kahl, M., Beck, R., Waldman, J., Hebart, H., Einsele, H. & Jahn, G. Modification of human cytomegalovirus tropism

through propagation in vitro is associated with changes in the viral genome. *J Gen Virol* **80 (Pt 11),** 2867–77 (1999).

179. Wilkinson, G. W., Davison, A. J., Tomasec, P., Fielding, C. A., Aicheler, R., Murrell, I., Seirafian, S., Wang, E. C., Weekes, M., Lehner, P. J., Wilkie, G. S. & Stanton, R. J. Human cytomegalovirus: taking the strain. *Med Microbiol Immunol* **204,** 273–84 (2015).

180. Grefte, A., Harmsen, M. C., van der Giessen, M., Knollema, S., van Son, W. J. & The, T. H. Presence of human cytomegalovirus (HCMV) immediate early mRNA but not ppUL83 (lower matrix protein pp65) mRNA in polymorphonuclear and mononuclear leukocytes during active HCMV infection. *J Gen Virol* **75 (Pt 8),** 1989–98 (1994).

181. Gerna, G., Zipeto, D., Percivalle, E., Parea, M., Revello, M. G., Maccario, R., Peri, G. & Milanesi, G. Human cytomegalovirus infection of the major leukocyte subpopulations and evidence for initial viral replication in polymorphonuclear leukocytes from viremic patients. *J Infect Dis* **166,** 1236–44 (1992).

182. Halwachs-Baumann, G., Wilders-Truschnig, M., Desoye, G., Hahn, T., Kiesel, L., Klingel, K., Rieger, P., Jahn, G. & Sinzger, C. Human trophoblast cells are permissive to the complete replicative cycle of human cytomegalovirus. *J Virol* **72,** 7598–602 (1998).

183. Sinclair, J. Human cytomegalovirus: Latency and reactivation in the myeloid lineage. *J Clin Virol* **41,** 180–5 (2008).

184. Soderberg-Naucler, C., Fish, K. N. & Nelson, J. A. Growth of human cytomegalovirus in primary macrophages. *Methods* **16,** 126–38 (1998).

185. Soderberg-Naucler, C., Fish, K. N. & Nelson, J. A. Reactivation of latent human cytomegalovirus by allogeneic stimulation of blood cells from healthy donors. *Cell* **91,** 119–26 (1997).

186. Friedman, H. M., Macarak, E. J., MacGregor, R. R., Wolfe, J. & Kefalides, N. A. Virus infection of endothelial cells. *J Infect Dis* **143,** 266–73 (1981).

187. Speir, E., Modali, R., Huang, E. S., Leon, M. B., Shawl, F., Finkel, T. & Epstein, S. E. Potential role of human cytomegalovirus and p53 interaction in coronary restenosis. *Science* **265,** 391–4 (1994).

188. Balfour H. H., J., Sifakis, F., Sliman, J. A., Knight, J. A., Schmeling, D. O. & Thomas, W. Age-specific prevalence of Epstein-Barr virus infection among individuals aged 6-19 years in the United States and factors affecting its acquisition. *J Infect Dis* **208,** 1286–93 (2013).

189. Cohen, J. I. Epstein-Barr virus infection. *N Engl J Med* **343,** 481–92 (2000).

190. Crawford, D. H., Swerdlow, A. J., Higgins, C., McAulay, K., Harrison, N., Williams, H., Britton, K. & Macsween, K. F. Sexual history and Epstein-Barr virus infection. *J Infect Dis* **186,** 731–6 (2002).

191. Henke, C. E., Kurland, L. T. & Elveback, L. R. Infectious mononucleosis in Rochester, Minnesota, 1950 through 1969. *Am J Epidemiol* **98,** 483–90 (1973).

192. Luzuriaga, K. & Sullivan, J. L. Infectious mononucleosis. *N Engl J Med* **362,** 1993–2000 (2010).

193. Callan, M. F., Tan, L., Annels, N., Ogg, G. S., Wilson, J. D., O'Callaghan, C. A., Steven, N., McMichael, A. J. & Rickinson, A. B. Direct visualization of antigen-specific CD8+ T cells during the primary immune response to Epstein-Barr virus In vivo. *J Exp Med* **187,** 1395–402 (1998).

194. Djaoud, Z., Guethlein, L. A., Horowitz, A., Azzi, T., Nemat-Gorgani, N., Olive, D., Nadal, D., Norman, P. J., Munz, C. & Parham, P. Two alternate strategies for innate immunity to Epstein-Barr virus: One using NK cells and the other NK cells and gammadelta T cells. *J Exp Med* **214,** 1827–1841 (2017).

195. Balfour H. H., J., Holman, C. J., Hokanson, K. M., Lelonek, M. M., Giesbrecht, J. E., White, D. R., Schmeling, D. O., Webb, C. H., Cavert, W., Wang, D. H. & Brundage, R. C. A prospective clinical study of Epstein-Barr virus and host interactions during acute infectious mononucleosis. *J Infect Dis* **192,** 1505–12 (2005).

196. Jenson, H. B. Acute complications of Epstein-Barr virus infectious mononucleosis. *Curr Opin Pediatr* **12,** 263–8 (2000).

197. Katano, H., Ali, M. A., Patera, A. C., Catalfamo, M., Jaffe, E. S., Kimura, H., Dale, J. K., Straus, S. E. & Cohen, J. I. Chronic active Epstein-Barr virus infection associated with mutations in perforin that impair its maturation. *Blood* **103,** 1244–52 (2004).

198. Kimura, H. & Cohen, J. I. Chronic Active Epstein-Barr Virus Disease. *Front Immunol* **8,** 1867 (2017).

199. Cohen, J. I., Jaffe, E. S., Dale, J. K., Pittaluga, S., Heslop, H. E., Rooney, C. M., Gottschalk, S., Bollard, C. M., Rao, V. K., Marques, A., Burbelo, P. D., Turk, S. P., Fulton, R., Wayne, A. S., Little, R. F., Cairo, M. S., El-Mallawany, N. K., Fowler, D., Sportes, C., Bishop, M. R., Wilson, W. & Straus, S. E. Characterization and treatment of chronic active Epstein-Barr virus disease: a 28-year experience in the United States. *Blood* **117,** 5835–49 (2011).

200. Kimura, H., Morishima, T., Kanegane, H., Ohga, S., Hoshino, Y., Maeda, A., Imai, S., Okano, M., Morio, T., Yokota, S., Tsuchiya, S., Yachie, A., Imashuku, S., Kawa, K., Wakiguchi, H., Japanese Association for Research on Epstein-Barr, V. & Related, D. Prognostic factors for chronic active Epstein-Barr virus infection. *J Infect Dis* **187,** 527–33 (2003).

201. Kimura, H., Ito, Y., Kawabe, S., Gotoh, K., Takahashi, Y., Kojima, S., Naoe, T., Esaki, S., Kikuta, A., Sawada, A., Kawa, K., Ohshima, K. & Nakamura, S. EBV-associated T/NK-cell lymphoproliferative diseases in nonimmunocompromised hosts: prospective analysis of 108 cases. *Blood* **119,** 673–86 (2012).

202. Quintanilla-Martinez, L., Kumar, S., Fend, F., Reyes, E., Teruya-Feldstein, J., Kingma, D. W., Sorbara, L., Raffeld, M., Straus, S. E. & Jaffe, E. S. Fulminant EBV(+) T-cell lymphoproliferative disorder following acute/chronic EBV infection: a distinct clinicopathologic syndrome. *Blood* **96,** 443–51 (2000).

203. Epstein, M. A., Achong, B. G. & Barr, Y. M. Virus Particles in Cultured Lymphoblasts from Burkitt's Lymphoma. *Lancet* **1,** 702–3 (1964).

204. Magrath, I. T. Non-Hodgkin's lymphomas: epidemiology and treatment. *Ann N Y Acad Sci* **824,** 91–106 (1997).

205. Carbone, A. Emerging pathways in the development of AIDS-related lymphomas. *Lancet Oncol* **4,** 22–9 (2003).

206. Glaser, S. L., Lin, R. J., Stewart, S. L., Ambinder, R. F., Jarrett, R. F., Brousset, P., Pallesen, G., Gulley, M. L., Khan, G., O'Grady, J., Hummel, M., Preciado, M. V., Knecht, H., Chan, J. K. & Claviez, A. Epstein-Barr virus-associated Hodgkin's disease: epidemiologic characteristics in international data. *Int J Cancer* **70,** 375–82 (1997).

207. Chiang, A. K., Tao, Q., Srivastava, G. & Ho, F. C. Nasal NK- and T-cell lymphomas share the same type of Epstein-Barr virus latency as nasopharyngeal carcinoma and Hodgkin's disease. *Int J Cancer* **68,** 285–90 (1996).

208. Swinnen, L. J. Organ transplant-related lymphoma. *Curr Treat Options Oncol* **2,** 301–8 (2001).

209. Camilleri-Broet, S., Davi, F., Feuillard, J., Seilhean, D., Michiels, J. F., Brousset, P., Epardeau, B., Navratil, E., Mokhtari, K., Bourgeois, C., Marelle, L., Raphael, M. & Hauw, J. J. AIDS-related primary brain lymphomas: histopathologic and immunohistochemical study of 51 cases. The French Study Group for HIV-Associated Tumors. *Hum Pathol* **28,** 367–74 (1997).

210. Glaser, S. L., Clarke, C. A., Gulley, M. L., Craig, F. E., DiGiuseppe, J. A., Dorfman, R. F., Mann, R. B. & Ambinder, R. F. Population-based patterns of human immunodeficiency virus-related Hodgkin lymphoma in the Greater San Francisco Bay Area, 1988-1998. *Cancer* **98,** 300–9 (2003).

211. Yu, M. C. & Yuan, J. M. Epidemiology of nasopharyngeal carcinoma. *Semin Cancer Biol* **12,** 421–9 (2002).

212. Parkin, D. M., Bray, F., Ferlay, J. & Pisani, P. Estimating the world cancer burden: Globocan 2000. *Int J Cancer* **94,** 153–6 (2001).

213. Lo, K. W., To, K. F. & Huang, D. P. Focus on nasopharyngeal carcinoma. *Cancer Cell* **5,** 423–8 (2004).

214. Yu, M. C., Ho, J. H., Lai, S. H. & Henderson, B. E. Cantonese-style salted fish as a cause of nasopharyngeal carcinoma: report of a case-control study in Hong Kong. *Cancer Res* **46,** 956–61 (1986).

215. Lung, M. L., Cheung, A. K., Ko, J. M., Lung, H. L., Cheng, Y. & Dai, W. The interplay of host genetic factors and Epstein-Barr virus in the development of nasopharyngeal carcinoma. *Chin J Cancer* **33,** 556–68 (2014).

216. Hildesheim, A. & Wang, C. P. Genetic predisposition factors and nasopharyngeal carcinoma risk: a review of epidemiological association studies, 2000-2011: Rosetta Stone for NPC: genetics, viral infection, and other environmental factors. *Semin Cancer Biol* **22,** 107–16 (2012).

217. Dai, W., Zheng, H., Cheung, A. K. & Lung, M. L. Genetic and epigenetic landscape of nasopharyngeal carcinoma. *Chin Clin Oncol* **5,** 16 (2016).

218. Mosialos, G., Birkenbach, M., Yalamanchili, R., VanArsdale, T., Ware, C. & Kieff, E. The Epstein-Barr virus transforming protein LMP1 engages signaling proteins for the tumor necrosis factor receptor family. *Cell* **80,** 389–99 (1995).

219. Price, A. M. & Luftig, M. A. To be or not IIb: a multi-step process for Epstein-Barr virus latency establishment and consequences for B cell tumorigenesis. *PLoS Pathog* **11,** e1004656 (2015).

220. Shannon-Lowe, C., Rickinson, A. B. & Bell, A. I. Epstein-Barr virus-associated lymphomas. *Philos Trans R Soc Lond B Biol Sci* **372** (2017).

221. Gutierrez, M. I., Ibrahim, M. M., Dale, J. K., Greiner, T. C., Straus, S. E. & Bhatia, K. Discrete alterations in the BZLF1 promoter in tumor and non-tumor-associated Epstein-Barr virus. *J Natl Cancer Inst* **94,** 1757–63 (2002).

222. Fang, C. Y., Lee, C. H., Wu, C. C., Chang, Y. T., Yu, S. L., Chou, S. P., Huang, P. T., Chen, C. L., Hou, J. W., Chang, Y., Tsai, C. H., Takada, K. & Chen, J. Y. Recurrent chemical reactivations of EBV promotes genome instability and enhances tumor progression of nasopharyngeal carcinoma cells. *Int J Cancer* **124,** 2016–25 (2009).

223. Hong, G. K., Gulley, M. L., Feng, W. H., Delecluse, H. J., Holley-Guthrie, E. & Kenney, S. C. Epstein-Barr virus lytic infection contributes to lymphoproliferative disease in a SCID mouse model. *J Virol* **79,** 13993–4003 (2005).

224. Imai, S., Koizumi, S., Sugiura, M., Tokunaga, M., Uemura, Y., Yamamoto, N., Tanaka, S., Sato, E. & Osato, T. Gastric carcinoma: monoclonal epithelial malignant cells expressing Epstein-Barr virus latent infection protein. *Proc Natl Acad Sci U S A* **91,** 9131–5 (1994).

225. Raab-Traub, N. & Flynn, K. The structure of the termini of the Epstein-Barr virus as a marker of clonal cellular proliferation. *Cell* **47,** 883–9 (1986).

226. Lin, J. C., Wang, W. Y., Chen, K. Y., Wei, Y. H., Liang, W. M., Jan, J. S. & Jiang, R. S. Quantification of plasma Epstein-Barr virus DNA in patients with advanced nasopharyngeal carcinoma. *N Engl J Med* **350,** 2461–70 (2004).

227. Alfieri, S., Iacovelli, N. A., Marceglia, S., Lasorsa, I., Resteghini, C., Taverna, F., Mazzocchi, A., Orlandi, E., Guzzo, M., Bianchi, R., Fanti, D., Pala, L., Racca, S., Dvir, R., Quattrone, P., Gloghini, A., Volpi, C. C., Granata, R., Bergamini, C., Locati, L., Licitra, L. & Bossi, P. Circulating pre-treatment Epstein-Barr virus DNA as prognostic factor in locally-advanced nasopharyngeal cancer in a non-endemic area. *Oncotarget* **8,** 47780–47789 (2017).

228. Yates, J. L., Warren, N. & Sugden, B. Stable replication of plasmids derived from Epstein-Barr virus in various mammalian cells. *Nature* **313,** 812–5 (1985).

229. Schepers, A., Pich, D. & Hammerschmidt, W. A transcription factor with homology to the AP-1 family links RNA transcription and DNA replication in the lytic cycle of Epstein-Barr virus. *EMBO J* **12,** 3921–9 (1993).

230. Murata, T. Encyclopedia of EBV-Encoded Lytic Genes: An Update. *Adv Exp Med Biol* **1045,** 395–412 (2018).

231. Ersing, I., Nobre, L., Wang, L. W., Soday, L., Ma, Y., Paulo, J. A., Narita, Y., Ashbaugh, C. W., Jiang, C., Grayson, N. E., Kieff, E., Gygi, S. P., Weekes, M. P. & Gewurz, B. E. A Temporal Proteomic Map of Epstein-Barr Virus Lytic Replication in B Cells. *Cell Rep* **19,** 1479–1493 (2017).

232. Torrents, E. Ribonucleotide reductases: essential enzymes for bacterial life. *Front Cell Infect Microbiol* **4,** 52 (2014).

233. Lembo, D. & Brune, W. Tinkering with a viral ribonucleotide reductase. *Trends Biochem Sci* **34,** 25–32 (2009).

234. Jordan, A. & Reichard, P. Ribonucleotide reductases. *Annu Rev Biochem* **67,** 71–98 (1998).

235. Nordlund, P. & Reichard, P. Ribonucleotide reductases. *Annu Rev Biochem* **75,** 681–706 (2006).

236. Cotruvo, J. A. & Stubbe, J. Class I ribonucleotide reductases: metallocofactor assembly and repair in vitro and in vivo. *Annu Rev Biochem* **80,** 733–67 (2011).

237. Langelier, Y., Bergeron, S., Chabaud, S., Lippens, J., Guilbault, C., Sasseville, A. M., Denis, S., Mosser, D. D. & Massie, B. The R1 subunit of herpes simplex virus ribonucleotide reductase protects cells against apoptosis at, or upstream of, caspase-8 activation. *J Gen Virol* **83,** 2779–89 (2002).

238. Dufour, F., Sasseville, A. M., Chabaud, S., Massie, B., Siegel, R. M. & Langelier, Y. The ribonucleotide reductase R1 subunits of herpes simplex virus types 1 and 2 protect cells against TNFalpha- and FasL-induced apoptosis by interacting with caspase-8. *Apoptosis* **16,** 256–71 (2011).

239. Huang, Z., Wu, S. Q., Liang, Y., Zhou, X., Chen, W., Li, L., Wu, J., Zhuang, Q., Chen, C., Li, J., Zhong, C. Q., Xia, W., Zhou, R., Zheng, C. & Han, J. RIP1/RIP3 binding to HSV-1 ICP6 initiates necroptosis to restrict virus propagation in mice. *Cell Host Microbe* **17,** 229–42 (2015).

240. Perkins, D., Pereira, E. F., Gober, M., Yarowsky, P. J. & Aurelian, L. The herpes simplex virus type 2 R1 protein kinase (ICP10 PK) blocks apoptosis in hippocampal neurons, involving activation of the MEK/MAPK survival pathway. *J Virol* **76,** 1435–49 (2002).

241. Mack, C., Sickmann, A., Lembo, D. & Brune, W. Inhibition of proinflammatory and innate immune signaling pathways by a cytomegalovirus RIP1-interacting protein. *Proc Natl Acad Sci U S A* **105,** 3094–9 (2008).

242. Brune, W., Menard, C., Heesemann, J. & Koszinowski, U. H. A ribonucleotide reductase homolog of cytomegalovirus and endothelial cell tropism. *Science* **291,** 303–5 (2001).

243. Kwon, K. M., Oh, S. E., Kim, Y. E., Han, T. H. & Ahn, J. H. Cooperative inhibition of RIP1-mediated NF-kappaB signaling by cytomegalovirus-encoded deubiquitinase and inactive homolog of cellular ribonucleotide reductase large subunit. *PLoS Pathog* **13,** e1006423 (2017).

244. Patrone, M., Percivalle, E., Secchi, M., Fiorina, L., Pedrali-Noy, G., Zoppe, M., Baldanti, F., Hahn, G., Koszinowski, U. H., Milanesi, G. & Gallina, A. The human cytomegalovirus UL45 gene product is a late, virion-associated protein and influences virus growth at low multiplicities of infection. *J Gen Virol* **84,** 3359–70 (2003).

245. Paladino, P., Marcon, E., Greenblatt, J. & Frappier, L. Identification of herpesvirus proteins that contribute to G1/S arrest. *J Virol* **88,** 4480–92 (2014).

246. Sakaue-Sawano, A., Kurokawa, H., Morimura, T., Hanyu, A., Hama, H., Osawa, H., Kashiwagi, S., Fukami, K., Miyata, T., Miyoshi, H., Imamura, T., Ogawa, M., Masai, H. & Miyawaki, A. Visualizing spatiotemporal dynamics of multicellular cell-cycle progression. *Cell* **132,** 487–98 (2008).

247. Yang, B., Li, X., Lei, L. & Chen, J. APOBEC: from mutator to editor. *J Genet Genomics* **44,** 423–437 (2017).

248. Rickinson, A. & Kieff, E. in *Fields Virology* (eds Knipe, D. & Howley, P. M.) 2nd, 2655–2700 (Lippincott Williams Wilkins, 2007).

249. Whitehurst, C. B., Ning, S., Bentz, G. L., Dufour, F., Gershburg, E., Shackelford, J., Langelier, Y. & Pagano, J. S. The Epstein-Barr virus (EBV) deubiquitinating enzyme BPLF1 reduces EBV ribonucleotide reductase activity. *J Virol* **83,** 4345–53 (2009).

250. Kraus, R. J., Yu, X., Cordes, B. A., Sathiamoorthi, S., Iempridee, T., Nawandar, D. M., Ma, S., Romero-Masters, J. C., McChesney, K. G., Lin, Z., Makielski, K. R., Lee, D. L., Lambert, P. F., Johannsen, E. C., Kenney, S. C. & Mertz, J. E. Hypoxia-inducible factor-1alpha plays roles in Epstein-Barr virus's natural life cycle and tumorigenesis by inducing lytic infection through direct binding to the immediate-early BZLF1 gene promoter. *PLoS Pathog* **13,** e1006404 (2017).

251. Hagemeier, S. R., Barlow, E. A., Kleman, A. A. & Kenney, S. C. The Epstein-Barr virus BRRF1 protein, Na, induces lytic infection in a TRAF2- and p53-dependent manner. *J Virol* **85,** 4318–29 (2011).

252. Verma, D., Thompson, J. & Swaminathan, S. Spironolactone blocks Epstein-Barr virus production by inhibiting EBV SM protein function. *Proc Natl Acad Sci U S A* **113,** 3609–14 (2016).

253. Starrett, G. J., Luengas, E. M., McCann, J. L., Ebrahimi, D., Temiz, N. A., Love, R. P., Feng, Y., Adolph, M. B., Chelico, L., Law, E. K., Carpenter, M. A. & Harris, R. S. The DNA cytosine deaminase APOBEC3H haplotype I likely contributes to breast and lung cancer mutagenesis. *Nat Commun* **7,** 12918 (2016).

254. Takada, K. Cross-linking of cell surface immunoglobulins induces Epstein-Barr virus in Burkitt lymphoma lines. *Int J Cancer* **33,** 27–32 (1984).

255. Borza, C. M. & Hutt-Fletcher, L. M. Alternate replication in B cells and epithelial cells switches tropism of Epstein-Barr virus. *Nat Med* **8,** 594–9 (2002).

256. Tsai, M. H., Raykova, A., Klinke, O., Bernhardt, K., Gartner, K., Leung, C. S., Geletneky, K., Sertel, S., Munz, C., Feederle, R. & Delecluse, H. J. Spontaneous

lytic replication and epitheliotropism define an Epstein-Barr virus strain found in carcinomas. *Cell Rep* **5,** 458–70 (2013).

257. Molesworth, S. J., Lake, C. M., Borza, C. M., Turk, S. M. & Hutt-Fletcher, L. M. Epstein-Barr virus gH is essential for penetration of B cells but also plays a role in attachment of virus to epithelial cells. *J Virol* **74,** 6324–32 (2000).

258. Suspne, R., Henry, M., Guillot, S., Wain-Hobson, S. & Vartanian, J. P. Recovery of APOBEC3-edited human immunodeficiency virus G-¿A hypermutants by differential DNA denaturation PCR. *J Gen Virol* **86,** 125–9 (2005).

259. Stenglein, M. D., Burns, M. B., Li, M., Lengyel, J. & Harris, R. S. APOBEC3 proteins mediate the clearance of foreign DNA from human cells. *Nat Struct Mol Biol* **17,** 222–9 (2010).

260. Geoui, T., Buisson, M., Tarbouriech, N. & Burmeister, W. P. New insights on the role of the gamma-herpesvirus uracil-DNA glycosylase leucine loop revealed by the structure of the Epstein-Barr virus enzyme in complex with an inhibitor protein. *J Mol Biol* **366,** 117–31 (2007).

261. Mol, C. D., Arvai, A. S., Sanderson, R. J., Slupphaug, G., Kavli, B., Krokan, H. E., Mosbaugh, D. W. & Tainer, J. A. Crystal structure of human uracil-DNA glycosylase in complex with a protein inhibitor: protein mimicry of DNA. *Cell* **82,** 701–8 (1995).

262. Robbiani, D. F. & Nussenzweig, M. C. Chromosome translocation, B cell lymphoma, and activation-induced cytidine deaminase. *Annu Rev Pathol* **8,** 79–103 (2013).

263. Suspene, R., Aynaud, M. M., Koch, S., Pasdeloup, D., Labetoulle, M., Gaertner, B., Vartanian, J. P., Meyerhans, A. & Wain-Hobson, S. Genetic editing of herpes simplex virus 1 and Epstein-Barr herpesvirus genomes by human APOBEC3 cytidine deaminases in culture and in vivo. *J Virol* **85,** 7594–602 (2011).

264. Sanjuan, R. & Domingo-Calap, P. Mechanisms of viral mutation. *Cell Mol Life Sci* **73,** 4433–4448 (2016).

265. Janini, M., Rogers, M., Birx, D. R. & McCutchan, F. E. Human immunodeficiency virus type 1 DNA sequences genetically damaged by hypermutation are often abundant in patient peripheral blood mononuclear

cells and may be generated during near-simultaneous infection and activation of CD4(+) T cells. *J Virol* **75,** 7973–86 (2001).

266. Kim, E. Y., Lorenzo-Redondo, R., Little, S. J., Chung, Y. S., Phalora, P. K., Maljkovic Berry, I., Archer, J., Penugonda, S., Fischer, W., Richman, D. D., Bhattacharya, T., Malim, M. H. & Wolinsky, S. M. Human APOBEC3 induced mutation of human immunodeficiency virus type-1 contributes to adaptation and evolution in natural infection. *PLoS Pathog* **10,** e1004281 (2014).

267. Stenglein, M. D. & Harris, R. S. APOBEC3B and APOBEC3F inhibit L1 retrotransposition by a DNA deamination-independent mechanism. *J Biol Chem* **281,** 16837–41 (2006).

268. Larue, R. S., Lengyel, J., Jonsson, S. R., Andresdottir, V. & Harris, R. S. Lentiviral Vif degrades the APOBEC3Z3/APOBEC3H protein of its mammalian host and is capable of cross-species activity. *J Virol* **84,** 8193–201 (2010).

269. Leonard, B., Hart, S. N., Burns, M. B., Carpenter, M. A., Temiz, N. A., Rathore, A., Vogel, R. I., Nikas, J. B., Law, E. K., Brown, W. L., Li, Y., Zhang, Y., Maurer, M. J., Oberg, A. L., Cunningham, J. M., Shridhar, V., Bell, D. A., April, C., Bentley, D., Bibikova, M., Cheetham, R. K., Fan, J. B., Grocock, R., Humphray, S., Kingsbury, Z., Peden, J., Chien, J., Swisher, E. M., Hartmann, L. C., Kalli, K. R., Goode, E. L., Sicotte, H., Kaufmann, S. H. & Harris, R. S. APOBEC3B upregulation and genomic mutation patterns in serous ovarian carcinoma. *Cancer Res* **73,** 7222–31 (2013).

270. Leonard, B., McCann, J. L., Starrett, G. J., Kosyakovsky, L., Luengas, E. M., Molan, A. M., Burns, M. B., McDougle, R. M., Parker, P. J., Brown, W. L. & Harris, R. S. The PKC/NF-kappaB signaling pathway induces APOBEC3B expression in multiple human cancers. *Cancer Res* **75,** 4538–47 (2015).

271. Bryant, D. M., Datta, A., Rodriguez-Fraticelli, A. E., Peranen, J., Martin-Belmonte, F. & Mostov, K. E. A molecular network for de novo generation of the apical surface and lumen. *Nat Cell Biol* **12,** 1035–45 (2010).

272. Salsman, J., Zimmerman, N., Chen, T., Domagala, M. & Frappier, L. Genome-wide screen of three herpesviruses for protein subcellular localization and alteration of PML nuclear bodies. *PLoS Pathog* **4,** e1000100 (2008).

273. Salamango, D. J. & Johnson, M. C. Characterizing the murine leukemia virus envelope glycoprotein membrane-spanning domain for its roles in interface alignment and fusogenicity. *J Virol* **89,** 12492–500 (2015).

274. Sanjana, N. E., Shalem, O. & Zhang, F. Improved vectors and genome-wide libraries for CRISPR screening. *Nat Methods* **11,** 783–4 (2014).

275. Albin, J. S., Hache, G., Hultquist, J. F., Brown, W. L. & Harris, R. S. Long-term restriction by APOBEC3F selects human immunodeficiency virus type 1 variants with restored Vif function. *J Virol* **84,** 10209–19 (2010).

276. Jagannathan, M., Nguyen, T., Gallo, D., Luthra, N., Brown, G. W., Saridakis, V. & Frappier, L. A role for USP7 in DNA replication. *Mol Cell Biol* **34,** 132–45 (2014).

277. Davis, Z. H., Verschueren, E., Jang, G. M., Kleffman, K., Johnson, J. R., Park, J., Von Dollen, J., Maher, M. C., Johnson, T., Newton, W., Jager, S., Shales, M., Horner, J., Hernandez, R. D., Krogan, N. J. & Glaunsinger, B. A. Global mapping of herpesvirus-host protein complexes reveals a transcription strategy for late genes. *Mol Cell* **57,** 349–60 (2015).

278. Shimizu, N., Yoshiyama, H. & Takada, K. Clonal propagation of Epstein-Barr virus (EBV) recombinants in EBV-negative Akata cells. *J Virol* **70,** 7260–3 (1996).

279. Ni, Z., Olsen, J. B., Emili, A. & Greenblatt, J. F. Identification of mammalian protein complexes by lentiviral-based affinity purification and mass spectrometry. *Methods Mol Biol* **781,** 31–45 (2011).

280. Liu, G., Zhang, J., Larsen, B., Stark, C., Breitkreutz, A., Lin, Z. Y., Breitkreutz, B. J., Ding, Y., Colwill, K., Pasculescu, A., Pawson, T., Wrana, J. L., Nesvizhskii, A. I., Raught, B., Tyers, M. & Gingras, A. C. ProHits: integrated software for mass spectrometry-based interaction proteomics. *Nat Biotechnol* **28,** 1015–7 (2010).

281. Cui, X. A., Zhang, H. & Palazzo, A. F. p180 promotes the ribosome-independent localization of a subset of mRNA to the endoplasmic reticulum. *PLoS Biol* **10,** e1001336 (2012).

282. Li, H. & Durbin, R. Fast and accurate short read alignment with Burrows-Wheeler transform. *Bioinformatics* **25,** 1754–60 (2009).

283. McKenna, A., Hanna, M., Banks, E., Sivachenko, A., Cibulskis, K., Kernytsky, A., Garimella, K., Altshuler, D., Gabriel, S., Daly, M. & DePristo, M. A. The Genome Analysis Toolkit: a MapReduce framework for analyzing next-generation DNA sequencing data. *Genome Res* **20,** 1297–303 (2010).

284. Li, H., Handsaker, B., Wysoker, A., Fennell, T., Ruan, J., Homer, N., Marth, G., Abecasis, G. & Durbin, R. The Sequence Alignment/Map format and SAMtools. *Bioinformatics* **25,** 2078–9 (2009).

285. Li, H. A statistical framework for SNP calling, mutation discovery, association mapping and population genetical parameter estimation from sequencing data. *Bioinformatics* **27,** 2987–93 (2011).

286. Koboldt, D. C., Zhang, Q., Larson, D. E., Shen, D., McLellan, M. D., Lin, L., Miller, C. A., Mardis, E. R., Ding, L. & Wilson, R. K. VarScan 2: somatic mutation and copy number alteration discovery in cancer by exome sequencing. *Genome Res* **22,** 568–76 (2012).

287. Borozan, I., Zapatka, M., Frappier, L. & Ferretti, V. Analysis of Epstein-Barr virus genomes and expression profiles in gastric adenocarcinoma. *J Virol* **92** (2018).

288. Katoh, K. & Standley, D. M. MAFFT multiple sequence alignment software version 7: improvements in performance and usability. *Mol Biol Evol* **30,** 772–80 (2013).

289. Ebrahimi, D., Anwar, F. & Davenport, M. P. APOBEC3 has not left an evolutionary footprint on the HIV-1 genome. *J Virol* **85,** 9139–46 (2011).

290. Lee, Y. N., Malim, M. H. & Bieniasz, P. D. Hypermutation of an ancient human retrovirus by APOBEC3G. *J Virol* **82,** 8762–70 (2008).

291. Narvaiza, I., Linfesty, D. C., Greener, B. N., Hakata, Y., Pintel, D. J., Logue, E., Landau, N. R. & Weitzman, M. D. Deaminase-independent inhibition of parvoviruses by the APOBEC3A cytidine deaminase. *PLoS Pathog* **5,** e1000439 (2009).

292. Zhang, W., Du, J., Evans, S. L., Yu, Y. & Yu, X. F. T-cell differentiation factor CBF-beta regulates HIV-1 Vif-mediated evasion of host restriction. *Nature* **481,** 376–9 (2011).

293. Bogerd, H. P., Tallmadge, R. L., Oaks, J. L., Carpenter, S. & Cullen, B. R. Equine infectious anemia virus resists the antiretroviral activity of equine APOBEC3 proteins through a packaging-independent mechanism. *J Virol* **82,** 11889–901 (2008).

294. Desai, P. & Person, S. Incorporation of the green fluorescent protein into the herpes simplex virus type 1 capsid. *J Virol* **72,** 7563–8 (1998).

295. Goldstein, D. J. & Weller, S. K. Factor(s) present in herpes simplex virus type 1-infected cells can compensate for the loss of the large subunit of the viral ribonucleotide reductase: characterization of an ICP6 deletion mutant. *Virology* **166,** 41–51 (1988).

296. DeLuca, N. A., McCarthy, A. M. & Schaffer, P. A. Isolation and characterization of deletion mutants of herpes simplex virus type 1 in the gene encoding immediate-early regulatory protein ICP4. *J Virol* **56,** 558–70 (1985).

297. Desai, P., Ramakrishnan, R., Lin, Z. W., Osak, B., Glorioso, J. C. & Levine, M. The RR1 gene of herpes simplex virus type 1 is uniquely trans activated by ICP0 during infection. *J Virol* **67,** 6125–35 (1993).

298. Cohen, D., Adamovich, Y., Reuven, N. & Shaul, Y. Hepatitis B virus activates deoxynucleotide synthesis in nondividing hepatocytes by targeting the R2 gene. *Hepatology* **51,** 1538–46 (2010).

299. Kitab, B., Satoh, M., Ohmori, Y., Munakata, T., Sudoh, M., Kohara, M. & Tsukiyama-Kohara, K. Ribonucleotide reductase M2 promotes RNA replication of hepatitis C virus by protecting NS5B protein from hPLIC1-dependent proteasomal degradation. *J Biol Chem* **294,** 5759–5773 (2019).

300. Iyer, L. M., Aravind, L. & Koonin, E. V. Common origin of four diverse families of large eukaryotic DNA viruses. *J Virol* **75,** 11720–34 (2001).

301. Sakowski, E. G., Munsell, E. V., Hyatt, M., Kress, W., Williamson, S. J., Nasko, D. J., Polson, S. W. & Wommack, K. E. Ribonucleotide reductases reveal novel viral diversity and predict biological and ecological features of unknown marine viruses. *Proc Natl Acad Sci U S A* **111,** 15786–91 (2014).

302. Zhao, Y., Temperton, B., Thrash, J. C., Schwalbach, M. S., Vergin, K. L., Landry, Z. C., Ellisman, M., Deerinck, T., Sullivan, M. B. & Giovannoni, S. J. Abundant SAR11 viruses in the ocean. *Nature* **494,** 357–60 (2013).

303. Mocarski, E. S., Guo, H. & Kaiser, W. J. Necroptosis: The Trojan horse in cell autonomous antiviral host defense. *Virology* **479-480,** 160–6 (2015).

304. Sitki-Green, D., Covington, M. & Raab-Traub, N. Compartmentalization and transmission of multiple epstein-barr virus strains in asymptomatic carriers. *J Virol* **77,** 1840–7 (2003).

305. Kenney, S. C. & Mertz, J. E. Regulation of the latent-lytic switch in Epstein-Barr virus. *Semin Cancer Biol* **26,** 60–8 (2014).

306. Chakraborty, S., Veettil, M. V. & Chandran, B. Kaposi's Sarcoma Associated Herpesvirus Entry into Target Cells. *Front Microbiol* **3,** 6 (2012).

307. Blasig, C., Zietz, C., Haar, B., Neipel, F., Esser, S., Brockmeyer, N. H., Tschachler, E., Colombini, S., Ensoli, B. & Sturzl, M. Monocytes in Kaposi's sarcoma lesions are productively infected by human herpesvirus 8. *J Virol* **71,** 7963–8 (1997).

308. Wu, W., Vieira, J., Fiore, N., Banerjee, P., Sieburg, M., Rochford, R., Harrington W., J. & Feuer, G. KSHV/HHV-8 infection of human hematopoietic progenitor (CD34+) cells: persistence of infection during hematopoiesis in vitro and in vivo. *Blood* **108,** 141–51 (2006).

309. Kim, I. J., Flano, E., Woodland, D. L., Lund, F. E., Randall, T. D. & Blackman, M. A. Maintenance of long term gamma-herpesvirus B cell latency is dependent on CD40-mediated development of memory B cells. *J Immunol* **171,** 886–92 (2003).

310. Thielen, B. K., McNevin, J. P., McElrath, M. J., Hunt, B. V., Klein, K. C. & Lingappa, J. R. Innate immune signaling induces high levels of TC-specific deaminase activity in primary monocyte-derived cells through expression of APOBEC3A isoforms. *J Biol Chem* **285,** 27753–66 (2010).

311. Akhtar, J. & Shukla, D. Viral entry mechanisms: cellular and viral mediators of herpes simplex virus entry. *FEBS J* **276,** 7228–36 (2009).

312. Edgar, R. C. MUSCLE: multiple sequence alignment with high accuracy and high throughput. *Nucleic Acids Res* **32,** 1792–7 (2004).

313. Bouckaert, R., Heled, J., Kuhnert, D., Vaughan, T., Wu, C. H., Xie, D., Suchard, M. A., Rambaut, A. & Drummond, A. J. BEAST 2: a software

platform for Bayesian evolutionary analysis. *PLoS Comput Biol* **10,** e1003537 (2014).

314. Hughes R. G., J. & Munyon, W. H. Temperature-sensitive mutants of herpes simplex virus type 1 defective in lysis but not in transformation. *J Virol* **16,** 275–83 (1975).

315. Park, D., Lalli, J., Sedlackova-Slavikova, L. & Rice, S. A. Functional comparison of herpes simplex virus 1 (HSV-1) and HSV-2 ICP27 homologs reveals a role for ICP27 in virion release. *J Virol* **89,** 2892–905 (2015).

316. DeLuca, N. A. & Schaffer, P. A. Physical and functional domains of the herpes simplex virus transcriptional regulatory protein ICP4. *J Virol* **62,** 732–43 (1988).

317. OhAinle, M., Kerns, J. A., Malik, H. S. & Emerman, M. Adaptive evolution and antiviral activity of the conserved mammalian cytidine deaminase APOBEC3H. *J Virol* **80,** 3853–62 (2006).

318. Sawyer, S. L., Emerman, M. & Malik, H. S. Ancient adaptive evolution of the primate antiviral DNA-editing enzyme APOBEC3G. *PLoS Biol* **2,** E275 (2004).

319. Daugherty, M. D. & Malik, H. S. Rules of engagement: molecular insights from host-virus arms races. *Annu Rev Genet* **46,** 677–700 (2012).

320. Van Valen, L. A new evolutionary law. *Evolutionary Theory* **1,** 1–30 (1973).

321. Cantrell, M. A., Scott, L., Brown, C. J., Martinez, A. R. & Wichman, H. A. Loss of LINE-1 activity in the megabats. *Genetics* **178,** 393–404 (2008).

322. Wagstaff, B. J., Kroutter, E. N., Derbes, R. S., Belancio, V. P. & Roy-Engel, A. M. Molecular reconstruction of extinct LINE-1 elements and their interaction with nonautonomous elements. *Mol Biol Evol* **30,** 88–99 (2013).

323. Horie, M., Honda, T., Suzuki, Y., Kobayashi, Y., Daito, T., Oshida, T., Ikuta, K., Jern, P., Gojobori, T., Coffin, J. M. & Tomonaga, K. Endogenous non-retroviral RNA virus elements in mammalian genomes. *Nature* **463,** 84–7 (2010).

324. Gilbert, C. & Feschotte, C. Genomic fossils calibrate the long-term evolution of hepadnaviruses. *PLoS Biol* **8** (2010).

325. Gifford, R. J. Viral evolution in deep time: lentiviruses and mammals. *Trends Genet* **28,** 89–100 (2012).

326. Yoshikawa, R., Izumi, T., Nakano, Y., Yamada, E., Moriwaki, M., Misawa, N., Ren, F., Kobayashi, T., Koyanagi, Y. & Sato, K. Small ruminant lentiviral Vif proteins commonly utilize cyclophilin A, an evolutionarily and structurally conserved protein, to degrade ovine and caprine APOBEC3 proteins. *Microbiol Immunol* **60,** 427–36 (2016).

327. Malik-Soni, N. *Investigation of Epstein-Barr virus-host interactions during latent and lytic infection* Thesis (2014).

328. Dong, Q., Smith, K. R., Oldenburg, D. G., Shapiro, M., Schutt, W. R., Malik, L., Plummer, J. B., Mu, Y., MacCarthy, T., White, D. W., McBride, K. M. & Krug, L. T. Combinatorial Loss of the Enzymatic Activities of Viral Uracil-DNA Glycosylase and Viral dUTPase Impairs Murine Gammaherpesvirus Pathogenesis and Leads to Increased Recombination-Based Deletion in the Viral Genome. *MBio* **9** (2018).

329. Mostafa, H. H., Thompson, T. W., Konen, A. J., Haenchen, S. D., Hilliard, J. G., Macdonald, S. J., Morrison, L. A. & Davido, D. J. Herpes Simplex Virus 1 Mutant with Point Mutations in UL39 Is Impaired for Acute Viral Replication in Mice, Establishment of Latency, and Explant-Induced Reactivation. *J Virol* **92** (2018).

330. Van Etten, J. L. & Meints, R. H. Giant viruses infecting algae. *Annu Rev Microbiol* **53,** 447–94 (1999).

331. Dunigan, D. D., Cerny, R. L., Bauman, A. T., Roach, J. C., Lane, L. C., Agarkova, I. V., Wulser, K., Yanai-Balser, G. M., Gurnon, J. R., Vitek, J. C., Kronschnabel, B. J., Jeanniard, A., Blanc, G., Upton, C., Duncan, G. A., McClung, O. W., Ma, F. & Van Etten, J. L. Paramecium bursaria chlorella virus 1 proteome reveals novel architectural and regulatory features of a giant virus. *J Virol* **86,** 8821–34 (2012).

332. Lanzkron, S., Strouse, J. J., Wilson, R., Beach, M. C., Haywood, C., Park, H., Witkop, C., Bass, E. B. & Segal, J. B. Systematic review: Hydroxyurea for the treatment of adults with sickle cell disease. *Ann Intern Med* **148,** 939–55 (2008).

333. Noble, S. & Goa, K. L. Gemcitabine. A review of its pharmacology and clinical potential in non-small cell lung cancer and pancreatic cancer. *Drugs* **54,** 447–72 (1997).

334. Apseloff, G. Therapeutic uses of gallium nitrate: past, present, and future. *Am J Ther* **6,** 327–39 (1999).

335. Yarbro, J. W. Mechanism of action of hydroxyurea. *Semin Oncol* **19,** 1–10 (1992).

336. Bernstein, L. R. Mechanisms of therapeutic activity for gallium. *Pharmacol Rev* **50,** 665–82 (1998).

337. Plunkett, W., Huang, P., Xu, Y. Z., Heinemann, V., Grunewald, R. & Gandhi, V. Gemcitabine: metabolism, mechanisms of action, and self-potentiation. *Semin Oncol* **22,** 3–10 (1995).

338. Harabuchi, Y., Takahara, M., Kishibe, K., Nagato, T. & Kumai, T. Extranodal Natural Killer/T-Cell Lymphoma, Nasal Type: Basic Science and Clinical Progress. *Front Pediatr* **7,** 141 (2019).

339. Aozasa, K., Takakuwa, T., Hongyo, T. & Yang, W. I. Nasal NK/T-cell lymphoma: epidemiology and pathogenesis. *Int J Hematol* **87,** 110–117 (2008).

340. Haverkos, B. M., Pan, Z., Gru, A. A., Freud, A. G., Rabinovitch, R., Xu-Welliver, M., Otto, B., Barrionuevo, C., Baiocchi, R. A., Rochford, R. & Porcu, P. Extranodal NK/T Cell Lymphoma, Nasal Type (ENKTL-NT): An Update on Epidemiology, Clinical Presentation, and Natural History in North American and European Cases. *Curr Hematol Malig Rep* **11,** 514–527 (2016).

341. Rudiger, T., Weisenburger, D. D., Anderson, J. R., Armitage, J. O., Diebold, J., MacLennan, K. A., Nathwani, B. N., Ullrich, F., Muller-Hermelink, H. K. & Non-Hodgkin's Lymphoma Classification, P. Peripheral T-cell lymphoma (excluding anaplastic large-cell lymphoma): results from the Non-Hodgkin's Lymphoma Classification Project. *Ann Oncol* **13,** 140–9 (2002).

342. Vose, J., Armitage, J., Weisenburger, D. & International, T. C.L. P. International peripheral T-cell and natural killer/T-cell lymphoma study: pathology findings and clinical outcomes. *J Clin Oncol* **26,** 4124–30 (2008).

343. Arber, D. A., Weiss, L. M., Albujar, P. F., Chen, Y. Y. & Jaffe, E. S. Nasal lymphomas in Peru. High incidence of T-cell immunophenotype and Epstein-Barr virus infection. *Am J Surg Pathol* **17,** 392–9 (1993).

344. Sidagis, J., Ueno, K., Tokunaga, M., Ohyama, M. & Eizuru, Y. Molecular epidemiology of Epstein-Barr virus (EBV) in EBV-related malignancies. *Int J Cancer* **72,** 72–6 (1997).

345. De Bruin, E. C., McGranahan, N., Mitter, R., Salm, M., Wedge, D. C., Yates, L., Jamal-Hanjani, M., Shafi, S., Murugaesu, N., Rowan, A. J., Gronroos, E., Muhammad, M. A., Horswell, S., Gerlinger, M., Varela, I., Jones, D., Marshall, J., Voet, T., Van Loo, P., Rassl, D. M., Rintoul, R. C., Janes, S. M., Lee, S. M., Forster, M., Ahmad, T., Lawrence, D., Falzon, M., Capitanio, A., Harkins, T. T., Lee, C. C., Tom, W., Teefe, E., Chen, S. C., Begum, S., Rabinowitz, A., Phillimore, B., Spencer-Dene, B., Stamp, G., Szallasi, Z., Matthews, N., Stewart, A., Campbell, P. & Swanton, C. Spatial and temporal diversity in genomic instability processes defines lung cancer evolution. *Science* **346,** 251–6 (2014).

346. Cho, R. J., Alexandrov, L. B., den Breems, N. Y., Atanasova, V. S., Farshchian, M., Purdom, E., Nguyen, T. N., Coarfa, C., Rajapakshe, K., Prisco, M., Sahu, J., Tassone, P., Greenawalt, E. J., Collisson, E. A., Wu, W., Yao, H., Su, X., Guttmann-Gruber, C., Hofbauer, J. P., Hashmi, R., Fuentes, I., Benz, S. C., Golovato, J., Ehli, E. A., Davis, C. M., Davies, G. E., Covington, K. R., Murrell, D. F., Salas-Alanis, J. C., Palisson, F., Bruckner, A. L., Robinson, W., Has, C., Bruckner-Tuderman, L., Titeux, M., Jonkman, M. F., Rashidghamat, E., Lwin, S. M., Mellerio, J. E., McGrath, J. A., Bauer, J. W., Hovnanian, A., Tsai, K. Y. & South, A. P. APOBEC mutation drives early-onset squamous cell carcinomas in recessive dystrophic epidermolysis bullosa. *Sci Transl Med* **10** (2018).

347. Sieuwerts, A. M., Willis, S., Burns, M. B., Look, M. P., Meijer-Van Gelder, M. E., Schlicker, A., Heideman, M. R., Jacobs, H., Wessels, L., Leyland-Jones, B., Gray, K. P., Foekens, J. A., Harris, R. S. & Martens, J. W. Elevated APOBEC3B correlates with poor outcomes for estrogen-receptor-positive breast cancers. *Horm Cancer* **5,** 405–13 (2014).

348. Faltas, B. M., Prandi, D., Tagawa, S. T., Molina, A. M., Nanus, D. M., Sternberg, C., Rosenberg, J., Mosquera, J. M., Robinson, B., Elemento, O., Sboner, A., Beltran, H., Demichelis, F. & Rubin, M. A. Clonal evolution of chemotherapy-resistant urothelial carcinoma. *Nat Genet* **48,** 1490–1499 (2016).

349. Schmitt, C., Lucius, R., Synowitz, M., Held-Feindt, J. & Hattermann, K. APOBEC3B is expressed in human glioma, and influences cell proliferation and temozolomide resistance. *Oncol Rep* **40,** 2742–2749 (2018).

350. Land, A. M., Wang, J., Law, E. K., Aberle, R., Kirmaier, A., Krupp, A., Johnson, W. E. & Harris, R. S. Degradation of the cancer genomic DNA deaminase APOBEC3B by SIV Vif. *Oncotarget* **6,** 39969–79 (2015).

351. Li, M. M. & Emerman, M. Polymorphism in human APOBEC3H affects a phenotype dominant for subcellular localization and antiviral activity. *J Virol* **85,** 8197–207 (2011).

Appendices

APPENDIX A

Differential Evolution of Antiretroviral Restriction Factors in Pteropid Bats As Revealed by *APOBEC3* Gene Complexity.

This appendix section was adapted with permission from:

Hayward JA, et al. Mol Biol Evol. (2018). ***35****(7):16261637.*

Authors: Joshua A Hayward[1,2], Mary Tachedjian[3], Jie Cui[4], Adam Z. Cheng[5], Adam Johnson[1], Michelle L. Baker[3], Reuben S. Harris[5,6], Lin-Fa Wang[7] & Gilda Tachedjian[*,1,2,8,9]

Affiliations:

[1] Health Security Program, Life Sciences Discipline, Burnet Institute, Melbourne, VIC, Australia.

[2] Department of Microbiology, Monash University, Clayton, VIC, Australia.

[3] Australian Animal Health Laboratory, Health and Biosecurity Business Unit, CSIRO, Geelong, VIC, Australia.

[4] Key Laboratory of Special Pathogens and Biosafety, Center for Emerging Infectious Diseases, Wuhan Institute of Virology, Chinese Academy of Sciences, Wuhan, China.

[5] Department of Biochemistry, Molecular Biology, and Biophysics, Institute for Molecular Virology, University of Minnesota, Minneapolis, MN.

[6] Howard Hughes Medical Institute, University of Minnesota, Minneapolis, MN.

[7] Programme in Emerging Infectious Diseases, Duke-NUS Medical School, Singapore.

[8] School of Science, College of Science, Engineering and Health, RMIT University, Melbourne, VIC, Australia.

[9] Department of Microbiology and Immunology at the Doherty Institute for Infection and Immunity, The University of Melbourne, Melbourne, VIC, Australia.

∗ Corresponding author: E-mail: gildat@burnet.edu.au

A.1 Summary

Bats have attracted attention in recent years as important reservoirs of viruses deadly to humans and other mammals. These infections are typically nonpathogenic in bats raising questions about innate immune differences that might exist between bats and other mammals. The *APOBEC3* gene family encodes antiviral DNA cytosine deaminases with important roles in the suppression of diverse viruses and genomic parasites. Here, we characterize pteropid *APOBEC3* genes and show that species within the genus *Pteropus* possess the largest and most diverse array of *APOBEC3* genes identified in any mammal reported to date. Several bat APOBEC3 proteins are antiviral as demonstrated by restriction of retroviral infectivity using HIV-1 as a model, and recombinant A3Z1 subtypes possess strong DNA deaminase activity. These genes represent the first group of antiviral restriction factors identified in bats with extensive diversification relative to homologues in other mammals.

A.2 Author Contributions

I cloned and tested each of the newly characterized bat *APOBEC3* genes for functional deaminase activity using a rifampicin resistance mutagenesis assay in *E. coli*. I generated the data for **Figure A.5.1** as well as the corresponding text and methods, reproduced below.

A.3 Results

Bat APOBEC3 Proteins Are Potent DNA Mutators

We tested the activity of the bat A3 proteins for which expression was verified by assessing their ability to cause mutations in *E. coli* though a rifampicin mutagenesis assay, utilizing human A3B and A3G as positive controls because they are known to be expressed and enzymatically active in *E. coli* (Holden et al. 2008; Shi et al. 2015). Mutations in the *rpoB* gene increase with mutagenic stress mediated by A3 (Harris et al. 2002; Shi et al. 2015). Mutational frequencies above background levels were only observed for A3Z1 proteins, and we found that four bat A3Z1s showed a 10-fold or greater increase in mutation frequency (**Figure A.5.1A**). In particular, A3Z1c isomer B showed over 1000-fold increase above empty vector and 100-fold above A3Z1c isomer A. To determine if the difference in mutation frequency correlated with differences in mutation signatures, we sequenced a PCR-amplified portion of the rpoB gene known to harbor hotspots for rifampicin resistance. Bat A3 mutation signatures were compared against human A3B and A3G (**Figure A.5.1B**), which have dinucleotide sequence preferences for 5-TC and 5-CC, respectively. We found that bat A3Z1c isomer A was highly specific for causing mutation at a known 5-TCG hotspot at nucleotide position 1585, which is also the preferred target site for A3B (Shi et al. 2015). In contrast, A3Z1c isomer B targeted sites at position 1565, 1585, and 1592, which have 5-TCT, 5-TCG, and 5-TCC contexts, respectively. Decreased specificity may account for the high mutation frequency observed in the rifampicin mutagenesis assays. These results show that bat A3 proteins are functionally active and can mutate cytosines in a diverse range of dinucleotide contexts.

A.4 Materials and Methods

Rifampicin Mutagenesis Assay

Bat A3 cDNAs were PCR amplified from parental vectors and subcloned into pET24(+) vectors (EMD Biosciences). Plasmids were transformed into calcium competent C43 (DE3) strain *E. coli* (gift from Dr. Do-Hyung Kim) and grown in LB plates with kanamycin. Single colonies were selected and grown in LB with kanamycin for 28 h to ensure stationary phase growth. Thereafter, cultures were spread on either rifampicin plates or serially diluted in M9 salt media and spread on kanamycin plates. Colony counts were obtained after 18 h. *rpoB* mutation frequency was obtained by dividing the number of viable colonies on rifampicin plates by colonies on kanamycin plates and correcting for the dilution factor. A portion of the *rpoB* gene was PCR amplified using primers: forward 5-TTGGCGAAATGGCGGAAAACC and reverse 5-CACCGACGGATACCACCTGCTG. PCR products were enzymatically purified using Exonuclease I and rSAP (NEB). Purified fragments were sequenced using the forward primer (GeneWiz, NJ).

A.5 Figures

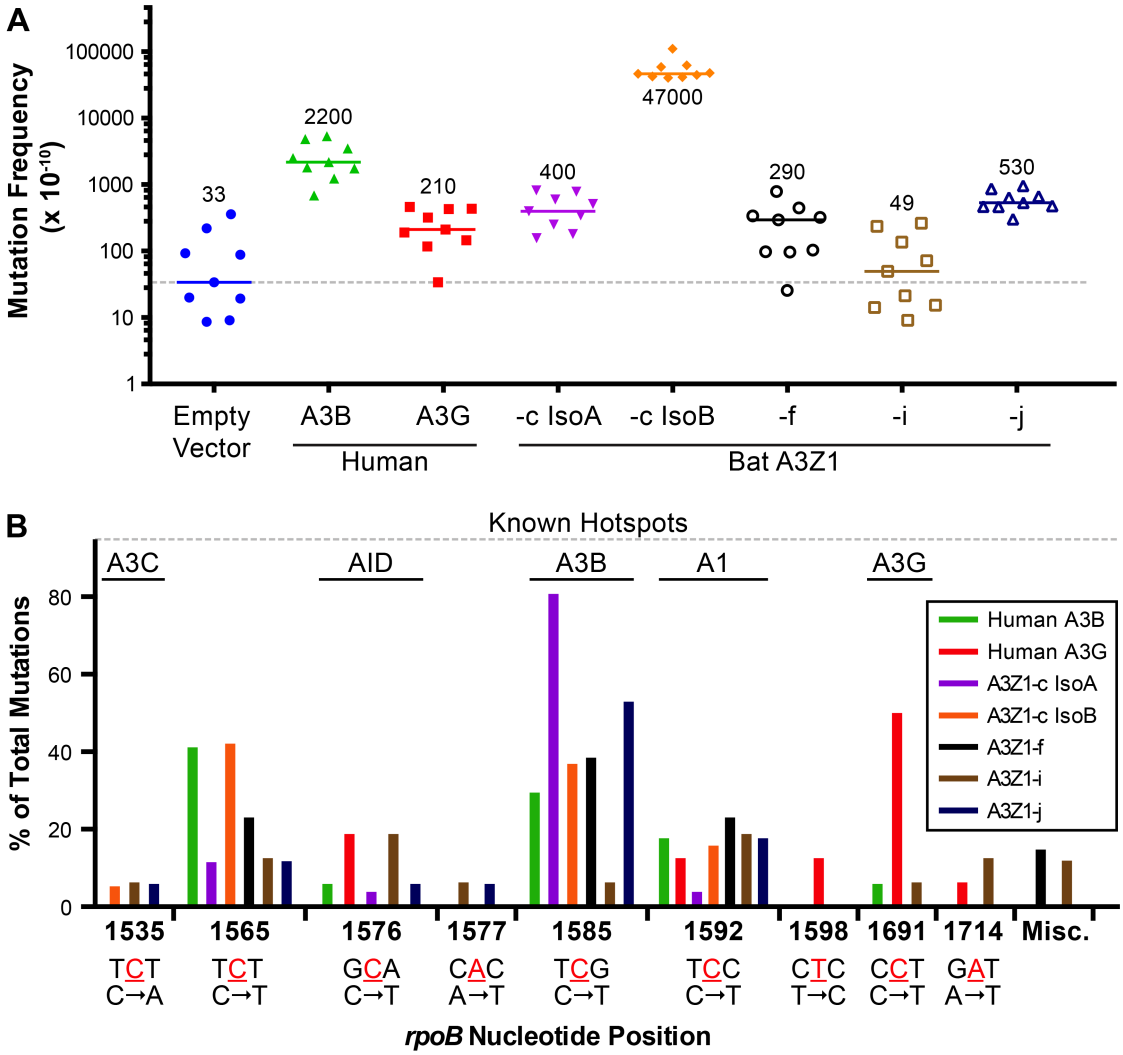

Figure A.5.1: Functional analysis of bat A3 proteins.
A) A3 proteins were transformed in C43 (DE3) *E. coli* to measure mutational frequency in the *rpoB* gene. Each point represents an independent sample and bars represent median mutation frequency with numerical values above.
(**B**) Mutation signatures in a portion of the *rpoB* gene by PCR amplification and Sanger sequencing. Position of the mutated nucleotide is underlined and in red with nucleotide changes below. Known hotspots targeted by related proteins are provided above. A1, APOBEC1; A3, APOBEC3; AID, Activation-induced deaminase.

APPENDIX B

APOBEC3H Subcellular Localization Determinants Define Zipcode for Targeting HIV-1 for Restriction

This appendix section was adapted with permission from:

Salamango DJ, et al. Mol Cell Biol. (2018). ***38****(23):e00356-18.*

Authors: Daniel J. Salamango[1,2,3], Jordan T. Becker[1,2,3], Jennifer L. McCann[1,2,3], Adam Z. Cheng[1,2,3], Özlem Demin[4], Rommie E. Amaro[4], William L. Brown[1,2,3], Nadine M. Shaban[1,2,3] & Reuben S. Harris[1,2,3,5]

Affiliations:

[1] Department of Biochemistry, Molecular Biology and Biophysics, University of Minnesota, Minneapolis, Minnesota, USA.

[2] Masonic Cancer Center, University of Minnesota, Minneapolis, Minnesota, USA.

[3] Institute for Molecular Virology, University of Minnesota, Minneapolis, Minnesota, USA.

[4] Department of Chemistry and Biochemistry, University of San Diego, La Jolla, California, USA.

[5] Howard Hughes Medical Institute, University of Minnesota, Minneapolis, Minnesota, USA.

Address correspondence to Daniel J. Salamango, dsalaman@umn.edu, or Reuben S. Harris, rsh@umn.edu.

B.1 Summary

APOBEC enzymes are DNA cytosine deaminases that normally serve as virus restriction factors, but several members, including APOBEC3H, also contribute to cancer mutagenesis. Despite their importance in multiple fields, little is known about cellular processes that regulate these DNA mutating enzymes. We show that APOBEC3H exists in two distinct subcellular compartments, cytoplasm and nucleolus, and that the structural determinants for each mechanism are genetically separable. First, native and fluorescently tagged APOBEC3Hs localize to these two compartments in multiple cell types. Second, a series of genetic, pharmacologic, and cell biological studies demonstrate active cytoplasmic and nucleolar retention mechanisms, whereas nuclear import and export occur through passive diffusion. Third, APOBEC3H cytoplasmic retention determinants relocalize APOBEC3A from a passive cell-wide state to the cytosol and, additionally, endow potent HIV-1 restriction activity. These results indicate that APOBEC3H has a structural zipcode for subcellular localization and selecting viral substrates for restriction.

B.2 Author Contributions

I performed immunofluorescence microscopy of untagged APOBEC3H splice variants (SV182/183/200). I generated the data for **Figure B.5.1A**, assisted in editing the text, and wrote the corresponding methods, reproduced below.

B.3 Results

Subcellular distribution of A3H

Previous studies have described A3H localization as predominantly cytoplasmic [34, 62, 97, 351], so we were surprised when immunofluorescence experiments using an A3H-specific polyclonal antibody detected two distinct subcellular pools of native A3H in HeLa cells (cytoplasmic and nuclear) (**Figure B.5.1A**, top). To confirm that this localization pattern was not due to an artifact of the immunofluorescence procedure, we added an N-terminal mCherry (mCh) fluorescence tag and still observed dual localization in 293T cells, indicating that this localization pattern is independent of detection method and cell type (**Figure B.5.1A**, bottom). In addition, two C-terminal splice variants of 182 and 200 residues in length had indistinguishable localization patterns, demonstrating that shared residues 1 to 182 govern both localization mechanisms (**Figure B.5.1A**, top and bottom).

B.4 Materials and Methods

Immunofluorescence

Approximately 25,000 HeLa cells were plated on acid-washed and polylysine-treated 22- by 22- by 1.5-mm coverslips (12-541-B; Fisherbrand, Minneapolis, MN) in a 6-well plate and after 24 h were transfected with 500 ng of the indicated A3 plasmids, 1.5 μl TransIT-LT1 (2304; Mirus), and 100 μl serum-free RPMI 1640 (Corning, Corning, NY). After 48 h, medium was removed and coverslips were washed with phosphate-buffered saline (PBS), fixed in 4% methanol-free formaldehyde (28906; Thermo Scientific) for 15 min, and rinsed 3 times for 5 min each in PBS with gentle

rocking. Cells were permeabilized with 0.2% Triton X-100 in PBS for 10 min, washed three time for 5 min each in PBS, and then incubated in blocking buffer (0.0028 M KH_2PO_4, 0.0072 M K_2HPO_4, 5% goat serum [Gibco], 5% glycerol, 1% cold water fish gelatin [Sigma-Aldrich], 0.04% sodium azide, pH 7.2) for 1 h. Cells were washed in PBS and then incubated in rabbit anti-A3H primary antibody (NBP1-91682; Novus, Littleton, CO) at 1:200 diluted in blocking buffer overnight at 4°C. Cells were washed three times for 5 min each with PBS and then incubated in goat anti-rabbit secondary antibodyfluorescein isothiocyanate (FITC) (111095144; Jackson Laboratories, Bar Harbor, ME) at 1:1,000 dilution in blocking buffer for 1 h at room temperature. Coverslips were mounted on precleaned slides (Gold Seal Rite-On) using one drop (10 to 15 μl) of mounting medium (prepared by dissolving 1 g n-propyl gallate [Sigma] in 30 ml glycerol overnight, adding 0.35 ml 0.1 M KH_2PO_4, adjusting the pH to 8 to 8.5 with K_2HPO_4, and adding water to obtain a final volume of 50 ml). Slides were imaged on a Nikon inverted Ti-E deconvolution microscope and analyzed using NiS Elements including deconvolution of images.

B.5 Figures

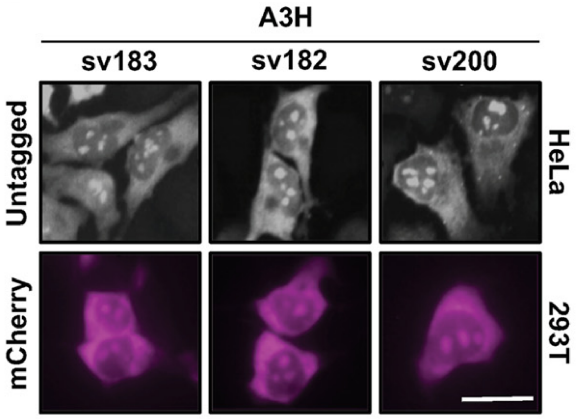

Figure B.5.1: Evidence for cytoplasmic and nucleolar A3H.
(**A**) Representative images of native A3H and mCherry-tagged (mCh) splice variants. Scale bar, 10 μm.

APPENDIX C

Genetic and Mechanistic Basis for APOBEC3H Alternative Splicing, Retrovirus Restriction, and Counteraction by HIV-1 Protease

This appendix section was adapted with permission from:

Ebrahimi D, et al. Nat Commun. (2018). ***9****(1):4137.*

Authors: Diako Ebrahimi[1], Christopher M. Richards[1], Michael A. Carpenter[1,2], Jiayi Wang[1], Terumasa Ikeda[1,2], Jordan T. Becker[1], Adam Z. Cheng[1], Jennifer L. McCann[1], Nadine M. Shaban[1], Daniel J. Salamango[1], Gabriel J. Starrett[1,4], Jairam R. Lingappa[3], Jeongsik Yong[1], William L. Brown[1] & Reuben S. Harris[1,2]

Affiliations:

[1] Department of Biochemistry, Molecular Biology and Biophysics, Masonic Cancer Center, Institute for Molecular Virology, Center for Genome Engineering, University of Minnesota, Minneapolis, MN 55455, USA.

[2] Howard Hughes Medical Institute, University of Minnesota, Minneapolis, MN 55455, USA.

[3] Departments of Global Health, Medicine and Pediatrics, University of Washington, Seattle, WA 98104, USA.

[4] Present address: Center for Cancer Research, National Cancer Institute, National Institutes of Health, Bethesda, MD 20892, USA.

These authors contributed equally: Diako Ebrahimi, Christopher M. Richards.

Correspondence and requests for materials should be addressed to R.S.H. (email: rsh@umn.edu)

C.1 Summary

Human APOBEC3H (A3H) is a single-stranded DNA cytosine deaminase that inhibits HIV-1. Seven haplotypes (IVII) and four splice variants (SV154/182/183/200) with differing antiviral activities and geographic distributions have been described, but the genetic and mechanistic basis for variant expression and function remains unclear. Using a combined bioinformatic/experimental analysis, we find that SV200 expression is specific to haplotype II, which is primarily found in sub-Saharan Africa. The underlying genetic mechanism for differential mRNA splicing is an ancient intronic deletion [del(ctc)] within A3H haplotype II sequence. We show that SV200 is at least fourfold more HIV-1 restrictive than other A3H splice variants. To counteract this elevated antiviral activity, HIV-1 protease cleaves SV200 into a shorter, less restrictive isoform. Our analyses indicate that, in addition to Vif-mediated degradation, HIV-1 may use protease as a counter-defense mechanism against A3H in >80% of sub-Saharan African populations.

C.2 Author Contributions

I purified A3H splice variants (SV200/187x/183) from HIV-1 viral particles produced from 293T cells and measured *in vitro* cytosine deaminase activity. Activity was also normalized to A3H protein packaging within viral particles. These experiments were performed in anticipation for reviewer feedback, but ultimately not included in the final manuscript. I assisted in editing the text.

C.3 Results

Packaging Efficiency and Activity of APOBEC3H Splice Variants

There was similarly strong Vif-deficient HIV-1 restriction activities for APOBEC3H SV182/3 and SV200, but the activity of the latter splice variant was likely underestimated due to lower enzyme amounts in viral particles (and potentially also to proteolytic cleavage). We therefore sought to quantify the *in vitro* deaminase activities of untagged A3H haplotype II SV200, a mutant mimicking cleaved SV200 with a stop codon at amino acid 187 (SV187x), and SV183 from purified HIV-1 particles. 293T cells were co-transfected with HIV-1ΔVif and different A3 proteins, and viral particles were then purified from the supernatant. Similar HIV-1 p24 levels were observed for all conditions, but A3H SV183 was packaged at 7-10 fold higher levels than either SV200 or SV187x (**Figure C.5.1A**). A3H SV183 from these viral particles additionally showed the highest raw deaminase activity per viral particle and was increased upon RNase treatment (**Figure C.5.1B**). However, after normalization for total A3H protein level within each viral particle, A3H SV200 and SV187x showed the highest *in vitro* deamination, consistent with higher HIV-1 restriction activity from these split variants (**Figure C.5.1B**).

C.4 Materials and Methods

Cell Culture and Virus Production

Approximately 250,000 293T cells were plated into 6-well plates. After 24 hours, cells were co-transfected with HIV-1ΔVif and A3 constructs for virus production and protein expression. After 48 hours, cell supernatant was collected, filtered, and

purified using a 20% sucrose cushion. The viral pellet was then split in half for either immunoblot for viral proteins and A3 packaging, or for *in vitro* deaminase assays as previously described [34]. A3 protein abundance in viral particles was quantified by densitometric analyses on ImageJ. A3 deaminase activity was quantified by densitometric analyses on ImageJ by dividing product band intensity by the sum of product and substrate band intensities. Normalized A3 deaminase activity was calculated by dividing the raw percent deaminase activity by relative A3 protein abundance in viral particles.

C.5 Figures

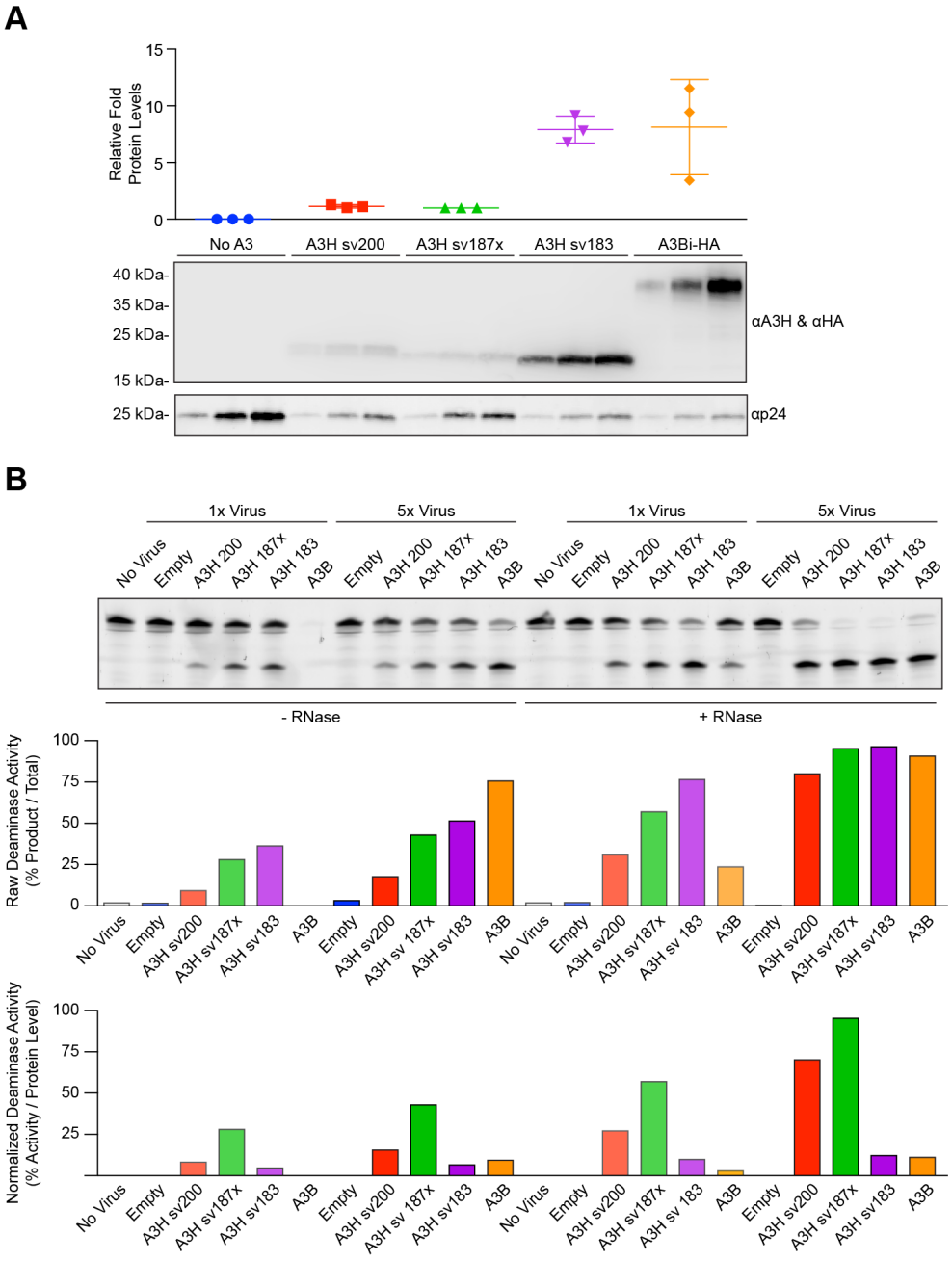

Figure C.5.1: Packaging Efficiency and Activity of APOBEC3H Splice Variants.

Figure C.5.1 (Continued):
(**A**) Immunoblot of A3 proteins in HIV-1ΔVif particles (bottom) and corresponding quantification (top).
(**B**) Representative TBE-urea PAGE analysis of A3 DNA deaminase activity from viral particles with or without RNase treatment and at two arbitrary volumes of virus (top). Quantification of raw and relative A3 deaminase activity (bottom).